Rutting of Granular Pavements

by Gregory Kenneth Arnold

Thesis submitted to The University of Nottingham

For the degree of Doctor of Philosophy, August 2004

ABSTRACT

The rutting of granular pavements was studied by examining the permanent deformation behaviour of granular and subgrade materials used in a Northern Ireland, United Kingdom pavement field trial and accelerated pavement tests at CAPTIF (Transit New Zealand's test track) located in Christchurch New Zealand. Repeated Load Triaxial (RLT) tests at many different combinations of confining stress and vertical cyclic stress for 50,000 loading cycles was conducted on the granular and subgrade materials. Moisture content was not varied in the RLT tests, although it was recognised that the resulting permanent strain depends on moisture content. However, the aim of the RLT tests was to derive relationships between permanent strain and stress level. These relationships were later used in finite element models to predict rutting behaviour and magnitude for the pavements tested in Northern Ireland and the CAPTIF test track. Predicted rutting behaviour and magnitude were compared to actual rut depth measurements during full scale pavement tests to validate the methods used.

ACKNOWLEDGEMENTS

I am extremely grateful for the support and assistance provided during my study, especially:

Andrew Dawson, University of Nottingham, as my supervisor for providing assistance, research direction and timely comments on thesis.

Dr David Hughes and Dr Des Robinson of Queens University of Belfast for their assistance.

Transit New Zealand through David Alabaster, who provided accelerated pavement test data from their test track CAPTIF.

The Engineering and Physical Sciences Research Council (EPSRC) for sponsoring the research project.

Department of the Environment (DOE) Northern Ireland, United Kingdom for funding the construction of the field trial.

Professor CDF Rodgers of the The University of Birmingham for the thorough examination of this thesis.

DEDICATION

This thesis is dedicated to my late father, Trevor Arnold. His ambitious, positive and fun attitude was a constant form of encouragement to aim high but still have fun along the way.

TABLE OF CONTENTS

Appendices

Table of Figures

List of Tables

CHAPTER 1 INTRODUCTION, OBJECTIVES AND SCOPE

1.1 BACKGROUND

The Romans can be considered as pioneers in road construction. Throughout Europe they established a vast network of roads primarily for military purposes. The layout seldom varied; two trenches were dug 5m apart to act as drainage ditches, and the soil between was excavated down to a firm foundation on which a multilayer granular base was laid using materials locally available (Croney and Croney, 1991). The thickness of pavement was modified to take account of the strength of the soil foundation. In most cases the pavements built by Romans in other parts of Europe were surfaced with flat quarried stone to maintain the common appearance familiar to visitors from Rome.

After the Romans, roads were needed again to transport surplus crops to barter with other villages. This led to the development of small market towns surrounded by satellite village communities. Long distance coach travel became important with the growing wealth of the 17th and 18th centuries. This necessitated more permanent roads between towns. Roads were either a bed of comparatively large pitched stone blinded by dry fines, as preferred by Thomas Telford, or were constructed with smaller angular material watered to assist granular interlock, as preferred by John Louden Macadam (Lay, 1984).

The modern pavement of today is derived from Macadam with a base of small angular rock material (granular) with a uniform grading overlying the soil foundation. But it is unlike Macadam as it is often surfaced with a smooth waterproof layer. This surface can contribute to the structural strength of the pavement as with an asphalt base, or simply waterproof the pavement as with a chipseal (sprayed seal surface). Both the modern pavement and the earlier pavements had primarily the same aim of protecting the underlying weaker soil foundation from wheel loads while providing a long lasting trafficable road. Modern pavements are commonly referred to as flexible pavements. Thin or low volume pavements represent approximately 95% of pavements in the UK (British Road Federation, 1999).

Flexible pavements fail either by cracking or rutting. For thinly surfaced asphalted granular pavements the avoidance of rutting is the major design consideration. Most current pavement thickness design guides (HMSO 1994, TRL 1993, Austroads 1992) assume that rutting occurs only in the subgrade soil foundation. The thickness of the unbound granular sub-base layer is, thus, determined from the subgrade condition (California Bearing Ratio and/or vertical compressive strain) and design traffic (including traffic during construction). The assumption that rutting with repetitive traffic loading occurs only within the sub-grade is assumed to be assured through the requirement of the unbound granular materials (UGMs) to comply with material specifications. These specifications are based on recipes of quarried crushed rock that have shown in the past to provide adequate performance rather than a test to determine the magnitude of rutting for the design traffic loading.

Granular pavement layers play an important role in the pavement. They are required to provide a working platform for the construction of the asphalt base layers and reduce compressive stresses on the subgrade and tensile stresses in the asphalt base. For thin-surfaced pavements the granular material contributes to the full structural strength of the pavement. It is therefore important that the granular materials have adequate stiffness and do not deform. Material specifications usually ensure this is the case. Permanent strain tests in the Repeated Load Triaxial (RLT) apparatus commonly show a wide range of performances for granular materials even though all comply with the same specification (Thom and Brown, 1989). Accelerated pavement tests show the same results and also report that 30% to 70% of the surface rutting is attributed to the granular layers (Arnold, 2001; Little, 1993; Pidwerbesky, 1996; Korkiala-Tanttu et al, 2003).

Furthermore, recycled aggregates and other locally available but marginal quality materials considered suitable for use in unbound pavement layers can often fail the Highways Agency's material specifications (HMSO 1994) and thus their use is restricted. There is potential for the permanent strain test in the RLT (or similar) apparatus to assess the suitability of these alternative materials for use at various depths within the pavement (e.g. sub-base and lower sub-base). Current pavement design methods and material specifications should include a test on the rutting behaviour under repeated loading. This allows for evaluation of a material's performance, in terms of the amount of rutting expected to occur for the design traffic loading.

1.2 INTRODUCTION TO THE PROJECT

This thesis is the result of three years of research undertaken at the University of Nottingham and Queens University Belfast to complete an EPSRC funded project, *Investigation into aggregate shakedown and its influence on pavement performance*. The laboratory study was conducted at the University of Nottingham while the field trial and finite element modelling was completed at Queens University of Belfast. Results from this three year study were supplemented with research projects completed by the Author for Transit New Zealand. These research projects involved the analysis and reporting of tests conducted at Transit New Zealand's accelerated pavement testing facility (CAPTIF) located in Christchurch, New Zealand. The Transit New Zealand research was undertaken in 3 segments: completed by the Author before, during (enabled by a 3 month break from studies) and immediately after completion of the EPSRC funded project.

The study is primarily an examination of the permanent strain/deformation behaviour of granular materials used in flexible pavements by the use of the Repeated Load Triaxial (RLT) apparatus. Results are categorised into three possible observations of permanent strain behaviour based on the shakedown concept (Dawson and Wellner, 1999) and are used to develop relationships that define stress boundaries between the different behaviour types. A constitutive model is also developed to predict permanent strain from loading stress and number of loads. The shakedown relationship was used in an elasto-plastic finite element model to predict rutting behaviour of a pavement as a whole, while the constitutive model was used in a pavement stress analysis to predict surface rut depth of the pavement.

To validate the methods to predict rutting behaviour and rut depth, pavement test data was utilised. A pavement was constructed in Northern Ireland (work based at Queens University Belfast) with two different aggregates on an access road to a landfill. The pavement was instrumented to record strain and stresses caused by passing lorries. Other pavement test data used were the results from an accelerated pavement test conducted at Transit New Zealand's CAPTIF located in Christchurch, New Zealand. Raw data from stress and strain gauges from the CAPTIF tests was further analysed for this thesis. Unbound granular materials (UGM) and the subgrade soil from the CAPTIF test were shipped to the University of Nottingham for Repeated Load Triaxial testing, as were the Northern Ireland materials.

1.3 OBJECTIVES

The overall aim of this research is,

To present and validate a method to predict rutting in thinly surfaced unbound granular pavements.

The objectives for this thesis are to:

1. Examine and report the repeated load permanent strain behaviour of granular materials with respect to stress in the Repeated Load Triaxial (RLT) apparatus;

2. Determine relationships of shakedown range behaviour with respect to loading stress using RLT results;

3. Analyse results (in terms of surface rutting and strains) of accelerated pavement tests conducted at Transit New Zealand's test track CAPTIF on several pavements with variations in granular material type and pavement depth, with the aim of obtaining results for future validation of models and better understanding where in the pavement deformation occurs;

4. Report on the design, construction, instrumentation and monitoring of a pavement test section constructed in Northern Ireland for the purpose of assessing the effects of two granular material types on surface rutting under 100mm of asphalt cover;

5. Utilise facilities and material models readily available in the commonly used ABAQUS Finite Element Package to incorporate the shakedown behaviour relationships and validate/modify with results from the Northern Ireland and New Zealand trials;

6. Develop a constitutive model for the prediction of permanent strain in granular pavement materials with respect to loading stress from RLT data;

7. Use the constitutive model and the stress distribution from pavement analysis to calculate the rutting of the Northern Ireland and New Zealand trials and compare with measured rut depth.

1.4 SCOPE

The study consisted of four broad areas: laboratory testing (Chapter 3); pavement trials (Chapters 4 and 5); predicting pavement deformation behaviour, in terms of shakedown ranges (Chapter 6); and calculating permanent strain to predict surface rutting of a pavement (Chapters 7). A summary of what is covered in each of the main chapters are detailed as follows:

The literature review (Chapter 2) aims to cover all the background information required for the forthcoming chapters from Repeated Load Triaxial testing, finite element modelling, pavement design, permanent strain modelling and the shakedown concept. Chapter 3 *Laboratory Testing*, covers the materials tested, laboratory tests (predominantly the Repeated Load Triaxial test) and includes limited analysis of the results in terms of the shakedown concept and resilient behaviour.

Results from three New Zealand accelerated pavement tests having in excess of 1 million wheel passes are reported in Chapter 4. Chapter 5 reports the pavement trial in Northern Ireland from design, construction monitoring and analysis of the results.

Chapter 6 uses the ABAQUS finite element package to incorporate the shakedown range stress boundaries derived from the laboratory study to predict shakedown range behaviour of the pavement trials documented in Chapters 4 and 5. Results are compared to actual shakedown range behaviour determined from the pavement trials for validation of the shakedown range prediction method.

Chapter 7 reports on detailed analysis of the RLT permanent strain data in Chapter 3 to develop a model to predict permanent strain from stress level and number of load cycles. The model developed is used to compute permanent strain from computed stresses within a pavement which is added together along the centre of the load to predict rut depth. Rutting is calculated for each pavement trial in this way and compared to the actual measured results.

Further analysis, using the methods to determine rutting behaviour (Chapter 6) and rut depth prediction are utilised for a range of applications are included in Chapter 8 *Discussion*. The applications included: determining the optimum asphalt cover thickness; assessment of standard UK Highway designs; and a methodology to assess alternative materials.

CHAPTER 2 LITERATURE REVIEW

2.1 INTRODUCTION

This literature review aims to cover all the background information required for the forthcoming Chapters from Repeated Load Triaxial testing, finite element modelling, pavement design and permanent strain modelling. The emphasis is on granular materials used in flexible pavements in terms of their permanent strain/rutting behaviour which is the prime focus of this research. Some of this literature review provides reference material for such items as stress invariants *p* and *q* (Section 2.4.3) that will be utilised throughout this thesis as an efficient means for characterising a stress state consisting of both axial and radial stresses.

Topics covered begin with current methods of pavement design and review of material specifications in terms of their inadequacies for consideration of the permanent strain/rutting behaviour of granular pavement layers that has been observed to occur in accelerated pavement tests. The Repeated Load Triaxial apparatus is introduced as a means of assessing the permanent strain behaviour of granular materials. Factors that affect the permanent strain and briefly the resilient strain behaviour of granular materials are discussed followed by an introduction to theoretical models proposed by researchers for permanent strain behaviour. This is followed by a review of finite element modelling of pavements for the analysis of pavements.

Finally, the concept of shakedown is introduced to cater for the many different permanent strain behaviours that are observed and predicted by the many permanent strain model forms. The shakedown concept is taken further in this thesis to characterise permanent strain behaviour and utilised in finite element modelling of a pavement to predict the permanent strain behaviour of the pavement as a whole.

2.2 PAVEMENT DESIGN

2.2.1 Thickness Design Charts

Pavement design involves the selection of materials and determination of layer thicknesses to ensure the design life is met. Material quality is ensured through compliance with specifications (Section 2.3). The thickness of the various pavement layers is typically determined using design charts from pavement design manuals (HMSO 1994, TRL 1993, Austroads 1992). Figure 2.1 (Austroads, 1992) shows the chart used to design thin surfaced granular pavements in New Zealand and Australia.

Pavement design charts typically rely on two inputs: the subgrade strength in terms of CBR (California Bearing Ratio); and design traffic loading in terms of ESAs (Equivalent Standard Axles). The California Bearing Ratio (AASHTO 1978) is one of the most widely known parameters for characterising the bearing capacity of soils and unbound granular materials (Sweere, 1990). Equivalent Standard Axles (ESAs) (Equation 2.1) are used in design as a means of combining the many different axle types and loads into one axle type and load.

$$ESA = \left[\frac{Single\_Axle\_load}{80kN}\right]^4$$

Equation 2.1

where,
ESA = Equivalent Standard Axle (80kN dual tyred single axle); and
Single_Axle_load = Actual axle load on a single axle (kN).

The origins of Equation 2.1 stem from the AASTHO road test (1962) and is often referred to as the fourth power law. AASHO (1962) calculated a damage law exponent of 4 based on a comparison of the number of axle passes to reach the end of the pavement life between the reference axle and the axle load in question. The pavement end of life in the AASHO (1962) tests was defined by reaching a certain pavement serviceability index value which considers factors such as rut depth, roughness and cracking. This fourth power relationship has been investigated by other researchers throughout the world. Power values between 1 and 8 were found for different pavement structures and failure mechanisms (Cebon, 1999; Kinder and Lay, 1988, Pidwerbesky, 1996, Arnold et al, 2004a and b).

The pavement thickness design charts were produced from experience of observed pavement performance and, more recently, from many linear elastic analyses of pavements using the principles of mechanistic pavement design as described in Section 2.2.2.

2.2.2 Mechanistic Pavement Design

Mechanistic pavement design involves using the theory of linear elastic analysis to calculate strains at critical locations in the pavement (Figure 2.2). In linear elastic analysis, each pavement layer is characterised by a value of resilient modulus (stress over associated elastic strain) and Poisson's ratio (ratio of radial strain to axial strain in direction of loading). These resilient strains at critical locations are used in empirical relationships known as strain criterians to determine the life of the pavement in terms of numbers of ESAs (Equation 2.1). There are strain criteria that determine the maximum allowable tensile stains in the base of bound layers and the maximum allowable vertical compressive strain in the subgrade. It is assumed cracking is a result of tensile strains at the base of bound layers while wheel track rutting is a result of vertical strains on the top of the subgrade. However, a major criticism of the subgrade strain criterion is the neglect of the permanent deformation of the pavement structure layers that contribute up to 70% of the surface rutting (Arnold et al, 2001; Little, 1993; Pidwerbesky, 1996; Korkiala-Tanttu et al, 2003). Cracking is not always a result of tensile strains in the base of bound layers but is often generated from the top, propaga ing downwards. After many years of involvement with pavement monitoring, the UK Transport Research Laboratory have only extremely rarely found any evidence for bottom-up cracking on the major highways in the UK, whereas innumerable examples of top-down cracking exist (Thom et al., 2002).

Top down cracking is a result of surface heaving combined with the hardening/embrittlement of the asphalt surface due to ageing/oxidisation caused by the environment (e.g. ultra violet radiation). Furthermore, the Transport Research Laboratory noted that asphaltic materials have continued to gain in stiffness throughout their lives, reducing considerably the strains caused by traffic loading (Thom et al., 2002), thus reducing the amount of rutting that could occur in the pavement layers.

Linear elastic analysis of pavements is a gross-approximation of real behaviour. In real pavements, loading is transient and not uniform (de Beer et al, 2002), the soil and granular layers (the pavement foundation) have markedly non-linear stress-strain relationships (Hicks and Monosmith, 1971) and are anisotropic (Karasahin & Dawson, 2000; Tutumluer and Seyhan, 2000), and the bituminous layer has properties which are sensitive to loading rate and to temperature (Brown, 1996). Another limitation of linear elastic models is stress states that exceed the yield strength of the unbound granular material often due to high tensile stresses being calculated. In linear elastic analysis the shear strength of the material is not considered.

2.3 MATERIAL SPECIFICATIONS (Aggregates)

In pavement design (Section 2.2) it is assumed that rutting will not occur within any of the pavement layers above the subgrade. Further, the pavement layers do not deteriorate or crack over the design life. Road controlling authorities ensure pavement material longevity through compliance with their relevant specifications. There are also construction specifications that detail methods of correct placement of materials in the pavement (e.g. compaction) to ensure their long term performance.

The current Specification for Highway Works (MCHW1, 2004) regulates the acceptance of road foundation materials by relatively simple index tests, for instance: the grading, plasticity of fines, CBR, number of crushed faces, weathering and flakiness. These tests are classed as characterisation tests as they do not directly measure the repeated load performance of aggregates resistance to deformation as do performance tests such as Repeated Load Triaxial tests (Section 2.5.1). However, some weathering tests in recipe based specifications do give an indication of resistance to deterioration over the design life and could be classed as a type of performance test.

2.4 STRESSES and STRAINS

Wheel loads on pavements result in a distribution and reduction of stresses throughout the pavement. As the vehicle passes over the pavement, the stress level in the pavement changes from a small to a higher value (Figure 2.3). This change in stress results in movement wi thin the pavement known as strains. Strains can also be divided into elastic (resilient) strains which are those that are recoverable and those that are non-recoverable known as permanent or plastic strains. Stresses act in 3-dimensions and all these stresses have an effect on how the material behaves. This section describes the insitu stresses caused by wheel loads and how these relate to insitu strain state that act in 3-dimensions.

2.4.1 Stresses and Strains in Flexible Pavement

The stresses acting on a given element in a material can be defined by its normal and shear stress components. It can be proven that for any general state of stress through any point in a body, three mutually perpendicular planes exist on which no shear stresses act. The resulting stresses on these planes are thus represented by a set of three normal stresses, called principal stresses σ_1, σ_2 and σ_3 (Figure 2.4(a) and Figure 2.5).

Stresses on a cubical element within a pavement structure due to traffic loading and unloading are shown in Figure 2.3 and Figure 2.4. Without traffic loading, a confining stress due to the overburden and previous stress history is applied to the element. As a wheel load approaches the element, the element is subjected to a simultaneous build-up in both the major principal and minor principal stresses.

These stresses also rotate about the centre element as shown in Figure 2.3 and Figure 2.4. This is referred to as the rotation of principal stresses.

If the element is not rotated (i.e. x, y, z reference system does not change) then, as the load approaches, the vertical and horizontal stresses increase. The shear stresses increase as the load approaches a point where they start decreasing until the load is directly above the particular element. At this point there is no shear stress on vertical and horizontal planes. As the load moves away a complete reversal of shear stress occurs (Figure 2.4(b)). This reversal of shear stresses is commonly referred to as principal stress rotation.

2.4.2 Repeated Load Behaviour

As a vehicle passes over the cubic element in a pavement a stress pulse is applied to it. These stress pulses are applied repeatedly in large numbers for the duration of the life of the pavement. The magnitude of these stress pulses will vary due to the wide range of vehicle types. However, for illustrative purposes it is assumed that each stress pulse is of the same magnitude. There is also an overburden pressure felt by the cylindrical element.

Figure 2.6 shows that the cylindrical element will deform in both the axial and radial direction with each stress pulse. The elastic deformation recovers after each load cycle. However, there is a small permanent deformation applied to the element during each load cycle. The amount and rate of permanent deformation accumulation is dependent on material properties, the stress level, and loading history. The accumulating (sometimes diminishing) non-recoverable deformation from each of the stress applications is the permanent deformation (Thom, 1988).

The deformations are also illustrated by means of the stress strain curve (Figure 2.7). Figure 2.7 shows the hysteresis loop behaviour experienced by the element during each load cycle as measured in the Repeated Load Triaxial apparatus. It is assumed in this plot that the permanent deformation rate reduces with the number of load cycles that is often the case for low stress levels. As described in Section

2.11.2 this behaviour is the case for the first few thousand cycles but depending on stress level permanent deformation rate may either: decrease; remain constant; or increase and quickly fail with increasing load cycles.

2.4.3 Stress Invariants (p and q)

A 3-dimensional stress system can be interpreted by considering the component principal stresses (Figure 2.5) divided into those stresses that tend to cause volume change (pressure) and those that cause shear distortion (shear stress).

The pressure which causes volume change is the mean principal stress and is defined as:

$$p = \frac{1}{3}(\sigma_1 + \sigma_2 + \sigma_3) \qquad \text{Equation 2.2}$$

where,
p = mean normal stress; and
σ_1, σ_2, σ_3 = principal stress components (Figure 2.5).

The octahedral shear stress is a measure of the distortional (shear) stress on the material, and is defined as (Gillett, 2003):

$$\tau_{oct} = \frac{1}{3}\sqrt{(\sigma_1 - \sigma_2)^2 + (\sigma_2 - \sigma_3)^2 + (\sigma_3 - \sigma_1)^2} \qquad \text{Equation 2.3}$$

where,
τ_{oct} = octahedral shear stress.

These two parameters are called stress invariants since they are independent of direction. Assuming axial symmetry in a pavement under a wheel load, the horizontal stresses are taken as equal. Therefore, the mean normal and shear stress invariants can be written as follows:

$$p = \frac{1}{3}(\sigma_1 + 2\sigma_3)$$ Equation 2.4

$$\tau_{oct} = \frac{\sqrt{2}}{3}(\sigma_1 - \sigma_3)$$ Equation 2.5

It is common, particularly in triaxial testing, to describe the shear stress invariant as deviator stress or principal stress difference, *q*:

$$q = \tau_{oct}\frac{3}{\sqrt{2}}$$ Equation 2.6, or

$$q = \sigma_1 - \sigma_3$$ Equation 2.7

where,
q = deviator stress or principal stress difference.

Trends in material performance will be the same with changes in deviator stress (*q*) and octahedral shear stress (τ_{oct}) as they are effectively interchangeable variables. However, the preference is to use deviator stress, *q* as representative of the shear stress invariant.

In keeping with standard soil mechanics practice, the effective principal stresses ($\sigma' = \sigma - u$) are used for determination of deviator stress, *q* and mean normal effective stress, *p'*. From Equation 2.7 it can be seen that the deviator stress is independent of pore water pressure as the same result is obtained if σ is replaced by σ' while the effective mean normal stress, *p'*, is must be calculated as in Equation 2.4 but with the pore water pressure subtracted.

2.4.4 Strain Invariants

Strain is defined as the deformation per unit of original length, and is dimensionless. Strains may also be translated into their appropriate invariants using the same approach that was used for stresses. The mean normal stress tends to cause volume change, which has a corresponding strain invariant called volumetric strain and is defined as:

$$\varepsilon_v = \varepsilon_1 + \varepsilon_2 + \varepsilon_3 \qquad \text{Equation 2.8}$$

where,

ε_v = volumetric strain; and

ε_1, ε_2, ε_3 = strains in direction of principal stress components (Figure 2.5).

The octahedral shear stress defined by Equation 2.3 causes the following shear strain similarly defined:

$$\varepsilon_s = \frac{2}{3}\sqrt{(\varepsilon_1 - \varepsilon_2)^2 + (\varepsilon_2 - \varepsilon_3)^2 + (\varepsilon_3 - \varepsilon_1)^2} \qquad \text{Equation 2.9}$$

where,

ε_s = shear strain.

Assuming symmetry under the wheel load the horizontal stresses and thus strains are equal. Therefore, the following strain invariants are derived:

$$\varepsilon_v = \varepsilon_1 + 2\varepsilon_3 \qquad \text{Equation 2.10}$$

$$\varepsilon_s = \frac{2}{3}(\varepsilon_1 - \varepsilon_3) \qquad \text{Equation 2.11}$$

In an anisotropic material change in mean normal stress, *p* also causes shear strain (ε_s) as well as volumetric strain (ε_v). Similarly, change in deviatoric stress, *q* causes volumetric and shear strains. Dilative or contractive materials also experience volumetric strains when there is a change in deviatoric stress.

2.4.5 Stress Paths and p-q Diagrams

A method to depict successive stress states that exist in material from unloaded to loaded is to plot a series of stress points (Boyce, 1976). These stress points (loaded and unloaded) have coordinates, namely the stress invariants: mean normal stress (p, Equation 2.4); and deviator stress (q, Equation 2.7). Plotting these stress points (loaded and unloaded) results in a stress path in p-q stress space. Usually the start (unloaded or minimum) and end (loaded or maximum) points are defined on the stress path. These are illustrated in Figure 2.8. Stress path characteristics including direction, length, start and end points all have a direct influence on resilient (elastic) and permanent strains (plastic). Thus a stress path is an important parameter in describing the nature of loading on a material. Testing stresses in a Repeated Load Triaxial apparatus are best defined by stress paths. However, often only the maximum stress invariants are reported.

2.4.6 Residual Stresses

Compaction of the granular pavement layers during construction results in the application of large vertical stresses. These vertical stresses are reported to cause lateral stresses to develop that become locked into the granular bases and subgrades (Sowers, et al., 1957; Uzan, 1985; Selig, 1987; Duncan and Seed, 1986).

It was shown by Selig (1987) that in a granular layer, large plastic lateral strain develops in the bottom of the layer during the first cycle of loading. Upon subsequent loading cycles, however, the response rapidly approaches an elastic condition. The lateral stress in the bottom of the granular layer, in both the loaded and unloaded condition, gradually increases up to about 50 load cycles. After 50 load cycles the lateral stresses in both the loaded and unloaded states were found to be in the order of 20 times greater than before the first load cycle. However, the horizontal stress in the unloaded condition was larger than the stress existing when fully loaded which was not the case when loading first started. This important finding suggests that tensile stresses at the base of the granular occur in the first few cycles but are quickly cancelled out by residual lateral stresses developing. The result is a net horizontal compressive stress state at the base of the granular layer.

Selig (1987) concluded that the residual lateral stress is the most important factor limiting permanent deformation of the bottom of the granular base. Further, the work of both Selig (1987) and Uzan (1985) indicates the need to properly consider the residual stresses that exist in a granular base in the analyses used in mechanistic based pavement design procedures (Section 2.2.2). Also, as described in the finite element modelling aspect of this project, an assumption of residual horizontal stresses was required.

Almeida, J. R. de. (1993) recognises that a pavement in its original state has residual lateral stresses which are under-estimated from the coefficient of earth pressure at rest, K_a (Equation 2.12). Almeida states that the residual stresses are likely to be of substantial magnitude which will increase the elastic stiffness of the material and change the stress distribution and recommends that a realistic estimate of horizontal residual stresses be made. However, Almeida recognises the actual value is not known as residual stresses are difficult to measure and predictive models for the residual stresses requires the stress history of the pavement during construction.

Rankine's theory of earth pressure (cited in Craig 1992) explained that a certain lateral horizontal stress must exist to ensure stress states do not exceed the Mohr-Coulomb failure envelope. These are defined by Equations 2.12 and 2.13 representing the active and passive lateral earth pressure states resepectively. The active state represents the minimum horizontal stress conditions that will be experienced by a vertical wall moving away from the surrounding soil, while the passive case represents the maximum lateral horizontal stress when the vertical wall moves towards the soil. Rankine showed that the two values of horizontal lateral stress (σ_{hr}) can be defined by Equations 2.12 and 2.13:

$$\sigma_{3a} = \sigma_1 K_a - 2cK_a \qquad \text{Equation 2.12}$$

$$K_a = \left(\frac{1 - \sin \phi}{1 + \sin \phi} \right)$$ Equation 2.13

$$\sigma_{3p} = \sigma_1 K_p - 2cK_p$$ Equation 2.14

$$K_p = \left(\frac{1 + \sin \phi}{1 - \sin \phi} \right)$$ Equation 2.15

where,

σ_{3a} = Horizontal lateral stress in the active state;

K_a = Coefficient of active earth pressure;

σ_{3p} = Horizontal lateral stress in the passive state;

K_p = Coefficient of passive earth pressure;

σ_1 = Overburden stress or major principal stress;

c = Mohr-Coulomb cohesion; and

ϕ = Mohr-Coulomb friction angle.

If the lateral strain in the soil is zero the corresponding lateral pressure is called earth pressure at rest. Since, the at rest condition does not involve failure of the soil, the Mohr-Coulomb criteria cannot be used to determine the pressure at rest. Triaxial tests are required in which the axial stress and all-round pressure are increased simultaneously such that the lateral strain in the specimen is maintained. For normally consolidated soils the lateral earth pressure at rest can be approximated by Equation 2.16:

$$\sigma_{3r} = \sigma_1^{'} K_0$$ Equation 2.16

$$K_0 = 1 - \sin \phi^{'}$$ Equation 2.17

where,

σ_{3r} = Horizontal lateral stress at rest;

σ'_1 = Overburden effective stress;

K_0 = Coefficient of earth pressure at rest (Equation 2.17);

ϕ' = Morh-Coulomb friction angle from effective stress.

The coefficient of lateral earth pressure at rest is considered an appropriate value to use for estimating the amount of residual stresses present in a granular material located in a pavement. For granular pavement materials the cohesion may be nil and the friction angle approximately 50 degrees. This results in the coefficient of lateral earth pressure at rest having a value of 0.23 (Equation 2.17). Granular materials are located relatively near the surface, say 200mm depth, and based on a density of 2400 kg/m^3 the overburden stress would be 5 kPa. Thus, the horizontal residual stress at rest evaluates as approximately 1.2 kPa. However, adding, say, 550kPa vertical stress from compaction and initial traffic loading the horizontal residual stress at rest is approximately 128 kPa. The high value of 128 kPa assumes that the materials do not relax and release some locked in residual stress once the load is removed. Therefore, a value of say 30kPa, maybe a more conservative estimate of the horizontal residual stresses.

Brown (1996) considered that ratios of horizontal to vertical stress as high as 6 are quite possible in practice due to the compaction of granular layers. Although some results from box tests on railway ballast reported by Stewart et al. (1985) indicated ratios up to as high as 11. As abov,e the overburden pressure is 5 kPa and therefore if the ratio of horizontal to vertical stress is taken as a value of 6 then again the horizontal stresses are estimated at 30 kPa.

2.4.7 Effect of Water/Suction

The cohesion, stiffness and resistance to deformation of the crushed stone material increases with decreases in moisture content (Theyse et al, 1999; Basma and Al-Suleiman, 1991). This is because a large component of the cohesion of the crushed stone is an apparent cohesion caused by soil suction. In studies of partially saturated soils (Croney and Coleman, 1952) suction is referred to as the matrix suction (s, Equation 2.18).

$$s = u_a - u_w \qquad \text{Equation 2.18}$$

where,
s = matrix sucion;
u_a = pore air pressure; and
u_w = pore water pressure.

Croney (1952) assumed $u_a = 0$ and defined suction as $-u_w$ under zero external stress. The effect of applied total stress p (Equation 2.2) was taken into account by use of a compressibility coefficient ($\propto$) as in Equation 2.19.

$$u = s + \propto p \qquad \text{Equation 2.19}$$

where,
s = soil suction as a negative quantity;
u = pore water pressure; and
p = total mean normal stress (Equation 2.2).

Effective stress (p') from Equation 2.20 is the total mean normal stress minus the pore water pressure (u).

$$p' = p - u \qquad \text{Equation 2.20}$$

It follows from Equation 2.19 that as suction is increased (i.e. a larger negative value) the pore water pressure reduces and thus the effective stress increases (Equation 2.20). Therefore, suction which is present in all partially saturated soils and granular materials has a significant effect on the effective stress. It is the effective stress which governs the effective level of confining stress or hydrostatic pressure, which, when increased, has the effect of increasing a material's strength. However, suction is not usually measured in the laboratory nor is it known in the field and therefore total stresses are normally used in studies of the repeated load behaviour of materials (Brown, 1996).

2.5 PERFORMANCE TESTS

Figure 2.3 illustrates the general stress regime experienced by an element of material in or below a pavement structure as a result of a moving wheel load within the plane of the wheel track, that is, the longitudinal plane. There are pulses of vertical and horizontal stress accompanied by a double pulse of shear stress with a sign reversal on the vertical and horizontal planes. Figure 2.4 shows the associated pattern of principal stresses illustrating the rotation of principal planes which takes place. Performance tests in the laboratory are those which attempt to reproduce the field situation. Clearly, for pavements this would demand complex test facilities. The Repeated Load Triaxial (RLT) (Shaw, 1980), hollow cylinder (Chan 1990) and k-mould (Semmelink et al, 1997) apparatuses can in various degrees simulate pavement loading on soils and granular materials.

Repeated Load Triaxial tests typically involve a repeated load to simulate many vehicle passes. Tests in the laboratory are usually element based where one set of stress conditions can only be tested at any one time. Therefore, to cover the full spectra of stresses that occur within the pavement many performance tests at different stress conditions are required. Wheel tracking and full scale accelerated pavement tests are also considered performance tests, but only triaxial type tests are discussed in this section.

2.5.1 Repeated Load Triaxial (RLT) Apparatus

The RLT apparatus tests cylindrical samples of soils or granular materials. Figure 2.9 illustrates a typical Repeated Load Triaxial apparatus test set up. For RLT tests the axial load supply is cycled for as many cycles as programmed by the user. The axial load type is usually programmed as a sinusoidal vertical pulse with a short rest period. Although possible for some RLT apparatuses, in this study the cell pressure was not cycled simultaneously with vertical load, but held constant. Two types of repeated load tests are usually conducted, being either a resilient or permanent deformation test. The most recent standard currently used for triaxial testing is the *prEN 13286-7 (2004) Unbound and hydraulically bound* *mixtures – Test methods – Part 7: Cyclic load triaxial test for unbound mixtures*. However, as triaxial testing is a research tool with the aim to simulate as closely as possible the range of conditions that will be experienced in a pavement it is common for a researcher to vary from this standard to assess material characteristics at other loading and environmental conditions expected in-service.

The resilient test determines the resilient (or elastic) modulus and Poisson's ratio (only possible if radial strains are measured in the test) for a full range of vertical and horizontal (cell pressure) combinations.

In a RLT test the principal stress in the x and y direction is the cell pressure and in the z direction the principal stress is the cell pressure plus the applied axial stress (as cell pressure acts all over the specimen including the top). Figure 2.10 shows the stresses acting on a RLT specimen during a test. The resilient test provides the elastic parameters needed for mechanistic pavement design (Section 2.2.2).

During a RLT test vertical stress, cell pressure, radial and vertical displacement on the specimen are recorded. The difference between the maximum and minimum displacement divided by the length over which this occurs gives the strain. Two types of strain are recorded: elastic/resilient (Equation 2.21); and permanent/plastic (Equation 2.22).

Resilient or elastic strain (ε) is defined by:

$$\varepsilon = \frac{\Delta L_{(N)}}{L_0\left(1-\varepsilon_{p(N-1)}\right)} \qquad \text{Equation 2.21}$$

Permanent strain (ε_p) is defined as:

$$\varepsilon_p = \frac{\Delta L_{(Total)}}{L_0} \qquad \text{Equation 2.22}$$

where,

L_0 = original specimen length (height or diameter);

$\Delta L_{(Total)}$= total plastic change in specimen length or difference in length from original length;

$\Delta L_{(N)}$ = resilient/elastic change in specimen length for N cycles; and

N = number of cycles.

Resilient modulus is then calculated by dividing the applied vertical deviator stress by the resilient strain for a constant cell pressure test (Equation 2.23). The Poisson's ratio is defined by Equation 2.24. Noting the minimum axial strain after each load cycle gives the permanent axial strain result for a test in which σ_d changes.

Resilient Modulus:

$$M_r = \frac{\sigma_d}{\varepsilon_a} \qquad \text{Equation 2.23}$$

Poisson's ratio:

$$\upsilon = \frac{-\varepsilon_r}{\varepsilon_a} \qquad \text{Equation 2.24}$$

where,

σ_d = maximum cyclic deviator axial stress

ε_r = radial strain; and

ε_a = axial strain.

The resilient modulus of a material according to 3-D Hooke's law equation is given by:

$$M_r = \frac{(\sigma_{1d} - \sigma_{3d})(\sigma_{1d} + 2\sigma_{3d})}{\varepsilon_{1r}(\sigma_{1d} + \sigma_{3d}) - 2\varepsilon_{3r}\sigma_{3d}} \qquad \text{Equation 2.25}$$

where,

M_r = calculated equivalent E-modulus (MPa);

ε_{1r} = measured axial resilient strain (μm/m);

ε_{3r} = measured radial resilient strain (μm/m);

σ_{1d} = difference in maximum and minimum principal axial stress (kPa); and

σ_{3d} = difference in maximum and minimum principal radial stress (kPa).

This assumes the material behaves linear-elastically for any individual stress stage.

For unbound granular materials it is usual to report resilient modulus versus bulk stress as the material's stiffness is highly stress-dependent. Established research (Hicks and Monismith, 1971) suggests a general relationship between these parameters as defined by Equation 2.27 (Section 2.7).

For a permanent deformation test at least 50,000 loading cycles are applied at one set of vertical and horizontal (cell pressure) combination. The amount of permanent strain versus load cycles is plotted. Currently, there is no standard method to interpret the result of the permanent strain test. Often a judgement is made as to whether the result is acceptable or not for the test stress level.

A major step towards implementation of the Repeated Load Triaxial test has been the standardisation of the test by various organisations worldwide such as CEN (2004), Australia Standards (1995) and AASHTO (1994). These test methods give a description of equipment, specimen preparation procedures and testing procedures.

The limitations of the RLT test are that only two of the maximum of six stress components are varied independently for complete general conditions (Hyde, 1974; Pappin, 1979; Chan, 1990). Only the vertical and horizontal stresses can be applied and this simulates the situation when the load is directly above the element. Principal stress rotation (Section 2.4.1) that occurs in a pavement from a passing wheel load cannot be duplicated in the Repeated Load Triaxial apparatus and is therefore a limitation of its ability to fully simulate vehicle loading.

2.5.2 K-mould Apparatus

The K-mould apparatus is the same as the RLT apparatus described in Section 2.5.1 except the confinement is achieved by elastic springs. Springs push cell walls against the cylindrical specimen with the effect that the lateral restraint increases as the granular specimen is being loaded vertically. Material parameters such as stress dependent elastic modulus and Poisson's ratio, cohesion and friction angle are determined from a single test specimen (Semmelink and de Beer, 1995). Springs containing the specimen give a controlled elastic modulus (or spring constant) in the horizontal or radial direction, E_3 and confining stress (σ_3) is determined by multiplying the elastic modulus by radial strain (ε_3):

$$\sigma_3 = - E_3\, \varepsilon_3 \qquad \text{Equation 2.26}$$

2.5.3 Hollow Cylinder Apparatus

The Hollow Cylinder Apparatus (HCA) is similar in principle to the Repeated Load Triaxial apparatus accept this device rotates principal stresses and as such better simulates actual stresses in the pavement under vehicle loading. Confining stress and an axial deviator stress can be applied in the same way as the RLT test (Section 2.5.1). However, it is also possible to apply a torque and vary the pressure in the centre of the cylinder from that outside the cylinder (Thom, 1988; Chan, 1990). Application of a torque generates shear stresses on the horizontal and vertical planes in the wall of the cylinder, whereas variation of internal pressure imposes variation in circumferential stress (Figure 2.11). While this improves the reproduction of the pavement stress state, it makes for a much more complex and expensive test. Also, as the wall thickness of the cylinder is 28mm this limits the maximum particle size to 4mm. Thus, tests cannot be carried out on most pavement materials at their normal gradings. However, Thom and Dawson

(1996) found that particle size did affect the magnitude of the strain but the form of the behaviour was similar.

2.6 FACTORS AFFECTING PERMANENT DEFORMATION OF UGMs

There are many factors that affect deformation behaviour/permanent strain of unbound granular materials (UGMs). Stress has the most significant effect on permanent strain, followed by number of load applications, insitu material factors (i.e. compacted density and moisture content) and source material properties (e.g. grading, fines content and aggregate type).

2.6.1 Effect of Stress

Morgan (1966) found in Repeated Load Triaxial (RLT) tests at a constant confining stress, that an increase in the accumulation of axial permanent strain was directly related to an increase in deviator stress (cyclic axial load). Conversely, it was found for a constant deviator stress that the accumulation of permanent strain increased with a reduction in confining stress. Clearly both confining stress and deviator stress has an effect on the accumulation of permanent strain. Many researchers have related the magnitude of permanent strain found in RLT tests to some kind of stress ratio of deviator stress (q) to mean normal stress (p) or confining stress (Barksdale, 1972; Lashine et al, 1971; Pappin, 1979; Paute et al., 1996; Lekarp and Dawson, 1998). Lekarp and Dawson (1998) also showed that an increase in stress path length in p-q space (Figure 2.8) increased the magnitude of permanent strain.

Another approach used by researchers is to use relationships of permanent strain to stress in terms of proximity to the static shear failure line (Maree, 1978 cited in Theyse, 2002; Barksdale, 1972; Raymond and Williams 1978; Thom 1988). It is assumed that stress states close to the shear failure line will result in higher magnitudes of permanent strain and stress states exceeding the failure line are not possible or will result in early failure of the material.

2.6.2 Effect of Variable and Constant Confining Pressure

The RLT test conditions in terms of variable confining pressure (VCP) or constant confining pressure (CCP) also affect the magnitude of permanent strain. Variable confining pressure best matches conditions in the field but is more difficult to test in the laboratory. Therefore, CCP conditions are commonly used in the RLT apparatus as done by Sweere (1990). This was justified by Sweere who reported that there is a correlation between testing at VCP and CCP. Apparently the result from testing at CCP is the same as testing at VCP, provided the CCP is half the maximum confining pressure in the VCP test, which is the average value.

2.6.3 Effect of Principal Stress Rotation

Chan (1990) observed the effect of shear stress reversal on permanent strain in hollow cylinder tests on crushed limestone both with and without the application of shear stress. The tests with shear stress reversal showed much higher permanent strain than tests with no shear stress. Higher permanent strains were also obtained from bi-directional compared with uni-directional shear reversal. Uni-directional shear reversal simulates the stress condition under a wheel load moving in one direction. It follows that bi-directional is the case where the wheel load moves forward and backwards over the same position. It was also found that the higher the ratio of shear stress to normal stress the higher the permanent strains.

Other tests by Thom and Dawson (1996) with the hollow cylinder apparatus found similar results to Chan (1990). Figure 2.12 (Thom and Dawson, 1996) shows that the permanent strain increased significantly when stress cycling was accompanied by principal stress rotation. Taking the points on Figure 2.12 it is clear that there is a significant increase in the rate of permanent strain development due to the effect of introducing principal stress rotation.

2.6.4 Effect of Number of Load Applications

For increasing load cycles (*N*) the accumulative permanent strain will always increase. How the cumulative permanent strain increases (i.e. deformation behaviour) varies. Paute et al (1996) found that the rate of increase in permanent strain with increasing load cycles decreases constantly to such an extent to define a limit value for the accumulation of permanent strain. On the other hand some researchers (Morgan, 1966; Barksdale, 1972; Sweere, 1990) have reported continuously increasing permanent strain under repeated loading. Further, Maree (1978, cited in Theyse, 2002) also found that for high stress states permanent strain increased at a constant rate but between 5,000 and 10,000 load cycles an exponential increase in permanent strain occurred resulting in failure shortly after.

According to Lekarp (1997) and Lekarp and Dawson (1998), the achievement of stable behaviour when permanent strain rate decreases with increasing load cycles can only occur when the applied stresses are low. Higher stresses would result in a continuous linear increase of permanent strain. Work by Kolisoja (1998) involving very large numbers of cycles, reveals that the development of permanent deformation may not be expressible as a simple function. This is because material that appears to be approaching a stable condition may then become unstable under further loading.

Three distinct types of behaviour of the development of permanent strain after the first 10,000 load cycles are observed from the range of literature (although researchers may have only observed one type of behaviour depending on the stress levels used):

A. decreasing permanent strain rate with increasing load cycles to a possible limiting permanent strain value;
B. linear increase in permanent strain with increasing load cycles; and

C. exponential increase in permanent strain and failure with increasing load cycles.

Given the range of equations (Table 2.1 after Lekarp, 1997), developed to predict permanent strain it seems that researchers probably only observed either A or B type of behaviour described above.

2.6.5 Effect of Moisture Content

Effect of moisture content can be related to its effect on soil suction and thus effective stress as defined in Section 2.4.7. Excess water in aggregates increases the pore water pressure through a reduction in the amount of suction (i.e. suction moving closer to zero) which in turn decreases the effective stress (Equation 2.20). This will reduce the shear strength and result in local permanent deformation transpiring as ruts in the surface. If the aggregate becomes saturated then suction that pulls particles/stones together reduces to zero and can become negative which results in de-compaction and the development of shallow shear and potholes. If the subgrade soil is an expansive clay and water is allowed to enter the foundation, the deterioration of the pavement may be exacerbated by damaging subgrade volume changes and differential heaving. Other signs of damage due to water infiltration are the pumping of water and fines through cracks and distress associated with frost heave.

High pore water pressures that reduce the amount of suction will occur in granular materials in the laboratory and field due to a combination of a high degree of saturation, low permeability and poor drainage. These conditions result in lowering the effective stress and consequently reducing stiffness and resistance to deformation (Haynes and Yoder, 1963; Barksdale, 1972; Maree et al., 1982; Thom and Brown, 1987; Dawson et al. 1996). Haynes and Yoder (1963) found the total permanent strain rose by more than 100% as the degree of saturation increased from 60 to 80%. A more modest increase of 68% in permanent strain was observed by Barksdale (1972) for tests on soaked specimens compared to those partially saturated. Thom and Brown (1987) reported a small increase in water content can trigger a dramatic increase in permanent strain. Analysing RLT permanent strain tests from Dodds et al. (1999) found the aggregate contaminated with 10% clay fines did not survive for 100,000 loading cycles when saturated, while the aggregate free from clay fines did survive.

2.6.6 Effect of Stress History

Accelerated pavement tests (Arnold et al., 2003) showed that if the load increased an initial sharp increase in surface deformation occurred despite the fact that prior to this increase the rate of permanent strain was minimal and either constant or decreasing with increasing load cycles. After the initial sharp rise in surface deformation with the larger wheel load the permanent strain rate stabilises to a constant or decreasing value. Because of stress history effects it is usually recommended that a new sample be used for RLT permanent strain tests at different stress levels. However, this is not always practical as a large number of tests are required to cover the full spectra of stress states that may occur within the pavement.

2.6.7 Effect of Density

Results for RLT permanent strain tests by Dodds et al. (1999) showed in all cases larger permanent strains for the samples compacted to a low density of 90% of MDD (Maximum Dry Density with vibrating hammer, BS 1377-4: 1990) compared with samples compacted at 95% of MDD. Other researchers report that the resistance to permanent deformation under repetitive loading is improved as a result of increased density (Holubec, 1969; Barksdale, 1972, 1991; Allen, 1973; Marek, 1977; Thom and Brown, 1988). Barksdale (1972) observed an average of 185% more permanent axial strain when the material was compacted at 95% instead of 100% of the maximum compactive density obtained from the drop hammer test.

2.6.8 Effect of Grading, Fines Content, and Aggregate Type

Thom and Brown (1988) conducted RLT permanent strain tests on crushed dolomitic limestone at a range of gradings and compaction level. They found when un-compacted, the specimens with uniform grading resulted in the least permanent strain.

The effect of increasing fines content generally increases the magnitude of deformation in RLT permanent strain tests (Barksdale, 1972, 1991; Thom and Brown, 1988). Dodds et al. 1999 confirm this result as the material with 10% fines added showed the highest deformations. Pore water pressure development was observed by Dodds et al, 1999 to be higher for materials with higher fines content. Pore water pressure reduces the effective stress and thus reduces the beneficial level of confinement.

Allen (1973) recognised that angular materials, such as crushed stone, undergo smaller permanent deformations compared to materials such as gravel with rounded particles. This is because angular materials develop better particle interlock compared to rounded materials and thus have higher shear strength.

2.7 FACTORS AFFECTING RESILIENT RESPONSE OF UGMs

The previous section discussed factors that affected the permanent deformation of unbound granular materials (UGMs). Generally, if resistance to permanent deformation is low then the material's stiffness/resilient modulus (Equation 2.23) is low and thus resilient strains are high. Therefore, the same factors that result in higher permanent strains discussed in Section 2.6 generally result in lower stiffnesses. Thom and Brown (1989) found the ranking of materials in terms of their stiffnesses was not the same as ranking materials in terms of their resistance to deformation. A material with the lowest stiffness did not have the lowest resistance to deformation.

The major effect on resilient behaviour is stress, where granular layers of a pavement have markedly non-linear stress strain relationships. As the pavement design procedures rely on accurate calculation of resilient strains at key locations within the pavement many studies have focused on the non-linear resilient properties of granular materials. Researchers (e.g. Hicks and Monismith (1971), Uzan (1985), Thom and Brown (1989) and Sweere (1990)) have shown a very high degree of dependence on confining pressure and sum of principal stresses for the resilient modulus of untreated granular materials. A common relationship used for defining the resilient modulus with respect to stress is the Hicks and Monismith (1971) k-θ model (Equation 2.27).

$$M_r = K_1 \left(\frac{\theta}{p_0} \right)^{K2} \qquad \text{Equation 2.27}$$

where,

M_r = Resilient modulus (Equation 2.23);

θ = bulk stress = sum of the principal stresses ($\sigma_1 + \sigma_2 + \sigma_3$); and

K_1 and K_2 are constants.

p_0 = reference stress to ensure consistency in units (either 1 kPa or 100 kPa).

The k-θ model (Equation 2.27) proposed by Seed et al. (1967), Brown & Pell (1967), and Hicks (1970) is one of the most widespread approaches to describe the resilient behaviour. For more complex pavement analysis the Boyce models (Boyce, 1980) are popular (Paute et al. 1996; Dawson et al. 1996). Hornych and Kerzrého (2002) have tested and modified the Boyce models to improve predictions of resilient behaviour measured at the LCPC test track located in France.

The ABAQUS finite element package used in this research models the non-linear behaviour of soils using a shear porous elasticity model available in the ABAQUS (1996) material library. The shear porous elasticity model is shown in Equation 2.28:

$$\frac{k}{(1+e_0)}\ln\left(\frac{p_0+p_t^{el}}{p+p_t^{el}}\right)=\frac{1+e^{el}}{1+e_0}-1 \qquad \text{Equation 2.28}$$

where,

k = logarithmic bulk modulus;

p = principal stress average (compression is +ve);

p_t^{el} = elastic tensile stress limit (tension is +ve);

p_0 = initial principal stress average (compression is +ve);

e_0 = initial void ratio (i.e. volume ratio that can be compressed); and

e^{el} = elastic volumetric strain.

In conjunction with the shear porous elasticity model a constant shear modulus, G, is required. The shear modulus G is calculated from Equation 2.29 as given in the ABAQUS (1996) manual:

$$q = 2Ge^{el} \qquad \text{Equation 2.29}$$

where,

q = principal stress difference or deviatoric stress;

G = shear modulus;

e^{el} = elastic volumetric strain resulting from a loading of q.

2.8 PERMANENT DEFORMATION MODELS OF GRANULAR MATERIALS

Over the years many researchers have begun to develop models for the prediction of permanent strain/rutting in unbound materials. Many of these relationships have been derived from permanent strain Repeated Load Triaxial tests. The aim of the models is to predict the magnitude of permanent strain from known loads and stress conditions. There are many different relationships reviewed in this section with quite different trends in permanent strain development. The differences in relationships are likely to be a result of the limited number of: load cycles and different stress conditions tested in the RLT apparatus. It is likely that more than one relationship is needed to fully describe the permanent strain behaviour of granular material.

For convenience and comparison, the relationships proposed for permanent strain prediction have been group in Table 2.1 (after Lekarp, 1997 except for those relationships from Theyse, 2002).

Table 2.1. Models proposed to predict permanent strain (after Lekarp, 1997 except relationships from Theyse, 2002).

Expression	Eqn.	Reference
$\varepsilon_{1,p} = a\varepsilon_r N^b$	2.30	Veverka (1979)
$K_p(N) = \dfrac{p}{\varepsilon_{v,p}(N)}$, $G_p(N) = \dfrac{q}{3\varepsilon_{s,p}(N)}$	2.31	Jouve et al. (1987)
$G_p = \dfrac{A_2\sqrt{N}}{\sqrt{N}+D_2}$, $\dfrac{G_p}{K_p} = \dfrac{A_3\sqrt{N}}{\sqrt{N}+D_3}$	2.32	Jouve et al. (1987)
$\dfrac{\varepsilon_{1,p}}{N} = A_1 N^{-b}$	2.33	Khedr (1985)
$\varepsilon_{1,p} = a + b\log(N)$	2.34	Barksdale (1972)
$\varepsilon_{1,p} = aN^b$	2.35	Sweere (1990)
$\varepsilon_{1,p} = (cN+a)(1-e^{-bN})$	2.36	Wolff & Visser (1994)
$\varepsilon^*_{1,p} = \dfrac{A_4\sqrt{N}}{\sqrt{N}+D_4}$	2.37	Paute et al. (1988)
$\varepsilon^*_{1,p} = A\left(1-\left(\dfrac{N}{100}\right)^{-B}\right)$	2.38	Paute et al. (1996)
$\varepsilon_{1,p} = \sum\varepsilon_N = \sum\dfrac{1}{N^h}\varepsilon_i$	2.39	Bonaquist & Witczak (1997)
$\varepsilon_{1,p} = \dfrac{q/a\sigma_3^b}{1-\left[\dfrac{(R_f q)/2(C\cos\phi+\sigma_3\sin\phi)}{(1-\sin\phi)}\right]}$	2.40	Barksdale (1972)
$\varepsilon_{1,p} = \varepsilon_{0.95S}\ln\left(1-\dfrac{q}{S}\right)^{-0.15} + \left\{\dfrac{a(q/S)}{1-b(q/S)}\right\}\ln(N)$	2.41	Lentz and Baladi (1981)

Parameters	
$\varepsilon_{1,p}$	= accumulated permanent strain after N load repetitions
$\varepsilon^*_{1,p}$	= additional permanent axial strain after first 100 cycles
$\varepsilon_{1,p}(N_{ref})$	= accumulated permanent axial strain after a given number of cycles N_{ref}, $N_{ref} > 100$
$\varepsilon_{v,p}$	= permanent volumetric strain for $N > 100$
$\varepsilon_{s,p}$	= permanent shear strain for $N > 100$
ε_N	= permanent strain for load cycle N
ε_i	= permanent strain for the first load cycle
ε_r	= resilient strain
K_p	= bulk modulus with respect to permanent deformation
G_p	= shear modulus with respect to permanent deformation
q	= deviator stress
p	= mean normal stress
q^0	= modified deviator stress= $\sqrt{2/3}\cdot q$
p^0	= modified mean normal stress= $\sqrt{3}\cdot p$
p^*	= stress parameter defined by intersection of the static failure line and the p-axis
p_0	= reference stress
L	= stress path length
σ_3	= confining pressure
N	= number of load applications
S	= static strength
$\varepsilon_{0.95S}$	= static strain at 95 percent of static strength
C	= apparent cohesion
ϕ	= angle of internal friction
fn$N$	= shape factor

Expression	Eqn.	Reference	Parameters	
$\varepsilon_{1,p} = 0.9\frac{q}{\sigma_3}$	2.42	Lashine et al. (1971)	R_f h	= ratio of measured strength to ultimate hyperbolic strength = repeated load hardening parameter, a function of stress to strength ratio
$\varepsilon_{s,p} = (\text{fn } N)L\left(\frac{q^0}{p^0}\right)^{2.8}_{\max}$	2.43	Pappin (1979)	A_1	= a material and stress-strain parameter given (function of stress ratio and resilient modulus)
			A2-A4, D2-D4	= parameters which are functions of stress ratio q/p
$A = \frac{\frac{q}{(p+p^*)}}{b\left(m-\frac{q}{(p+p^*)}\right)}$	2.44	Paute et al. (1996)	m *a, b, c, d* *A, B, t, u*	= slope of the static failure line = regression parameters (*A* is also the limit value for maximum permanent axial strain)
$\frac{\varepsilon_{1,p}(N_{ref})}{(L/p_0)} = a\left(\frac{q}{p}\right)^b_{\max}$	2.45	Lekarp and Dawson (1998)	*PD* σ_1^a	= permanent deformation (mm) = applied major principal stress
$\varepsilon_p(N) = A\left(1-\left(\frac{N}{100}\right)^{-B}\right)\times\left(\frac{1}{p_a}\right)^r\times\left(\frac{q}{p}\right)^s$	2.46	Akou et al. (1999)	*SR*	= shear stress ratio (a theoretical maximum value of 1 indicates the applied stress is at the limit of materials shear strength defined by *C* and ϕ)
$PD = dN + \frac{cN}{\left[1+\left(\frac{cN}{a}\right)^b\right]^{1/b}}$	2.47		*RD* *St* *PS*	= Relative Density (%) in relation to solid density = degree of saturation (%) = Plastic Strain (%)
$PD = dN + a(1-e^{-bN})$	2.48			
$PD = te^{aN} - ue^{-bN} - t + u$	2.49	Theyse (2002)		
$\log N = -13.43 + 0.29RD - 0.07St + 0.07PS - 0.02SR$	2.50			
$SR = \frac{\sigma_1^a - \sigma_3}{\sigma_3\left(\tan^2\left(45^0+\frac{\phi}{2}\right)-1\right)+2C\tan\left(45^0+\frac{\phi}{2}\right)}$	2.51			

2.9 ELASTO-PLASTICITY MODELS

2.9.1 Introduction

Granular materials can carry only limited tensile stress and can undergo plastic deformation under high compressive stress. One of the most common ways of simulating such material behaviour and limiting the tensile stress in finite element models is elasto-plasticity. If the stress is always less than the yield criterion, the material behaviour is assumed to be elastic. Otherwise, the material develops plastic flow and is considered to be an elastic-perfectly plastic material (Figure 2.13). Stress levels above the yield line are not possible and deformations will continue to take place until the stress can be reduced to below the yield stress through the load being redistributed to other parts in the structure/pavement.

Hardening can also be added to elasto-plastic models. Hardening is where the failure surface/yield line moves resulting in an increase in strength that occurs after a defined amount of permanent strain. In fact hardening can occur many times provided there is a relationship between the yield surface and permanent strain.

Mohr-Coulomb and Drucker-Prager criteria are commonly used for modelling granular materials (Chen 1994; Desai and Siriwardane 1984). They are generalised forms of the Tresca and Von Mises criteria, created by adding the friction angle, which develops hydrostatic pressure-dependent behaviour. Both criteria satisfy most of the characteristic behaviour of granular materials (Chen 1994, Chen and Han 1988).

2.9.2 Mohr-Coulomb Yield Criteria

The Mohr-Coulomb yield criterion has successfully simulated frictional material behavior since its development. The yield criterion is based on the maximum shear stress of the material. The Mohr-Coulomb model assumes a linear relationship between shear strength and normal stress (Figure 2.14 and Equation 2.52).

$$\tau_f = c + \sigma_n \tan\phi \qquad \text{Equation 2.52}$$

where,

τ_f = shear stress;

σ_n = normal stress;

c = apparent cohesion (includes suction); and

ϕ = angle of frictional resistance.

If the principal stresses $\sigma_1 \geq \sigma_2 \geq \sigma_3$ the Mohr-Coulomb criterion can be written as per Equation 2.53.

$$(\sigma_1 - \sigma_3) = 2c \cdot \cos\phi - (\sigma_1 + \sigma_3)\tan\phi \qquad \text{Equation 2.53}$$

The tensile strength of a material can be controlled by the cohesion in the Mohr-Coulomb failure criterion. Cohesion is a material constant and often varies with the size of the particles composing the granular material and the amount of suction (forces pulling particles together in partially saturated materials, Section 2.4.7). Small-grain granular materials (clay) often have higher cohesion than large-grain ones (gravel) because chemical bonds and capillary forces exist between grains (Craig 1992, Terzaghi, et al 1996). Hence, the behaviour of small-grain materials is governed more by cohesion, while that of large-grain ones is governed more by friction and interlocking between grains. The Tresca criterion is a special case of Mohr-Coulomb criterion when the angle of frictional resistance, ϕ = 0. That means the critical value of shear stress is constant and its value depends on the cohesion in the Tresca criterion, while it is a function of the normal stress in the Mohr-Coulomb criterion. The yield (or failure) surface of the Mohr-Coulomb criterion can be represented as a hexagonal pyramid extended to the compressive principal stress space (Figure 2.15). In finite element formulation, a six-faced Mohr-Coulomb yield surface causes numerical difficulties along each edge because the normal vector of the yield surface cannot be uniquely defined along edge lines.

2.9.3 Drucker-Prager Yield Criterion

For soils and unbound granular materials, unlike metals, there exists a number of yield criteria dependent on the hydrostatic stress component. Recognising this, Drucker and Prager (1952) extended the well known Von Mises yield condition to include the hydrostatic component of the stress tensor. The extended Von Mises yield condition in 3-dimensional principal stress space is a cone with the space diagonal as its axis (Figure 2.16). This criterion can also be defined as a Drucker-Prager yield surface, F_s, in a p (mean normal stress, Equation 2.2) versus q (principal stress difference, Equation 2.7) stress space given by Equation 2.54 and shown in Figure 2.17.

$$Fs = q - p \tan\beta - d = 0 \qquad \text{Equation 2.54}$$

where,

β = the angle of the yield surface in p-q stress space (Figure 2.17);

d = the q-intercept of the yield surface in p-q stress space (Figure 2.17);

q = principal stress difference, Equation 2.7; and

p = mean normal stress, Equation 2.2.

In finite element models of pavements many researchers define the Drucker-Prager criterion in slightly different components as per Equation 2.55.

$q = \mathrm{M}\,(p + \mathrm{p}^*)$ Equation 2.55

where,

M = $\tan\beta$ (β from Equation 2.54);

p* = $-d/\mathrm{M}$ (d from Equation 2.54).

The conical shape of the Drucker-Prager yield surface results in a circular cross-section only when viewed at right angles to the $\sigma_1=\sigma_2=\sigma_3$ stress tensor (Figure 2.15). Unlike the Mohr-Coulomb criterion the circular shape of the Drucker-Prager yield surface can be readily defined in finite element formulations.

For the linear Drucker-Prager model the ABAQUS general finite element package requires the yield surface to be defined as per the line plotted in Figure 2.17. The angle of the line, β, is inputted directly while the value of "*d*" the "*q-intercept*" (Figure 2.17) is not used. Instead a value on the yield line, σ_{0c}, is used. This value (σ_{0c}) is the yield stress where the confining stress is zero and is also shown in Figure 2.17.

Data to define the yield line are conventionally obtained from a series of triaxial constant strain or stress rate failure tests (monotonic shear failure tests) at different confining stresses (Figure 2.18). The yield stress for each failure test (i.e. the maximum stress value achieved in the test) is plotted in *p*-*q* stress space (Figure 2.19). From this plot a straight line is approximated through the data to obtain "*d*" the "*q-intercept*" and the angle of the line, β. It can be shown when confining stress is zero in triaxial test conditions, where $\sigma_2=\sigma_3$, that σ_{0c}, required by ABAQUS is calculated using Equation 2.56.

$$\sigma_{0c} = \frac{d}{(1 - 1/3\tan\beta)}$$ Equation 2.56

If the experimental data is not readily available, the yield line can be obtain from Mohr-Coulomb friction angle, ϕ, and cohesion, c. From geometry, trigonometry and the relationships between *p*-*q* stresses and principal stresses the Mohr-Coulomb failure line can be plotted in *p*-*q* space to represent a Drucker-Prager failure criterion. It can be shown that the angle of the failure line in *p*-*q* stress space, β, is defined by Equation 2.57 and the *q*-intercept, d is determined using Equation 2.58 for triaxial test conditions (ie. $\sigma_2=\sigma_3$).

$$\tan\beta = \frac{6\sin\phi}{3-\sin\phi} \qquad \text{Equation 2.57}$$

$$d = \frac{6c\cos\phi}{3-\sin\phi} \qquad \text{Equation 2.58}$$

Similarly, σ_{0c}, required by ABAQUS is calculated using Equation 2.56 above.

One weakness of the Drucker-Prager yield criterion is that the maximum strength in compression is the same as the maximum strength in extension (ie. for the cases when $\sigma_1>\sigma_2=\sigma_3$ and when $\sigma_1=\sigma_2>\sigma_3$) because its yield surface is circular on the plane, as demonstrated in Figure 2.15. That contradicts characteristics of granular materials. On the contrary, Mohr-Coulomb does show a difference between them by a hexagonal cross section, as demonstrated in Figure 2.15. Thus, the Drucker-Prager criterion could overestimate the strength in extension of a granular material.

In the ABAQUS (1996) general finite element package hardening can be added to the Drucker-Prager criterion. The hardening is defined by kinematic hardening models which assume associated plastic flow, where plastic strain is perpendicular to the yield surface. The hardening model consists of a linear kinematic hardening component that describes the translation of the yield surface in *p*-*q* stress space in relation to plastic strain. The hardening model is defined in terms of a table of permanent strain in relation to yield strength in terms of the cohesive parameter σ_{0c} (Equation 2.56). The result is an increasing yield surface as permanent strain occurs as shown in Figure 2.20.

2.10 FINITE ELEMENT MODELLING OF GRANULAR PAVEMENTS

2.10.1 Introduction

Current linear elastic programmes used in mechanistic design procedures (Section 2.2.2) can only approximate at best the variation of stiffness with stress for granular and subgrade soil materials. Hence, finite element modelling (FEM) is required to fully take into account the non-linear stress-strain relationships for these materials (e.g. Equation 2.27). Many researchers have customised general finite element packages to develop finite element programs specific to pavements. Some of these programs include DEFPAV (Snaith, 1976) developed at Queens University Belfast, FENLAP (Finite Element Non-Linear Analysis for Pavements) (Brunton & Almeida, 1992) developed at Nottingham, and ILLI-PAVE (Thompson et al. 2002) from University of Illinois. Other finite element programs like ANSYS (2002), Version 6.1 and ABAQUS (1996) Version 5.6 are general commercial finite element packages (FEP). Commercial finite element packages are more time consuming as they require the user to develop the geometry and choose (if available in the library) or program a suitable material model. Further, commercial FEP's cannot easily accommodate trial changes in pavement thickness as a new geometry needs to be created each time. However, commercial FEP's have the advantage of being readily available, allow for the analysis of complex geometries like the pavement's edge and undertake complex crack analysis (Mohammad et al. 2003).

2.10.2 Two Dimensional (2D) Axisymmetric Models

Axisymmetric problems are viewed as two-dimensional, but the *x* and *y*-directions are replaced by the radial (*r*) and axial (*z*) direction. The axisymmetric 2-D approach has been one of the common ways to analyse flexible pavement problems since Burmister created a layered linear elastic half-space solution in the 1940s. After the introduction of finite element methods, numerous axisymmetric 2-D finite element codes were developed for pavement analysis and design. Their prime objective was to include non-linear elastic constitutive models into the existing 2-D axisymmetric pavement analysis framework initially derived by Burmister (1945).

The axisymmetric domain is modelled using eight-node rectangular elements, with four nodes at the vertices and four nodes at the mid distance of the sides. Each node has two degrees of freedom, its vertical and horizontal displacement. Due to axial symmetry, the elements are complete rings in the circumferential direction and the nodal points at which they are connected are circular lines in plan view. This type of element has been extensively used in finite element applications (Almeida 1986; Zienkiewicz and Taylor 1989) for it yields a satisfactory level of accuracy despite its simplicity.

The advantage of modelling in 2-D is the less complex and symmetrical geometry and loading (Figure 2.21) which results in significantly less computing power. This was the prime reason why many finite element packages developed specifically for pavements used 2D axisymmetric geometry. These included ILLI-PAVE from the University of Illinois originally developed by Raad and Figueroa (1980) and later refined by Thompson et al. (1985, 1987 & 2002); DEFPAV, developed by Trinity College Dublin and Queens University Belfast (Snaith, 1976). FENLAP (Finite Element Non-Linear Analysis for Pavements) (Brunton & Almeida, 1992) developed at the University of Nottingham also uses an axisymmetric idealisation of the pavement structure under a vertical circular load. Neves & Correia (2003) successfully used FENLAP to model the anisotropic version of Boyce’s model (1980) for the non-linear behaviour of granular material. The CESAR-LCPC (Central

Laboratory of Chaussees France) assume a 2D axisymmetric model of the pavement and also utilises Boyce's model (Akou et al, 1999).

Other axisymmetric finite element packages developed for pavement analysis as reviewed in the Amedeus project (Amedeus, 2000) are AXIDIN and MICHPAVE. AXIDIN was developed at the Laboratorio Nacional de Engenharia Civil (Antunes, 1993). Its prime use was to undertake dynamic analyses of falling weight deflectometer (FWD) tests, although it can also analyse dynamic loads induced by heavy vehicles. MICHPAVE (Harichadran et al. 1989) was developed from ILLI-PAVE by Michigan State University and is similar except to reduce the number of finite elements MICHPAVE allows for a "flexible boundary" at the base to allow for displacement at depth. ILLI-PAVE only uses finite elements and therefore the boundaries must be placed at a large distance so their effect is negligible (Amedeus, 2000). Duncan et al. (1968) suggested that for finite element models the boundaries should extend to 50 times the radius of the loaded area in the vertical direction, while limited to 20 times the radius in the horizontal direction. Therefore, many finite elements are needed in finite element models that do not incorporate a flexible boundary like ILLI-PAVE which increases the computation time. The k-θ model (Equation 2.27) for granular materials is used in MICHPAVE and ILLI-PAVE.

Only a single circular wheel load can be analysed using a 2D-axisymetric approach and edge effects cannot be modelled. Further, there is no such problem as a truly 2D one; all 2D solutions are approximations of 3D solutions (Becker, 2004). Although, now that computing power has increased 3D geometries are being used due to the ability to model for example, more complex loading, pavement edges or crack propagation.

All commercial finite element packages including ABAQUS (1996) and ANSYS (2002) can readily model 2D-axisymetric idealisation. The main advantage is significantly reduced processing times due to the advantages of symmetry which reduces the number of elements. It is generally recommended that the first pavement analysis with non-linear models should be conducted using a simpler 2D model before moving onto a 3D model. This allows for validation of boundary conditions, models used and their parameters. Hoff et al. (1999) used an axisymmetric model in ABAQUS to incorporate a constitutive model for unbound granular materials based on hyperelasticity.

2.10.3 Two Dimensional (2D) Plane Strain and Plane Stress Models

Another 2D approximation is to assume either plane strain or plane stress models. Plane stress models assume very thin geometries where the σ_3 principal stress across the thickness is nil. This is clearly not the case for pavements containing no-tension materials and the use of a plane stress model is considered not suited for pavement analysis and as such no reference to its use has been found in the literature.

Plane strain models assume thickness in the horizontal plane is infinite. Geometry in the horizontal plane does not change so that strain is nil. Loading is assumed as a strip extending infinitely in the horizontal plane as shown in Figure 2.22. Generally, the use of plane strain models has not been favoured for routine pavement analysis. Jacobs et al. (1992) assumed a plane strain model for fracture/cracking analysis for overlay design of pavements . However, Jacobs et al. 1992 did use a 3D model to calibrate the plane strain model where the strip loading in the 2D model was changed until the results were similar to those obtained in the 3D model.

Long et al. (2002) used a plane strain model to simulate pavements tested by the HVS (Heavy Vehicle Simulator) in a rutting study described by Harvey and Popescu (2000). A complex non-linear visco-elastic model was used to model the asphalt layer. Initially the deformations computed were large and it was found necessary to reduce the plane strain load by one third to obtain deformations close to those measured in the HVS tests. The plane-strain model simulated actual passes of a wheel where computations were needed for each load cycle. Generally, computations were stopped after 7000 simulated wheel passes as this took several days. Due to the complexities of the material model a 3D model would not be practical due to the many more elements required which would significantly increase the computation times.

2.10.4 Three Dimensional (3D) Models

As computing power has increased 3D computer models are becoming more common, although as a first trial analysis in developing material models a 2D analysis is usually employed. Developing the 3D geometry is more complex where element types and degrees of freedom (DOF) need to be carefully chosen. Usually generalised commercially available finite element packages are used for 3D analysis due to their flexibility to model all types of geometries and material models as well as their interactions between the pavement layers.

Mohammad et al. (2003) analysed a 3D model in ANSYS on a typical three-layer flexible pavement system with a predefined crack. Further, Mohammad et al. (2003) analysed a more realistic non-uniform vertical and lateral pressure distribution of a wheel load.

Delft University of Technology have developed a 3D finite element package CAPA-3D (Scarpas et al. 1997 & 1998). CAPA-3D is a complex and general finite element programme and experience is needed to utilise its full capabilities. It can simulate a very broad range of soil and pavement engineering materials under a range of loads both dynamic and static (Amedeus, 2000). Airey et al. (2002) used the Delft 3D finite element package to simulate asphalt mixture performance in pavement structures using a constitutive model based tension and compressive strength of asphalt mixtures.

General finite element packages like SYSTUS (Amedeus, 2000), ANSYS (2002), CESAR (LCPC, Central Laboratory of Chaussees, France), DIANA (Delft University of Technology, Holland) and ABAQUS (1996) do not include tools especially dedicated to pavement analysis and design. The fields of application of these programmes are very broad, including but not limited to the analysis of aircraft, buildings and boats. The calculation method based on finite elements employed makes it possible to analyse numerous problems such as:

- static or dynamic analysis of linear or non-linear structures;
- 3D or 2D (i.e. plane strain, plane stress, or axisymmetric) geometries;
- dynamic analysis with determination of eigenmodes and eigenfrequencies,
- analysis of large displacements and large strains,
- analysis of second-order problems: stability and buckling; both linear and non-linear,
- definition of numerous interfaces of different natures: sliding, perfect sticking, variable friction;
- employ a range of material behaviour laws available in the library of material types;
- defining own material behaviour laws;
- defining any geometrical shape of the load distribution and its interface properties;
- study of fracture mechanics for analysis of issues such as reflective cracking in pavements;
- produce output of stresses, strains and displacements in all directions (e.g. principal, x, y, z or shear components) in both graphical and tabular form in each applications post-processor.

Schools of Engineering at universities should have access to one or more general finite element packages, although there are some limitations when applying their use to pavement design and analysis:

- general finite element packages are expensive and generally only available to pavement engineers through universities;
- installation and use is difficult with sometimes many weeks needed to gain competence in using the package through trial and error until confident in the pavement analysis and models chosen;
- changing the pavement depth (which is a key aspect in design) to assess its effect is not straightforward as often a new geometry is required and as this is the first stage of the finite element model development, i.e. boundaries, loads, materials and the finite element mesh need to be redefined.

2.11 SHAKEDOWN IN RELATION TO PAVEMENT DESIGN

2.11.1 Introduction

The literature review on models for permanent strain (Section 2.8) resulted in many different models, some of which indicate the permanent strain rate decreases with increasing strain rate (Khedr, 1985 (Eqn. 2.33); Barksdale, 1972 (Eqn. 2.34); Sweere, 1990 (Eqn. 2.35); Theyse, 2002 (Eqn. 2.47)). Paute et al. (1996) suggest there is a limit to the amount of permanent strain as per the asymptotic model proposed (Equation 2.38). In contrast, Wolf and Visser's (1994) relationship suggests that the permanent strain rate will eventually become constant.

Theyse (2002) recognised it is not possible to categorise the permanent strain behaviour by a single relationship. Three equations are proposed (2.47, 2.48 and 2.49). Equation 2.47 will predict a long term response of decreasing permanent strain rate and is suited for low stress conditions. The second equation (2.48) will predict a long term constant permanent strain rate and is suited for medium stress conditions, while the third equation is suited for high stress conditions where the permanent strain increases exponentially and eventually fails.

It appears the level of stress defines the type of permanent strain behaviour that can be expected. From a design perspective the level of stress which will result in a decreasing permanent strain rate is ideal as this represents stable conditions. These stable conditions can be considered as shakedown, where there exists a *shakedown limit stress* at the boundary between the points at which shakedown occurs and does not occur.

The possibility of using this *shakedown limit stress* as the design stress for pavements was first recognised by Sharp and Booker (1984) and Sharp (1985).

The shakedown concept has been applied to studies on wear of layered surfaces by Anderson and Collins (1995), Wong and Kapoor (1996) and Wong et al. (1997). These analyses all use the concept of *shakedown theory* to determine the long-term behaviour of the surface. The basic assumption is that the structure can be modelled by an homogeneous elastic/plastic material, in which case the structure will eventually either shakedown, i.e. the ultimate response will be purely elastic (reversible), or will fail in the sense that the structural response is always plastic (irreversible) however many times the load is applied. The critical load level separating these two types of behaviour is termed the *critical shakedown stress*.

Brett (1987, cited in Boulibibane 1999) used a time series analysis to study the variation of roughness and serviceability indices of a number of sections of roads in New South Wales and concluded that after 8 years at least 40% were operating in a shakendown state – so called “survivor pavements”. Both Sharp and Brett quote a number of other field observations supporting the view that many pavements do shakedown rather than deteriorate continuously.

The basic analysis of Booker and Sharp (1984) has been followed up by a number of investigators. Interest has centred on the calculation of the *critical shakedown stress*. This is difficult to compute exactly but lower and upper bounds can be obtained by methods similar to those employed in limit analysis for monotonic loadings. Lower bound analysis based on consideration of stress fields have been given by Sharp and Booker (1984), Raad et al. (1988), Raad et al. (1989a, b), Hossain and Yu (1996), Yu and Hossain (1998) and Boulbibane and Weichert (1997). Such analyses use finite element programs to calculate the elastic stress field and a linear programming procedure for finding the best lower bound for the shakedown load. For simplification, these calculations have assumed a two-dimensional (plane strain) idealisation, in which the quasi-circular loading area of a wheel is replaced by an infinite strip loading under an infinitely long cylinder.

2.11.2 Shakedown Ranges

The idea of a *critical shakedown stress* effectively relates to a one-dimensional stress value, typically the wheel load. However, Repeated Load Triaxial tests produce results of permanent strain behaviour in relation to stress level in 3 dimensions in terms of stress invariants p and q (Section 2.4.3). From a design perspective a critical shakedown stress value in terms of that due to a wheel load is not practical as the wheel loading cannot be changed. Further, deriving critical shakedown stress from lower and upper bound theorems and utilising ϕ (friction angle) and c (cohesion) from monotonic shear failure tests is both difficult and questionable. As discussed in the introduction of this section different permanent deformation behaviours are observed in granular materials.

Dawson and Wellner (1999) have applied the shakedown concept to describe the observed behaviour of UGMs in the RLT permanent strain test. Johnson (1986) in the study of shakedown in metals reported four possible deformation behaviour types under cyclic loading either: elastic; elastic shakedown; plastic shakedown or ratchetting (Figure 2.23). In view of these shakedown behaviour types Dawson and Wellner (1999) and Wellner and Gleitz (1999) proposed three behaviour ranges A, B or C considered possible to occur in permanent strain Repeated Load Triaxial tests

(RLT). The shakedown behaviour types are detailed in Figure 2.23 and Figure 2.24 and are described as follows:

- **Range A** is the plastic shakedown range and in this range the response shows high strain rates per load cycle for a finite number of load applications during the initial compaction period. After the compaction period the permanent strain rate per load cycle decreases until the response becomes entirely resilient and no further permanent strain occurs.

- **Range B** is the plastic creep shakedown range and initially behaviour is like Range A during the compaction period. After this time the permanent strain rate (permanent strain per load cycle) is either decreasing or constant. Also for the duration of the RLT test the permanent strain is acceptable but the response does not become entirely resilient. However, it is possible that if the RLT test number of load cycles were increased to perhaps 2 million load cycles the result could either be Range A or Range C (incremental collapse).

- **Range C** is the incremental collapse shakedown range where initially a compaction period may be observed and after this time the permanent strain rate increases with increasing load cycles.

These three shakedown behaviour Ranges were also derived based simply on the fact that it is possible to classify all permanent strain/rutting plots with number of load cycles in one of three types. Long term permanent strain rate is either: decreasing with increasing load cycles (i.e. Range A); remaining constant with increasing load cycles (i.e. Range B); or increasing with increasing load cycles with likely premature failure (i.e. Range C). Johnson (1986) identified four possible shakedown Ranges: elastic; elastic shakedown; plastic shakedown. Figures 2.23 and 2.24 show these three behaviour ranges. As shown in Figure 2.23 Johnson (1986) shows a fourth behaviour range labelled as *Elastic* that occurs from the first load. A purely elastic response from the very first load is considered unlikely in granular and soil materials but should it occur a Range A classification would be appropriate.

Generally, from plots of permanent strain/rutting versus cumulative load cycles classification into the appropriate shakedown range is obvious. However, for test results near the border of shakedown ranges the classification may be difficult. Werkmeister et al. (2001) proposed the use of cumulative permanent strain versus permanent strain rate plots to aid in determining the shakedown range. An example plot is shown in Figure 2.25 (after Werkmeister et al 2001). Range A response is shown on this plot as a vertical line heading downwards towards very low strain rates and virtually no change in cumulative permanent strain. The horizontal lines show a Range C response where the strain rate is not changing or is increasing and cumulative permanent strain increases. A Range B response is between a Range A and Range C response, typically exhibiting a constant, but very small, plastic strain rate per cycle.

To determine the stress conditions that result in Range A, B or C behaviour, RLT permanent strain tests at a range of testing stress conditions will be conducted. Therefore, from computed stresses within the pavement it will be possible to determine which behaviour range is expected as observed in RLT tests. From a design perspective achieving Range A behaviour is best, while Range B maybe acceptable provided the amount of rutting for the design traffic can be calculated.

2.12 SUMMARY

This literature review aims to cover all the background information required for the forthcoming chapters from Repeated Load Triaxial testing, finite element modelling, pavement design and permanent strain modelling. The emphasis is on granular materials used in flexible pavements in terms of their permanent strain/rutting behaviour which is the prime focus of this research. Some of this literature review provides reference material for such items as stress invariants *p* and *q* (Section 2.4.3) that will be utilised throughout this thesis as an efficient means for characterising a stress state consisting of both axial and radial stresses. Some key points from the literature review relevant to this forthcoming thesis are summarised below:

- Rutting of pavements is caused by the passage of heavy vehicles, whereafter each wheel pass the pavement deflects downwards and then rebounds leaving a irrecoverable downwards deformation, this accumulates and after millions of passes or sometimes less a significant rut forms (i.e. >20mm) and the pavement requires rehabilitation;

- Current design methods are based on the assumption that surface rutting is only a function of compressive subgrade strain. Pavement material specifications are designed to ensure constructed layers of imported material do not contribute to rutting;

- Accelerated pavement tests report that 30 to 70% of the surface rutting is a result of deformation of the granular layers;

- The Repeated Load Triaxial (RLT) (Shaw, 1980), hollow cylinder (Chan 1990) and k-mould (Semmelink et al, 1997) apparatuses can in various degrees simulate pavement loading on soils and granular materials;

- The limitations of the RLT test are that only two of the maximum of six stress components are varied independently for complete general conditions and only the vertical and horizontal stresses can be applied and this simulates the situation when the load is directly above the element;

- As a wheel load approaches the element in a pavement it is subjected to a simultaneous build-up in both the major and minor principal stresses, these stresses also rotate about the centre element and this is referred to as rotation of principal stresses;

- Compaction of the granular pavement layers during construction results in the application of large vertical stresses which cause lateral/residual stresses to develop that become locked into the granular bases and subgrades and these lateral/residual stresses should be considered in pavement analysis;

- The effect of stress, both loading and unloading, is the single biggest factor that affects the resilient and permanent strain behaviour of granular materials;

- Increases in moisture, low permeability and poor drainage of granular materials under repetitive loading have the effect of reducing the amount of suction that pulls stones together with a consequential reduction in stiffness and resistance to deformation;

- Elasto-plastic models are those that define the yield strength of a material and those commonly used for granular materials are either the Drucker-Prager or Mohr-Coulomb criteria;

- Finite element modelling can fully incorporate the non-linear resilient behaviour of granular materials along with their yield strength limitations to calculate stresses and strains within a pavement that are more realistic than those predicted by linear elastic models;

- There are many different relationships developed by researchers that predict permanent strain from number of load cycles and in some cases stress under loading usually defined by stress invariants p (mean principal stress) and q (principal stress difference or deviatoric stress);

- No single model is adequately able to predict long-term permanent strain observations, where the permanent strain rate is either decreasing, remaining constant, or increasing with failure imminent;

- These three types of behaviour can be defined by shakedown ranges A, B or C:
    - **Range A**: Long term permanent strain rate is decreasing and is considered to be stable, which is ideal for pavement design;
    - **Range B**: Long term permanent strain rate appears constant;
    - **Range C**: Permanent strain rate rapidly increases towards failure after an initial stage;

- The type of long term permanent strain behaviour or shakedown Range A, B or C relates to the loading stress conditions.

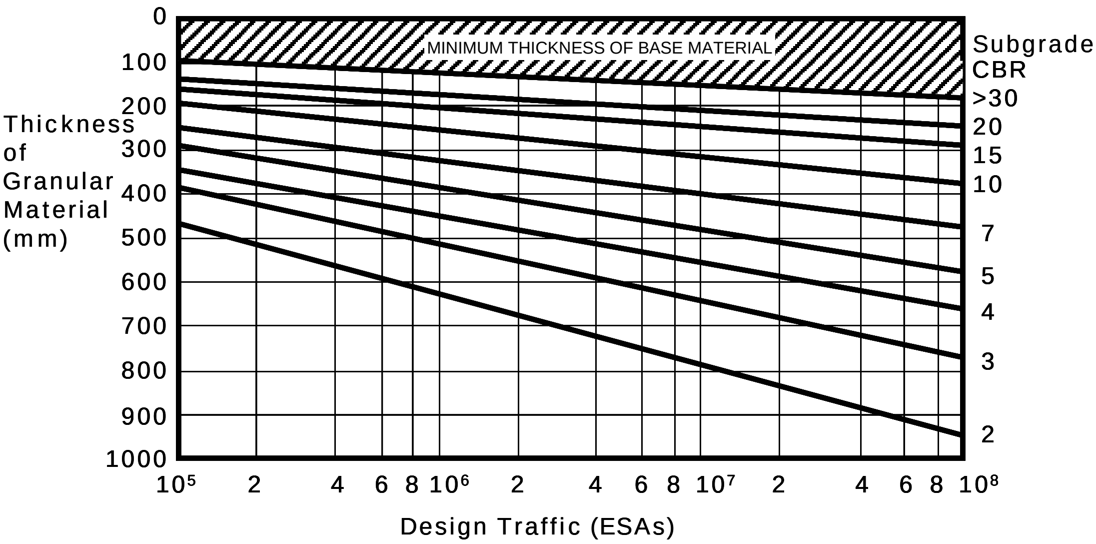

Figure 2.1. Pavement thickness design chart for thin-surfaced granular pavements (from Figure 8.4, Austroads, 1992)

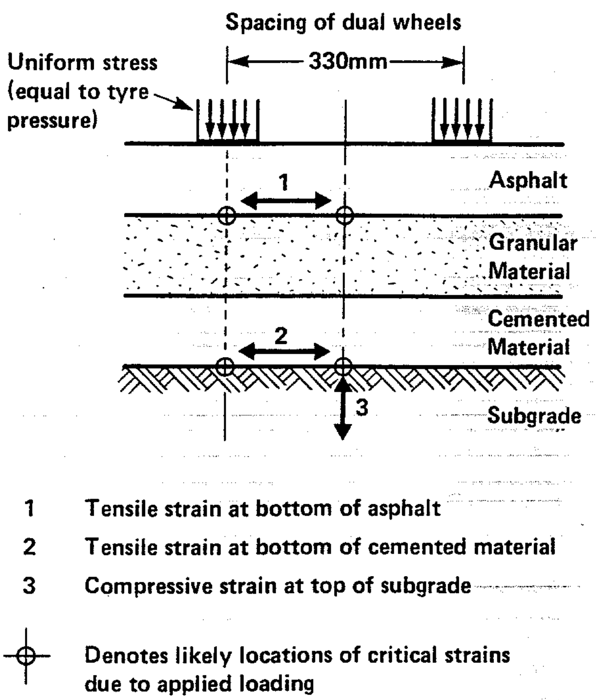

Figure 2.2. Mechanistic pavement design showing key strain locations.

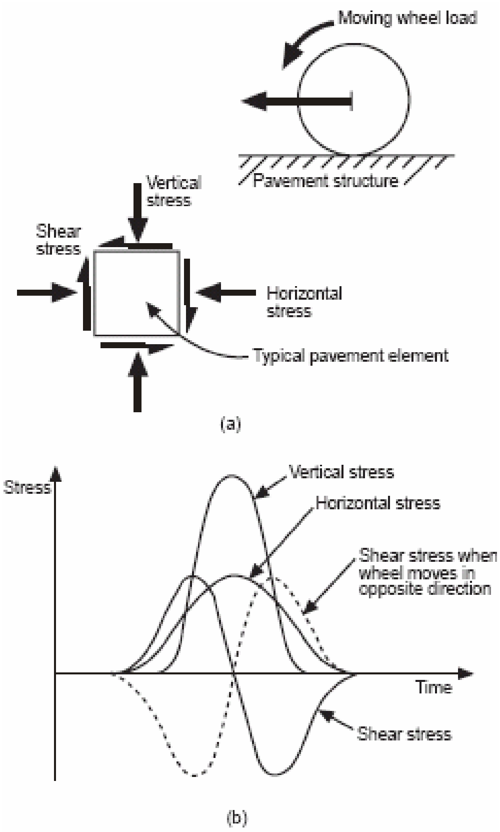

Figure 2.3 Stress conditions under a moving wheel load: (a) stresses on pavement element; (b) variation of stresses with time (after Brown, 1996).

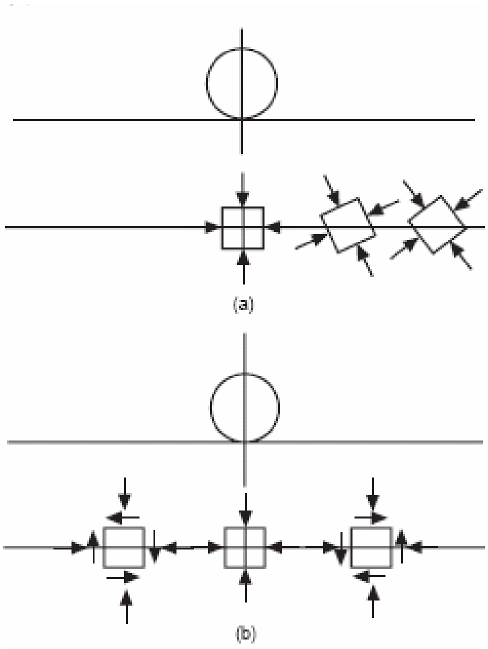

Figure 2.4. Stresses on a pavement element: (a) principal stresses - element rotates; (b) no rotation – shear stress reversal (after Brown, 1996).

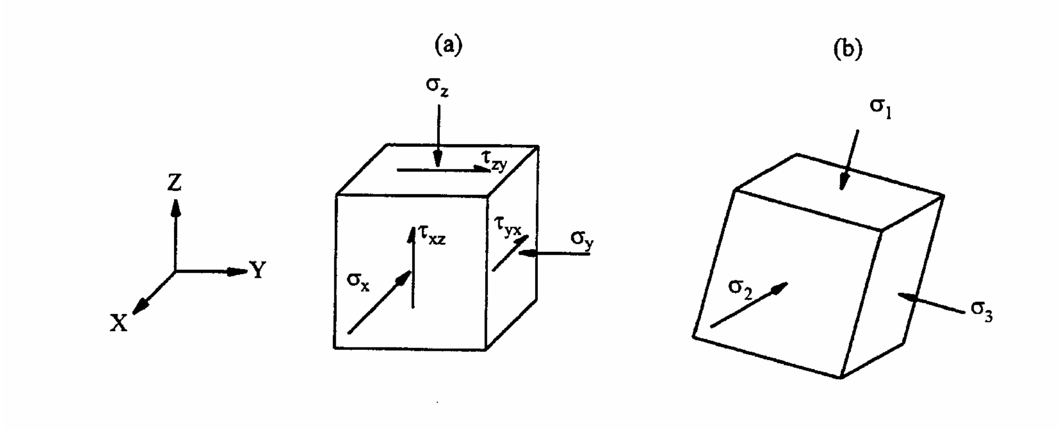

Figure 2.5. Stress components acting on an element (Lekarp, 1997).

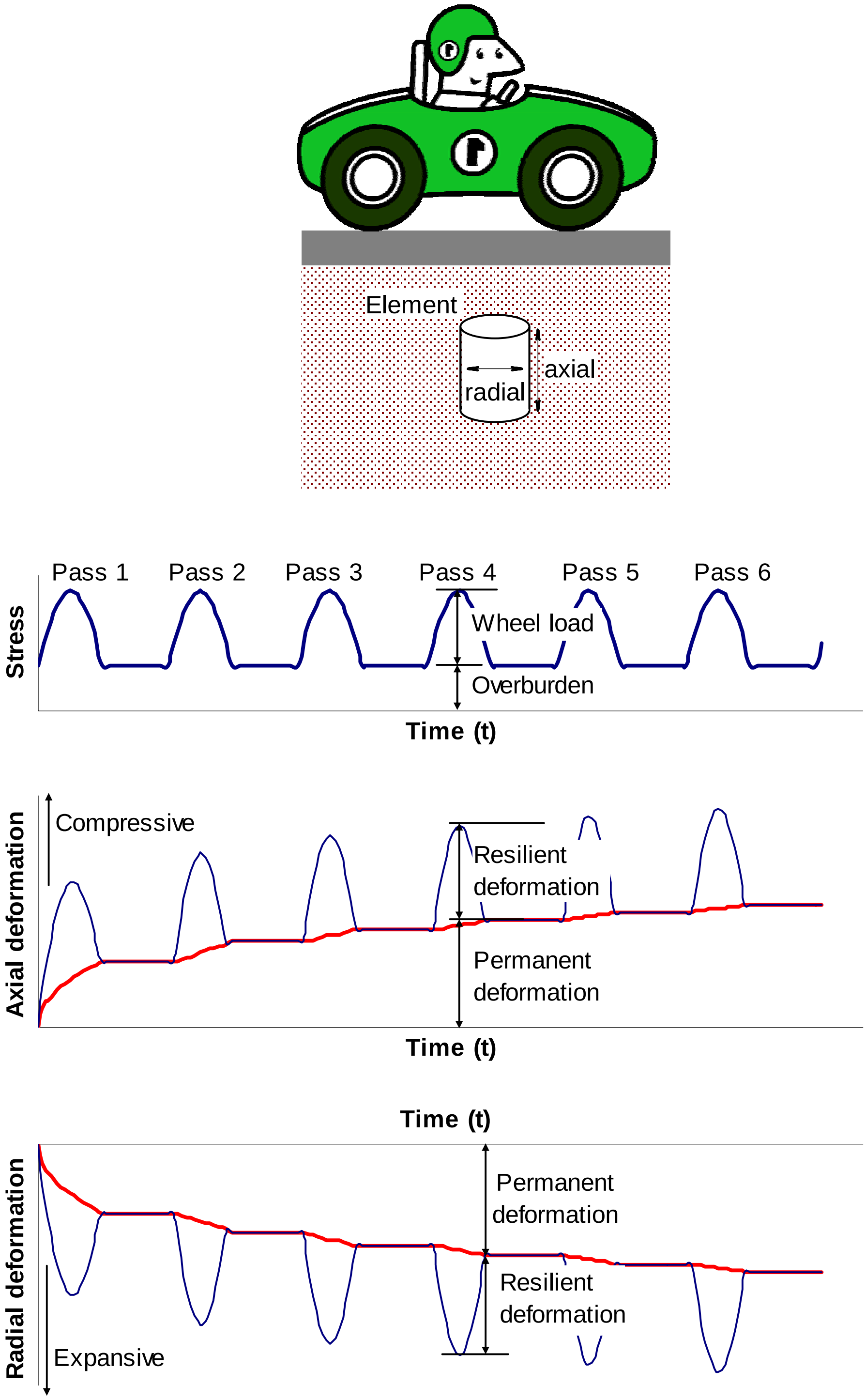

Figure 2.6. Loading in pavements under traffic.

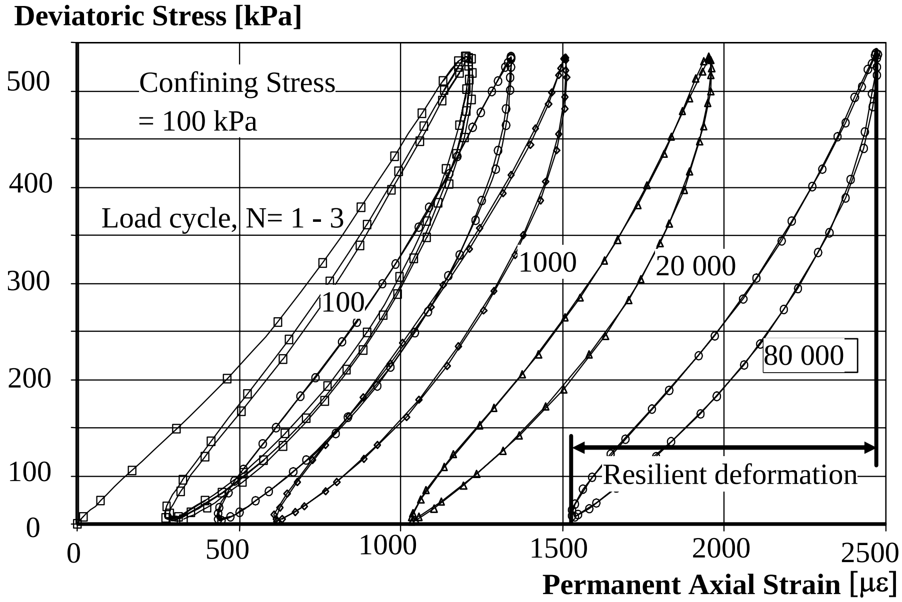

Figure 2.7. Stress-strain behaviour of materials under repeated loading (Werkmeister, 2003).

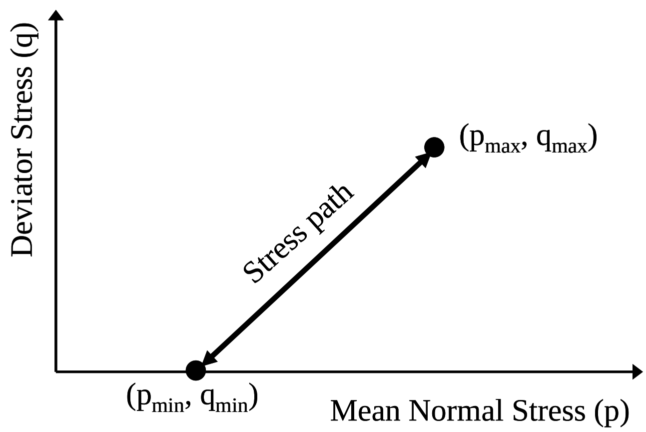

Figure 2.8. The definition of a stress path in p-q stress space.

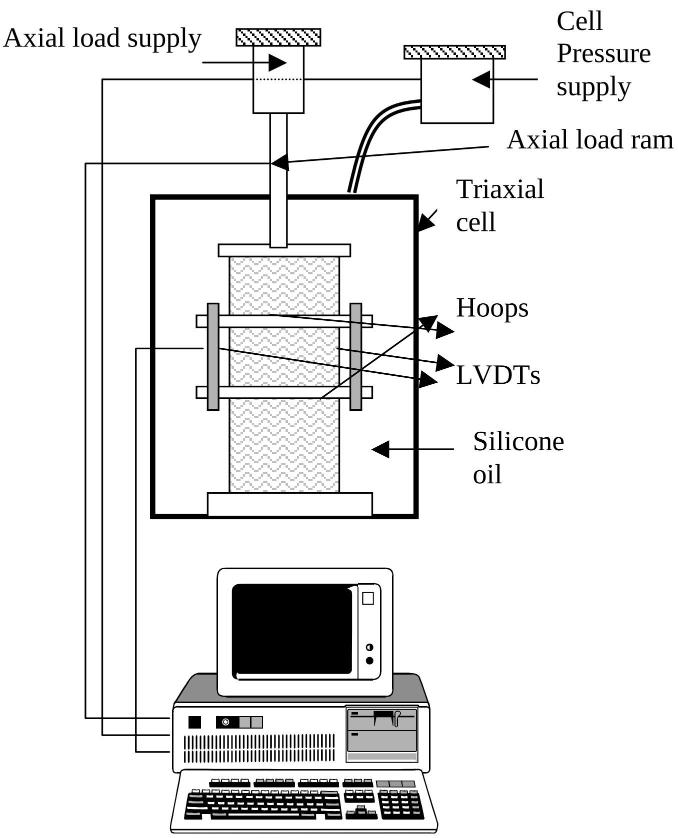

Figure 2.9. Repeated Load Triaxial (RLT) apparatus.

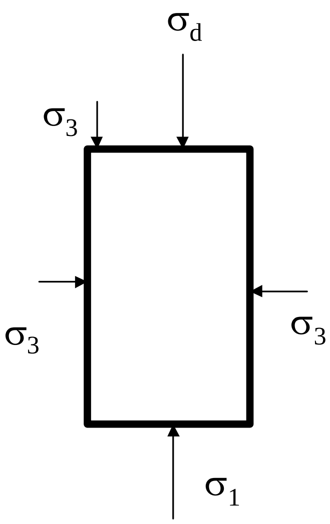

<u>where:</u>

σ_1 = major principal stress [kPa]

σ_3 = minor principal (confining) stress [kPa]

σ_d = cyclic deviator stress [kPa]

$\sigma_1 = \sigma_d + \sigma_3$

Figure 2.10. Stresses on a specimen in a RLT test.

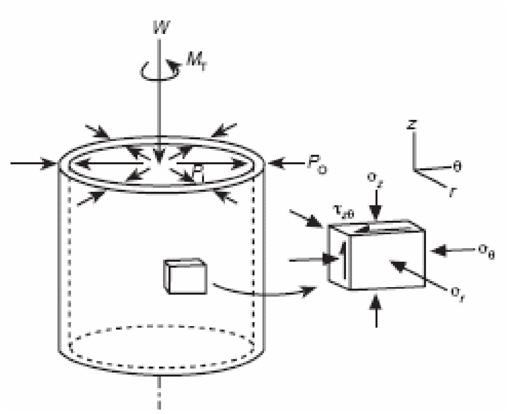

Figure 2.11 Stress conditions in a hollow cylinder apparatus (HCA).

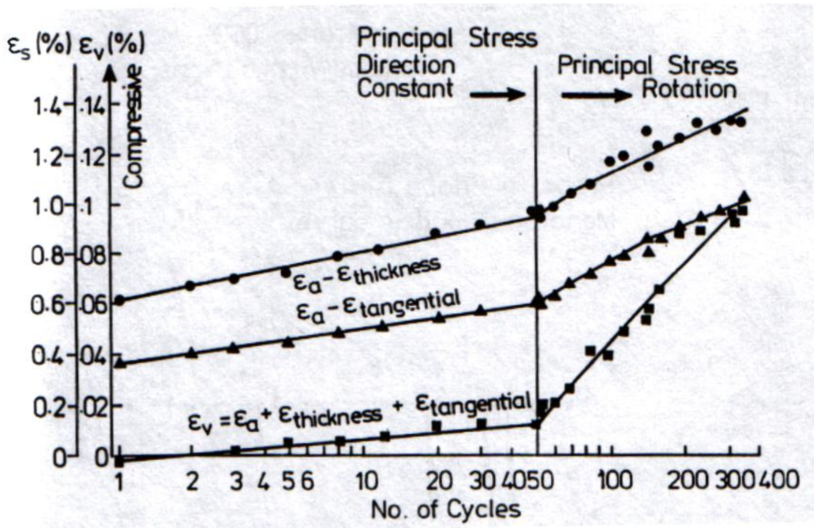

Figure 2.12. Effect of principal stress rotation on the accumulation of permanent strain (after Thom and Dawson, 1996).

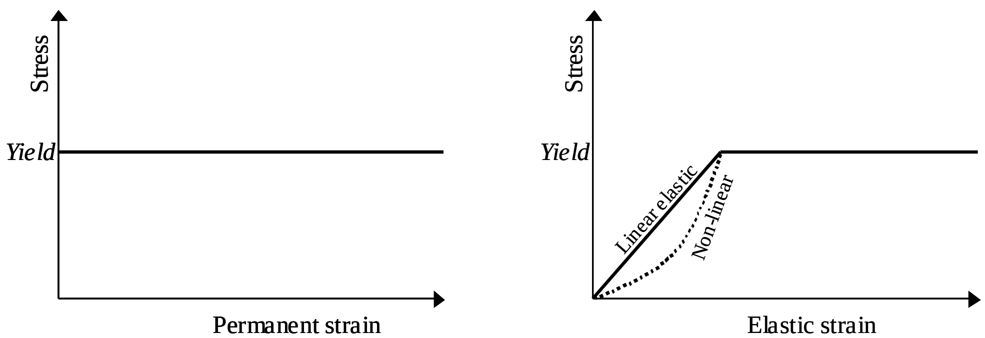

Figure 2.13. Elastic perfectly plastic behaviour assumed in elasto-plasticity models.

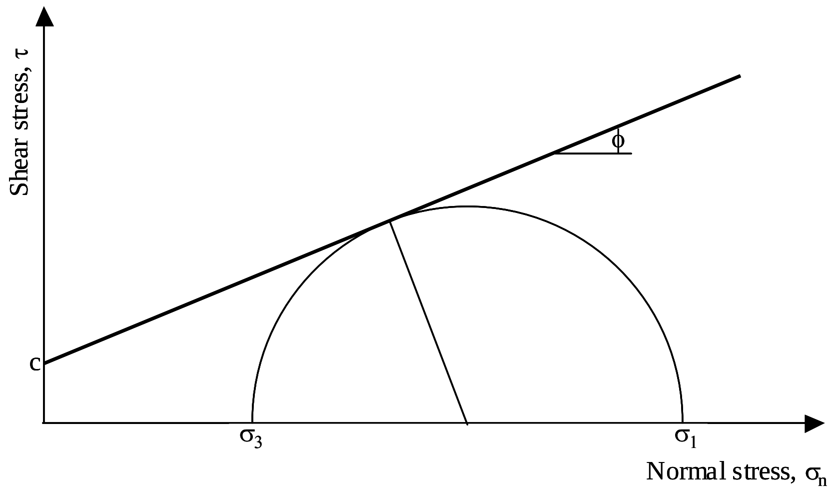

Figure 2.14. Traditional Mohr-Coulomb failure criteria/circles

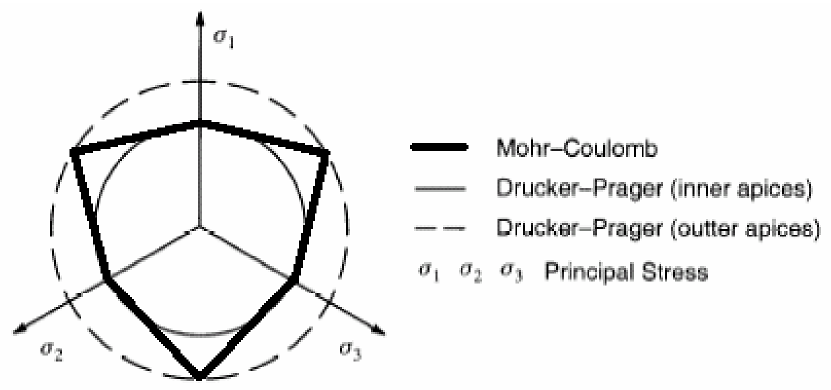

Figure 2.15. Cross-sections of Mohr-Coulomb and Drucker-Prager criteria.

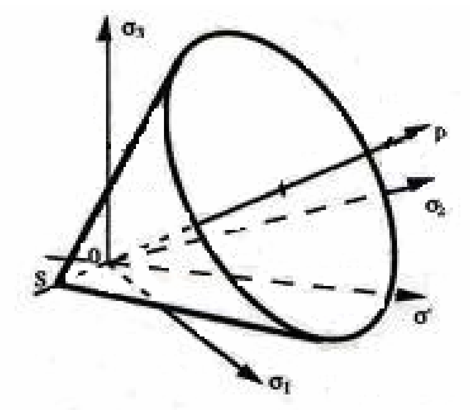

Figure 2.16. The Drucker-Prager conical surface principal stress space (after Guezouli et al. 1993).

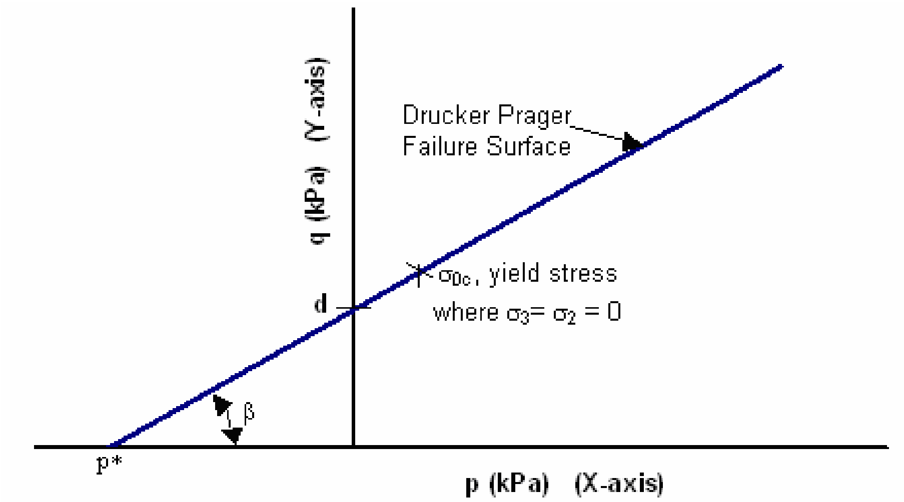

Figure 2.17. Drucker-Prager yield condition in 2D *p-q* stress space.

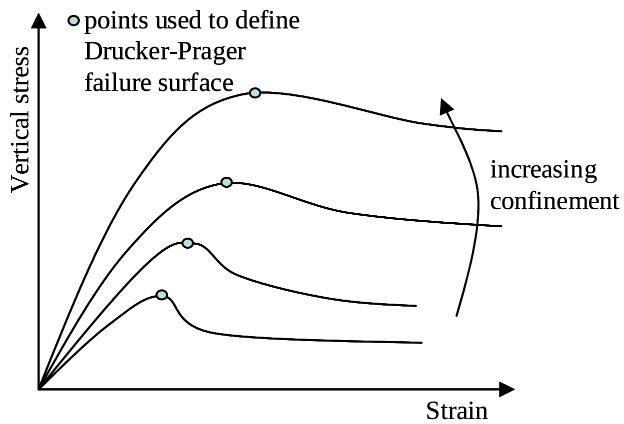

Figure 2.18. Monotonic shear failure test results from the triaxial apparatus.

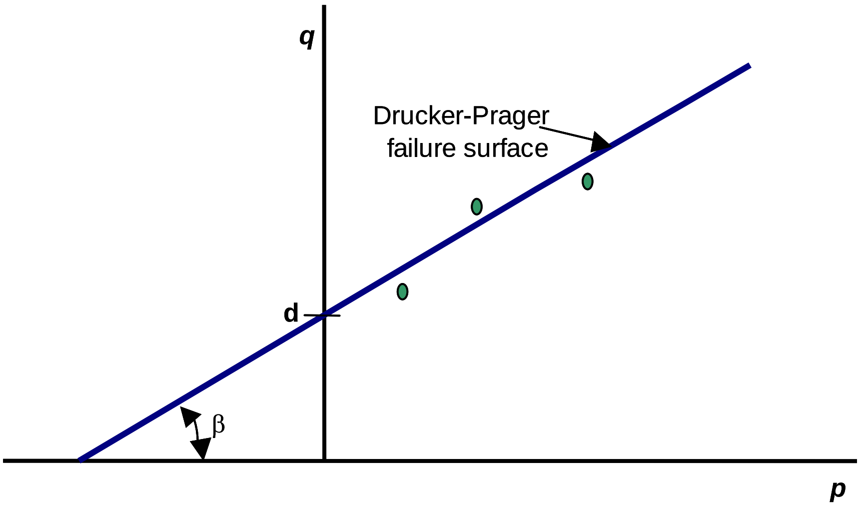

Figure 2.19. Yield stress values from Figure 2.18 plotted in *p*-*q* stress space to define the Drucker-Prager failure surface.

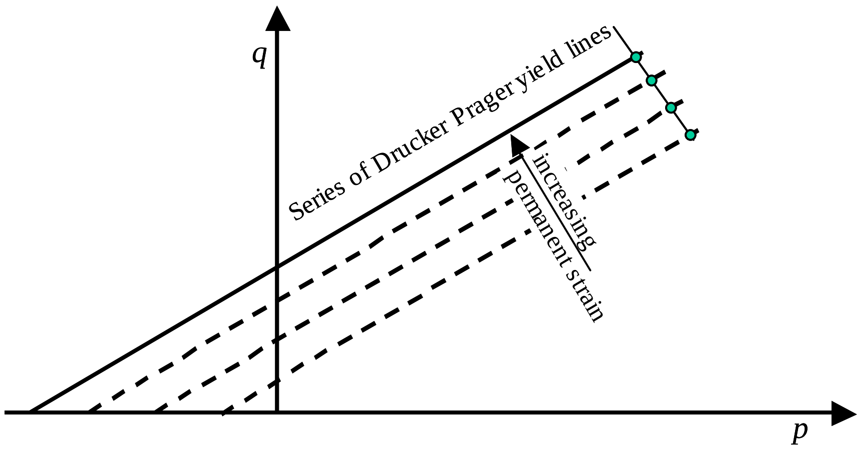

Figure 2.20. Series of Drucker-Prager yield lines that result as the material hardens/deforms.

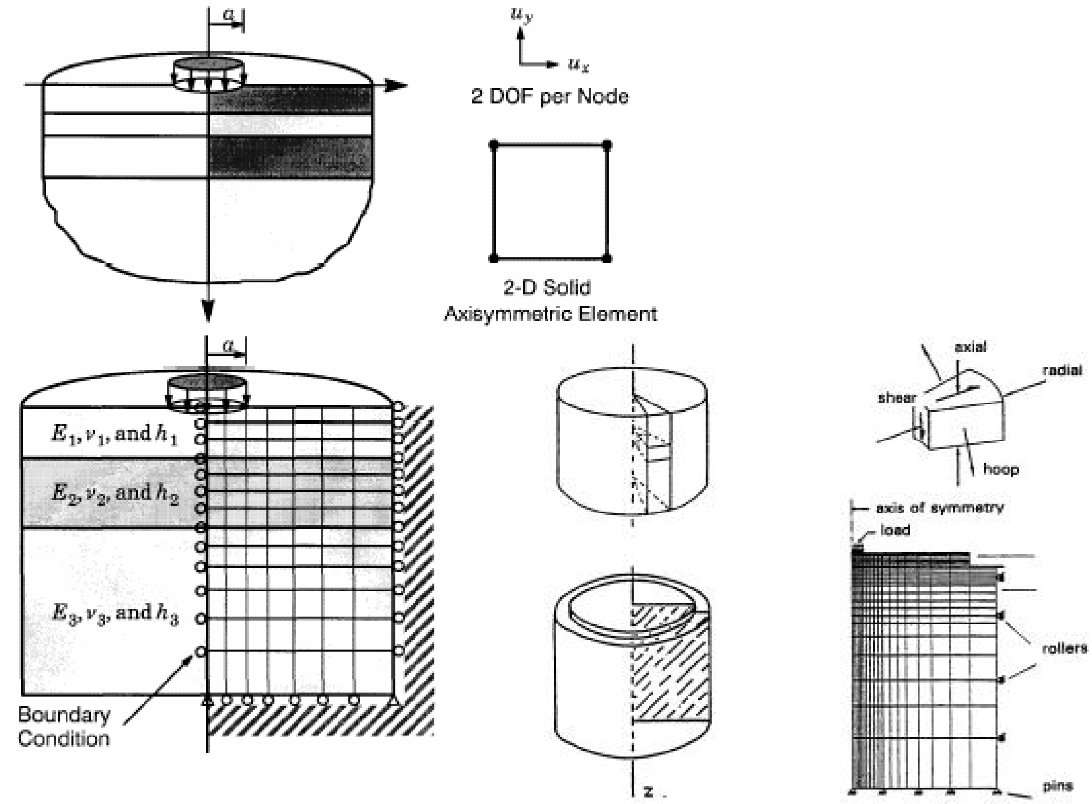

Figure 2.21. Axisymmetric 2D finite element model.

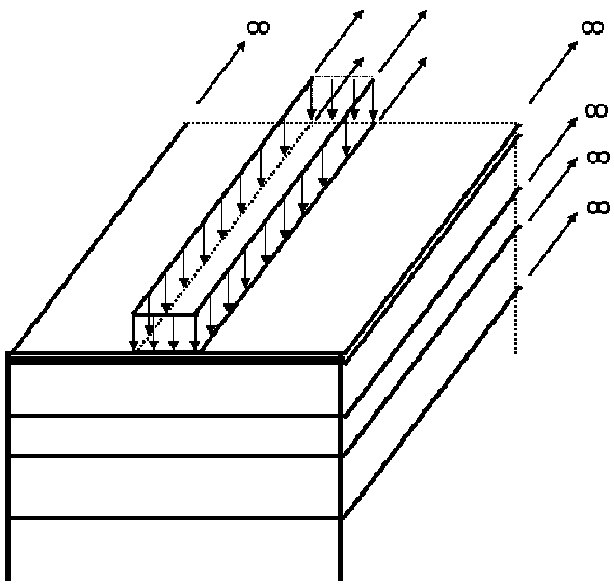

Figure 2.22. 2D plane strain finite element model.

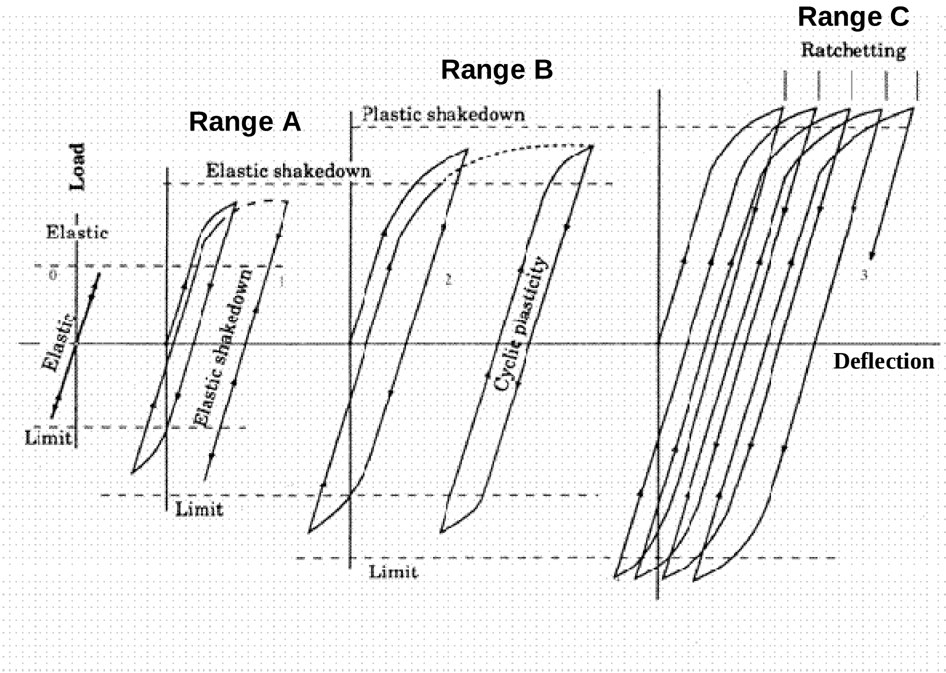

Figure 2.23. Elastic/plastic behaviour under repeated cyclic load (after Johnson, 1986)

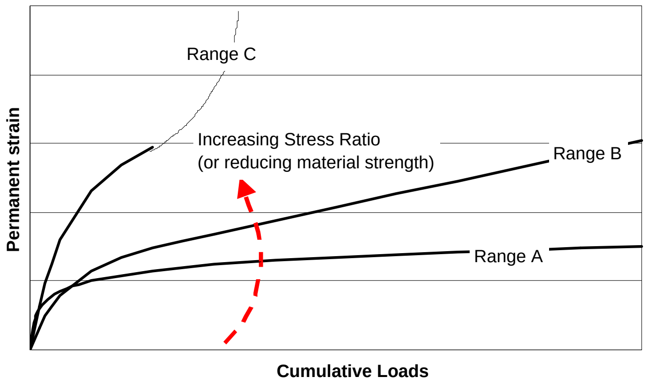

Figure 2.24. Shakedown range behaviours for permanent strain versus cumulative loading.

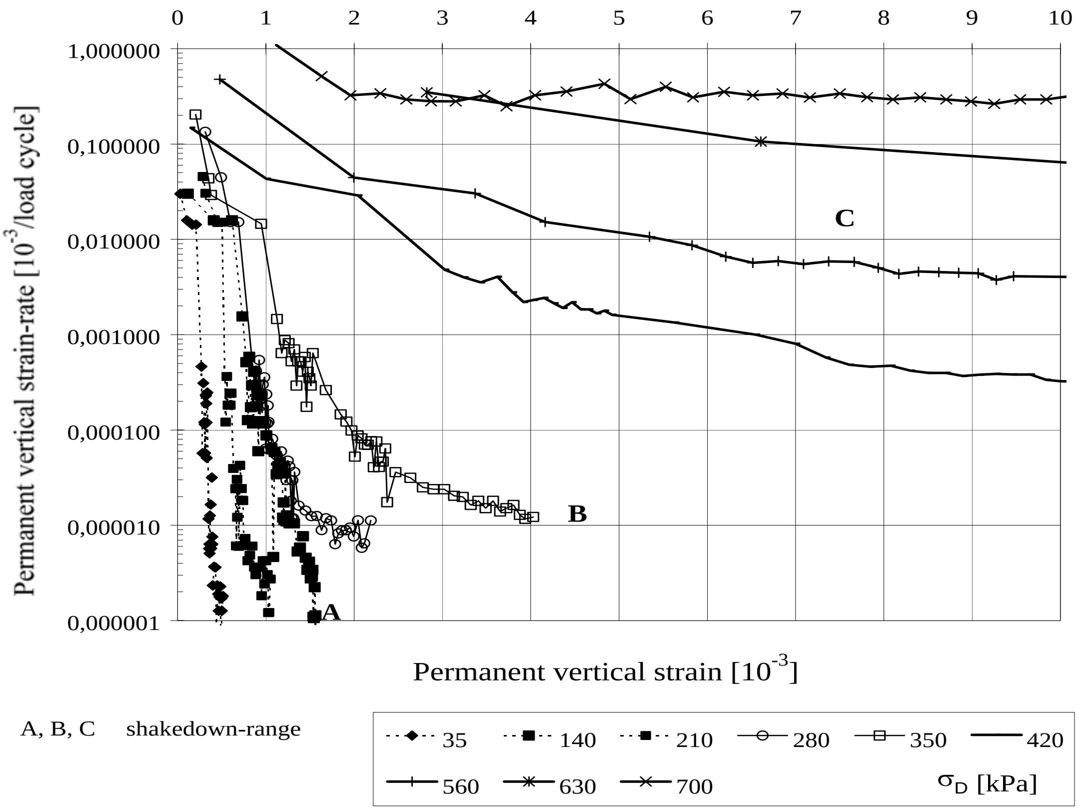

Figure 2.25. Cumulative permanent strain versus strain rate plot showing shakedown ranges (after Werkmeister et al 2001).

CHAPTER 3 LABORATORY TESTING

3.1 INTRODUCTION

One of the objectives of this study is to examine the permanent deformation behaviour of unbound granular materials in view of the shakedown behaviour ranges (Section 2.11.2). The aim is to incorporate the shakedown ranges/permanent deformation behaviour of UGMs into existing finite element techniques and pavement modelling for the purpose of predicting long term permanent deformation/rutting behaviour of the pavement. The shakedown concept has been described in Section 2.11.2 in terms of three permanent deformation behaviours referred to as shakedown Ranges A, B and C. Section 2.11.2 describes how to identify these ranges from Repeated Load Triaxial (RLT) permanent strain tests where permanent strain/rutting versus loading cycles is recorded. Repeated Load Triaxial apparatus simulates cyclic loading on cylindrical samples of unbound materials at specified testing stresses and is well suited for assessing the deformation behaviour of soil and granular materials at specific stress levels (Section 2.5.1).

Stress was identified in Section 2.6.1 to have the most significant effect on permanent strain. Further, many permanent strain models identified in Table 2.1 utilise stress condition, often characterised by stress invariants p and q (Section 2.4.3) as primary inputs. Thus, RLT permanent strain testing will be conducted on a range of materials with the aim to relate shakedown ranges A, B and C to testing stress invariants p and q. The testing stresses will be chosen to ensure the full spectra of stresses possible in a pavement are covered. A picture/pattern or relationship was therefore developed from the RLT tests to describe the stress conditions where the various shakedown ranges occur. Parameters for non-linear elastic resilient models are also determined. Results of these analyses will be used in pavement modelling in Chapter 6 *Finite Element Modelling* and Chapter 7 *Modelling Permanent Deformation* to predict the behaviour range (A, B and C) and surface rut depth of the pavement as a whole respectively. However, further analysis of the *raw* RLT permanent strain results was undertaken in Chapter 7 *Modelling Permanent Deformation* to develop a constitutive model for the prediction of permanent strain.

The range of unbound granular materials tested related to materials where full scale pavement test data were available. This will allow the predictions of shakedown behaviour range in Chapter 6 *Finite Element Modelling* and rut depth in Chapter 7 *Modelling Permanent Deformation* to be assessed against actual field results.

This chapter covers the materials, laboratory tests (predominantly Repeated Load Triaxial tests) and results. Limited analysis of the results in terms of the shakedown concept and resilient behaviour are also reported.

3.2 REPEATED LOAD TRIAXIAL APPARATUS (RLT)

This laboratory study evolved around the use of the University of Nottingham's Repeated Load Triaxial (RLT) apparatus (Figure 3.1). As discussed in Section 2.5.1 the RLT apparatus approximates cyclic loading of granular and soil materials. Tests for many load cycles (at least 50,000) at the same testing stresses (loaded and unloaded) are for permanent strain tests where the result is a plot of permanent strain (Equation 2.22) versus number of load cycles. Resilient modulus (Equation 2.23) is determined from many tests at different stress levels on the same specimen usually for 100 loading cycles at a time. The triaxial apparatus is also used for monotonic shear failure tests either strain or stress controlled.

The features of the University of Nottingham's 150mm diameter RLT apparatus for testing granular materials with particle sizes up to 40mm (Brown et al, 1989) are illustrated in Figure 3.2 and Figure 3.3 and are described as follows:

- use of closed loop servo-hydraulic loading systems for cycling both deviator and confining stresses;
- accurate measurement of axial and radial deformations directly on the test specimen using LVDTs and by cast epoxy strain hoops fitted with foil strain gauges respectively;
- measurement of axial load on the top platen;
- measurement of pore water pressure;
- computer control and data acquisition.

3.3 MATERIALS

A total of 6 unbound granular materials (UGMs) and one subgrade soil (a silty clay) were tested. These materials were chosen as they have been used in full scale pavement trials as described in Chapters 4 *New Zealand Accelerated Pavement Tests* and 5 *Northern Ireland Field Trial*. The Northern Ireland field trial pavement was constructed as part of this research project, while the Author was the key researcher (both before, during and after this research project) in the New Zealand Accelerated Pavement Tests at Transit New Zealand's CAPTIF (Canterbury Accelerated Pavement Testing Indoor Facility). This allows the predictions of deformation behaviour originally derived from RLT test results to be assessed against actual field measurements of rut depth. Four UGMs (*CAPTIF 1*, *2*, *3* and *4*) and the subgrade (*CAPTIF subgrade*) tested were used at CAPTIF located in Christchurch New Zealand. The other two UGMs (*NI Good* and *NI Poor*) were sourced from Northern Ireland and were used in the field trial built at Ballyclare in Northern Ireland, UK. The aggregates from Northern Ireland are both greywackes from the same quarry (Tullyraine's, Banbridge, Northern Ireland, UK) where one is of less quality and usually discarded as waste and has a slight red colour, hence named as *NI Poor* (red discarded aggregate) and *NI Good* (aggregate frequently used on highway projects in Northern Ireland). Table 3.1 summarises the different materials used in the pavement trials and tested in the RLT apparatus.

Table 3.1 Materials tested in the Repeat Load Triaxial apparatus.

Material Name	Description
NI Good	Premium quality crushed rock - graded aggregate with a maximum particle size of 40mm from Banbridge, Northern Ireland, UK.
NI Poor	Low quality crushed quarry waste rock - graded aggregate (red in colour) with a maximum particle size of 40mm from Banbridge, Northern Ireland, UK.
CAPTIF 1	Premium quality crushed rock – graded aggregate with a maximum particle size of 40mm from Christchurch, New Zealand.
CAPTIF 2	Same as CAPTIF 1 but contaminated with 10% by mass of silty clay fines.
CAPTIF 3	Australian class 2 premium crushed rock – graded aggregate with a maximum particle size of 20mm from Montrose, Victoria, Australia.
CAPTIF 4	Premium quality crushed rock – graded aggregate with a maximum particle size of 20mm from Christchurch, New Zealand.
CAPTIF Subgrade	Silty clay soil used as the subgrade for tests at CAPTIF from Christchurch, New Zealand.

3.3.1 CAPTIF Materials

The CAPTIF materials sourced in New Zealand (CAPTIF 1, 2 and 4) are all crushed alluvial gravel (greywacke) from a quarry located at Pound Road, Christchurch, New Zealand. The rock is angular, hard, light bluish-grey sandy medium gravel with minor silt. CAPTIF 1 and 4 materials comply with New Zealand’s national *Specification for Basecourse Aggregate* (TNZ M4, 2002). Compliance with this specification allows the use of these materials on state highways in the top 150mm layer of a thin surfaced (<25mm) unbound granular pavements. Further, CAPTIF 1 and 4 materials are well graded with nil plastic fines (plasticity index=0) with only 3% fines (i.e. mass passing the 75 μm sieve). Good performance is expected with CAPTIF 1 and 4 materials, while poor performance is expected for the CAPTIF 2 material, as although the same as CAPTIF 1, 10% by mass of silty clay fines were added to produce the CAPTIF 2 material.

The Australian material (CAPTIF 3) is similar to the premium New Zealand materials (CAPTIF 1 and 4). This material has nil plastic fines (plasticity index=0) and complies with the New Zealand specification (TNZ M4, 2002). In Australia, the material is considered as class 2 premium crushed rock. The source material is a rhyolite, acid igneous rock from Boral quarry at Montrose, Victoria, Australia. The rock is angular, rough, hard and blue-grey in colour.

The 1200mm thick subgrade used in all the tests at CAPTIF is classed as Waikari clay. Waikari clay is composed of quartz and minor feldspar with smectite and minor illite and kaolinite forming the clay mineral component (Pidwerbesky, 1996). The CAPTIF Subgrade is a clay with low plasticity with a Unified Classification System of *CL*. Laboratory charactirisation tests on the CAPTIF Subgrade (Pidwerbesky, 1996) found a Liquid Limit of 28%, a Plasticity Limit of 14%, a Plasticty Index of 14% and 72% by mass passing the 0.075mm sieve. This material was subjected to the same tests as the aggregate to enable complete deformation models of the CAPTIF pavements, which include both aggregate and subgrade layers, to be developed.

3.3.2 Northern Ireland Aggregates

Two aggregates from Northern Ireland were chosen for testing being those used in the field trial detailed in Chapter 5. They are both greywackes from the same quarry (Tullyraine's, Banbridge, Northern Ireland, UK) where one is of less quality and usually discarded as waste and has a slight red colour (*NI Poor*). These aggregates are later referred to as *NI Good* and *NI Poor*. The *NI Good* aggregate complies with the Highways Agency specification for sub-bases and is commonly used on highways in Northern Ireland. Based on its use the *NI Good* aggregate should show good performance in the tests. Although there is no history on the use of the *NI Poor* aggregate, it is expected the tests will show a weak material.

The greywacke, according to BS 812 Part 1: 1975, is part of the gritstone group of aggregates that embraces a large number of sandstone type deposits. Greywacke is one of the major sources of coarse aggregate in Northern Ireland. It outcrops in large areas of Counties Down and Armagh and comprises greywacke from both the Ordovician (505 M years ago) and Silurian (440 M years ago) period.

Greywackes are typically inter-bedded with marine shales or slates, and are associated with submarine lava flows. They are generally of marine origin and may have been deposited by turbidity currents. They are low-grade metamorphic rocks, which have been altered under the influence of heat and low pressure. The lower quality aggregate may be caused by inter-bedded red shales which is common for greywacke deposits. However, shale beds are typically only 10 to 40 cm thick while the red coloured lower quality aggregate encountered at the quarry in Banbridge was a large deposit with a bed thickness of at least 3m.

3.3.3 Particle Size Distribution (PSD)

All the materials when received were dried and broadly separated into different size fractions using the large sieves/drier in the concrete laboratory at the University of Nottingham. The resulting particle size distributions (PSD) compared with the limits posed in the New Zealand specification (TNZ M/4, 2002) as detailed in Figures 3.4, 3.5, and 3.6. Samples for laboratory testing were later re-mixed to the exact same PSD every time. This ensured consistent samples in triaxial tests, to minimise error resulting from differences in sample preparation. As discussed in Section 2.6.8, higher voids content caused by lack of fines in the PSD will have more potential for further densification causing greater deformation. In contrast higher fines content at high moisture contents can cause a build up of pore water pressure in a Repeated Load Triaxial test and weaken the sample.

Particle size distributions (PSD) show the CAPTIF 2 and 3 granular materials to have significantly more fines (10% passing the 0.075mm sieve) than the other materials. CAPTIF 1 and 4 aggregates have only 5 and 0% passing the 0.075mm sieve respectively.

Gradings for the two Northern Ireland materials are almost identical (Figure 3.6) except the *NI Poor* material had a higher percentage of larger stone sizes, in some cases up to 50mm in diameter. The similar gradings of the two materials indicates that the previously discarded *NI Poor* material may provide adequate performance and the use of the name *NI Poor* may be misguiding. However, the quarry owners report the *NI Poor* material strength reduces significantly when wet and its use is reserved for footpaths and carparks etc. Stones as large as 50mm cannot be included in the RLT tests as the recommended maximum particle size that can be tested is $1/5^{th}$ of the sample diameter. The University of Nottingham RLT apparatus test samples are 150mm diameter. Therefore, the as-received PSD of the NI Poor material was adjusted by replacing the mass of stones greater than 28mm by material between 9.51 and 14mm in diameter for the purpose of RLT testing. The adjusted grading is illustrated in Figure 3.6 (*NI Poor – RLT*) and as can be seen the effect brings it closer to the PSD of the *NI Good* material.

As discussed in Section 2.6.5 *Effect of Moisture Content* and 2.6.8 *Effect of Grading, Fines Content, and Aggregate Type* fines are likely to affect test results. Higher fines will reduce drainage and thus at high levels of saturation pore water pressures can build up and weaken the material which will result in higher deformations. In contrast greater fines content will reduce the amount of voids in the compacted material and thus limit the amount of densification and reduce the amount of deformation under repeated loading.

3.4 COMPACTION TESTS

To establish the target dry density and moisture content for materials tested in the Repeated Load Triaxial (RLT) apparatus compaction tests were undertaken. As these materials were granular and constructed in the field trials using vibrating steel rollers a vibrating hammer test was employed. Further, the New Zealand specification for field compaction of pavements (TNZ B2, 1997) requires a target compacted density of 97% of maximum dry density (MDD) and prior to sealing dried back to a moisture content 70% of optimum moisture content (OMC), where MDD and OMC are those values obtained from the vibrating hammer compaction test (British Standard BS 1377-4: 1990 - 3.7 *Method using vibrating hammer*). These targets were used for the construction of the Northern Ireland and New Zealand pavement tests. As the performance of pavements in the tests will be compared to predictions originally derived from RLT tests it is important the samples tested are the same density and moisture as the in-service values. Therefore, it was decided to use the same targets used in New Zealand for the construction of pavements (i.e. 97%MDD and 70%OMC) for the compacted RLT samples. However, the compaction targets for CAPTIF subgrade triaxial samples were the same moisture content and density achieved insitu at the test track, as fine grained soils are not suited for a vibrating hammer compaction test. RLT samples were compacted at the final target moisture content rather than at OMC and then dried back. Drying back the sample is not usually considered for RLT samples due to the difficulty in obtaining the target moisture content. Compacting at the target moisture content will have the effect of increasing the required compactive effort when preparing the RLT samples, compared to the effort required to compact at optimum.

For the granular materials vibrating hammer compaction tests were conducted in accordance with BS 1377-4: 1990 - 3.7 *Method using vibrating hammer*. To undertake the compaction test at least 5 samples are prepared at 5 different moisture contents and then compacted in a mould for 1 minute using a 600 to 800 Watt Kango Hammer. All the samples were prepared to their as received PSD as described in Section 3.3.3, with the exception that material greater than 20mm in diameter was removed, as required for the 100mm diameter mould. The effect of removing the material greater than 20mm was considered minor for the small sample weight (approximately 2kg) as it generally meant replacing one stone of greater than 20mm with a stone 14 to 20mm. The MDD and OMC and corresponding target values of 97%MDD and 70%OMC are shown in Table 3.2.

Table 3.2. Vibrating hammer compaction results.

	Vibratory hammer compaction.		Triaxial samples target	
Material	MDD (t/m^3)	OMC (%)	[1]DD (t/m^3)	[1]MC (%)
NI Good	1.90	5.00	1.84	3.5
NI Poor	2.10	7.51	2.03	5.25
CAPTIF 1	2.19	5.14	2.12	3.6
CAPTIF 2	2.28	4.67	2.21	3.27
CAPTIF 3	2.21	5.49	2.14	3.84
CAPTIF 4	2.17	5.64	2.10	3.95
CAPTIF Subgrade	-	-	1.84	8.50

1 With the exception of the CAPTIF Subgrade the dry density (DD) and moisture content (MC) were 0.97MDD (Maximum Dry Density) and 0.7OMC (Optimum Moisture Content) respectively.

In the compaction test each material achieved the same amount of compactive effort. The differences in MDD and OMC obtained are due to many factors such as: the source rock's solid density, inter particle friction, PSD and fines content. Ideally, total voids content from the solid density would be a more useful measure in comparing the MDD achieved for each material. However, it can be seen that aggregates with higher fines contents being CAPTIF 2 and CAPTIF 3 do result in the highest density due to the fact that the fines will fill the small void spaces between the stones. *NI Good* material achieved the lowest density most likely due to the solid rock having a low density.

3.5 RLT SAMPLE PREPARATION

Sample preparation involved re-mixing the dry material as per their particle size distribution (as received) to the weight required to achieve the compacted density for the sample. Water at the correct volume/weight was added last and a portable concrete mixer was used to thoroughly mix the granular material. A four piece aluminium split mould, bolted tightly together, with an inner silicon membrane attached was used to surround the sample during compaction. The inner membrane had studs attached for later attachment of steel threaded rods that would support the on-sample instrumentation.

Compaction was achieved in 6 layers with the use of a Kango Hammer as detailed in Figures 3.7 and 3.8. To ensure the compaction target was achieved evenly through the specimen, the sample was divided into three equal quantities. Compaction was checked regularly using $2/3^{rd}$ and $1/3^{rd}$ of the sample depth as targets for $1/3^{rd}$ and $2/3^{rd}$ of the sample weight respectively. A steel block was used to achieve a level surface to the correct sample height for the final layer as shown in Figure 3.9.

An output of this research was to develop a set of procedures for sample preparation. These procedures, entitled *11.18 Triaxial Testing*, are available from the online Quality Control Manual of the Pavement Research Building, NCPE, University of Nottingham and give a more complete description of sample preparation.

Generally, the samples prepared were adequate although occasionally the studs to support the instruments were not seated correctly. If this occurred the sample was emptied into the bucket and sample preparation re-started. To assist in the seating of the studs finer material of the aggregate was packed around the studs.

3.6 MONOTONIC SHEAR FAILURE TRIAXIAL TESTS

Monotonic shear failure tests were conducted on all materials for comparison with the RLT permanent strain results. As many pavements do not fail by shear, the RLT permanent strain tests are considered more representative of actual performance in the road. Nevertheless, the static Mohr-Coulomb yield strength parameters c and ϕ (Section 2.9.2) are well known. Further, it is commonly thought that safe stress states are those less than 70% of the static shear strength (Section 2.6.1).

Drucker-Prager (Section 2.9.3) and Mohr-Coulomb (Section 2.9.2) yield strength parameters were calculated for all materials and compared to the RLT permanent strain results and the shakedown behaviour Ranges A, B and C (Section 2.11.2) determined. Results of the monotonic shear failure tests were used as a guide for setting stress limits for the RLT tests, although bearing in mindTheyse’s (2002) observation that for fast repetitive loading, stress states in excess of the yield strength are possible.

Monotonic shear failure tests were conducted on 3 to 4 specimens for each material at different constant confining pressures of 25, 50, 75 and/or 100kPa. The shear failure test available on the University of Nottingham triaxial apparatus was a ramp test. The ramp test is a stress controlled test and was set to a constantly increasing stress of 5kPa per second until the sample failed. Strain controlled failure tests are considered best (Niekerk, et al. 2000) but were discounted as they cannot be performed on the Nottingham triaxial apparatus due to the large electrical noise from the LVDT in relation to the tiny displacement incrementssthat would be required each second.

Each triaxial sample for the ramp test was prepared as detailed in Section 3.5 except that on-sample instrumentation was not used. Instead, the deformation of the sample was measured using an external LVDT (Linear Variable Displacement Transformer). During the ramp tests vertical displacement versus load is electronically recorded. The maximum load achieved along with the cell pressure is noted as one stress state defining failure. This stress state was characterised in terms of stress invariants, p and q (Section 2.4.3). The results of at least 3 tests are required to define the Drucker-Prager yield line or surface in terms of slope and intercept (β and d, Figure 2.17) in p-q stress space. Mohr-Coulomb criteria (ϕ and c, Section 2.9.2) were then calculated from β and d as per Equations 2.57 and 2.58. Repeat tests were not conducted as the prime reason for the shear tests was to obtain an indication of stress limits for the Repeated Load Triaxial permanent strain tests. However, a fourth ramp test was sometimes needed as some samples did not fail within the loading limits (1200 kPa) of the triaxial apparatus when a 100kPa confining pressure was applied.

Figure 3.10 is the result of the monotonic shear failure tests at a range of cell pressures for the *NI Good* material. Similar tests were completed for all the materials and their failure surfaces determined as plotted in Figure 3.11. Table 3.3 shows the calculated Drucker-Prager yield failure parameters, intercept d and angle β in p-q stress space (Figure 2.19, Section 2.9.3). Also included are the values of Mohr-Coulomb cohesion (c) and friction angle (ϕ) (Section 2.9.2).

Table 3.3. Failure surfaces.

	Drucker-Prager (p-q stress space)		Mohr-coulomb	
Material	*d (kPa)*	β	*c (kPa)*	ϕ
NI Good	135	62	74	46
NI Poor	49	62	27	46
CAPTIF 1	61	64	35	50
CAPTIF 2	0	68	0	61
CAPTIF 3	103	61	55	44
CAPTIF 4	7	68	5	61
CAPTIF Subgrade	33	60	17	42

It should be noted that for CAPTIF 2 yield shear failure test results, the best fit straight line resulted in a negative intercept being calculated. A negative intercept or cohesion is not physically possible and therefore the straight line was forced through the origin.

Results of the monotonic shear failure tests show relatively high angles of internal friction for all materials. This means that as the level of confinement increases the yield strength will increase significantly. For a Drucker-Prager friction angle of 64 degrees (CAPTIF 1) then for every 1 kPa increase in confining stress will result in nearly a 2kPa ($\tan 64°$) increase in vertical deviatoric stress, q that can be sustained before failure. CAPTIF 3 material has the lowest friction angle of the materials and this maybe due to the dense grading that does not allow the build up of pore water pressure to dissipate.

The level of cohesive strength seen in most materials excluding CAPTIF 2 and CAPTIF 4 is due to the effect of matrix suction. Matrix suction is effectively negative pore water pressure that occurs in partially saturated materials. The effect of this suction is to pull particles together and significantly increase the apparent cohesion of the aggregate or soil. The importance of the matrix suction in determining the effective strength of partially saturated subgrades and granular materials is well understood and described by many authors (e.g. Theyse 2002, Oloo et al. 1997 and Brown 1996). Another reason for cohesive strength is the particle interlock having the effect of effectively joining stones to a limited degree. Individual stones have tensile strength some of which is transferred to an interlocked arrangement of stones. As pore water pressure was not measured during the shear failure tests, the cohesion is calculated based on total stress values. In reality, in partially saturated materials, the pore water pressure is a negative value and subtracting this value from the total mean princial stress (p) will mean that the principal effective stress, p', is to the right of the value of p. Effective cohesion, expressed ijn this way would be substantially reduced compared to the level of total cohesion. Hence, nearly all of the cohesion reported in Table 3.3 is expected to be due to suction or negative pore water pressure.

The yield strength parameters for the CAPTIF 2 and CAPTIF Subgrade materials are a surprise result. CAPTIF 2 is the same as CAPTIF 1 but with 10% by mass of silty clay soil (actually the CAPTIF Subgrade soil) added. It is expected the effect of this silty clay soil would be to reduce the friction angle due to the introduction of plasiticity to the aggregate and increase cohesion due to soil particles bonding together. However, the opposite occurred for the CAPTIF 2 material and is probably due to the CAPTIF Subgrade being a low plasticity clay (Section 3.3.1). The CAPTIF Subgrade which is a silty-clay soil showed an unexpected high friction angle, nearly as high as several granular materials, however, the friction angle determined from RLT tests defining when shakedown Range C (failure) occurs is significantly less (Table 3.4) and thus suggesting that the friction angle in Table 3.3 is in error.

Ideally the monotonic shear failure tests should have been repeated to reduce the errors in the results by identifying outliers, however, these errors willonly become apparent when comparing the stress states at which failure occurred in the RLT permanent strain tests.

3.7 RLT TEST CONDITIONS

The aim of RLT tests was to determine the effect of stress condition on permanent strain (see Section 3.1). RLT permanent strain tests are time consuming and many tests are needed to cover the full spectra of stresses expected within the pavement. To ensure sufficient RLT tests covering the required stress levels for the 6 granular and 1 subgrade material were conducted repeat tests with variations of particle size distribution, compacted density and moisture content could not be scheduled. However, as discussed in Sections 2.6 and 2.7, it is recognised that all these factors will affect the permanent and resilient strain behaviour. Nevertheless, the overall aim is to develop stress based models to predict the rutting behaviour and magnitude for actual pavement tests. Therefore, density and moisture content of the RLT specimens were close to those estimated in-service within the constructed pavement tests. RLT testing stresses are described in the fully loaded state in terms of stress invariants p (mean principal stress) and q (deviatoric stress) as defined in Section 2.4.3. Stress invariants are a convenient way of describing 3-dimensional stress states and are commonly used in relationships for permanent strain (Table 2.1).

To cover the full spectra of stresses expected in a pavement (Figure 3.12, after Jouve and Guezouli, 1993) a series of permanent strain tests was conducted at different combinations of cell pressure and cyclic vertical load. As shown in Figure 3.12 the bulk of the stresses calculated show the mean principal stress (p) varies from 50 to 300 kPa and the deviatoric stress (q) from 50 to 700 kPa. These ranges of stresses were confirmed with some pavement analysis using the CIRCLY linear elastic program (Wardle, 1980). Although at the base of the granular layers negative values of mean principal stress p were calculated, as a granular material has limited tensile strength negative values of mean principal stress were discounted. The results of the static shear failure tests plotted in *p*-*q* stress space (Figure 3.11) were used as an approximate upper limit for testing stresses.

It is common that a new specimen is used for each stress level. However, to reduce testing time multi-stage tests were devised and conducted. These tests involved applying a range of stress conditions on one sample. After application of 50,000 load cycles (if the sample had not failed) new stress conditions were applied for another 50,000 cycles. These new stress conditions were always slightly more severe (i.e. closer to the yield line) than the previous stress conditions.

For multi-stage testing it seemed sensible to simply increase the vertical cyclic stress each time, while keeping the cell pressure constant. Keeping cell pressure constant is common in many RLT standards (CEN 2000; Australia Standards 1995; and AASHTO 1994). For each cell pressure value a new specimen would be used. However, this testing approach (keeping cell pressure constant) does not adequately cover the full spectra of stresses for future interpolation for other stresses not tested. Further, it is nearly parallel with the yield line and will take many tests with increases in vertical load to cross through it, and therefore distinct differences between permanent strain behaviour may not occur (assuming the closer the testing stress is to yield then the higher the amount of permanent strain).

Testing stresses were chosen by keeping *p* (average of principal stresses) constant while increasing *q* (principal stress difference) for each new increasing stress level moving closer and occasionally above the yield line. Three samples for each material were tested at three different values of maximum mean principal stress *p* (75, 150 and 250 kPa). This covered the full spectra of stresses in *p*-*q* stress space for later interpolation of permanent strain behaviour in relation to stress level. An example of the stress paths tested in comparison with the monotonic shear failure line are shown in Figure 3.13 for the CAPTIF 1 aggregate. The stress paths along with the full results for all the materials tested are given in Appendix A.

For each stress path at least 50,000 load cycles were applied at a speed of 5 hertz. After 50,000 cycles the vertical stress level was increased and the cell pressure reduced in order to keep *p* (principal stress average) constant. Vertical loading was a sinusoidal pulse at 5 times a second. Review of other RLT permanent strain tests (Werkmeister et al. 2000; Dodds et al. 1999; and Niekerk, 2000) do show that the trend in behaviour (i.e. permanent strain rate is either decreasing (Range A), constant (Range B), or increasing (Range C)) is evident after 20,000 load cycles and therefore 50,000 load cycles is considered sufficient. However, for the later permanent strain modelling in Chapter 7 the 50,000 load cycles were extrapolated based on an assumed relationship to 2 million load cycles. Further, keeping the number of load cycles to 50,000 ensured sufficient time to complete the testing for the 6 aggregates and 1 subgrade material.

3.8 RESULTS

3.8.1 Data Processing

During Repeat Load Triaxial testing, at pre-set regular intervals of loading, vertical displacement with on-sample LVDTs was recorded at a frequency of 1000 times a second during load cycle intervals of: 0-10; 50-100; 190-200; 290-300; 390-400; 490-500; 590-600; 690-700; 790-800; 890-900; 990-1000; 1490-1500; 1990-2000; 2490-2500; 2990-3000; 3990-4000; 4990-5000; 7990-8000; 9990-10000; 14990-15000; 19990-20000; 24990-25000; 29990-30000; 34990-35000; 39990-40000; 44990-45000; 49990-50000 . The recorded data were processed in a spreadsheet along with a Visual Basic program to determine the average, maximum and minimum values for 10 loading cycles prior to the loading interval in question. There were many electrical spikes in the data which the programme first removed, then smoothed, before averaging. The data were further processed to calculate the permanent strain (Equation 2.22) versus number of load cycles as well as elastic strains (Equation 2.21) for each testing stress.

3.8.2 Permanent Strain and Shakedown Ranges

Permanent strain versus number of load cycles for the CAPTIF 1 material in the multi-stage RLT test where the maximum mean principal stress (*p*) for all the stages of the test is 250kPa as shown in Figure 3.14. This trend in results is similar to the other multi-stage RLT permanent strain tests where as the testing stress approaches the yield strength of the material, i.e. the rate of deformation gradually increases until a stress level is reached where the sample fails before the specified 50,000 cycles are completed.

The full results of the permanent strain tests along with some preliminary analysis in terms of assessing the shakedown range behaviours (A, B or C) as per Section 2.11.2 is shown in Appendix A. As a reminder shakedown Range A is where the rate of deformation is decreasing with increasing load cycles (i.e. stable behaviour). Shakedown Range C is excessive deformation leading to premature failure of the sample, while Range B is between Ranges A and C where the long term permanent strain rate is constant. To assist in determining the behaviour Ranges the permanent strain versus average permanent strain rate (permanent strain divided by total number of loads) is plotted as shown in Figure 3.14 for the maximum mean principal stress, *p*=250kPa for the CAPTIF 1 material. Appendix A shows the results of RLT permanent strain tests for other stress levels and materials reported graphically similar to Figure 3.14 .

After the shakedown range is determined for each testing stress the boundary between these ranges is interpolated assuming a linear function and plotted in *p-q* stress space. The boundary between shakedown Range A and B was taken as the best fit straight line through the highest vertical testing stress possible for shakedown Range A for the 3 tests at maximum principal stress *p*=75, 150 and 250kPa. A best fit straight line was fitted to the lowest vertical stresses where shakedown Range C occurred for the

B/C boundary. Figure 3.15 show the shakedown range boundaries for all the materials tested. For comparison the yield line is also shown. These shakedown range plots can then be used in predicting the likely performance of the material in the pavement as done in finite element modelling conducted in Chapter 6. It is assumed that if traffic induced stresses computed within the pavement material all plot below the shakedown Range A/B boundary in *p-q* stress space then stable/Range A behaviour of the material is expected.

The linear functions indicating the stress boundaries between shakedown Ranges A, B and C are summarised in Table 3.4 in terms of intercept (d) and slope (β). For comparison the equivalent Mohr-Coloumb parameters (c and ϕ) are determined.

Table 3.4. Shakedown range boundaries.

	Shakedown range boundary A-B				**Shakedown range boundary B-C**			
	p-q stress space		Mohr-Coloumb		*p-q* stress space		Mohr-Coloumb	
Material	*d (kPa)*	β *(°)*	*c (kPa)*	ϕ *(°)*	*d (kPa)*	β *(°)*	*c (kPa)*	ϕ *(°)*
NI Good	10	58	5	39	59	65	35	52
NI Poor	65	39	31	21	114	56	57	36
CAPTIF 1	39	48	19	28	63	61	34	44
CAPTIF 2	0	45	0	25	0	62	0	46
CAPTIF 3	32	54	16	34	33	65	20	52
CAPTIF 4	31	40	15	22	0	66	0	55
CAPTIF Subgrade	22	28	10	14	0	62	0	46

It should be noted that negative values of intercepts are not physically acceptable and in such cases that this did occur a best fit line was forced through the origin. This adjustment did not significantly affect the goodness of fit to the data points defining the shakedown boundaries.

Criteria defining the boundary between shakedown Range B and C beheaviour are in effect failure criteria, as Range C behaviour is when failure occurs. Therefore, the criteria defining monotonic shear failure (Table 3.3) should be close to the criteria defining the shakedown Range B/C boundary. This is the case for most materials (ie. friction angles are within 4 degrees) except the *NI Poor* and *CAPTIF 2* materials. The shakeown range boundary B/C had friction angles 6 degrees less than those determined from the shear failure tests for the *NI Poor* and *CAPTIF 2* materials. As it is considered the *NI Poor* and *CAPTIF 2* materials are weaker than the other materials (excluding the subgrade) it is likely the friction angles determined from the shakedown range boundary B/C are the more appropriate values to define when failure occurs.

The shakedown boundaries plotted in *p-q* stress space (stress invariants, Section 2.4.3) can be considered design criteria. Should the stress distribution in the pavement be known, then in theory these stresses could be plotted alongside the shakedown range boundaries in Figure 3.15 to make an assessment on the behaviour range expected for the pavement as a whole. Shakedown Range B/C boundary does represent failure in the RLT permanent strain tests and as expected it is plotted close to the yield line determined from monotonic shear failure tests. The shakedown Range B/C boundary for all the materials appears similar and indicates an unusual result that the CAPTIF Subgrade is as strong as the CAPTIF 1 material. Differences in material strength are better distinguished with the shakedown Range A/B boundary as the CAPTIF Subgrade is clearly shown to be the weakest material (i.e. Range A/B boundary has the flattest slope).

3.8.3 Elastic Strain and Non-Linear Elastic Modelling

The elastic strains were used to determine the constants in the non-linear porous elasticity model later used in finite element modelling (Chapter 6). Porous elasticity (Equation 2.28) is the only suitable available model in the ABAQUS finite element package as used in this study. ABAQUS was chosen because it is becoming the general finite element model of choice for universities. Further, it is outside the scope of the research (primarily concerned with permanent strain and rutting) to program in ABAQUS a more commonly used non-linear resilient model like the Boyce model as used by Akou et al. (1999), Jouve & Guezouli (1993); Schelt et al. (1993) and Wellner & Gleitz (1999).

For each new stage of a RLT permanent strain test, stress level and the average elastic resilient strain in the vertical and for some tests in the horizontal direction (i.e. when the hoops were working) were determined. The elastic resilient modulus (M_r) was then calculated as the ratio between the maximum vertical cyclic deviatoric stress and the recoverable vertical elastic strain (Equation 2.21). Poisson's ratio was also calculated when the radial hoops were measuring correctly, otherwise the Poisson's ratio was assumed to equal 0.35. The resilient modulus and Poisson's ratio are needed in linear elastic models such as BISAR and CIRCLY. As discussed in Section 2.7 the elastic modulus is non-linear and its value depends on the level of stress. For comparison of material resilient properties/stiffnesses the resilient strain data was fitted to the simple k-θ model (Equation 2.27). The k-θ model is commonly used (e.g. Muhammad et al. 2003 and Wellner & Gleitz 1999) and more generally understood (Brown, 1996).

The bulk stress along with resilient modulus was calculated at each stress level tested in the multi-stage RLT permanent strain tests. Results for all the materials are shown in Figure 3.16 while Table 3.5 lists the constants $k1$ and $k2$ for the bulk stress model (Equation 2.27 where p_0 = 1 kPa). The k-θ model only approximates the non-linear resilient behaviour with r^2 ranging from 0.04 (CAPTIF 3) to 0.97 (CAPTIF 4). It is uncertain why there was such a poor correlation with the CAPTIF 3 resilient moduli. Although, many researchers (Hicks, 1970; Hicks & Monismith, 1971; Brown and

Hyde, 1975; Boyce, 1980; Sweere, 1990; Kolisoja, 1997; and Uzan, 1985) have found the k-θ was not the best non-linear elastic model due to assumptions that have proven to be incorrect, these being: Poisson's ratio is constant; and deviatoric stress (q) having no influence. Included in Table 3.5 are the calculated resilient moduli for bulk stresses of 100, 400 and 800 kPa. As can be seen the CAPTIF 4 material is the stiffest for high bulk stresses while the CAPTIF 3 material has the highest stiffness at low bulk stresses. It is interesting to note that the CAPTIF 2 material contaminated with 10% clay fines has the 2nd highest stiffness for high bulk stresses. In contrast, the permanent strain tests (Appendix A) show CAPTIF 2 to have the highest deformation of the granular materials.

Table 3.5. Resilient moduli from k-θ model (Equation 2.27).

	Constants		**Elastic Modulus, $E = k_1\theta^{k2}$ (Eqn. 2.27) (MPa)**		
Material	***k1***	***k2***	**θ=100kPa**	**θ= 400kPa**	**θ= 800kPa**
NI Good	71.51	0.29	269	400	488
NI Poor	103.46	0.23	303	419	492
CAPTIF 1	29.87	0.43	215	390	526
CAPTIF 2	3.20	0.77	110	321	546
CAPTIF 3	325.04	0.05	414	446	462
CAPTIF 4	1.00	0.94	77	286	550
CAPTIF Subgrade	10.85	0.49	105	208	293

The non-linear elastic behaviour will be modelled in the ABAQUS finite element package detailed in Chapter 6 *Finite Element Modelling* using the shear porous elasticity model available in the ABAQUS material library. The model chosen was based on best fit to measured volumetric elastic/resilient strains from multi-stage RLT permanent strain tests. The shear porous elasticity model is defined by Equations 2.28 and 2.29.

The values of k, p_t^{el}, p_0, e_0 and G are required to define the porous elasticity model (Equations 2.28 and 2.29) in ABAQUS. Elastic tensile limit (p_t^{el}) was set at 6kPa (value kept low as unbound pavement materials cannot support tensile stresses) while p_0 was set at 0 kPa. In theory, the value of p_0 is not zero but rather equal to the confining stress which was not cycled. However, the confining stress was different for each stage of the RLT multi-stage test and only one value of p_0 can be assumed in ABAQUS porous elasticity model. Solver in Microsoft Excel was used to determine the other constants such that the absolute sum of the difference between calculated and measured values are minimised. Table 3.6 lists the porous elasticity constants determined for each material along with mean error being the difference between measured and calculated. It can be considered from the results that the fit of this model to the data is poor. However, as plotted in Figure 3.17, the porous elasticity is showing the correct trend in results. The shear modulus model (Equation 2.28) is a better fit to the measured data as plotted in Figure 3.18 with a mean error from 20 to 100 kPa (Table 3.6).

Porous elasticity can also be defined in ABAQUS using the Poisson's form of porous elasticity model. However, no sensible relationships with the measured data could be found with this model. Further, as discussed it is outside the scope of this study to program a new material model in ABAQUS and therefore the shear porous elasticity model will be persisted with in Chapter 6 *Finite Element Modelling*.

Table 3.6. Porous elasticity constants.

	Porous elasticity constants				Mean Error (e^{el}) (μ m/m)	Shear Modulus G (MPa)	Mean Error (q) (k Pa)
Material	p_0 (MPa)	k	p_t^{el} (MPa)	e_0			
NI Good	0	0.0008	0.006	0.0014	*388*	213	*40*
NI Poor	0	0.0007	0.006	0.0014	*895*	171	*60*
CAPTIF 1	0	0.0008	0.006	0.0015	*274*	220	*25*
CAPTIF 2	0	0.0008	0.006	0.00015	*265*	207	*98*
CAPTIF 3	0	0.0006	0.006	0.0009	*431*	222	*33*
CAPTIF 4	0	0.0007	0.006	0.0012	*342*	182	*96*
CAPTIF Subgrade	0	0.0008	0.006	0.0017	*288*	108	*22*

One reason for the poor relationships of the non-linear models to the measured resilient strains/moduli from the multi-stage RLT permanent strain tests is the testing stresses chosen (e.g. Figure 3.13). The stress paths chosen were such that for several tests (3 up to 10) although the maximum deviatoric stress, q increased, the maximum mean principal stress, p remained constant. For a constant mean principal stress, the resilient modulus calculated with the k-θ model and the volumetric strain calculated from the porous elasticity model would remain the same regardless of changes in q. This effect is clearly shown in Figure 3.17 where many measured points are plotted along the same value of mean principal stress, p. It is postulated that researchers whom developed non-linear elastic relationships were derived from triaxial data with only 1 or 2 tests at stresses with the same mean principal stress. Particularly when many testing regimes in RLT standards developed (CEN 2000, Australia Standards 1995 and AASHTO 1994) keep the confining stress the same and simply change deviatoric stress (q).

3.9 SUMMARY

This chapter was focussed around the Repeated Load Triaxial apparatus for the purpose of understanding the permanent strain behaviour of 6 granular and 1 subgrade soil materials with respect to a range of loading stresses. All the materials tested have been used in accelerated pavement tests in New Zealand (Chapter 4) and a Northern Ireland field trial (Chapter 5), with the aim that the results of future modelling can be validated. Preliminary tests were conducted to determine the RLT testing conditions which included the specimen density and moisture content obtained from vibrating hammer compaction tests and testing stress limits found from monotonic shear failure tests. Some preliminary analyses of the RLT test results were conducted for the purpose of finite element modelling in Chapter 6 while more detailed modelling of permanent strain will be undertaken in Chapter 7 *Modelling Permanent Deformation.*

To cover the full spectra of stresses expected in a pavement multi-stage RLT permanent strain tests were derived. Results of these tests were reported in terms of cumulative permanent strain versus number of loading cycles (usually 50,000) for each set of testing stresses. For each testing stress the shakedown range behaviour was determined in terms of ranges A (long term permanent strain rate is decreasing), B (long term permanent strain rate is constant) and C (long term permanent strain rate is increasing and often the specimen fails). The fully loaded testing stresses were plotted in p (mean principal stress) -q (deviatoric stress) stress space with each point labelled with either shakedown Range A, B or C. It was found that a stress boundary existed between the various shakedown ranges. The shakedown Range B/C boundary plotted close to the yield line (obtained from monotonic shear failure tests) while the shakedown Range A/B boundary had a much lower gradient than the B/C boundary (approximately half).

It was proposed that plots showing the shakedown range boundaries along with stresses computed in a pavement are useful in pavement analysis where the shakedown range expected of the pavement as a whole can be predicted. Achieving shakedown Range A is best as this predicts an ever decreasing permanent strain rate where the amount of permanent strain may reach a maximum value after which no further permanent strain will develop, unless the load is increased or the material weakens (e.g. through ingress of moisture). Shakedown range boundaries will be used to predict behaviour of the pavements used in accelerated pavement tests and a field trial via finite element modelling reported in Chapter 6.

Resilient properties were also analysed from the RLT tests and fitted using two non-linear elastic models. The first model was the k-θ model a commonly used model that relates resilient modulus to bulk stress (sum of the principal stresses). Results showed the fit was not good and varied depending on the material. The granular material that resulted in the highest permanent strain from the RLT tests had the highest resilient modulus/stiffness. The parameters of the shear porous elasticity model, which relates volumetric strain to stress level, were also obtained from the RLT resilient data. Porous elasticity is the only non-linear model recommended for use by soils available in the ABAQUS finite element package which was used in pavement finite element modelling (Chapter 6). The fit to the porous elasticity model was poor although the model showed the correct trend.

Figure 3.1. University of Nottingham Repeated Load Triaxial (RLT) apparatus.

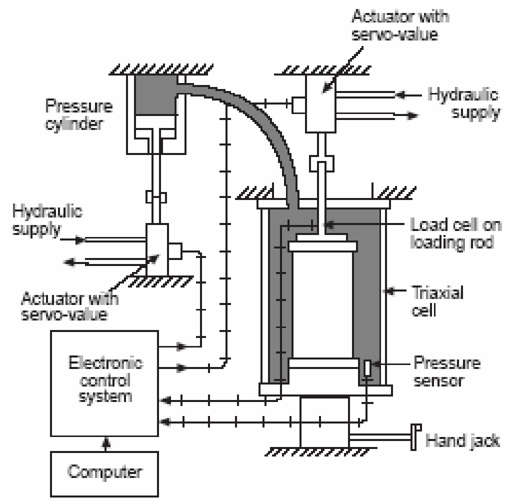

Figure 3.2. Schematic of University of Nottingham's RLT apparatus.

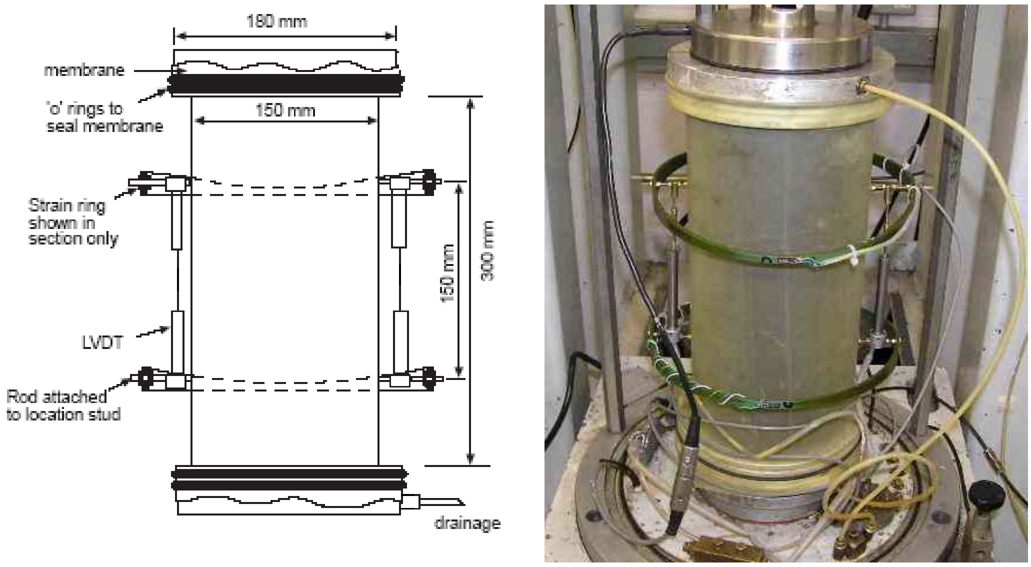

Figure 3.3. University of Nottingham's instrumented RLT sample enclosed in a silicon membrane.

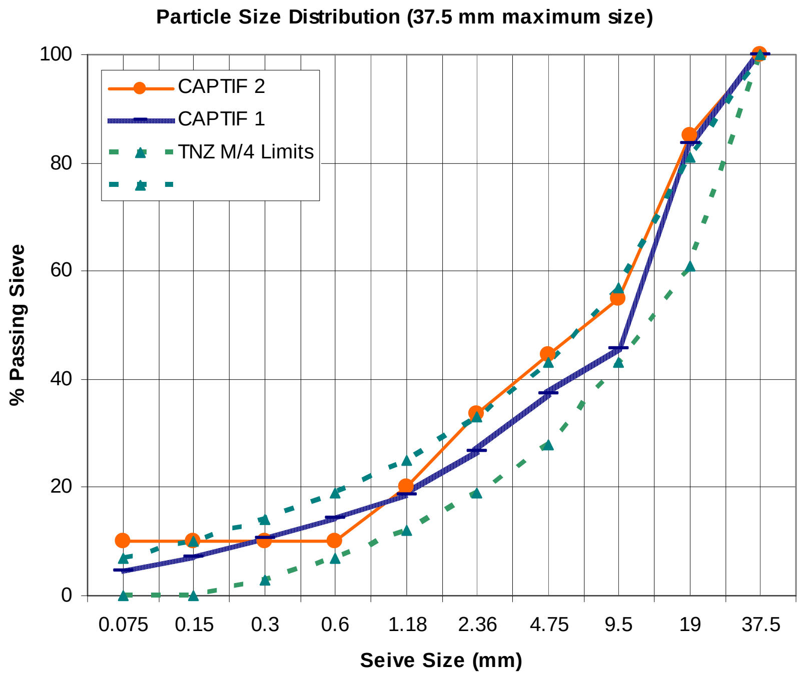

Figure 3.4. PSD of CAPTIF 1 and 2 aggregates (max. particle size of 37.5mm).

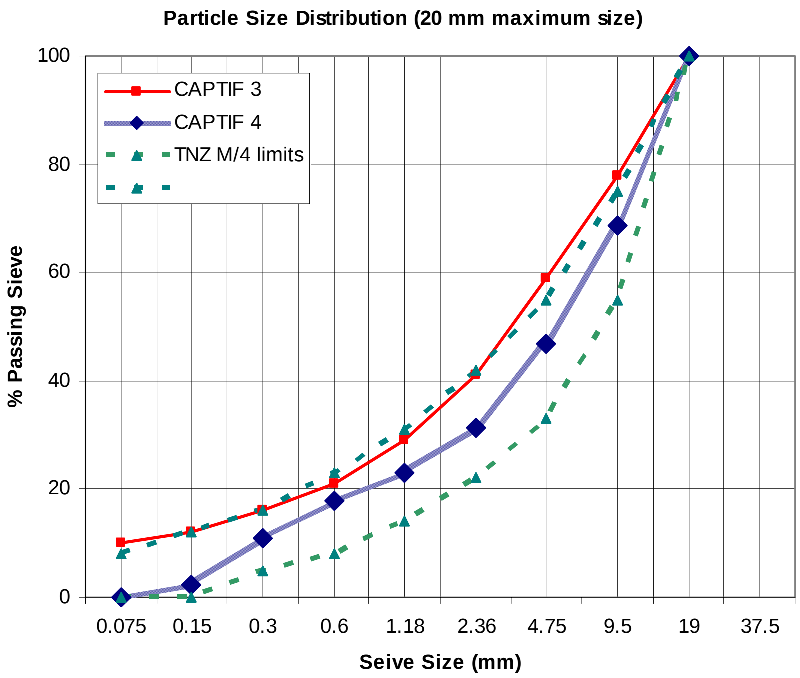

Figure 3.5. PSD of CAPTIF 3 and 4 aggregates (max. particle size of 20mm).

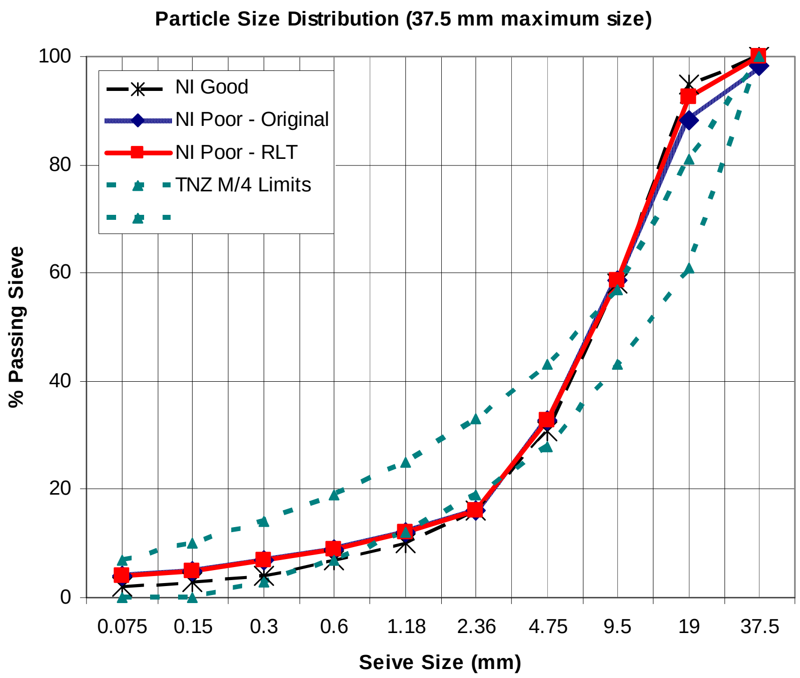

Figure 3.6. PSD for Northern Ireland aggregates includes adjusted grading for *NI Poor* RLT sample.

Figure 3.7. Adding material to compaction mould for RLT sample preparation.

Figure 3.8. Compacting material layers for RLT sample preparation.

Figure 3.9. The use of the end platen to ensure the correct finished height for the final layer.

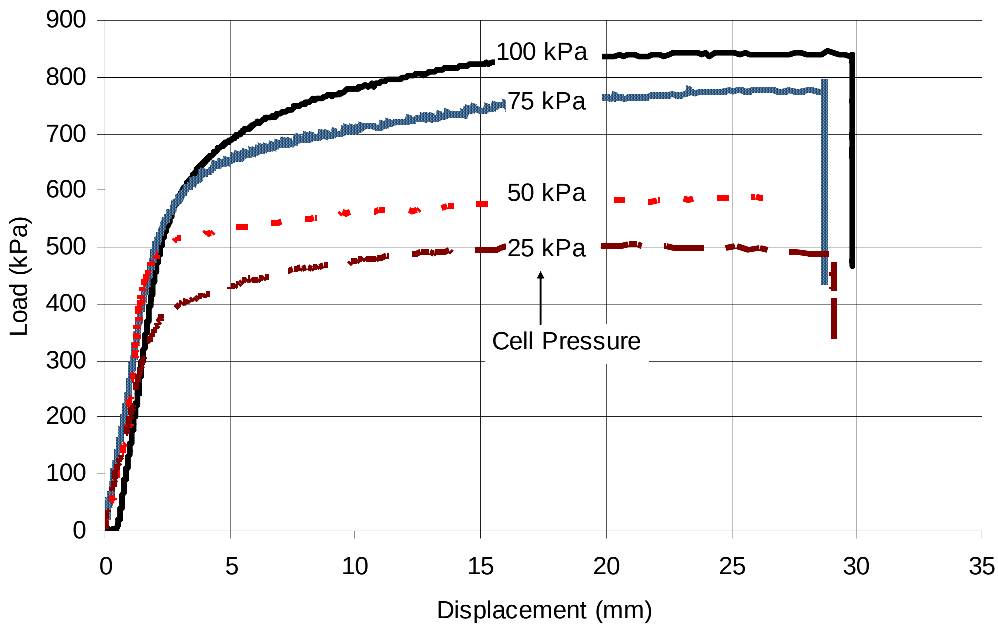

Figure 3.10. Monotonic shear failure tests for NI Good material.

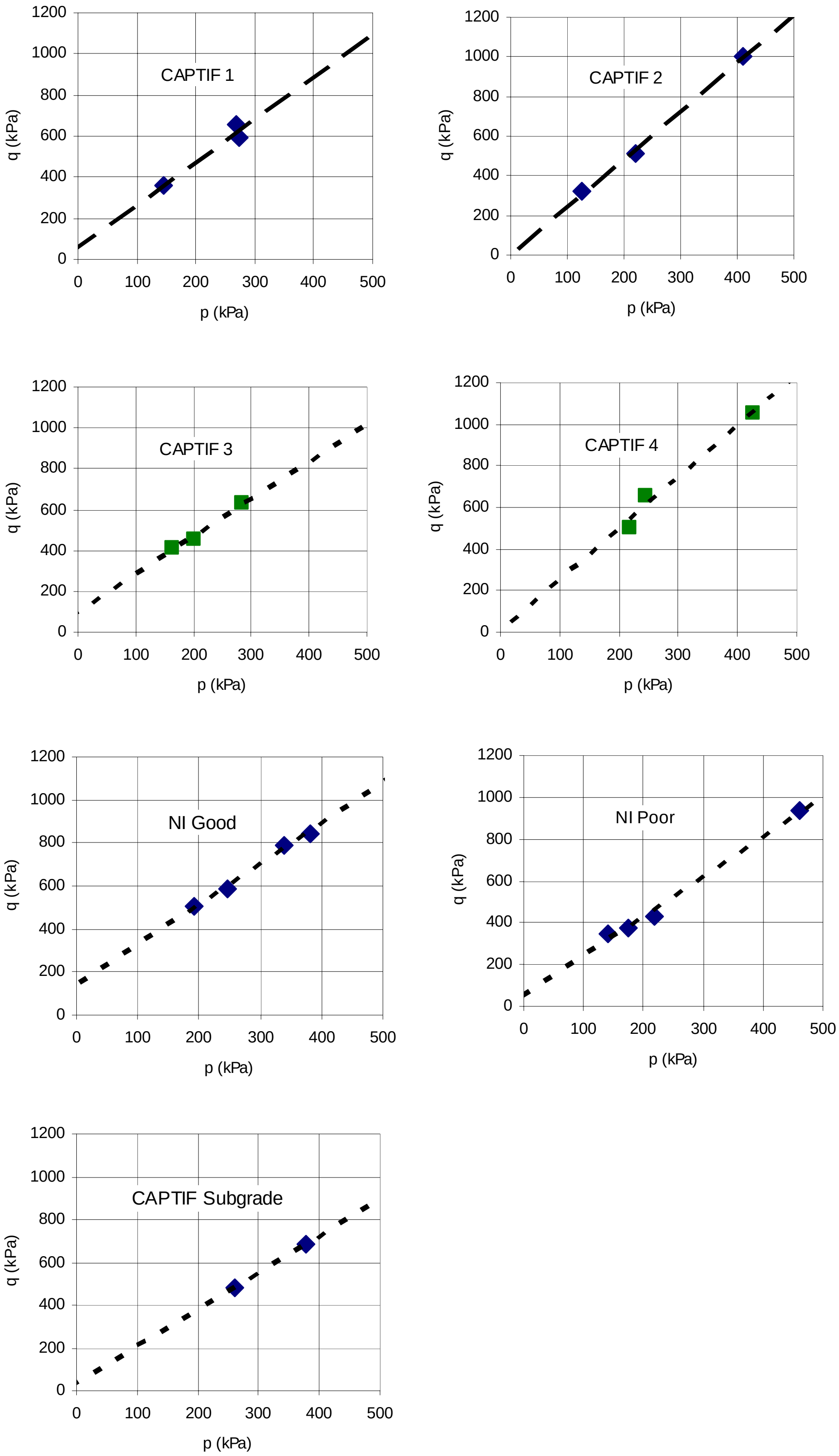

Figure 3.11. Yield surfaces from monotonic shear failure tests.

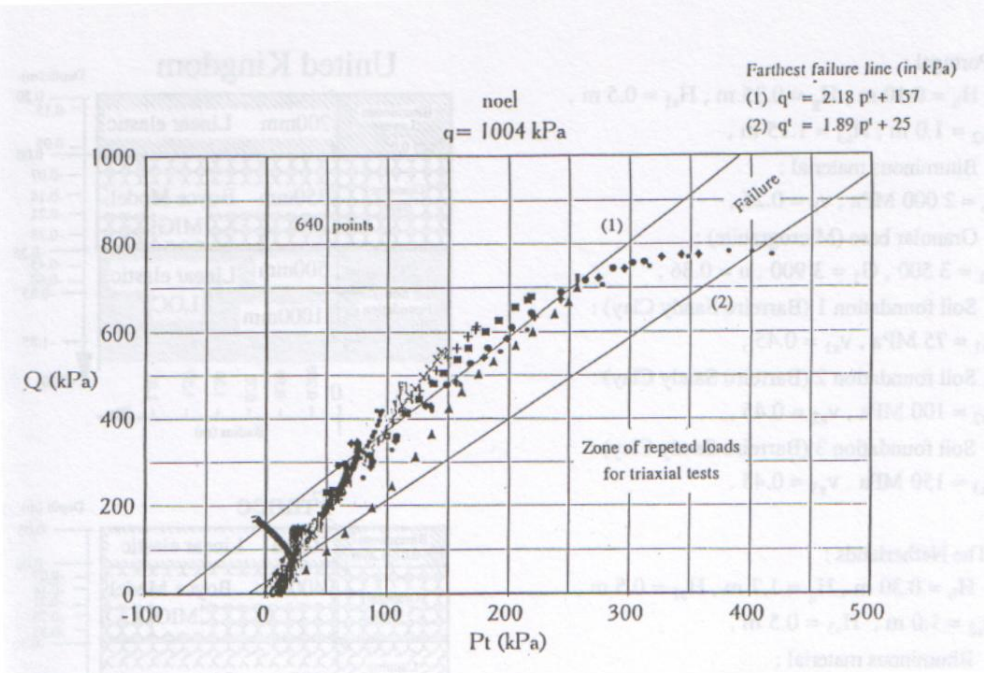

Figure 3.12. Representation of the stresses in the *p-q* space for all the Gauss points (after Jouve and Guezouli, 1993).

Stress Paths (kPa) – *CAPTIF 1 (Test 1, p=75kPa)*							
	$p=\frac{1}{3}(\sigma_1+2\sigma_3)$		[1] $q=\sigma_1-\sigma_3$		$\sigma_1=q+\sigma_3+$[2]k		[3] σ_3
A	*62*	76	*0*	43	*69*	112	58
B	*47*	77	*0*	91	*55*	145	43
C	*31*	77	*0*	139	*40*	179	27
D	*16*	77	*0*	183	*26*	209	11
E	*6*	73	*0*	203	*17*	220	0

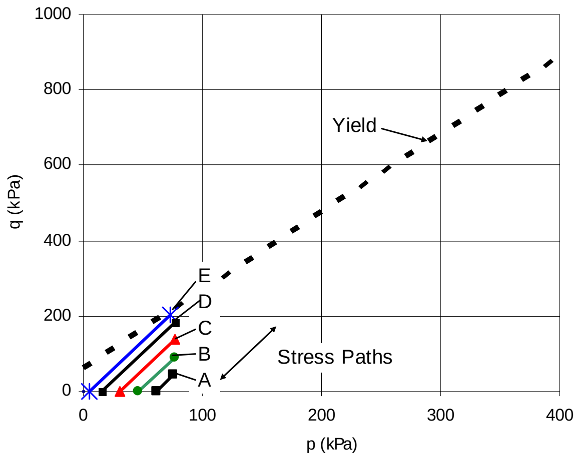

Stress Paths (kPa) – *CAPTIF 1 (Test 2, p=150kPa)*							
	$p=\frac{1}{3}(\sigma_1+2\sigma_3)$		[1] $q=\sigma_1-\sigma_3$		$\sigma_1=q+\sigma_3+$[2]k		[3] σ_3
A	*104*	149	*0*	135	*111*	247	100
B	*93*	154	*0*	183	*101*	284	88
C	*74*	151	*0*	229	*83*	313	70
D	*59*	150	*0*	274	*69*	343	54
E	*46*	152	*0*	319	*58*	376	40
F	*29*	151	*0*	367	*42*	409	22

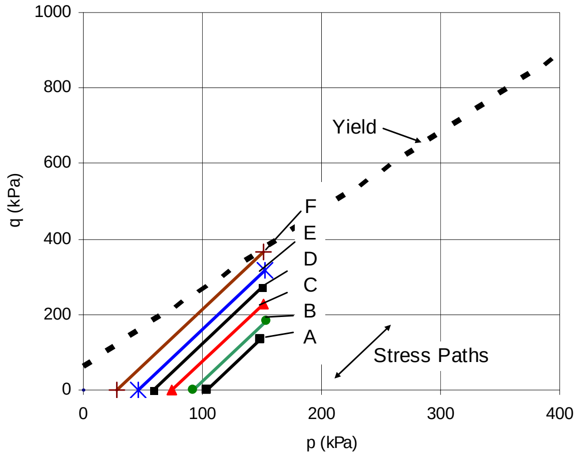

Stress Paths (kPa) – *CAPTIF 1 (Test 3, p=250kPa)*							
	$p=\frac{1}{3}(\sigma_1+2\sigma_3)$		[1] $q=\sigma_1-\sigma_3$		$\sigma_1=q+\sigma_3+$[2]k		[3] σ_3
A	139	247	0	324	149	473	134
B	122	247	0	376	130	506	118
C	110	250	0	419	119	538	105
D	88	243	0	465	98	563	83
E	78	249	0	515	90	604	72

1. q = cyclic vertical load (kPa).
2. k = top platen weight and minimum vertical load.
3. σ_3 = cell pressure (kPa).

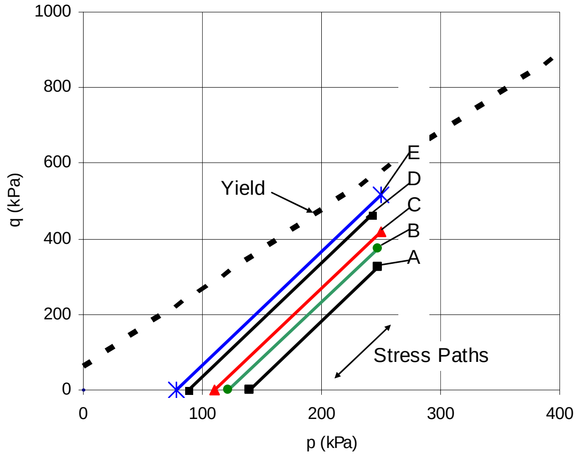

Figure 3.13. RLT permanent strain stress paths tested for CAPTIF 1 material.

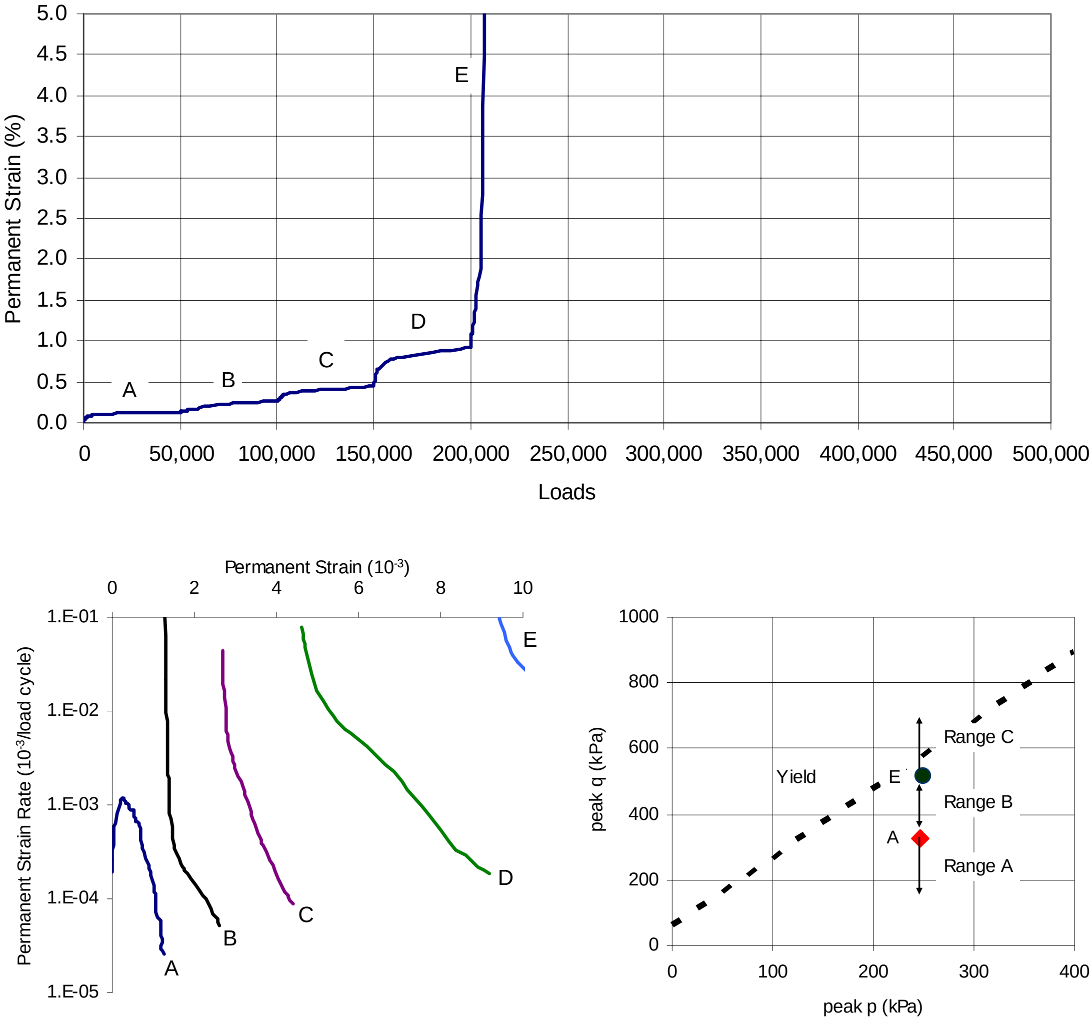

Figure 3.14. RLT permanent strain and shakedown boundary determination for CAPTIF 1 material, test 3 (p=250kPa).

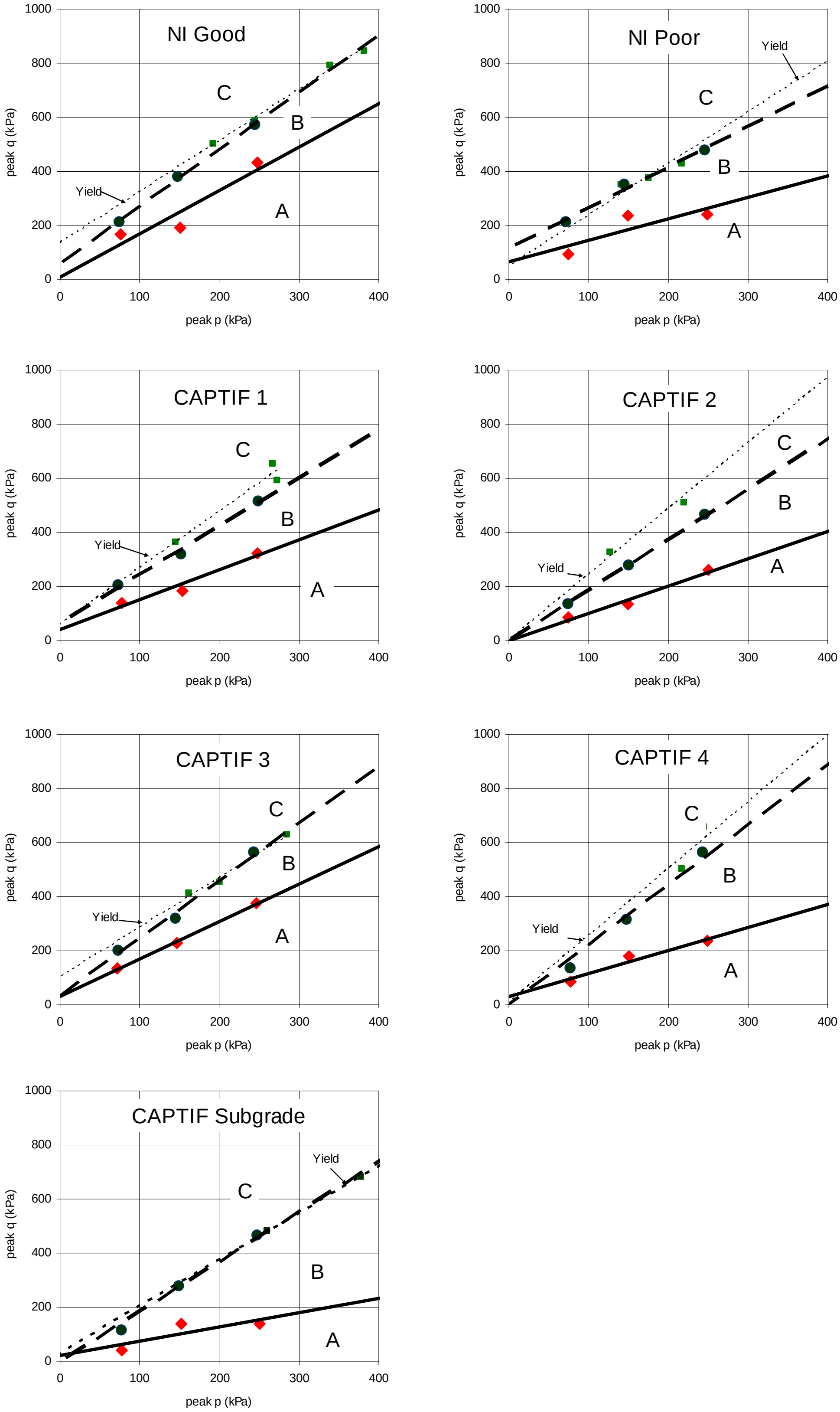

Figure 3.15. Shakedown range boundaries.

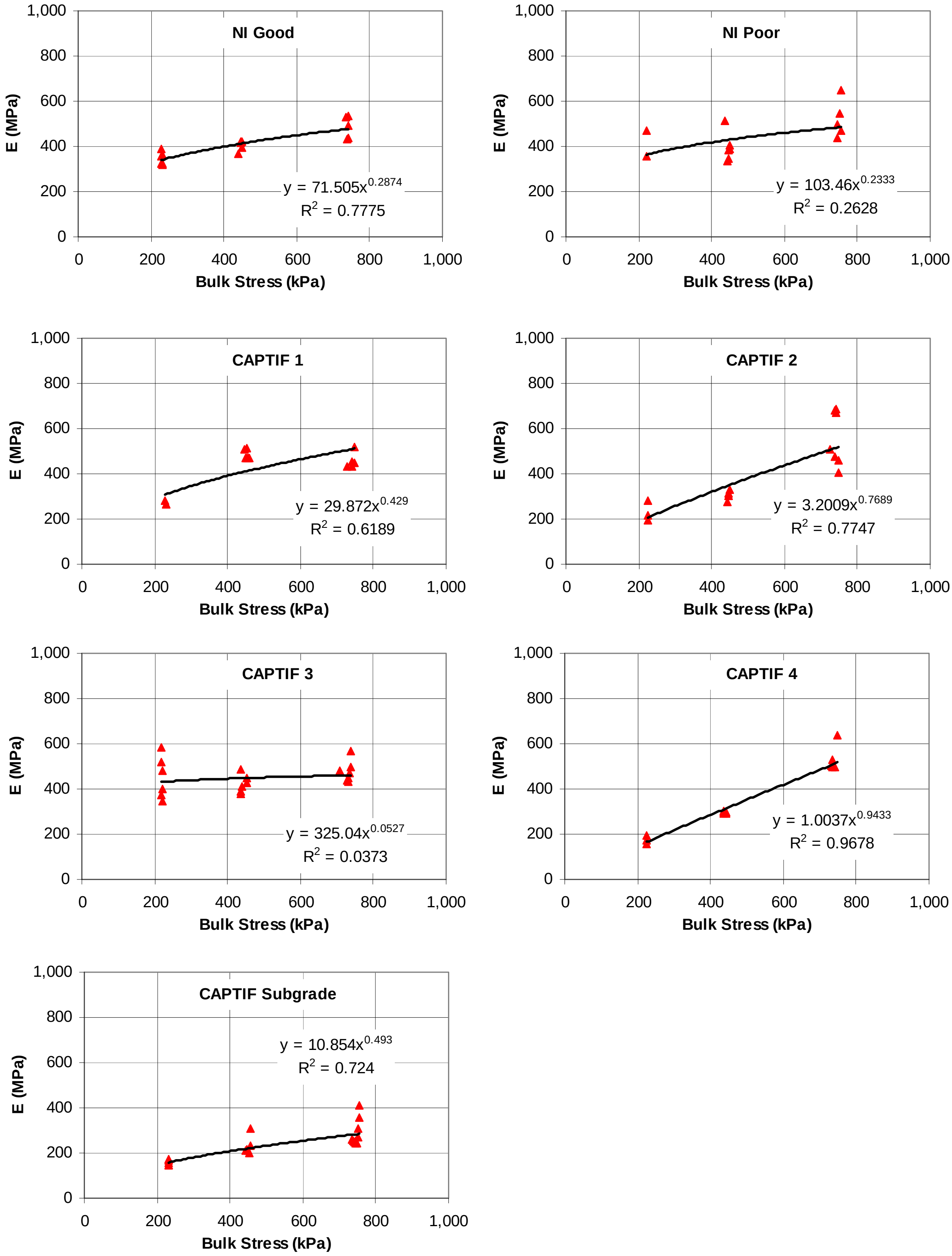

Figure 3.16. Elastic modulus versus bulk stress.

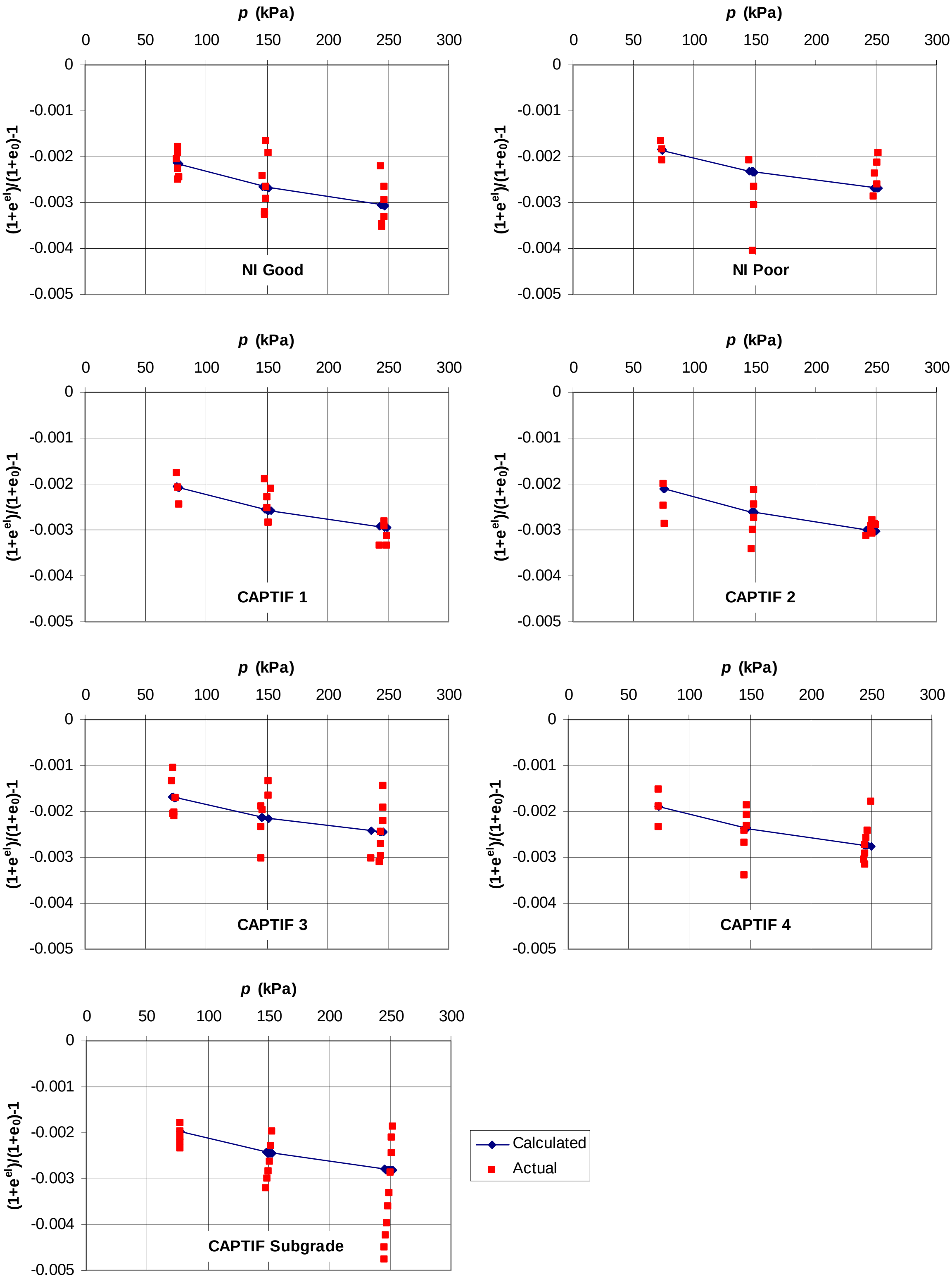

Figure 3.17. Comparison of porous elasticity model to measured data.

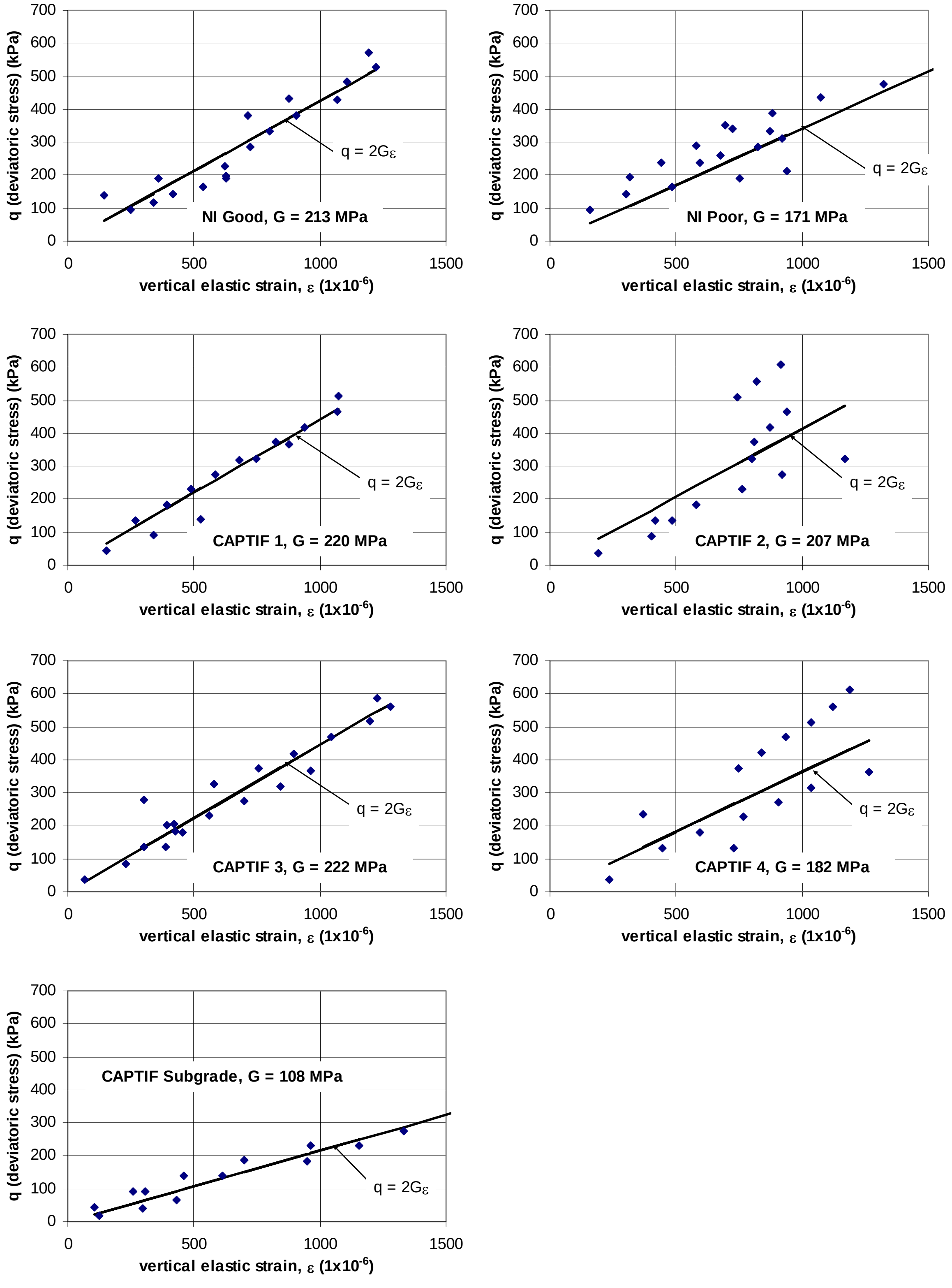

Figure 3.18. Comparison of shear modulus model with measured data.

CHAPTER 4 NEW ZEALAND ACCELERATED PAVEMENT TESTS

4.1 INTRODUCTION

4.1.1 Background and Scope

Full scale accelerated pavement tests (APTs) provide essential results to validate predictions derived from laboratory tests and pavement modelling. APTs and/or field trials are usually necessary before research from a desk and laboratory study are implemented in practice (Theyse et al, 1999). Transit New Zealand, the government agency responsible for highways in New Zealand, have been conducting accelerated pavement tests at CAPTIF (Canterbury Accelerated Pavement Testing Indoor Facility) since 1987 (Arnold et al. 1999). Data from three accelerated pavement tests (APTs) were further analysed as part of this thesis. Two of the APTs the Author was involved in as a key researcher before, during and after his studies at the University of Nottingham. The Author's involvement was to develop the research brief, analyse results and write the final reports (Arnold et al, 2001, 2003, 2004a, 2004b).

The original purpose of the APTs at CAPTIF were to: assess the difference in pavement wear of steel and air-bag suspensions (defined as the 1997 CAPTIF test, de Pont, 1997; de Pont and Pidwerbesky, 1995; de Pont et al, 1996); predicting pavement performance from Repeated Load Triaxial (RLT) tests on granular materials (defined as the 2001 CAPTIF test, Arnold et al, 2001); and determine the effect on pavement wear of an increase in mass limits for heavy vehicles (defined as the 2003 CAPTIF test, Arnold et al, 2003, 2004a and 2004b). Although the original purpose of the APTs were not directly relevant to this thesis, through the Author's involvement, a vast amount of data was made available for re-analysis in line with this thesis objectives. Data available from the APTs at regular loading intervals (up to 1 million) for a range of wheel loads (half axle loads of 40, 50 and 60kN) and pavements with different granular materials and depths include: surface profile (to calculate rutting); insitu measurements of both static and dynamic strains; insitu measurements of stress; surface deflections from the falling weight deflectometer (FWD); and trench data to assess the proportion of rutting in each pavement layer. The granular and subgrade materials used in the CAPTIF APTs were tested in the laboratory study (Chapter 3). This allows the prediction of shakedown range behaviour and rutting from pavement modelling of the APTs in Chapters 6 and 7 to be compared to what actually occurred for validation. However, the finite element modelling undertaken in Chapter 6 reflected analysis of pavement sections available at the time, being the 2001 (Arnold et al, 2001) CAPTIF tests. All the CAPTIF tests were utilised in the deformation modelling undertaken in Chapter 7.

Results of three APTs at CAPTIF are reported in this chapter in the context of this thesis. The CAPTIF 2001 test results are analysed more fully than the other tests and this reflects the greater involvement of the Author in this test and the timely availability of results during his study. The CAPTIF facility is described in this chapter, followed by descriptions of the pavement test sections, including: design; construction; instrumentation; and monitoring. Finally, the results are summarised with more emphasis on the CAPTIF 2001 test results. Key results useful for validating the pavement modelling, as undertaken in Chapters 6 and 7, are the plots of surface rutting with number of wheel passes for each pavement section and wheel load.

4.1.2 The Canterbury Accelerated Pavement Testing Indoor Facility (CAPTIF)

CAPTIF is located in Christchurch, New Zealand and is owned and operated by Transit New Zealand. It consists of a 58m long (on the centreline) circular track contained within a 1.5m deep x 4.0m wide concrete tank (Figure 4.1). A centre platform carries the machinery and electronics needed to drive the system. Mounted on this platform is a sliding frame that can move horizontally by 1m. This radial movement enables the wheel paths to be varied laterally and allows the two “vehicles” to operate in seperate wheel paths. An elevation view is shown in Figure 4.2.

At the ends of this frame, two radial arms connect to the Simulated Loading and Vehicle Emulator (SLAVE) units shown in Figure 4.3. These arms are hinged in the vertical plane so that the SLAVEs can be removed from the track during pavement construction, profile measurement etc. and are hinged in the horizontal plane to allow for vehicle bounce.

CAPTIF is unique among accelerated pavement test (APT) facilities in that it was specifically designed to generate realistic dynamic wheel forces. Other accelerated pavement testing facility designs attempt to minimise dynamic loading. The SLAVE units at CAPTIF are designed to have sprung and unsprung mass values of similar magnitude to those on actual vehicles and utilise standard heavy vehicle suspension components. The net result of this is that the SLAVEs apply dynamic wheel loads to the test pavement that are similar in character and magnitude to those applied by real vehicles. A more detailed description of the CAPTIF and its systems is given by Pidwerbesky (1995).

4.2 PAVEMENT SECTIONS

The CAPTIF 1, 2, 3 and Subgrade materials (Table 3.1) were tested in two separate APTs reported in: Arnold et al. (2001, 2003, 2004a and 2004b); and de Pont et al. (2001 and 2002). To accommodate the three different granular materials, the CAPTIF test track was divided into four segments. The 4th segment is an excluded area from the research study, due to the extra compaction from construction traffic that this segment receives, which, from experience, affects the results. Figures 4.4 and 4.5 detail how the pavements with different granular materials (Table 3.1) were split for the two CAPTIF tests (2001 and 2003). A typical pavement cross-section is shown in Figure 4.6.

The earlier CAPTIF test (de Pont, 1997; de Pont and Pidwerbesky, 1995; de Pont et al, 1996) was not split into sections as the same granular material was used (CAPTIF 4, Table 3.1). The cross-section for the earlier CAPTIF test was the same as shown in Figure 4.6 but the asphalt surface thickness was 90mm and the granular material layer was a thickness of 200mm.

There are a total of 8 pavement types tested at CAPTIF and these have been given unique identifications as shown in Table 4.1. The three CAPTIF tests have been defined by the year the first report was published, either 1997 (de Pont, 1997; de Pont and Pidwerbesky, 1995; and de Pont et al, 1996), 2001 (Arnold et al, 2001; and de Pont et al, 2001) or 2003 (Arnold et al, 2003, 2004a and 2004b). All CAPTIF APTs used the same 1200mm thickness of subgrade being the CAPTIF Subgrade (Table 3.1).

Table 4.1. CAPTIF test section IDs

ID	Granular Material (Table 3.1)	Granular Depth (mm)	CAPTIF Test	Asphalt Surface Depth (mm)
1	CAPTIF 1	275	2001	25
1a		275	2003	
1b		200	2003	
2	CAPTIF 2	275	2001	
3	CAPTIF 3	275	2001	
3a		275	2003	
3b		200	2003	
4	CAPTIF 4	200	1997	90

4.3 PAVEMENT DESIGN

4.3.1 2001 and 2003 CAPTIF tests

The pavement designs for the 2001 and 2003 CAPTIF tests were based on typical New Zealand pavements consisting of a thin-surface on an unbound granular layer overlying a soil subgrade. Design life was 1 million wheel passes of a standard dual tyred wheel load (half axle=40kN). Thickness of the granular layer was determined using guidelines in the Austroads (1992) Pavement Design Guide.

The designs involved a linear elastic analysis using CIRCLY (Wardle, 1980). However, due to the protection from the environment provided by the CAPTIF test building affecting pavement life, design of the pavement thickness was primarily based on past performance in previous CAPTIF tests to ensure a result within 1 million load cycles. A total of 275mm of granular material was decided for the 2001 CAPTIF test while two granular material thicknesses of 200 and 275mm were used in the 2003 CAPTIF tests to assess its effect on pavement life.

Another modification to usual pavement designs in New Zealand was to exclude the use of a sub-base granular material. A premium base quality granular material was used in the full depth of the pavement. This ensured that the resulting performance was influenced by the granular material of interest and not by a lower quality sub-base aggregate. Further, this lessened the complexity of pavement analysis and modelling. While a New Zealand pavement typically has a chipseal surfacing, a 25mm thick layer of fine asphaltic concrete was used instead as the chipseal would likely fail from flushing before the end of testing.

The subgrade for all the CAPTIF pavement sections was a silty clay, 1200mm thick, which has a nominal in-situ CBR (California Bearing Ratio) value of 11%. The thicknesses of granular material were either 200 or 275mm as detailed in Table 4.1.

4.3.2 1997 CAPTIF test

The starting point for the design of the 1997 CAPTIF test was the New Zealand design guide at the time (National Roads Board, 1989) with a nominal design life for the pavement of 1.5 million equivalent standard axle loads (ESA). However, this was modified to provide a pavement typical to Northern Hemisphere pavements, where the funding originated, that consisted of a structural asphalt layer, while ensuring the pavement constructed will or nearly meet the failure criteria (cracking and/or rutting) within the 1.5 million wheel passes. Hence, a relatively thin structural asphalt layer of 90mm over 200mm of granular material (CAPTIF 4, Table 3.1) was used.

4.4 PAVEMENT INSTRUMENTATION

The response of the pavement during the CAPTIF tests was monitored using instruments installed in each pavement section (Table 4.1). Each pavement section was instrumented with 36 Emu strain coils (for measuring displacement) and 3 stress gauges. Figure 4.7 shows a typical layout of instrumentation in a CAPTIF pavement test section.

The soil strain instrumentation used at CAPTIF is the Emu strain coil system (Janoo et al, 1999) purchased from the University of Nottingham. Emu strain coils were fabricated at CAPTIF using Nottingham guidelines and relay boards, triggering systems and software were developed at the University of Canterbury. This system operates as follows: a static reading on the Emu strain coils is taken for reference with the vehicles stationary and away from the Emu strain coil locations. The SLAVE vehicle is then run up to the test speed and the measurement parameters are entered into the controlling computer. When the vehicle speed is within the acceptable tolerance (±0.5km/h) of the test value, the operator begins taking readings. Infra red trigger beams detect the approach of the vehicle to be measured. Each sensor in the array is scanned simultaneously when triggered so that a continuous bowl shape of strain versus distance travelled is obtained. The Emu strain coil sensors work on the principle of inductance coupling of free-floating wire-wound disks. Sets of Emu strain coils are placed vertically above each other to enable vertical strains to be recorded at varying depths in the pavement and subgrade material. The system measures displacement relative to each Emu strain coil, as the wheel load passes over the Emu strain coil locations. These recorded displacements are converted to strain by dividing by the distance between the strain gauges.

Emu strain coils were installed in conjunction with the placement of the granular and subgrade pavement layers. Figure 4.8 shows the method used for Emu coil installation where, prior to compaction of the granular or subgrade layer, the loose material of the new layer is swept aside so as to reveal the previous compacted layer. A horizontal beam with markings that show the transverse locations of the

Emu coils is made to span between the station location markers on the tank walls. This is used, together with a ruler at right angles to the beam, a perspex plate to position the 3 coils, and a small spirit level, to accurately place the coils. The placement of the Emu coils was a time consuming process as it is important to ensure the coils are in perfect vertical alignment and that they are lying perfectly flat. Janoo et al (1999) found the combined effect of a tilt of 8 degrees and lateral movement at 12mm indicated a maximum variation of 2% on the calculated strain. After the placement of the coils the hole is filled in and the layer compacted along with the rest of the pavement layer, to ensure the pavement at the coil locations is representative of the rest of the pavement section.

Vertical stress caused by a passing wheel load was measured at the subgrade surface level using the Dynatest SOPT (SOil Pressure Transducers) instrument for the 2001 and 2003 CAPTIF tests only. These gauges have been specifically developed for use in pavements by Dynatest Consulting Ltd. They are installed in a similar manner to the Emu gauges.

4.5 CONSTRUCTION

The test pavement at CAPTIF is constructed in a series of vertical layers. Subgrade soil and aggregate materials were placed in lifts not exceeding 150mm in thickness. Each layer was compacted with at least seven passes of the Wacker plate compactor. Spot density and height readings are taken to ensure the targets for compaction and layer thicknesses are achieved. The final aggregate surface was trimmed using the tractor with the laser-guided blade and then compacted using a 4 tonne steel/rubber combo roller. After each layer the appropriate Emu strain coil instruments were installed (Figure 4.8) and the disturbance to the layer repaired.

Prior to applying the asphalt surfacing, the aggregate surface was swept with a power broom and then heavily tack coated. A 25mm layer of 10mm asphaltic concrete (AC) was placed by a paving machine over the entire track in one layer for the 2001 and 2003 CAPTIF tests, while the 1997 CAPTIF tests the 90mm AC layer was placed in two equal layers. The sealing crew used a footpath roller behind the paving machine. Once the paving machine had completed the circular test track and left the building, the entire surface was rolled with a 3.5 tonne steel drum roller.

4.6 PAVEMENT LOADING

For the 2001 and 2003 CAPTIF tests, the wheel paths of the two vehicles on the circular test track were separated for the purpose of assessing the relative damaging effect of the pavement due to different suspension types and wheel loads. For the 1997 CAPTIF tests steel and air-bag suspensions were used for each wheel path, while the wheel load was the same (50kN on a single tyre). The two wheel paths for the 2001 CAPTIF tests were at two different loads of 40kN and 50kN load on dual tyres, while steel suspension was used for both wheel loads. For the 2003 CAPTIF tests 40kN and 60kN wheel loads were tested, but with air bag suspension systems being used. Accelerated pavement loading was conducted at a speed of 45km/hr and a wheel wander of ±50mm with a normal distribution. Testing was stopped periodically to undertake pavement testing. The number of wheel passes for each pavement test section (Table 4.1) and load is summarised in Table 4.2. After 1 million wheel passes for the 40kN loads (2001 and 2003 CAPTIF tests) the load was increased to either 50kN or 60kN for the remainder of the test. A reason for this change, was to determine the effect on an already trafficked road, should legal mass limits of heavy vehicles increase (de Pont et al, 2001; Arnold et al, 2003).

Table 4.2. Pavement loading for each test section and wheel path (Table 4.1).

Pavement ID (Table 4.1)	Load (kN) 0 –1 M passes	Load (kN) > 1 M passes	Wheel type & suspension	Tyre Pressure (kPa)	Equivalent axle load (tonnes)	Total Wheel passes (M)
Lighter Wheel Path: **1, 2, 3**	40	50	dual/steel	750	8 (<1M) 10 (>1M)	1.32
Heavier Wheel Path: **1, 2, 3**	50	50	dual/steel	750	10	1.32
Lighter Wheel Path: **1a, 1b, 3a, 3b**	40	60	dual/air-bag	750	8 (<1M) 12 (>1M)	1.4
Heavier Wheel Path: **1a, 1b, 3a, 3b**	60	60	dual/air-bag	750	12	1.4
Inside Wheel Path: **4**	50	50	single/air-bag	750	10	1.7
Outside Wheel Path: **4**	50	50	single/steel	750	10	1.7

4.7 PAVEMENT TESTING

Prior to pavement loading and at the completion of 15, 25, 35, 50, 100, 150, 200, 250, 300, 400, 500, 600, 700, 800, 900 and 1000 thousand load cycles various tests were undertaken. These tests monitored the surface deformation, structural condition and insitu strains and stresses:

Surface deformation:

- Longitudinal profile in the wheel path centreline using the laser profiler;

- Transverse profile at each of the 58 stations around the track using the CAPTIF profilometer (Figure 4.9).

Structural condition:

- The structural condition/deflection of the pavement was measured using the Dynatest Falling Weight Deflectometer at each station in each wheel path.

Insitu strain and stress response measurements:

- The pavement response to vehicle loading was measured by recording the Emu strain coil signals caused by the passing vehicle at the test speed (45km/h) and at 15km/h. Each Emu strain coil pair/stress cell was measured over 3 laps to verify the repeatability of the measurements.

4.8 RESULTS

4.8.1 Introduction

The key results for validating the pavement modelling undertaken in Chapters 6 and 7 are plots of permanent deformation at the surface versus number of loading cycles for each pavement type and loading (Table 4.2). Permanent deformation is reported for all pavement tests (1997, 2001 and 2003). Insitu measurements of stresses and strains and measurements from post-mortem trenches were further analysed for the 2001 CAPTIF test (Pavement IDs 1, 2 and 3: Table 4.1). This reflects the greater involvement of the Author with the 2001 CAPTIF test and the timely availability of the results in line with this research.

4.8.2 Surface Deformation

Transverse profile was measured at regular loading intervals at all 1m station points. This information was used in a spreadsheet to calculate the vertical surface deformation. Vertical surface deformation (VSD) is more conveniently measured at CAPTIF with the transverse profilometer, as it is the maximum vertical difference between the current level and the start reference level of the pavement. Further, the measurement of VSD is more stable in comparison to straight edge measurements that are influenced by shoving on the edges of the wheel paths. Rut depth is determined using a straight edge across the pavement and considers the upward shoving at the edges of the wheel path (Figure 4.10). However, the edges of the pavement at CAPTIF move downwards which distorts the straight edge rut depth as shown in Figure 4.11. This is particularly the case when one wheel path has a heavier load than the other as shown in Figure 4.11. Although VSD is considered best for describing surface deformation the straight edge rut depth has also been calculated.

A typical result showing the progression of surface deformation for one of the stations is shown in Figure 4.12. Vertical surface deformation (VSD) and straight edge rut depth for each pavement section (Table 4.1) was calculated as the average value determined from approximately 10 measurements at 1 m stations for the 2001 and 2003 tests and from 52 measurements for the 1997 test (Pavement ID 4, Table 4.1). Results of the surface deformations were grouped in terms of the pavement types (Table 4.1) as shown from Figures 4.13 to 4.20.

The plots of deformation versus number of load cycles were further analysed to determine the pavements' overall behaviour in terms of shakedown Ranges A, B or C as defined in Section 2.11.2. This overall behaviour shown as surface rutting is a consequence of the deformation of underlying pavement material elements, where each material element will deform differently, dependent on the level of stress. Thus, the material elements that make up the pavement will exhibit the full shakedown ranges A, B or C. As a brief reminder Range A is where the deformation rate is decreasing rapidly and Range C is failure or increasing deformation rate, while Range B is everything that is not Range A or C. To assist in determining the shakedown Ranges, deformation versus deformation rate was plotted as shown alongside the surface deformation plots (Figures 4.13 to 4.20).

The deformation rate was calculated as the average slope for a selected range of points to smooth out the resulting values.

For all pavement test sections it can be safely assumed that Range C did not occur as none of the sections failed after 1 million passes. Therefore, the deformation behaviour observed is either Range A or B. Range A is assigned conservatively where it is considered that the rate of deformation is decreasing and it appears that the magnitude of cumulative deformation is reaching an upper limit. Applying this criterion requires judgement, from reviewing both the trend in surface deformation versus load cycles and the deformation versus deformation rate plots. For the 2001 and 2003 tests the load for the lighter (40kN) wheel path was increased to either 50kN (2001 test) or 60kN (2002 test) after 1 million wheel passes. This change in load caused a "hiccup" in the deformation for both wheel paths, possibly due to the several weeks' rest, before testing continued, after the 1 million wheel passes. During this, it is hypothesised, any build up of residual stresses (Section 2.4.6) had relaxed. Although, this is an interesting result, the deformation results after 1 million wheel passes for the 2001 and 2003 tests were ignored, for assigning the behaviour ranges A or B, along with the associated final deformation and rate of deformation. The final deformation rate for the 2001 and 2003 tests was taken as the average slope from 700,000 to 1,000,000 wheel passes, while the final vertical surface deformation (VSD) value was that at 1 million wheel passes.

Table 4.3. Long term deformation behaviour.

Pavement ID (Table 4.1)	Load (kN)	Shakedown Range	Final Rate VSD/Wheel Passes (mm x 10^{-6})	Final VSD (mm)
1	40 50	B B	3.2 6.1	6.0 11.2
1a	40 60	B B	2.7 5.0	5.9 10.8
1b	40 60	B B	3.4 4.8	6.5 11.5
2	40 50	B B	3.3 4.6	6.7 9.6
3	40 50	B B	3.1 3.1	5.2 6.2
3a	40 60	B A	2.9 0.65	6.0 9.4
3b	40 60	B A	2.2 0.77	6.0 11.4
4	50 – Air 50 - Steel	A A	0.66 1.2	9.7 10.8

Range A behaviour was observed in pavement Test Section 4 and the 60kN wheel load in 3a and 3b. Pavement Test Section 4 had the thickest asphalt cover (90mm) compared to only 25mm for the other sections and thus the better performance obtained is as expected. However, a Range A response in the 60kN wheel path for Sections 3a and 3b is unexpected especially as the lighter 40kN wheel path resulted in a Range B response. It can only be postulated, that, should many more loads be applied in the 40kN wheel path for Sections 3a and 3b, that a Range A response would also be observed. The extra loads will result in greater VSD which in turn causes vertical and lateral movement of the granular material underneath. Lateral movement of granular material will result in a build up of opposing lateral stresses that will restrict the development of further deformation (see also discussion of residual stresses in Section 2.4.6). Another interesting result is that, after the loading stopped for several weeks and was then re-applied, the deformation rate increased dramatically and then decreased for Sections 3a

(Figure 4.18) and 3b (Figure 4.19). This behaviour lends itself to changing the behaviour range assigned from A to B for Sections 3a and 3b. However, this maybe due to continuous loading building up the lateral residual stresses which when unloading for a period of time, these lateral stresses relax.

The final vertical surface deformations (VSD) for each pavement test section shows (as expected) the heavier load results in a higher VSD (except Section 3 – 50kN as because of surfacing repairs this result can be excluded, Figure 4.17). Apart from Test Sections 3a and 3b increasing wheel load also increases the rate of VSD development. Pavement Test Section 2, with the CAPTIF 2 granular material (which is CAPTIF 1 material but contaminated with 10% of clay fines) shows less deformation than pavement Test Section 1, being the original CAPTIF 1 material. This is due to an indoor environment of CAPTIF and thus keeping the granular materials becoming “too wet”. CAPTIF 2 material when wet would likely result in rapid pavement failure due to the clay fines reducing the frictional resistance between aggregate particles (Section 2.6.8).

4.8.3 Insitu Deformation – 2001 test

The Emu strain coils were also used to give an indication of deformation within the pavement layers. At regular loading intervals voltage was recorded for each Emu strain coil pair without wheel loading. This voltage was converted to distance for determining the Emu strain coil spacings at various numbers of wheel passes. Assuming the bottom Emu strain coil is fixed, the reduced level of each Emu strain coil was determined. Of interest, is the change in reduced level during the test. Results are plotted in Figure 4.21, where the erratic results that occurred in the first 100,000 wheel passes were excluded. For comparison, the change in reduced level, from the surface profiles at Emu strain coil locations (transverse distance=1.35m, Figure 4.12) was included in these plots. In general, the trend shows the Emu strain coils are moving downwards to greater depths in the pavement. This result is most pronounced in pavement Test Section 2 (Table 4.1).

Including the reduced levels calculated from the start of the test yields the results shown in Figure 4.22. With the exception of Test Section 2, the reduced level of the Emu strain coils moves up and down. After 1 million load cycles, the reduced level of the Emu strain coils are within 0.3mm for the 1 and 3 pavement test sections (Table 4.1) from their start positions. Test Section 2 shows a definite trend downwards, where the greatest amount of deformation occurs in the top of the subgrade.

Change in Emu strain coil pair spacings in relation to the spacings at 5,000 and 100,000 were also plotted in Figures 4.22 and 4.23 respectively. Ignoring the initial readings, the trend is a reduction in Emu strain coil spacings, where the aggregate and top subgrade layers are deforming the most (ie. show the greatest change in spacing).

To give an indication on where the deformation is occurring, the change in Emu strain coil spacing was further analysed. The proportion of the total change in spacing was determined at the 900,000 wheel pass points for Test Sections 2 and 3 results, while ignoring values less than 100,000 wheel passes. For Test Section 1 proportions were calculated from the 1000,000 data as results at 900,000 were questionable. Table 4.4 shows the percentage of deformation calculated from the change in Emu strain coil spacings.

Table 4.4. Deformation in each layer at 900,000 wheel passes from changes in Emu strain coil spacings after 100,000 wheel passes.

	1 (Table 4.1)		2 (Table 4.1)		3 (Table 4.1)	
AG (113mm)	-0.22mm	12%	-0.50mm	18%	-0.29	20%
AG (188mm)	-0.16mm	9%	-0.44mm	16%	-0.29	20%
AG (263mm)	-0.32mm	17%	-0.32mm	11%	-0.24	17%
SG (338mm)	-0.42mm	23%	-0.80mm	29%	-0.35	24%
SG (413mm)	-0.33mm	18%	-0.30mm	11%	-0.17	12%
SG (488mm)	-0.28mm	15%	-0.17mm	6%	-0.050	3%
SG (563mm)	-0.11mm	6%	-0.26mm	9%	-0.050	3%
Aggregate (AG)	-0.70mm	38%	-1.26mm	45%	-0.82mm	57%
Subgrade (SG)	-0.90mm	62%	-1.56mm	55%	-0.88mm	43%
Total	-1.84mm	100%	-2.79mm	100%	-1.44mm	100%
Surface (profile) – 900,000 minus 100,000 VSD	-1.31mm	-	-2.11mm	-	-0.88mm	-

Analyses of the static Emu strain coil spacings show approximately 40% to 60% of the deformation occurs in the granular layers. The granular material in pavement Test Section 2 shows the greatest magnitude in deformation. Test Section 2 is constructed with the CAPTIF 2 material which has 10% clay fines added and thus this extra deformation within the granular material is expected. Differences between the surface profile and that determined from movement of the Emu strain coils is likely to be a result of the accumulating error in the Emu strain coil measurement. It is also observed, that the surface profile deformation shown is less than the maximum vertical surface deformation. This is because the value is taken on top of the instruments, which are placed between the two tyres (i.e. transverse distance 1.35m, Figure 4.12). Further, the proportion of deformation seen between the tyres, may not be the same as what would have occurred directly under the tyre. The upper portion of the pavement does not “feel” the full load of the tyres, as the load is spread laterally at an angle of approximately 30 degrees, as shown in Figure 4.25. Figure 4.25 shows the classical bearing capacity failure, where a wedge is pushed downwards underneath the tyres, while besides the wedge the soil is pushed outwards and upwards. The bearing capacity failure mechanism and the effect of load spreading is suspected to have the effect of pushing the top two Emu strain coils upwards. This upwards movement may be cancelled due to the combined wedge of the two tyres pushing the coils downwards.

4.8.4 Structural Condition

Pavement deflections were measured with the Dynatest Falling Weight Deflectometer at various intervals during the testing. The deflection measurements were not back-analysed to estimate pavement layer moduli as this was not necessary for this study. Rather, the peak deflections have been plotted as an indication of how the pavements' competence, in terms of stiffness, changes during the accelerated pavement testing. Figures 4.26, 4.27, and 4.28 show the average peak deflections measured during testing of the pavement sections (Table 4.1).

Apart from pavement Test Sections 1a and 1b, deflection does not increase with increasing load cycles. This suggests the pavements are as structurally sound after 1 million passes as when first constructed. Further, the results indicate that deflection measurements are not a very good indicator of remaining life of the pavement.

4.8.5 Resilient Strain and Stress Measurements

Vertical strains and stresses were measured under the range of loads and speeds at frequent intervals. Tables 4.5, 4.6, 4.7, and 4.8 are the median response values for each pavement test section (Table 4.1). Median values are used to eliminate the bias from outliers and nil values that occurs when average values are calculated. During testing peak dynamic vertical strains were recorded at regular intervals, as shown in Figures 4.29, 4.30, & 4.31 for the pavement test sections and for the

1997, 2001 and 2003 tests. Dynamic peak vertical stress at regular loading intervals was measured for the 2003 tests in the heavier wheel path (60kN) and is plotted in Figure 4.32.

The trend in strain measurements varies by different pavement test section, granular material and depth. All the strain measurements were reviewed to determine how strains change at each depth with increasing numbers of load cycles. In general, the strains decease for those measured in the aggregate, indicating an increase in stiffness with increasing loads. This increase in stiffness is probably due to the granular materials re-arranging into a tighter and denser arrangement and/or the build up of lateral residual stresses, which have the effect of increasing the confining stress. Increases in confining stress cause an increase the bulk stress and thus, according to the Hicks (1970) k-θ model (Equation 2.27), the stiffness/resilient modulus increases for granular materials.

Strains measured in the subgrade soil show significantly higher strains than granular materials. Further, the strains tend to increase with increasing load cycles. Pore water pressure build up in the fine grained soil under repetitive loading is a likely reason for the measured strains to increase. The general trend in increasing vertical stress at the top of the subgrade is another reason for the increasing strains in the subgrade soil.

In Figure 4.31, the 3a and 3b Test Sections showed an increase in strain resulting from an increase in wheel load from 40kN to 60kN that occurred after 1 million loads. However, for the other sections the change in load resulted in some erratic results in measured strains as shown in Figure 4.30.

The measured stress values (Figure 4.32) show erratic results, although the trend shows the stress increases as the number of wheel passes increases.

Table 4.5. Measured vertical stresses and strains for 40kN load in 40kN wheel path for 2001 tests.

40kN load @ 6km/hr (tyre pressure =750kPa)		Pavement ID (Table 4.1) (40kN Wheel Path)		
		1	2	3
Material	Depth (mm)	Strain (micro-m/m)		
Aggregate	112.5	880	740	760
	187.5	720	700	740
	262.5	780	860	540
Subgrade	337.5	2240	3700	980
	412.5	2500	1780	1000
	487.5	2100	1320	*rejected*
	562.5	1000	940	980
		Stress (kPa)		
Top of subgrade (300)		77	92	77

Table 4.6. Measured vertical stresses and strains for 40kN load in 40kN wheel path for 2003 tests.

40kN load @ 6km/hr (tyre pressure =750kPa)		Pavement ID (Table 4.1) (40kN Wheel Path)			
		1a	1b	3a	3b
Material	Depth (mm)	Strain (micro-m/m)			
Aggregate	112.5	1004	1264	852	1432
	187.5	905	754	459	749
	262.5	685		463	
Subgrade	262.5		1746		2537
	337.5	2261	1323	1846	1373
	412.5	1555	-	1267	954
	487.5	1113	-	387	1130
	562.5	511	415	352	512

** Stress not measured in 40kN wheel path and in 50kN wheel path both stress and strain were not measured.*

Table 4.7. Measured stresses and strains for 60kN load in 60kN wheel path for 2003 tests.

60kN load @ 6km/hr (tyre pressure =750kPa)		Pavement ID (Table 4.1) (60kN Wheel Path)			
		1a	1b	3a	3b
Material	Depth (mm)	Strain (micro-m/m)			
Aggregate	112.5	1799	1151	1329	1530
	187.5	1557	1564	664	1621
	262.5	1189		572	
Subgrade	262.5		3219		4281
	337.5	3007	2120	3152	4260
	412.5	3870	1739	2147	1841
	487.5	1189	637	601	1306
	562.5	902	597	393	1496
		Stress (kPa)			
Top of subgrade		131.5 *(300mm)*	307 *(225mm)*	150.5 *(300mm)*	223.5 *(225mm)*

Table 4.8. Measured stresses and strains for 50kN load for both wheel paths in 1997 tests.

Material	Depth (mm)	**Measured**
Surface deflection (mm):		
Asphalt	0	0.9
Horizontal strain ($\mu m/m$):		
Asphalt	90	487
Vertical strain ($\mu m/m$):		
Granular	280	908
Subgrade	380	2120
Subgrade	480	1174

4.8.6 Insitu Stiffness – 2001 tests

The strains and stresses measured in the bottom of the granular layer were also analysed. Measured values of strain and stress were used to calculate the resilient modulus for the 2001 pavement test sections (1, 2 and 3). The resilient modulus calculated was simply measured vertical stress divided by measured vertical strain. These results were plotted against bulk stress in a similar manner used to report resilient moduli from Repeated Load Triaxial (RLT) tests (Figure 3.16). Further details of the calculations are given in Arnold et al. (2001). Bulk stress is the sum of the principal stresses and its value can be related to the resilient modulus with Equation 2.27 (Hicks 1970).

Horizontal stress was not measured in the pavement and therefore to calculate bulk stress it was assumed to be nil. Linear elastic analysis confirms this assumption, that horizontal stresses directly beneath the centre of the wheel load in the bottom of the granular layer are negligible. However, in a pavement due to surrounding aggregate, there is expected to be a level of confinement or horizontal stress. This level of confinement is unknown but is estimated to be around 30kPa from recommendations of other researchers (Section 2.4.6). Results of bulk stress versus resilient modulus from measured stresses and strain are shown in Figure 4.33. These results of calculated insitu stiffnesses show all the materials to be highly non-linear with respect to stress, the CAPTIF 3 material (Table 3.1) having the highest stiffness, while the CAPTIF 2 material (Table 3.1) having the lowest stiffness.

4.8.7 Post Mortem – 2001 tests

After completion of 1 million wheel passes, a further 320,000 wheel passes of a 50kN dual tyred load were conducted on the 2001 tests (1, 2 & 3 Table 4.1). At the end of this second test three trenches were excavated in each section (i.e. 1, 2 and 3, Table 4.1). The asphalt surface was cut with a saw while the aggregate was carefully removed to reveal the subgrade surface. Using a beam spanning the tank walls the depth to the subgrade at regular transverse intervals was measured. The final reduced level of the subgrade surface was determined. Deformation was calculated as the difference between the before and after reduced levels.

To determine the amount of deformation on the aggregate surface, the before and after reduced levels of the asphalt surface were used. Further, the deformation of the subgrade was subtracted. This assumption was correct as upon excavation the asphalt layer followed the same shape as the deformed surface of the aggregate.

Reduced levels of the before and after asphalt and subgrade surfaces of one cross-section in each section are shown in Figure 4.34. From these results an average deformation was calculated for the aggregate and subgrade. It is shown that approximately half of the deformation is attributed to the aggregate layer (Table 4.9).

Table 4.9. Average deformation and percentages in aggregate and subgrade layers.

		Subgrade		Aggregate		Total
Section (Table 4.1)	Stn.	Value (mm)	% of Total	Value (mm)	% of Total	Value (mm)
1	5	2.0	27%	5.3	73%	7.3
	7	4.2	63%	2.5	38%	6.7
	8	2.8	53%	2.5	47%	5.3
2	18	3.3	42%	4.7	58%	8.0
	20	3.7	49%	3.8	51%	7.5
	22	1.8	30%	4.3	70%	6.2
3	33	0.0	0%	6.5	100%	6.5
	34	-1.2	-22%	6.5	122%	5.3
	36	-4.3	-93%	9.0	193%	4.7

Results of the post-mortem show that over half the deformation occurs in the granular materials. Section 3 shows an unusual result where the subgrade level has remained the same or increased. It is unsure if this is a real result or an error of some type.

4.9 SUMMARY

This chapter reports results from three accelerated pavement tests at Transit New Zealand's CAPTIF (1997, 2001, 2003). The granular and subgrade materials used in these tests were shipped to the University of Nottingham and tested in the triaxial apparatus (Chapter 3). Results from the CAPTIF tests will be compared with predictions on deformation behaviour (Range A, B or C defined in Section 2.11.2) and surface deformation as undertaken in Chapter 6 *Finite Element Modelling* and 7 *Modelling Permanent Deformation* respectively. A key output from review of these CAPTIF tests is surface deformation/rutting with respect to loading, number of load cycles and pavement type. Insitu stresses and strains were also examined to gain an understanding in the mechanisms that occur in granular pavements under repetitive loading. Permanent deformations within the pavement layers were analysed from static Emu strain coil readings and excavated trenches in the 2001 tests. It was found that approximately half of the surface rut depth can be attributed to deformation in the aggregate layers.

Figure 4.1. Transit New Zealand's pavement testing facility CAPTIF.

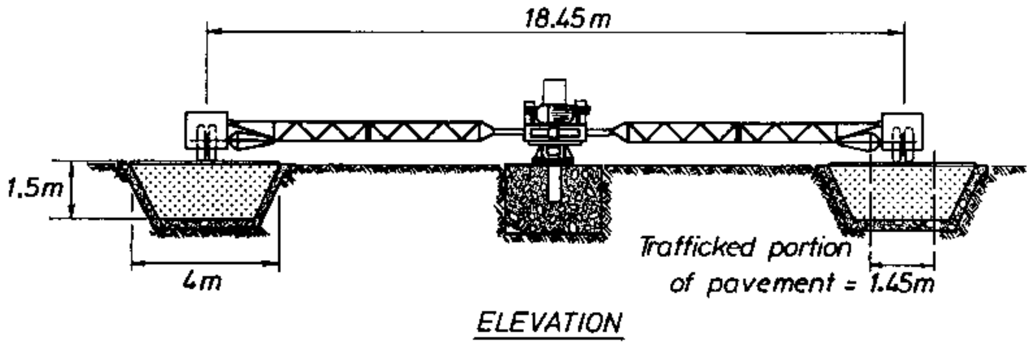

Figure 4.2. Elevation view of CAPTIF.

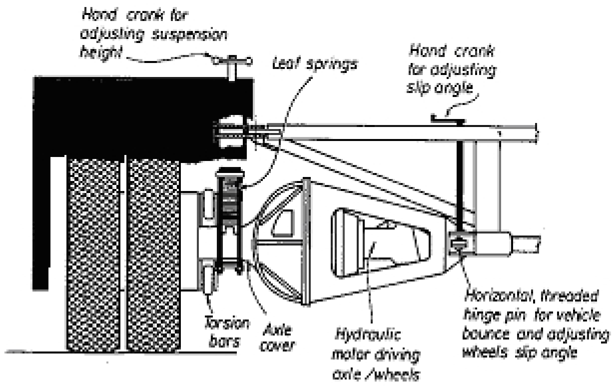

Figure 4.3. The CAPTIF SLAVE unit.

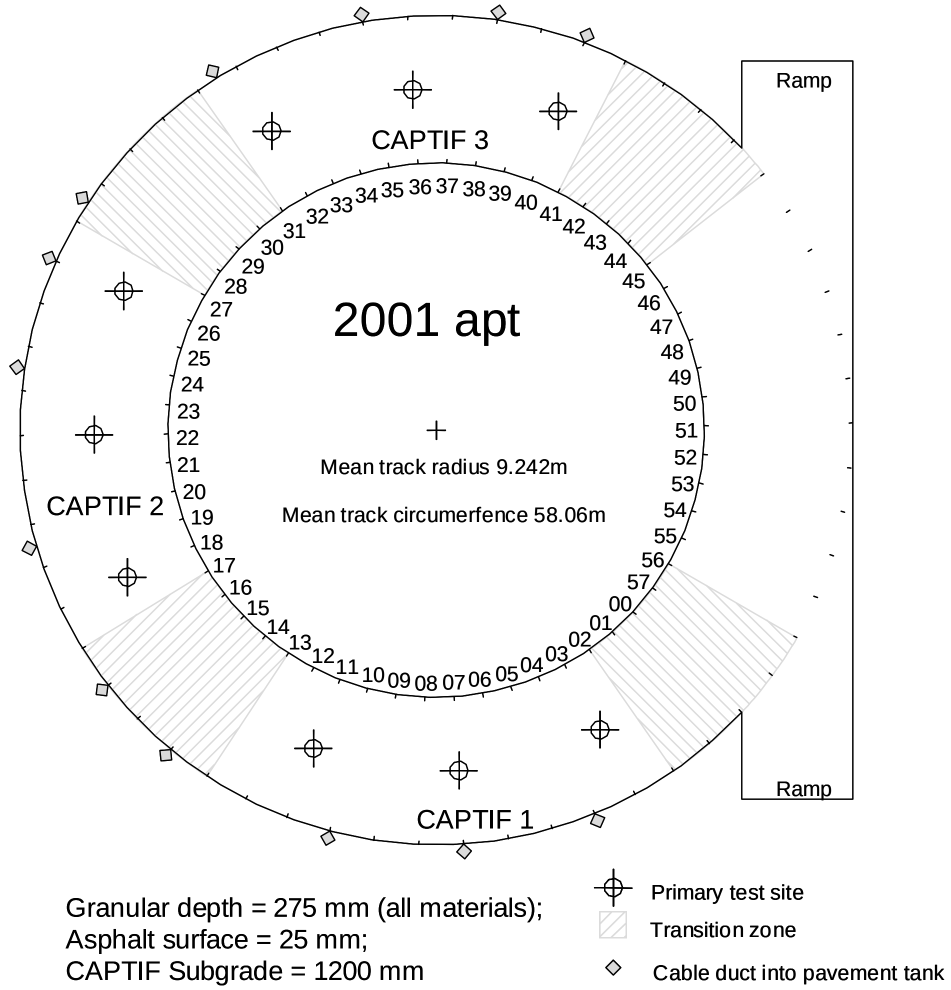

Figure 4.4. Layout of CAPTIF granular test sections for the 2001 test.

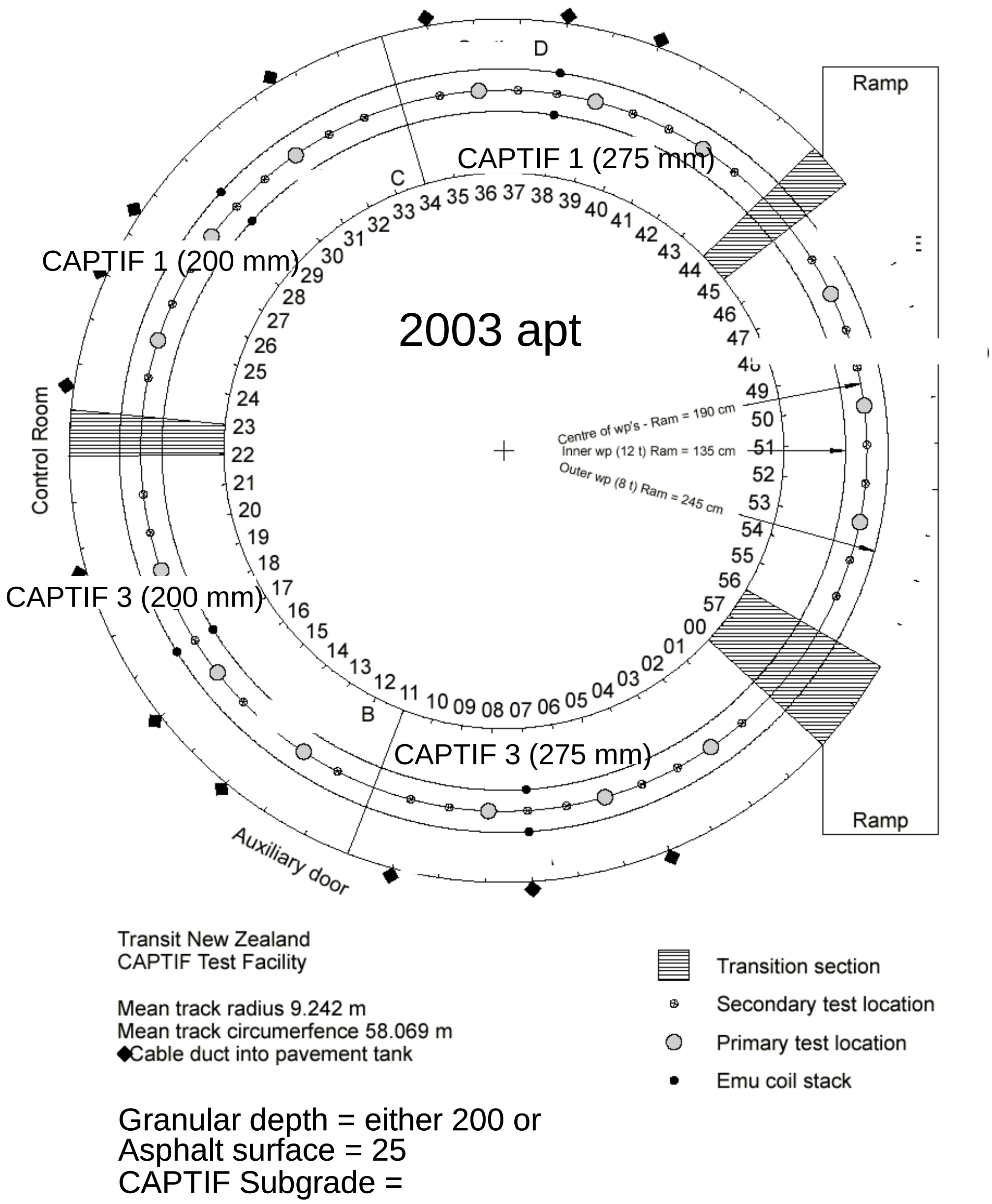

Pleas check the revisions to this figure

Figure 4.5. Layout of CAPTIF granular test sections for the 2003 test.

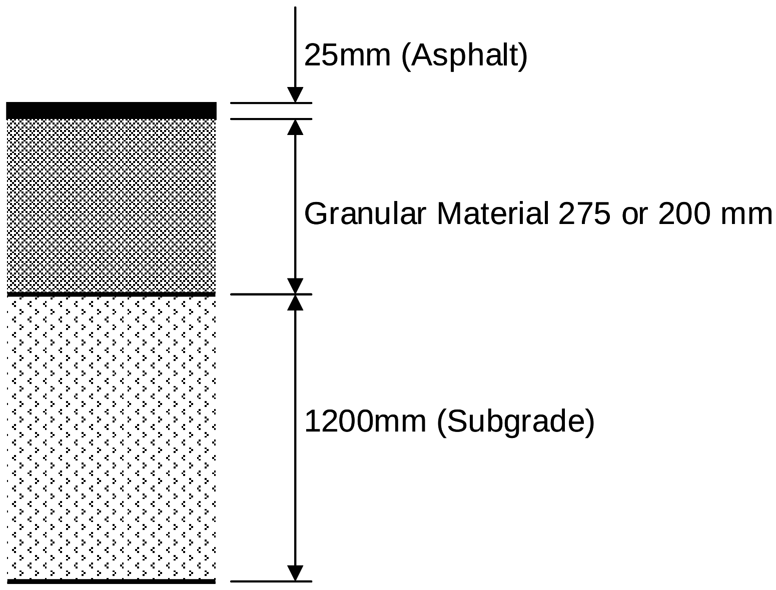

Figure 4.6. Pavement cross-section for CAPTIF 1, 2 and 3 aggregate trials.

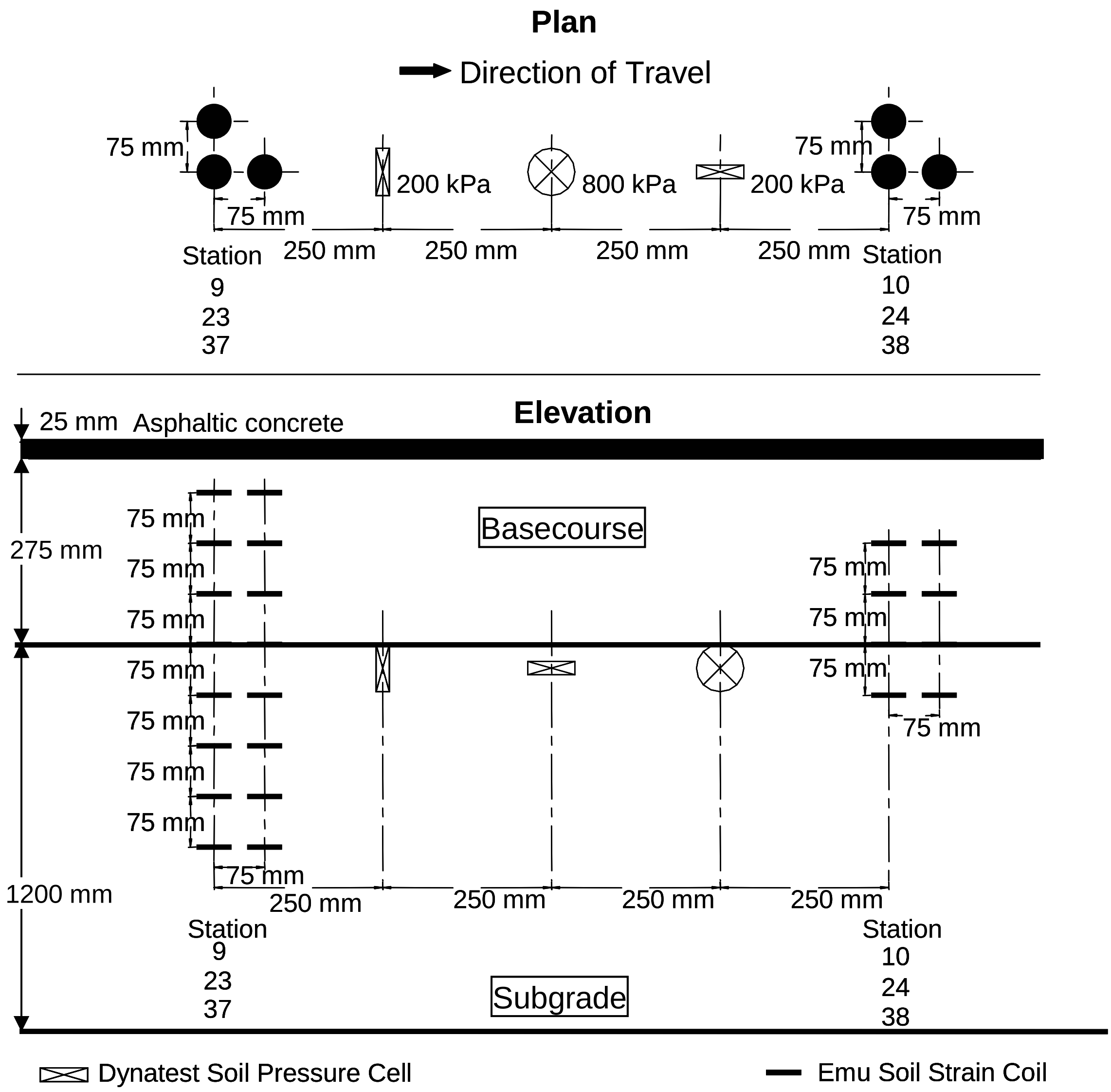

Figure 4.7. Layout of CAPTIF pavement instrumentation.

Figure 4.8. Emu strain coil installation.

Figure 4.9. Transverse profile measured using the CAPTIF profilometer.

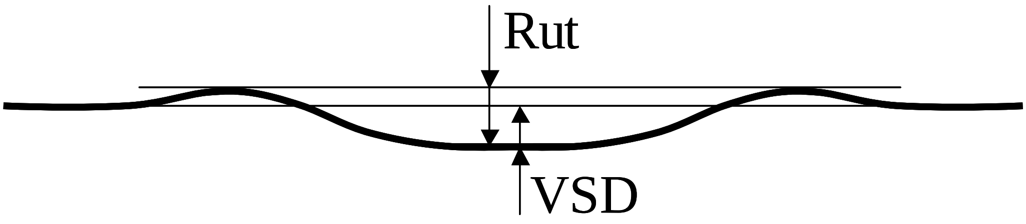

Figure 4.10. The different measures of pavement deformation.

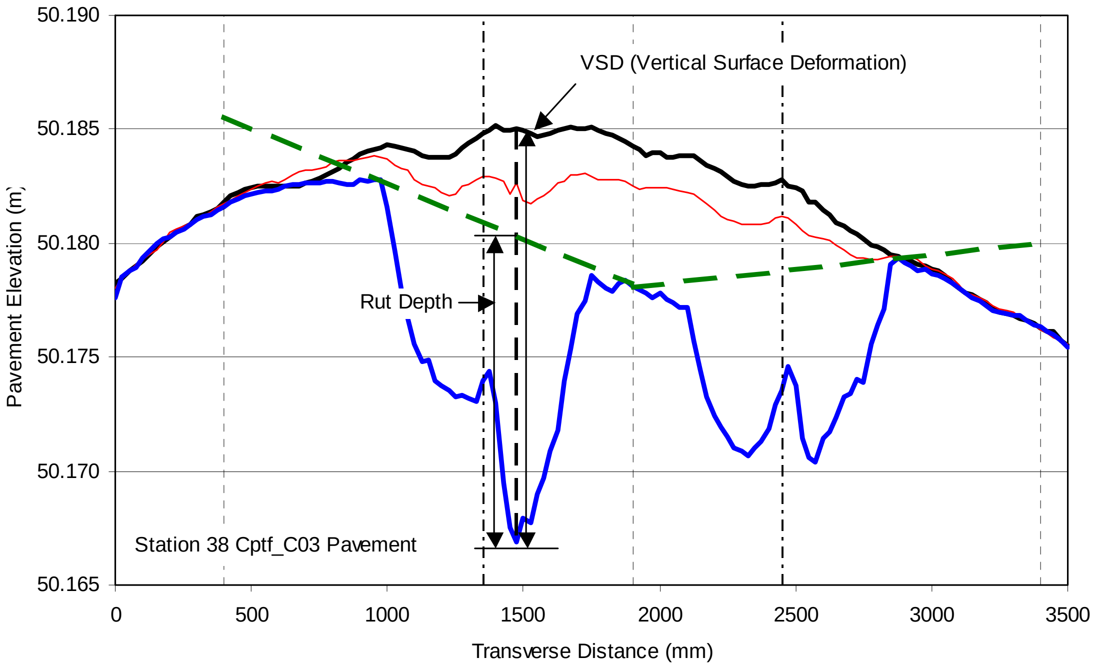

Figure 4.11. Typical measurement of rut depth and VSD at CAPTIF (after Arnold et al, 2004b).

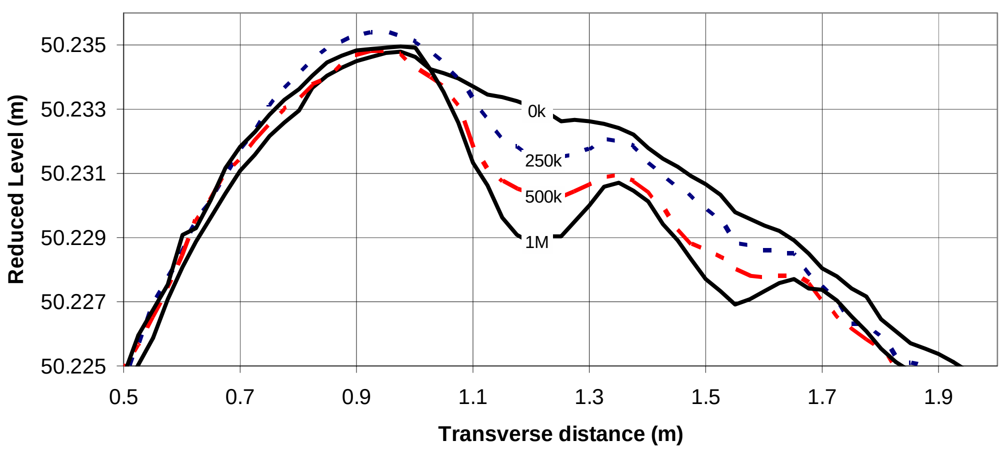

Figure 4.12. Typical CAPTIF transverse profile.

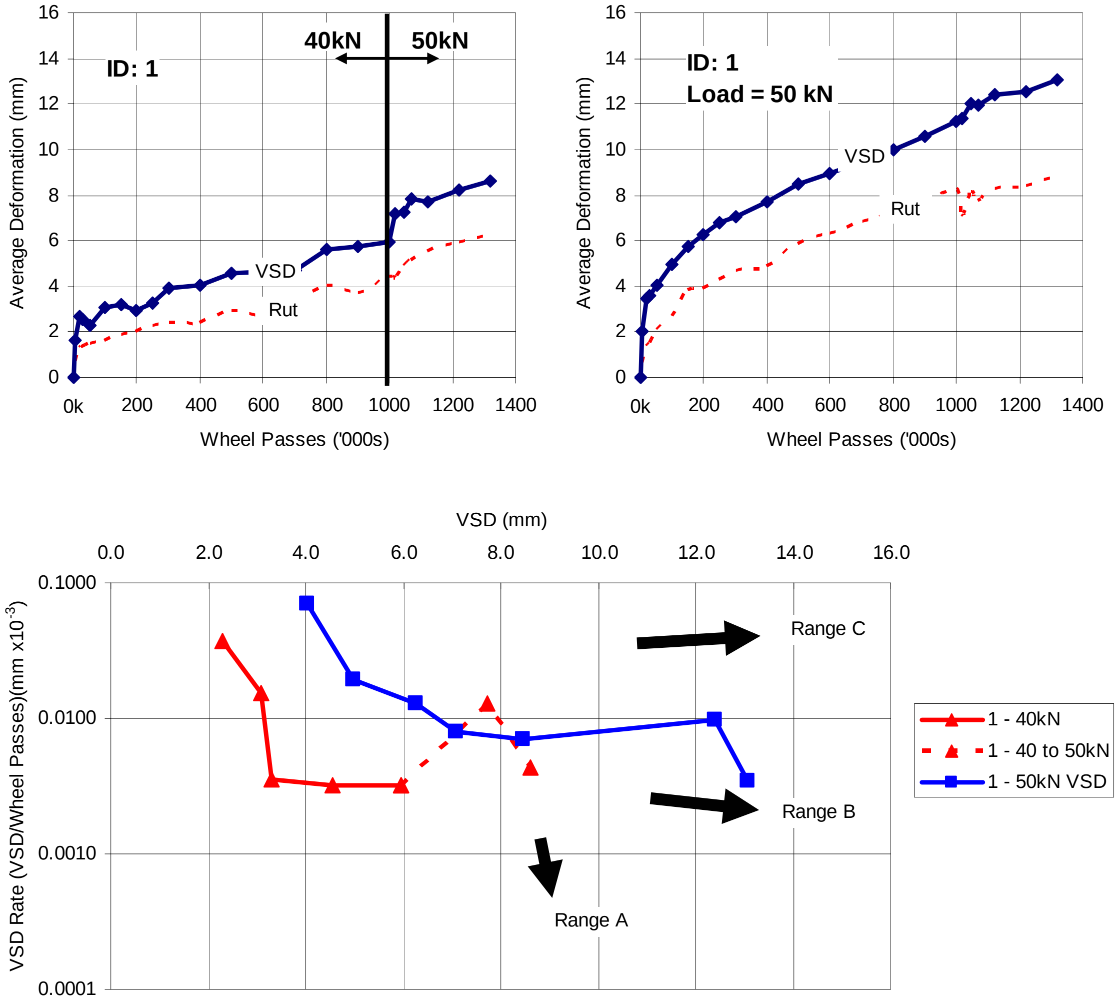

Figure 4.13. Average vertical surface deformation (VSD) and rut depth with load cycles for pavement Test Section 1.

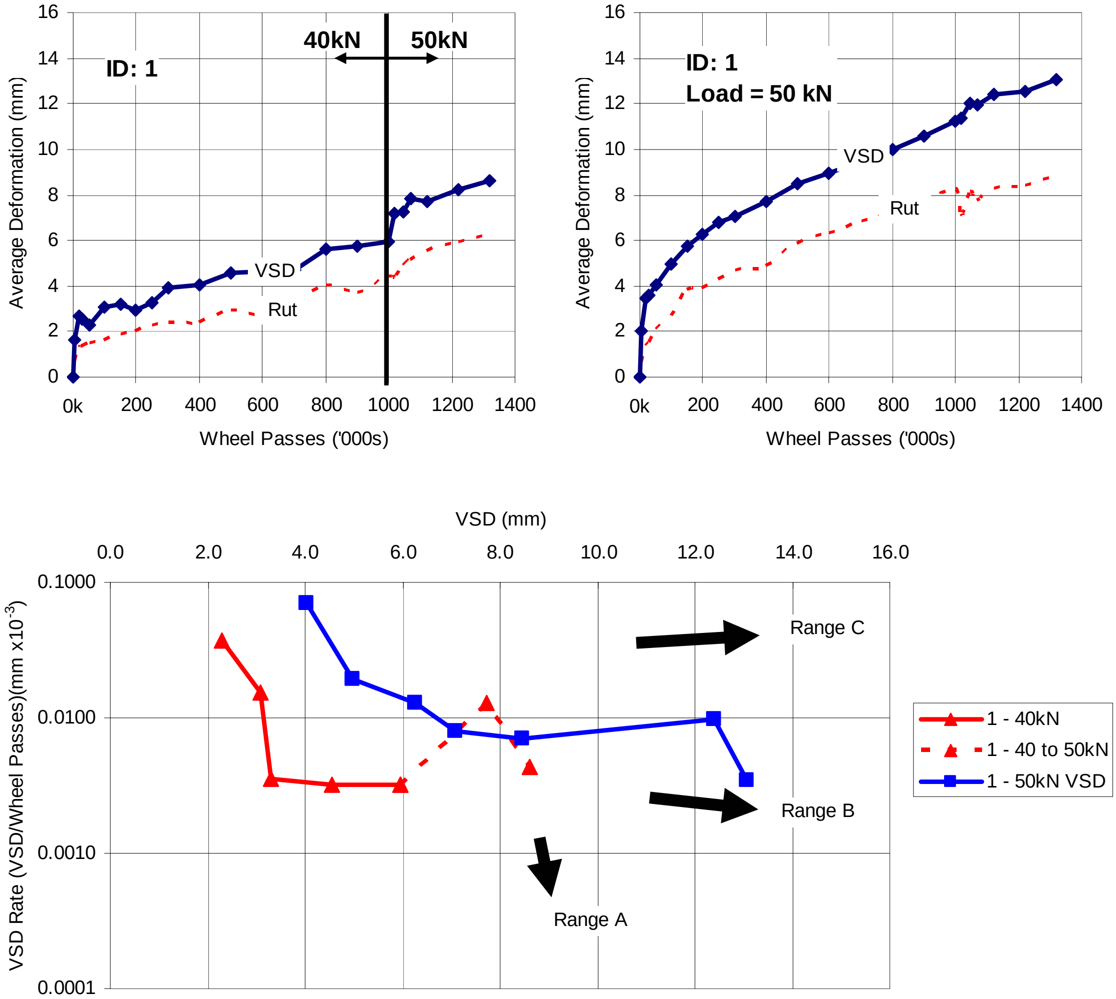

Figure 4.14. Average vertical surface deformation (VSD) and rut depth with load cycles for pavement Test Section 1a .

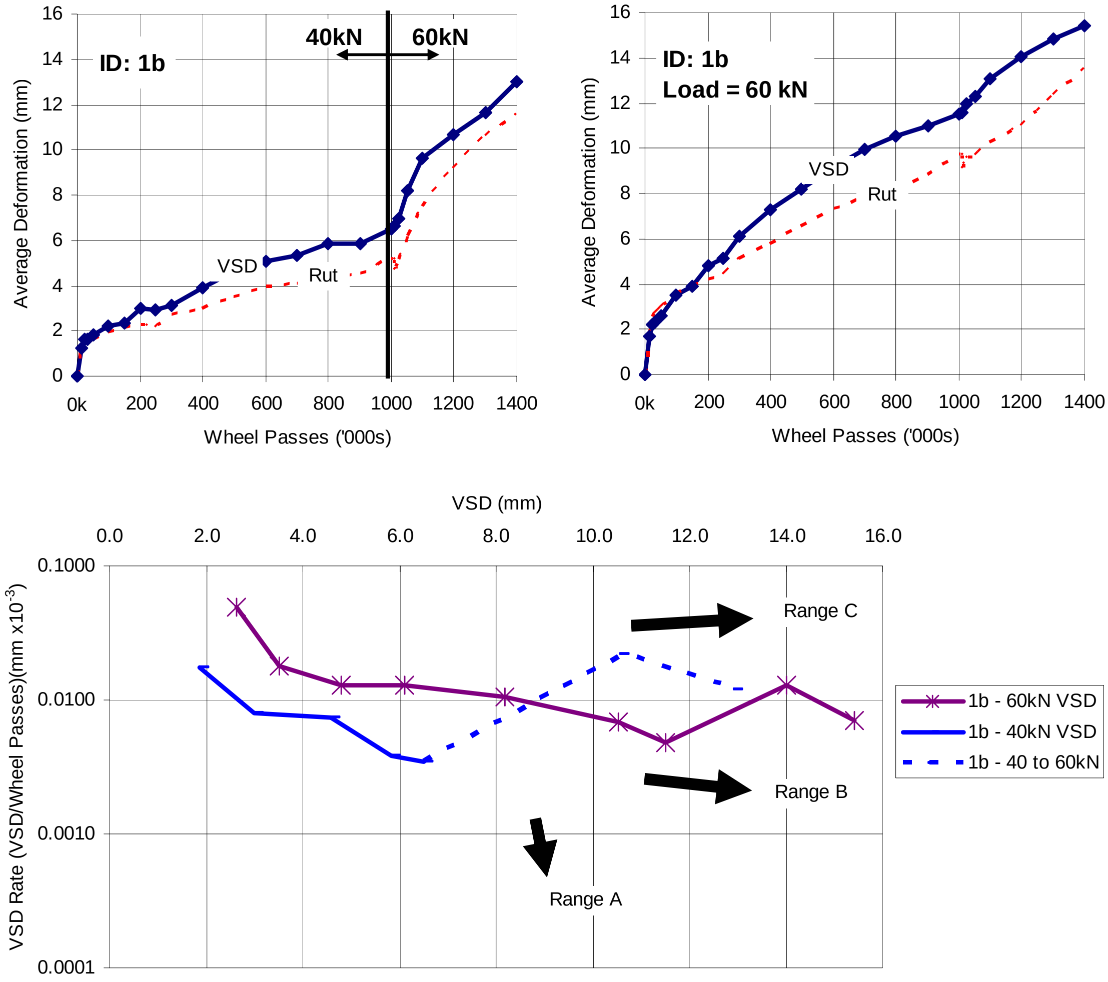

Figure 4.15. Average vertical surface deformation (VSD) and rut depth with load cycles for pavement Test Section 1b.

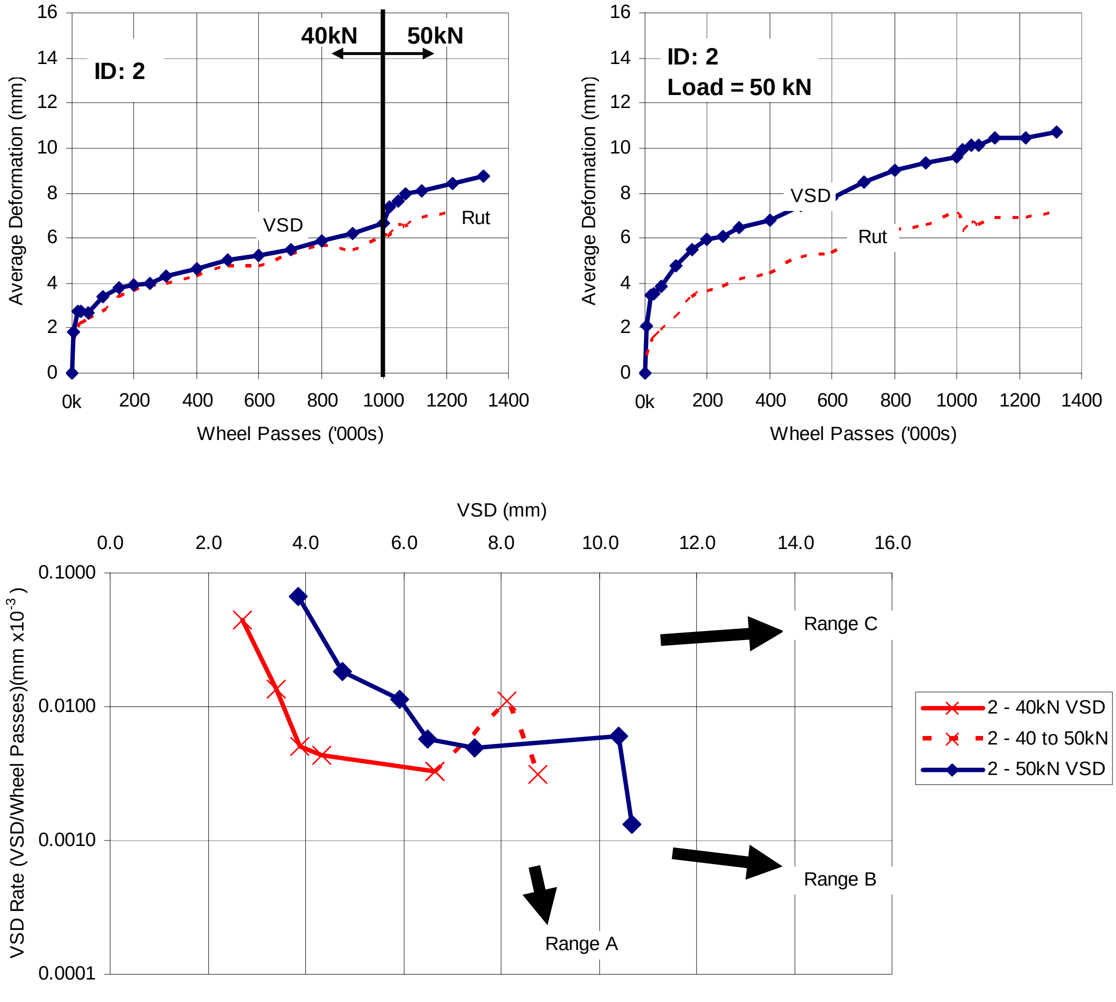

Figure 4.16. Average vertical surface deformation (VSD) and rut depth with load cycles for pavement Test Section 2.

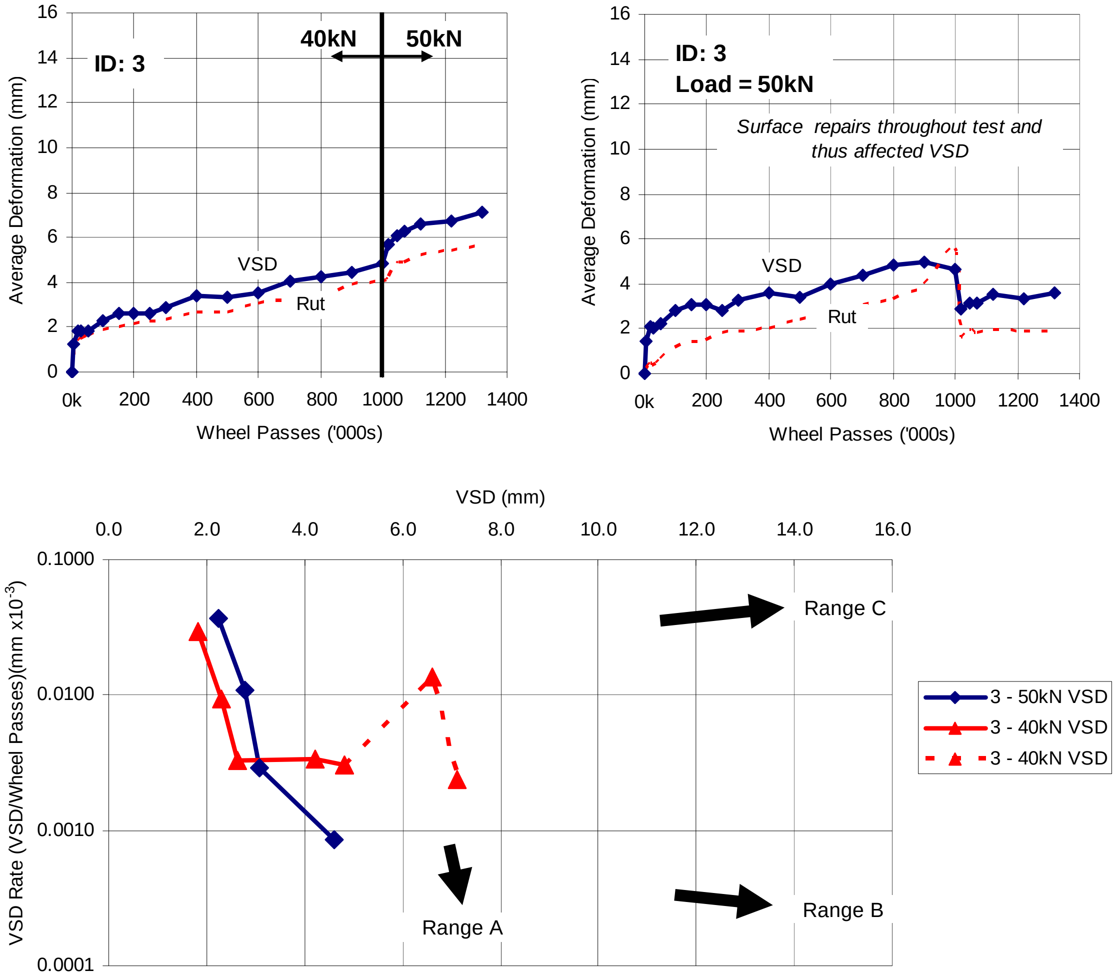

Figure 4.17. Average vertical surface deformation (VSD) and rut depth with load cycles for pavement Test Section 3.

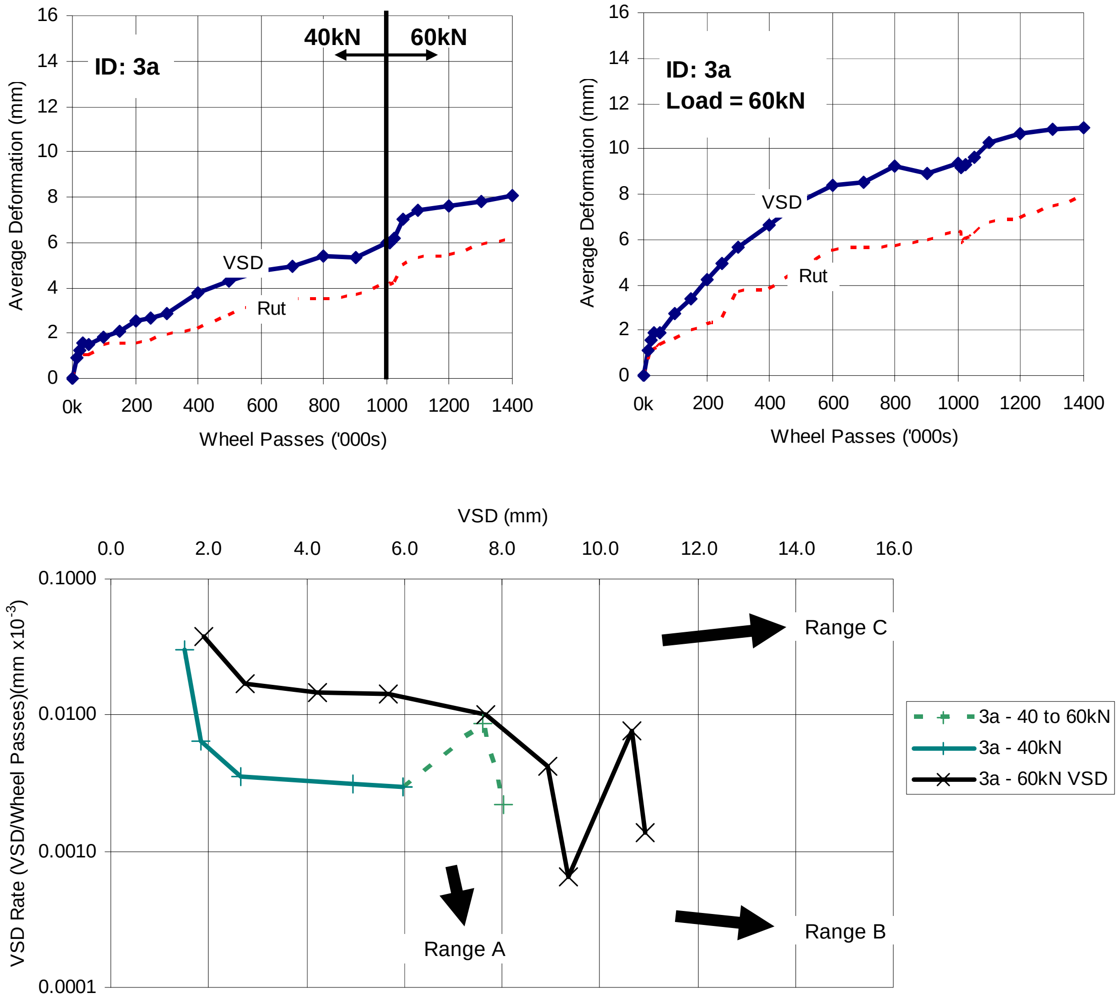

Figure 4.18. Average vertical surface deformation (VSD) and rut depth with load cycles for pavement Test Section 3a.

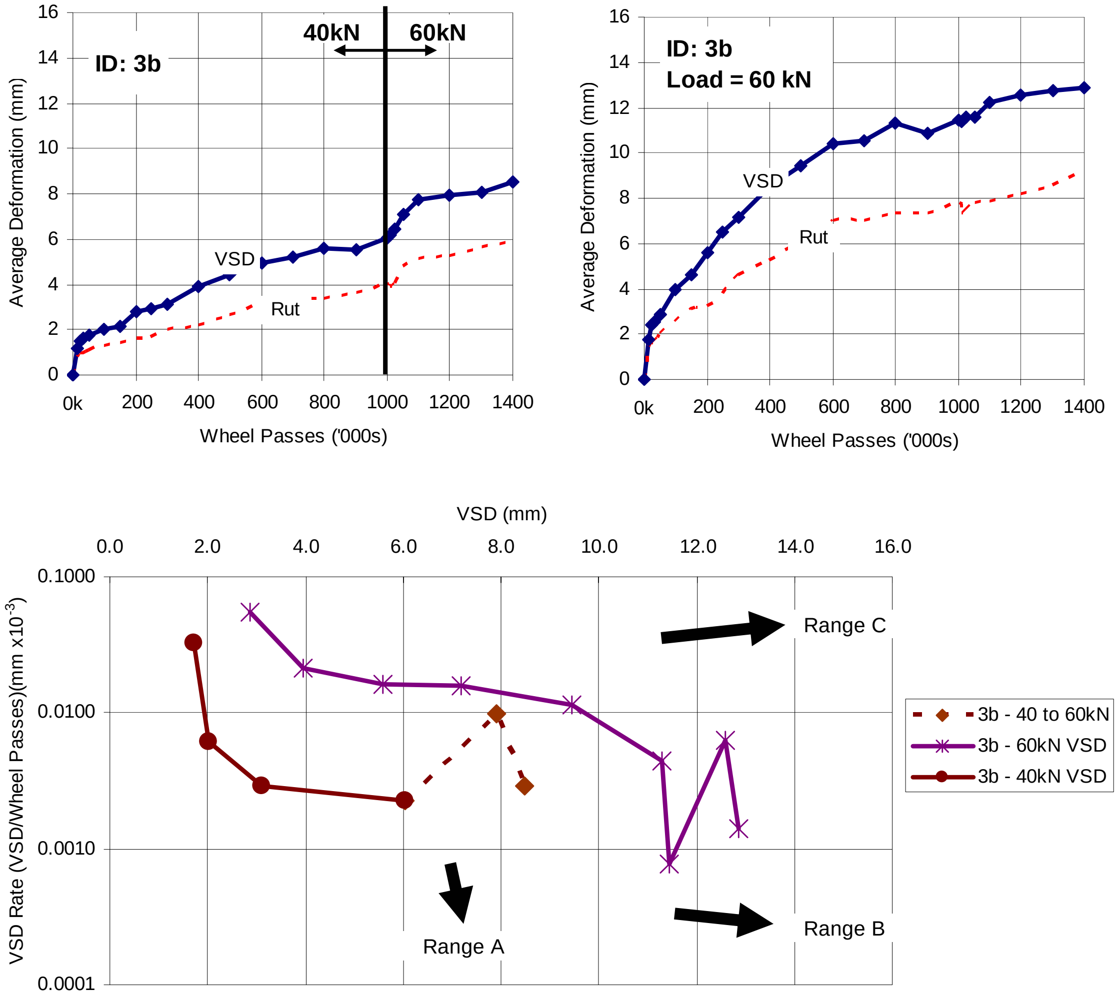

Figure 4.19. Average vertical surface deformation (VSD) and rut depth with load cycles for pavement Test Section 3b.

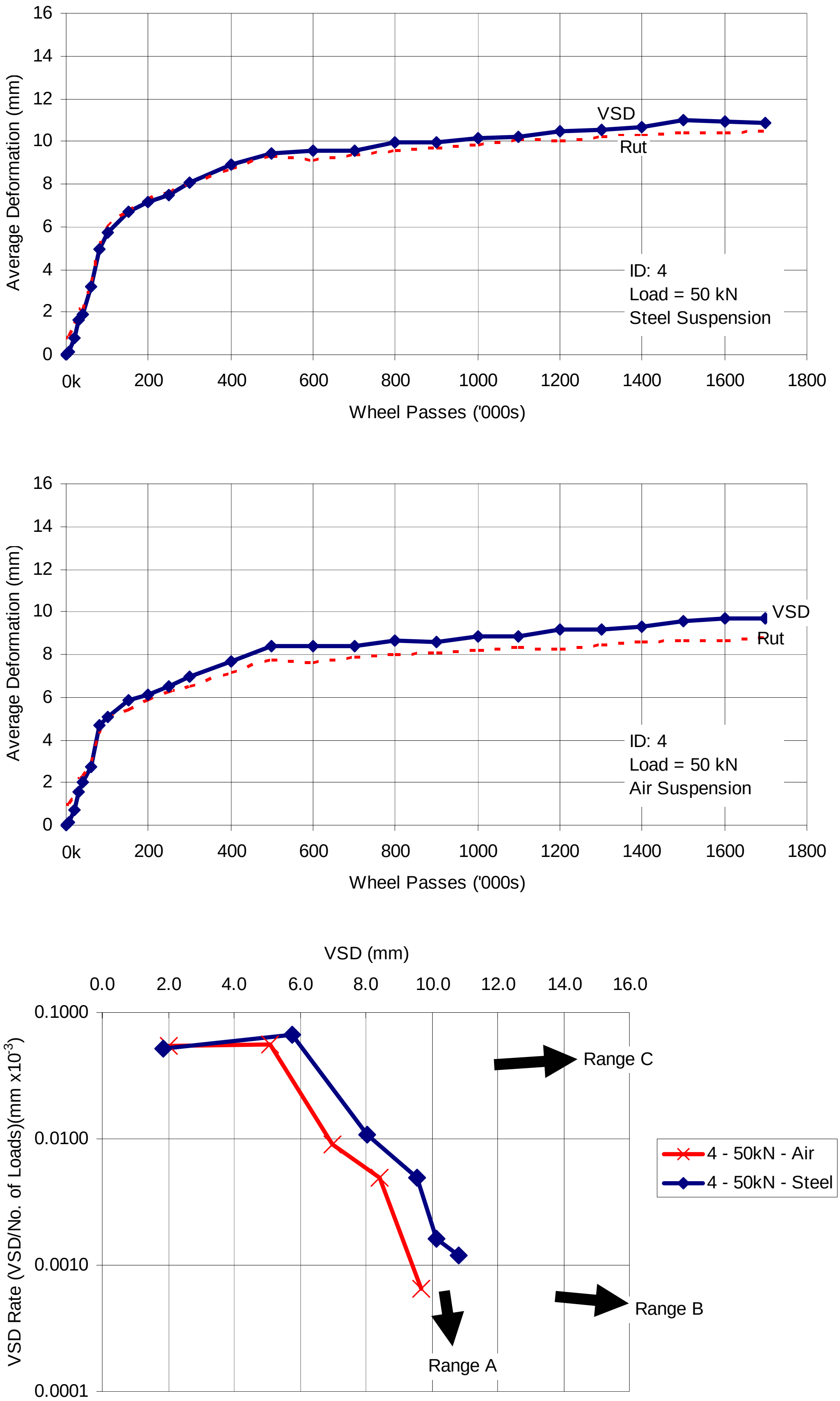

Figure 4.20. Average vertical surface deformation (VSD) and rut depth with load cycles for pavement Test Section 4.

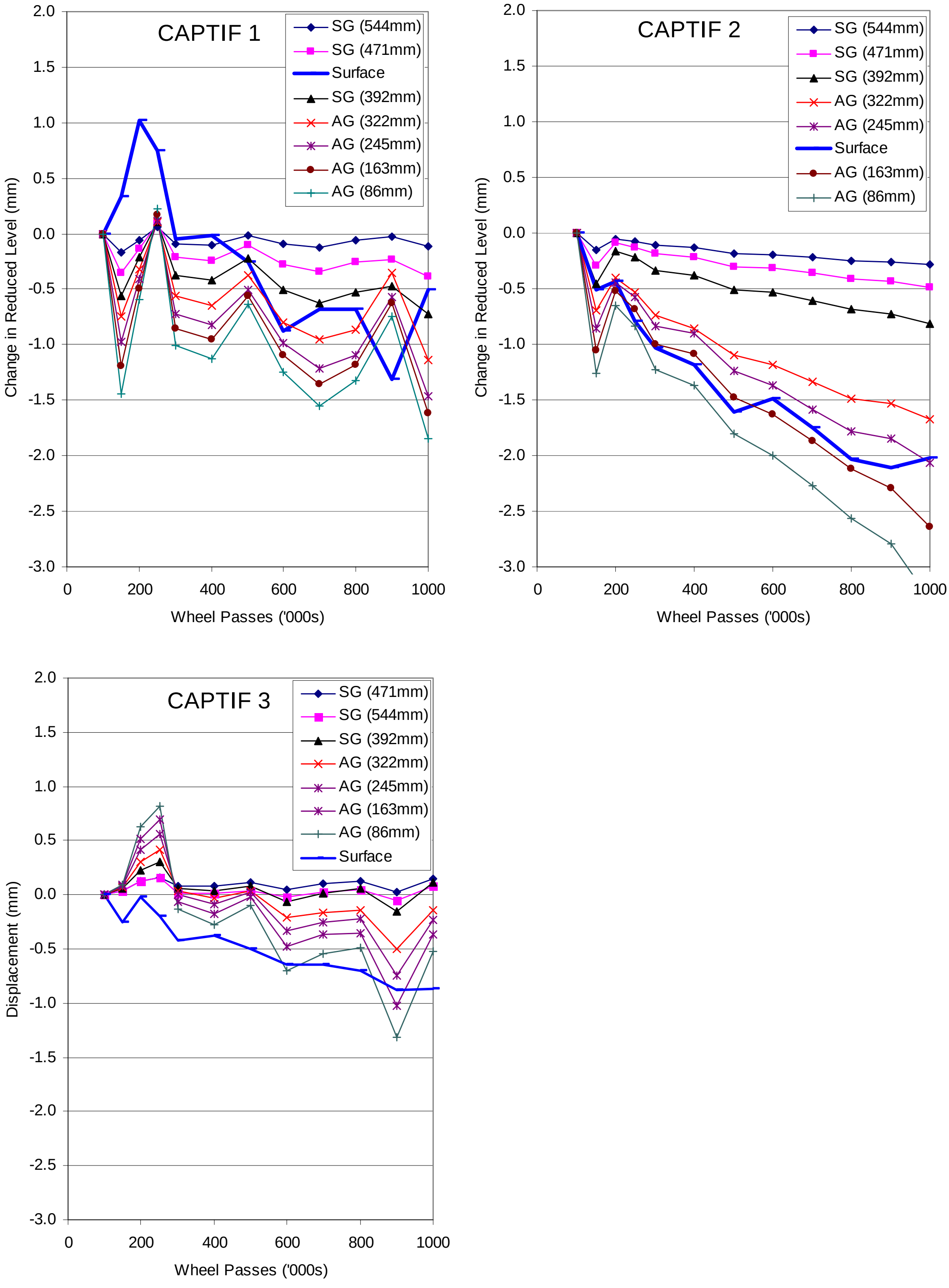

Figure 4.21. Change in reduced level of Emu strain coils starting at 100,000 wheel passes.

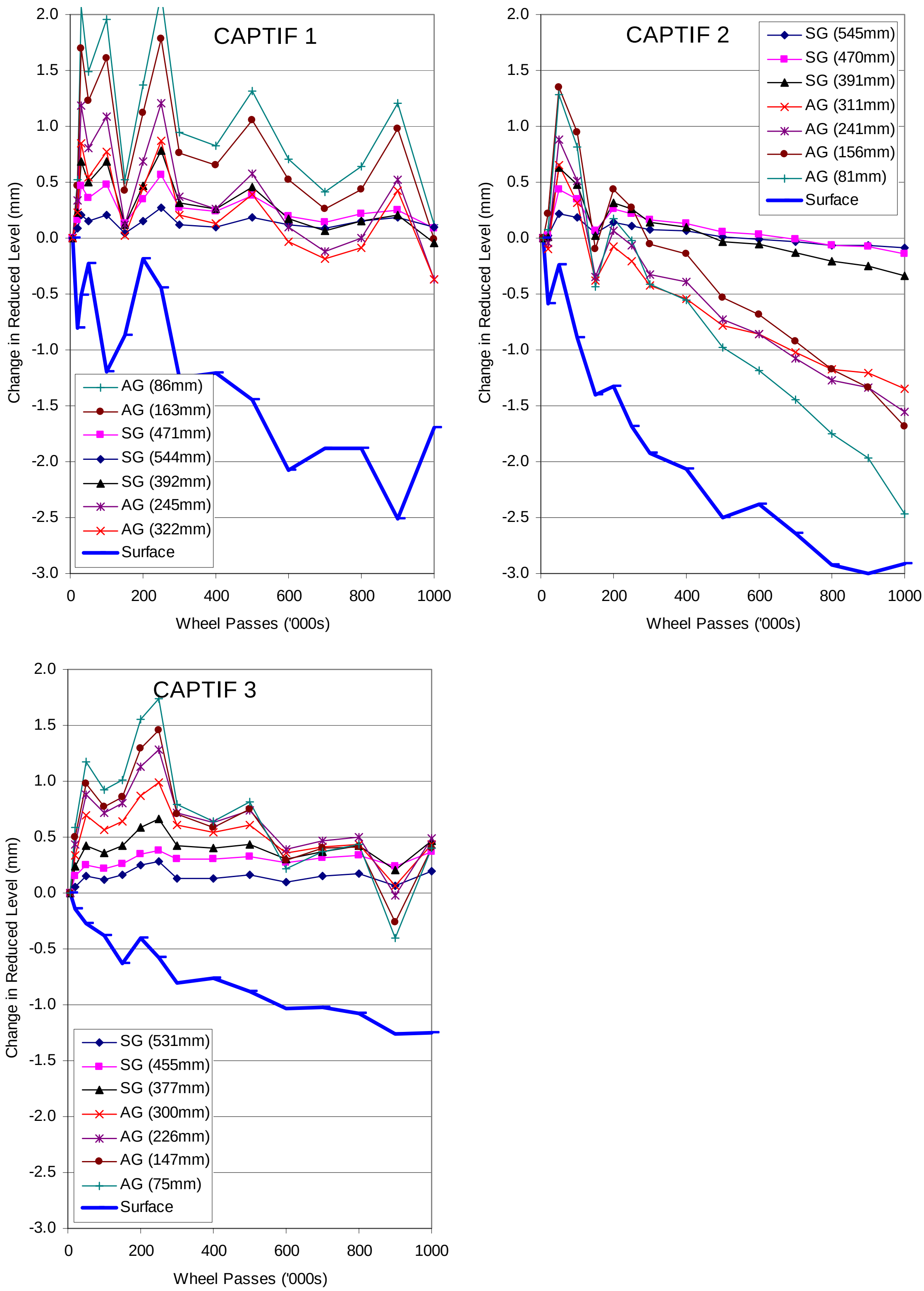

Figure 4.22. Change in reduced level of Emu strain coils starting at 5k wheel passes.

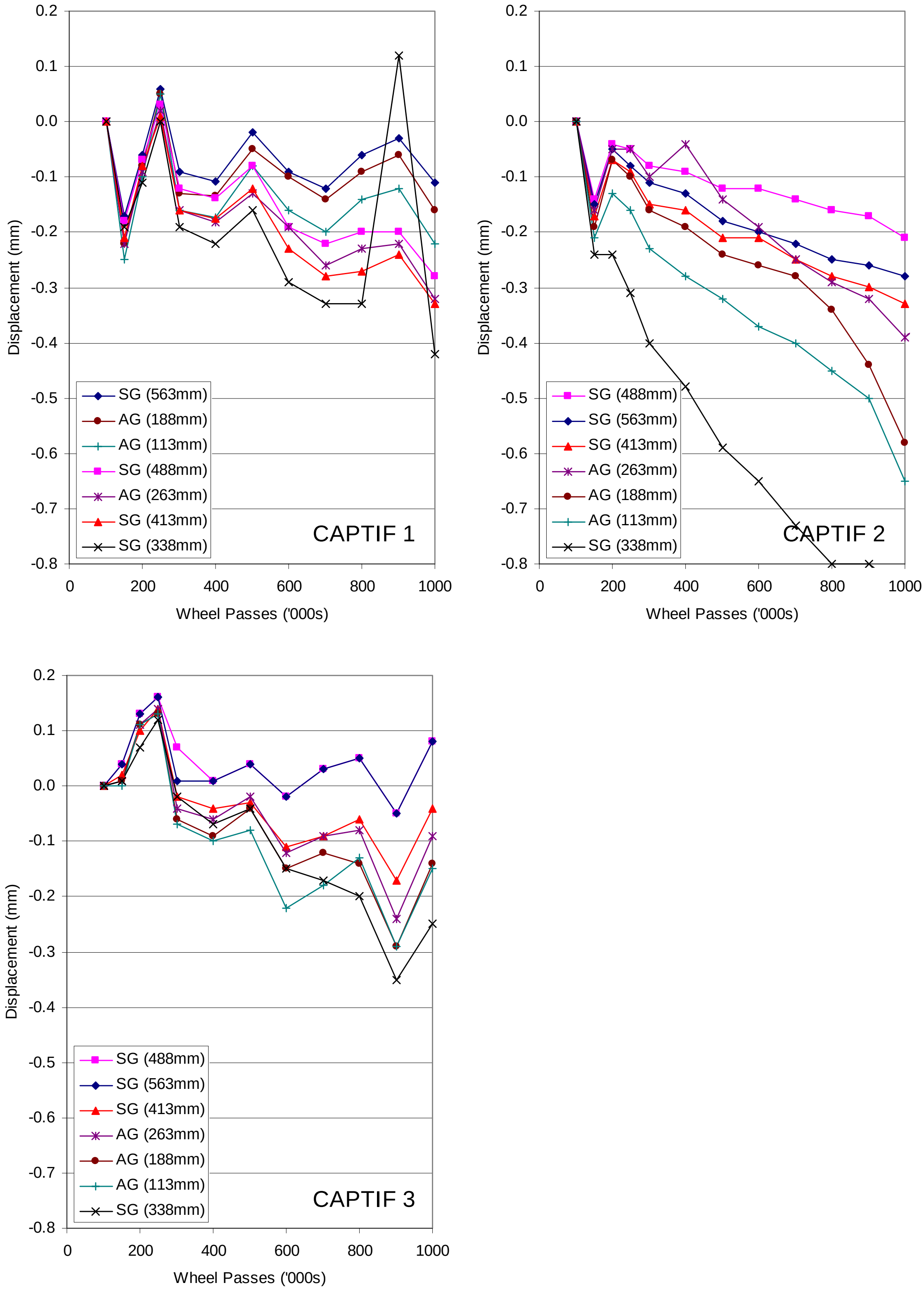

Figure 4.23. Change in spacing of Emu coil pairs from 100,000 wheel passes.

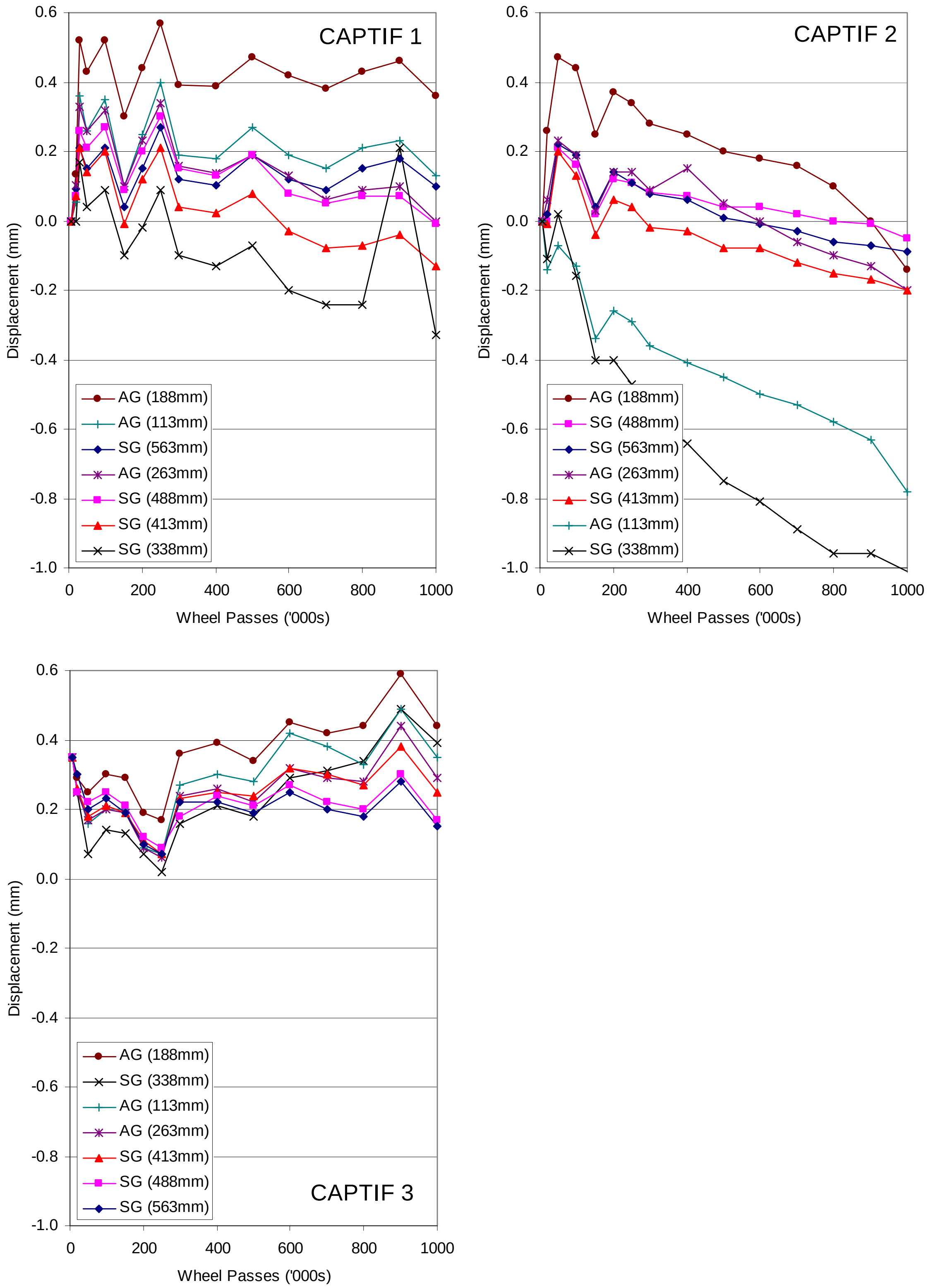

Figure 4.24. Change in spacing of Emu coil pairs from 5k wheel passes.

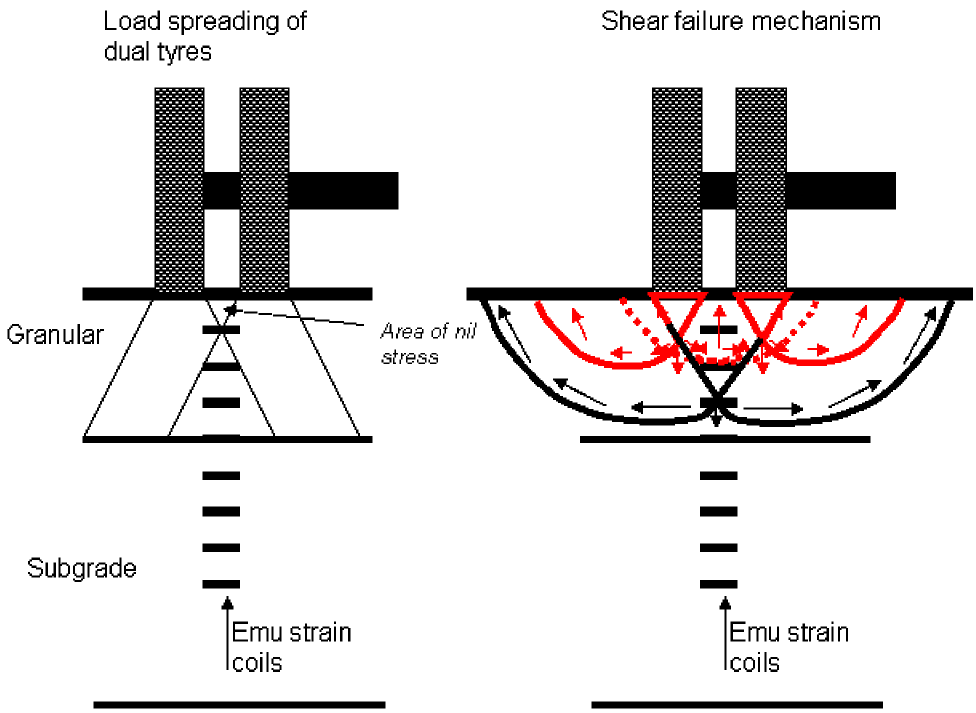

Figure 4.25. Effect of dual tyres on Emu strain coil movement.

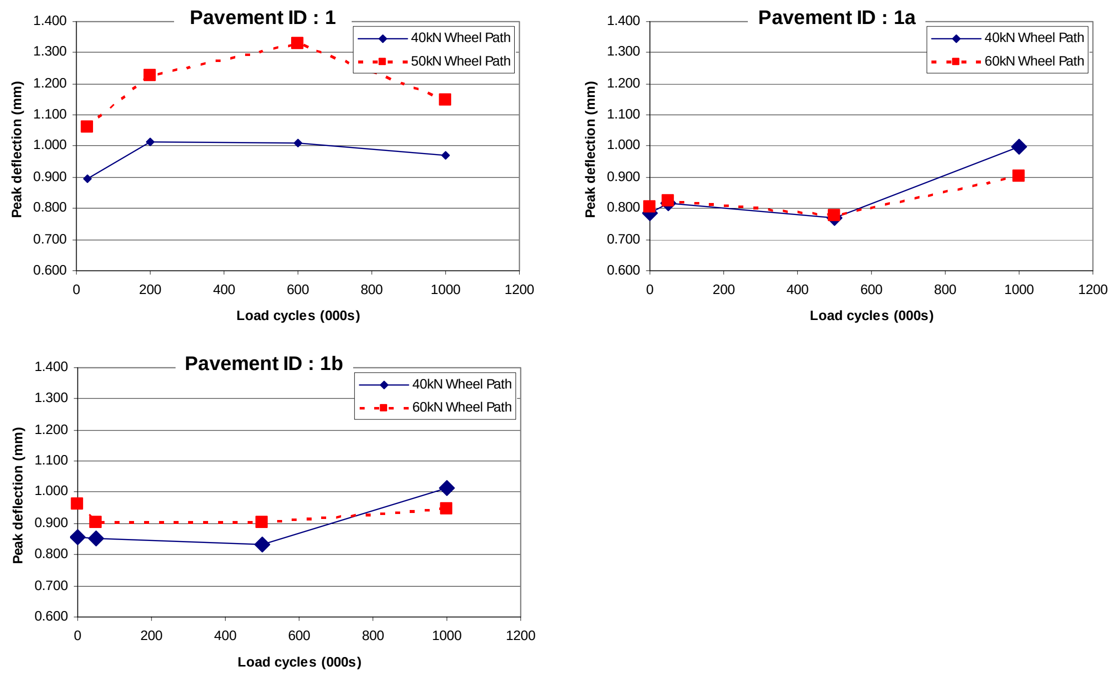

Figure 4.26. Average peak deflection with increasing wheel passes for the Test Sections 1, 1a and 1b (Table 4.1).

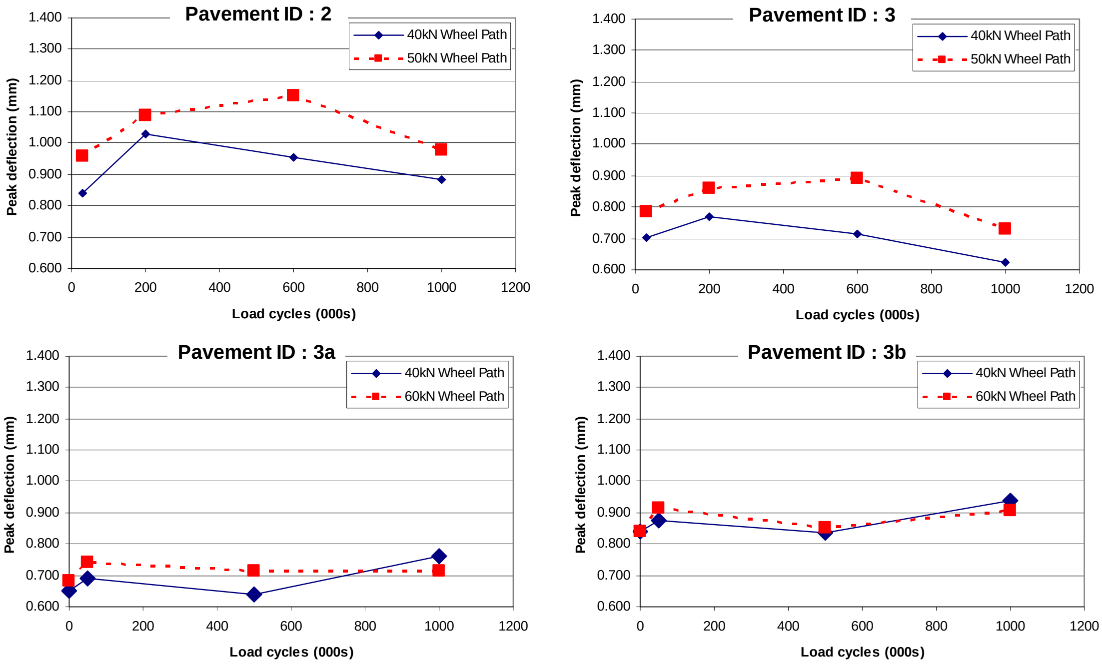

Figure 4.27. Average peak deflection with increasing wheel passes for the Test Sections 2, 3, 3a and 3b (Table 4.1).

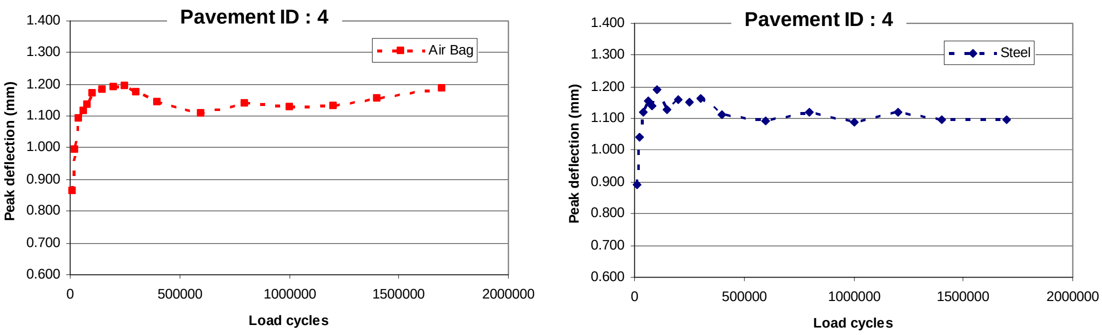

Figure 4.28. Average peak deflection with increasing wheel passes for the Test Section 4 (Table 4.1).

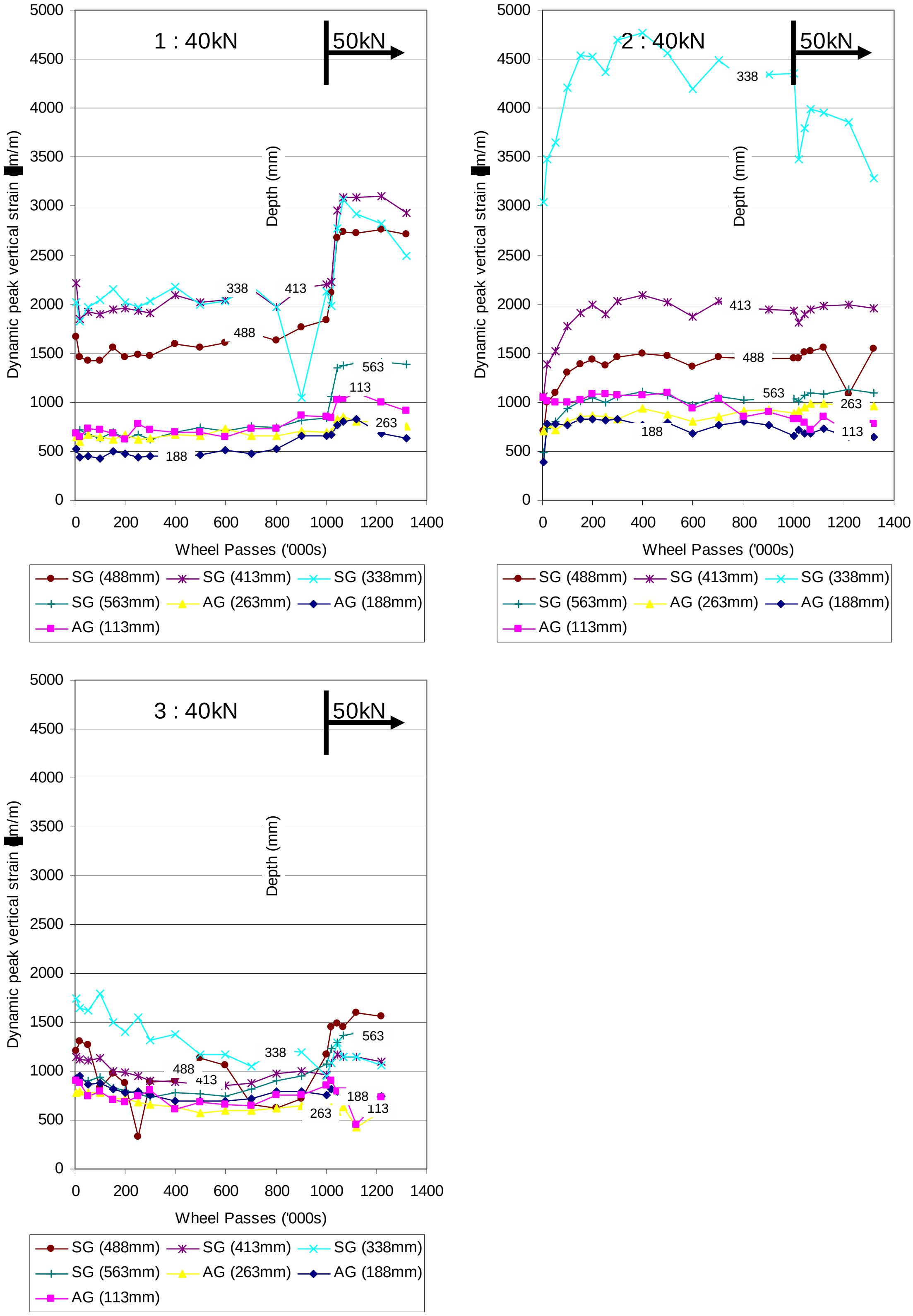

Figure 4.29. Peak dynamic vertical strains with increasing load cycles for 2001 tests (Test Sections 1, 2 & 3 Table 4.1).

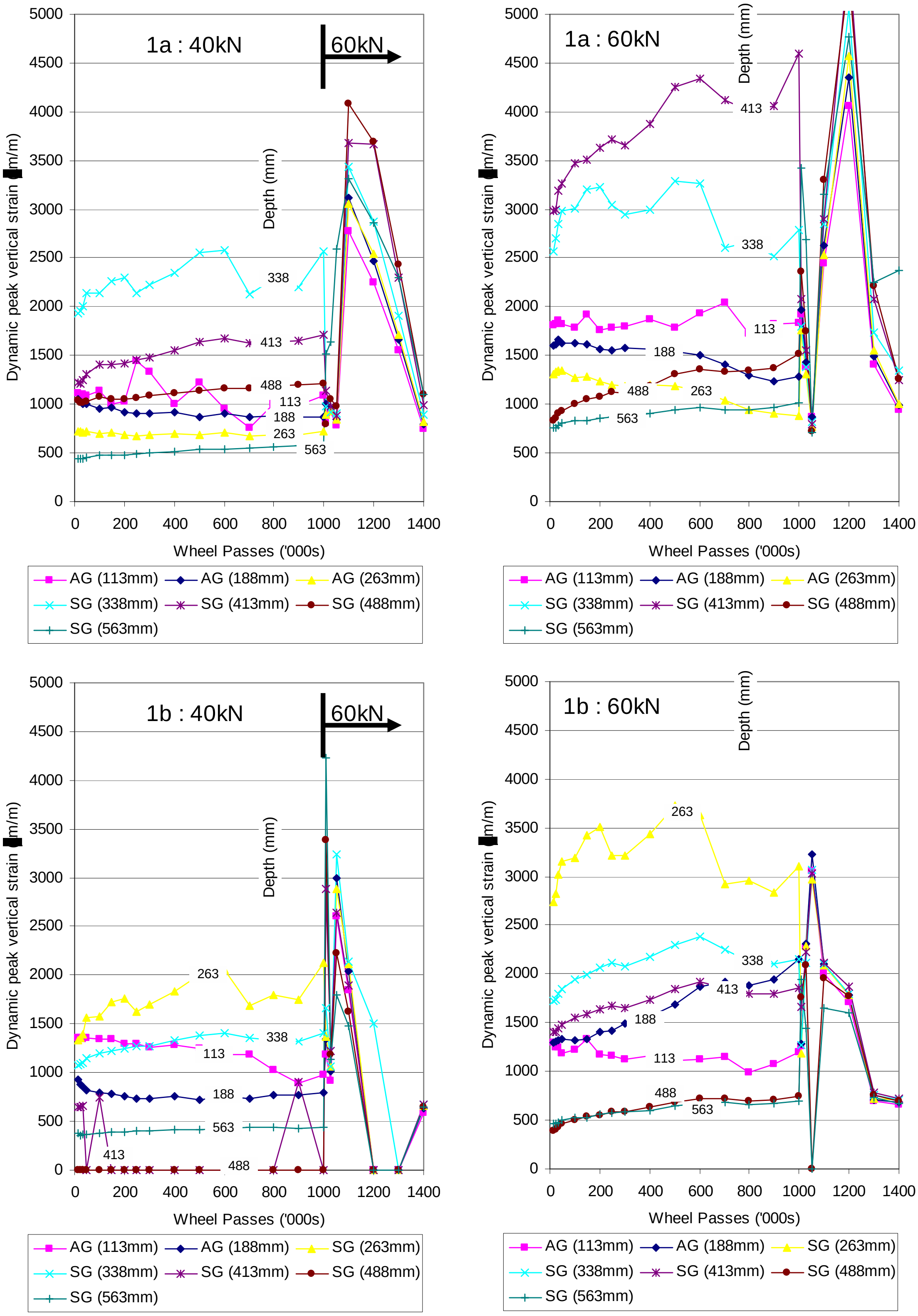

Figure 4.30. Peak dynamic vertical strains with increasing load cycles for 2003 tests (Test Sections 1a & 1b Table 4.1).

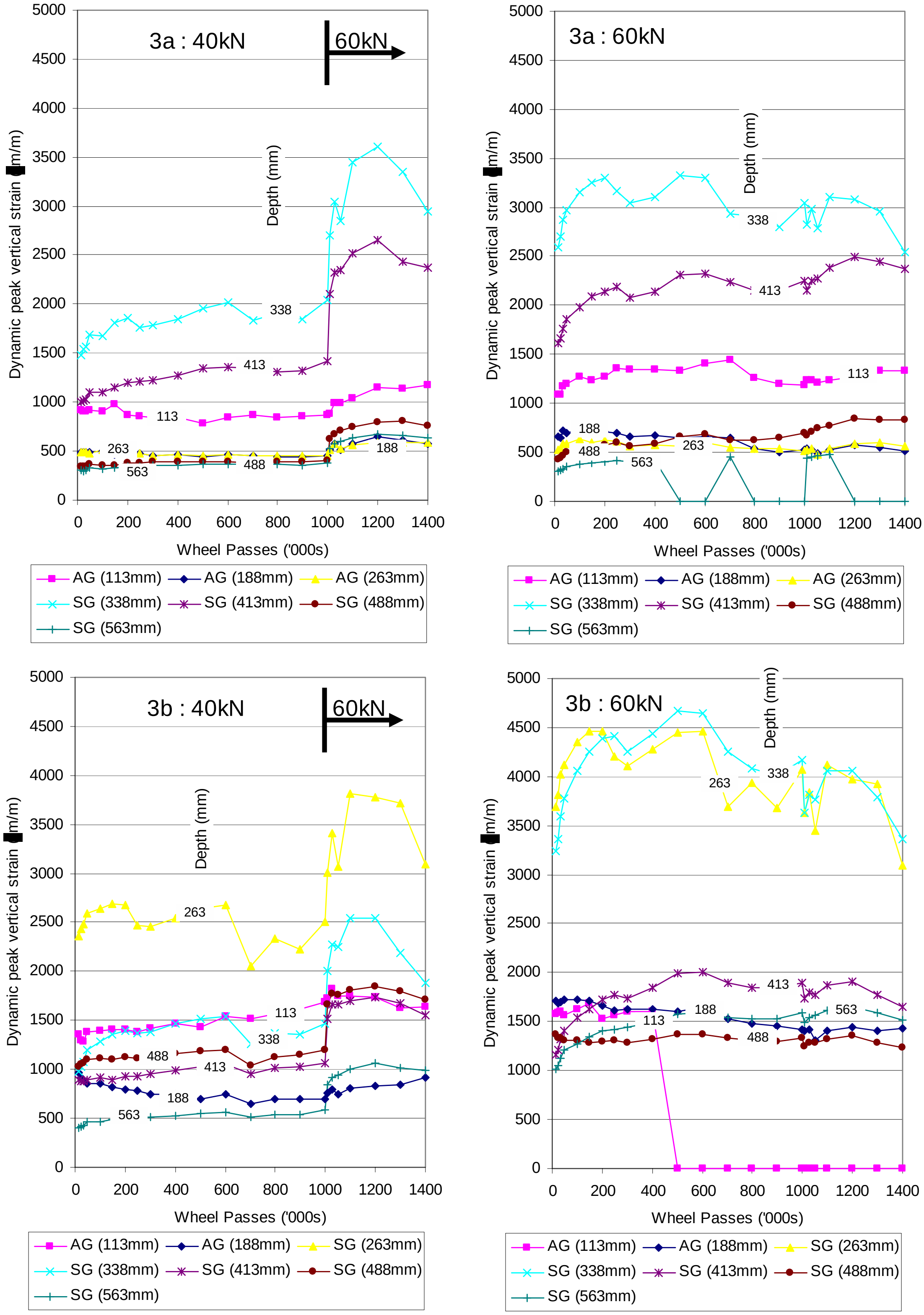

Figure 4.31. Peak dynamic vertical strains with increasing load cycles for 2003 tests (Test Sections 3a & 3b Table 4.1).

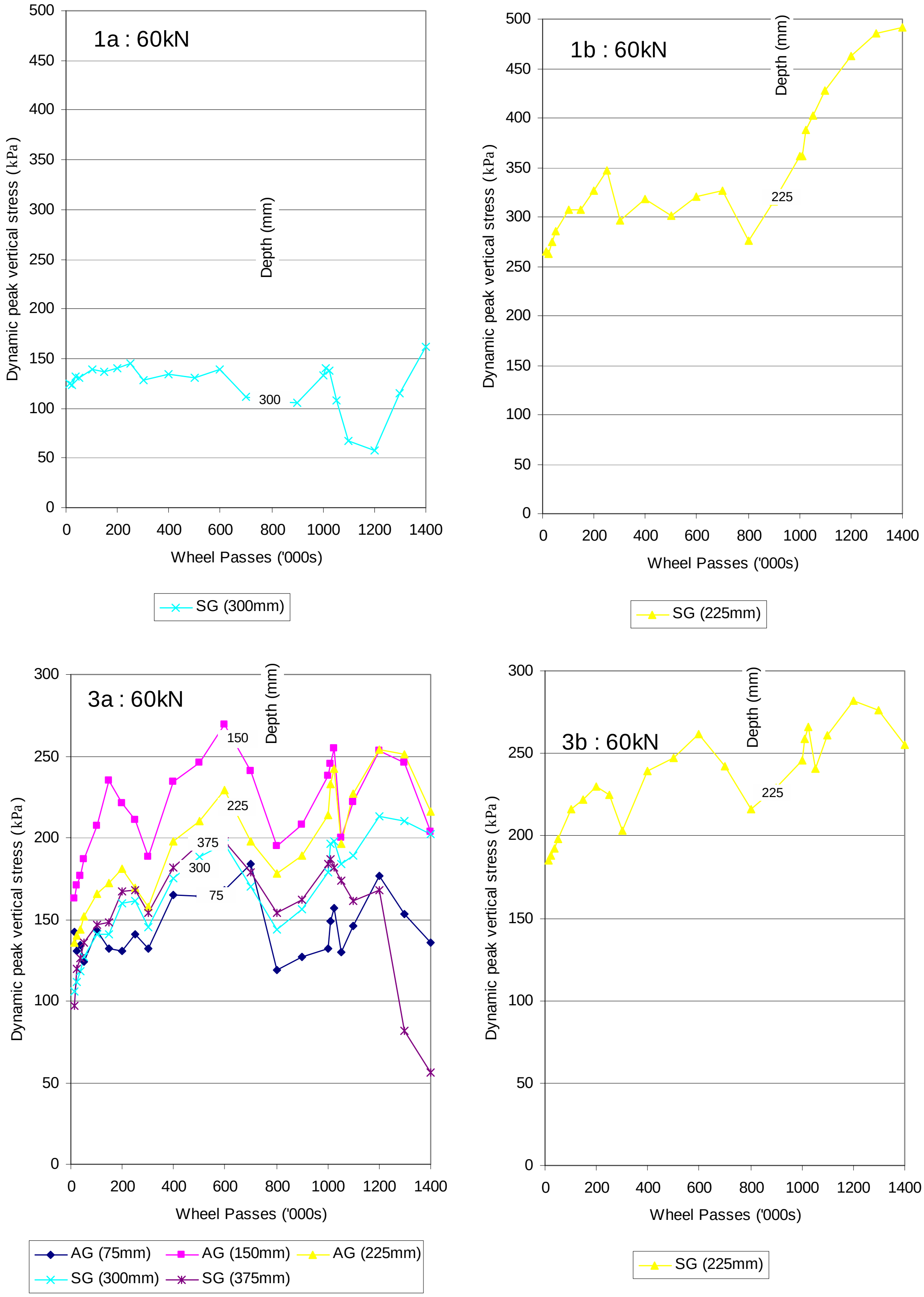

Figure 4.32. Peak dynamic vertical stress with increasing load cycles for 2003 tests in the 60kN wheel path (Test Sections 1a, 1b, 3a & 3b Table 4.1).

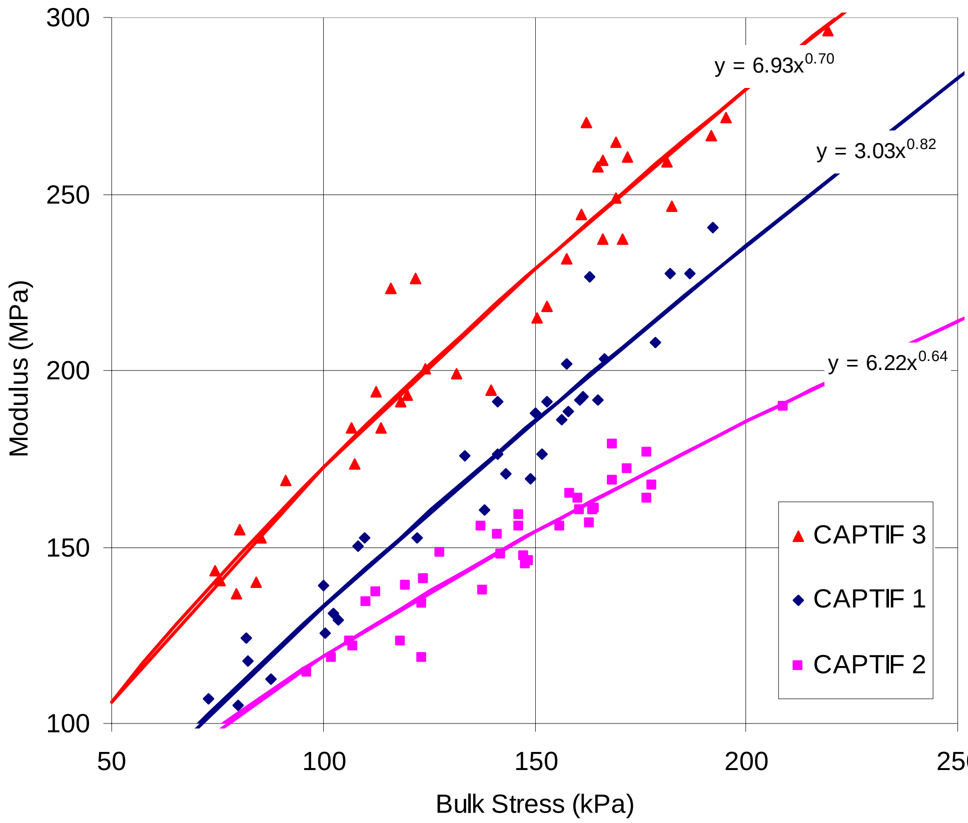

Figure 4.33. Modulus versus bulk stress from measured stresses and strain.

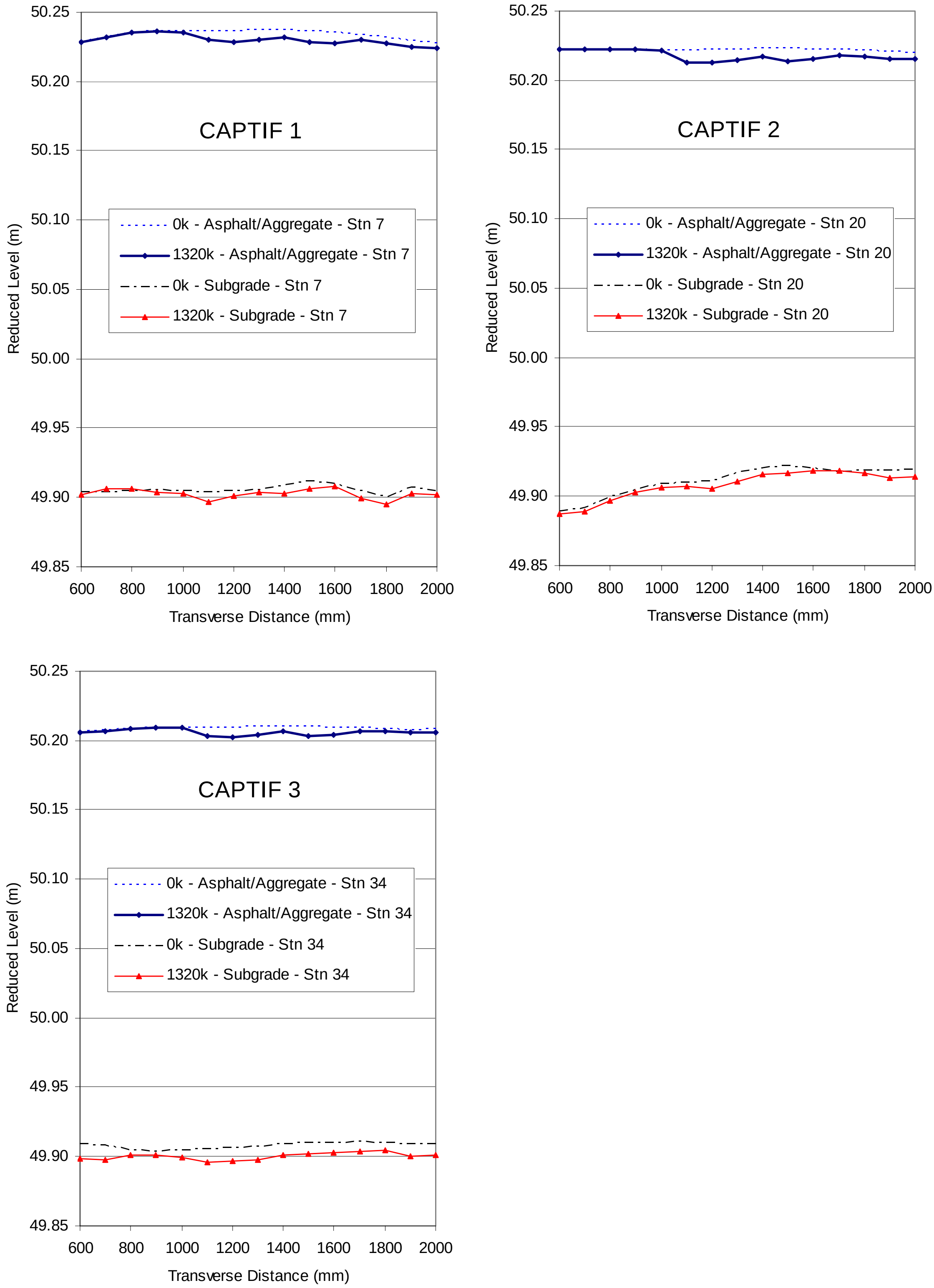

Figure 4.34. Reduced levels of aggregate and subgrade surfaces before and after testing.

CHAPTER 5 NORTHERN IRELAND FIELD TRIAL

5.1 INTRODUCTION

To complement the results from the New Zealand accelerated pavement tests (Chapter 4) a field trial was conducted in Northern Ireland. The field trial differs from the New Zealand tests as it is a actual road used by lorries in an outdoor environment. Two granular materials (NI Good and NI Poor, Table 3.1) as tested in the laboratory study (Chapter 3) were used in the Northern Ireland field trial. This field trial will be later used in finite element and permanent deformation modelling (Chapters 6 and 7 respectively). There are many factors that affect pavement performance including the environment, residual/confining stresses, shear stress reversal and influence of the pavement structure as a whole that cannot be fully simulated in the laboratory nor the Finite Element Model (FEM). Therefore, a key result from the Northern Ireland field trial is surface rutting with respect to number of wheel passes that can be compared against predictions of rutting behaviour (Range A, B or C, Section 2.11.2) and rut depth.

The field trial was sponsored by the Department of the Environment (DOE) Northern Ireland, United Kingdom and constructed on a straight section of road accessing the Ballyclare landfill in Northern Ireland, UK. The section chosen was just before the weighbridge allowing the weight of all heavy vehicles passing over the trial to be recorded. Further, a concrete kerb on the left hand side allowed permanent reference markers to be placed for repeat measurements of rutting. Figure 5.1 shows the locality plan. Instrumentation was used in the pavement trial to measure stresses and strains, while a profiler was used to obtain the transverse profile for the calculation of rutting.

This chapter reports the process of design, construction and monitoring of the Northern Ireland field trial. Insitu strains and stresses are reported along with wheel loads. Rutting is calculated for each section at regular loading intervals and the shakedown behaviour range is determined (Range A, B or C, Section 2.11.2). Finally, the difficulties found in monitoring the field trial are discussed along with recommendations for establishing future field trials.

5.2 DESIGN

The results from the RLT tests were categorised into 3 behaviour ranges A, B and C (Section 3.8.2). Range A is stable behaviour while Range C is incremental collapse and Range B is between Ranges A and C (Section 2.11.2). Stress level was the primary factor influencing the permanent deformation behaviour and thus shakedown range as indicated in Figure 3.15. Ideally, the aim of the field trial is to show these three different shakedown ranges. However, it is likely during the time frame of the study there will be insufficient number of wheel loads to enable a confident determination of the shakedown ranges.

The pavement types trialled were two sections varying only in the unbound granular material type (i.e. *NI Good* or *NI Poor*, Table 3.1) and surfaced with a structural asphalt layer. Discussion with the site owner and the use of a dynamic cone penetrometer revealed that the subgrade was very strong and consisted of predominantly rock material. Therefore, to ensure the strong subgrade material did not influence the shear zones caused by a dual lorry tyre (width approx 700mm) a large thickness of granular material was required. Granular thickness was chosen as the minimum thickness to ensure the lines of potential shear failure (i.e. bearing failure, Craig 1992), that extend downwards by 1.5 times the tyre diameter/width, are not influenced by the solid rock subgrade that was typically found at the site. A granular thickness of at least 700mm was thought best but was limited to 450mm at the time of design to keep within budget constraints. ????? Prof Rogers Question (originally labelled to page 154) needs answering here.

Linear elastic analyses on a range of pavement cross-sections with various asphalt thicknesses were undertaken to determine suitable asphalt thicknesses to trial. The program used in New Zealand and Australia for mechanistic pavement design, CIRCLY (Wardle, 1980) was utilised for the linear elastic analyses. A moduli of 200 MPa with a Poisson's ratio of 0.35 was assigned to the granular materials as an approximate estimate based on RLT test results (Table 3.5) and considered appropriate for a preliminary analyses of the pavements (Austroads, 1992). A moduli of 3000 MPa with a Poisson's ratio of 0.35 was assumed for the asphalt layer being based on recommendations in the Austroads Pavement Design Guide (Austroads, 1992).

Results of the linear elastic analyses were reported in terms of stress invariants *p* (mean principal stress) and *q* (principal stress difference) (Section 2.4.3) calculated to occur in the centre of the wheel load at depth increments of 10mm within the granular materials. A horizontal residual stress of 30kPa was added to the stresses computed under a wheel load for the calculation of stress invariants *p* and *q*. The value of 30kPa was considered appropriate to account for the lateral stresses developed during compaction and the material's self weight (see Section 2.4.6). Further, the horizontal stress added did account for the shortcomings of linear elastic analyses where large tensile stresses were computed at the base of granular layers (Akou et al, 1999). Stress invariants *p* and *q* calculated without (nil) and with 30kPa horizontal residual stress added were plotted for a range of asphalt cover thicknesses (40 to 100mm) along with the shakedown Range A/B boundary determined for the NI Good and NI Poor materials (Figure 3.15) as shown in Figures 5.2 and 5.3. These plots of stresses in the granular material show that the asphalt cover thickness influences the shakedown range predicted, Figure 5.3, with the 30 kPa residual stress being a more realistic estimate. As expected, Range B was predicted for pavements with thin asphalt cover while stable behaviour (Range A) was predicted for thick asphalt cover. Based on these predictions the field trial was planned to be constructed with a range of asphalt thicknesses and split into two sections each varying only by aggregate type (*NI Good* or *NI Poor*).

The final design of the field trial was also influenced by the allowable budget, site restrictions, construction and pavement instrumentation limitations, in addition to the requirements for varying asphalt thickness. Due to budget restraints the design thickness of aggregate was limited to 450mm. The asphalt thickness was aimed to vary continuously from 40mm, being the thinnest for construct-ability reasons, to a thickness of 100mm over a length of 15 metres per section in order to observe its influence on rutting behaviour.

Two sections were built side by side in order to comparatively test the *NI Good* and *NI Poor* aggregates. Further, it was thought for ease of constructing constant thicknesses of aggregate layers that the excavation would taper to allow the thickness of aggregate to be the same everywhere. The design longitudinal cross-section is shown in Figure 5.4. As later discussed in Section 5.6 *Construction* the design requirements were not achieved. Asphalt cover thickness varied randomly from 80 to 120mm and the aggregate depth varied from 600 to 800mm.

For setting out during construction, design drawings based on a level survey at 1 metre intervals were developed. This detailed survey was primarily conducted for the purposes of establishing the instrument locations. An example of design cross-section drawings for set-out showing instrument locations is shown in Figure 5.5.

5.3 STRAIN MEASUREMENT

It was proposed early in the study to instrument the field trial to measure pavement response under load. Strain was measured dynamically under wheel loading at a range of locations. However, the measurement of dynamic resilient strain is not pivotal to the direction of this thesis that aims to show permanent deformation behaviour and magnitude can be predicted from models derived from Repeated Load Triaxial testing undertaken in Chapter 3. The results of strain measurements will be useful in determining the reasons for differences (if any) between predicted rutting (Chapter 7) and what actually occurred. A total of 48 Emu strain coils for each section were installed in a regular array in three transverse locations (Figure 5.10). The basis of the Emu strain coil configuration was derived from experience with the New Zealand accelerated pavement tests (as per Figure 4.7).

5.3.1 Instruments

Strain was measured using the Emu Strain System developed by the University of Nottingham. This strain system utilises Emu strain coil pairs installed in the pavement at a range of locations. In each section of the two aggregate types (*NI Good* and *NI Poor*) three transverse locations were instrumented with Emu strain coils.

The Emu strain coils are electrical inductance devices which operate in pairs. Each Emu strain coil consists of a circular non-conducting disc (Phenolic Fabric-Carp Grade material) with a groove around its circumference. Fine gauge wire is wound around the disc in the groove terminating with a more substantial wire that is later used to connect to the instrument reader/transmitter (Figure 5.6). The Emu strain coils used in the trial were 100mm diameter and contained 80 turns of 35 gauge fine wire (0.25mm diameter). Ten metres of cable was then attached, the wire on the disc was sealed with silicon, and then the completed disc with wire attached was dipped in "Magnolia" Compound 3106 Epoxy Resin (a waterproof sealant similar to Shellac).

The University of Nottingham Emu strain measuring system is based on the principle that when an alternating current is passed through a Emu strain coil of wire an alternating magnetic field is generated. Another Emu strain coil placed within this field will have an alternating current induced in it. The magnitude of the induced current is proportional to the magnitude flux density, which in turn is nonlinearly related to the distance between the two Emu strain coils. Thus, a pair of sending and receiving Emu strain coils provides a non-contacting displacement, or strain, measuring device. Dynamic measurements are determined from the voltage shift generated by the relative movement of the Emu strain coil pair. Both the static and dynamic signals are amplified and conditioned to provide separate, continuous, d.c. voltages, which is logged by an analog-to-digital data acquisition system in a computer.

5.3.2 Calibration

The Emu strain coil pairs were calibrated before installing in the pavement using the calibrating rig shown in Figure 5.7. For three Emu strain coil spacings of 120, 150 and 180mm the static voltage was recorded and the maximum dynamic voltage achieved by two turns of the micrometer (1.27mm). Initially, many more spacings and turns of the micrometer were calibrated but it was found that the voltage versus displacement followed standard power and linear relationships. Therefore, to calibrate the Emu strain coil pairs only 3 points are needed to determine the constants for the equations relating voltage to displacement. Typical relationships showing static distance versus voltage for both static and dynamic readings is shown in Figure 5.8. To determine the dynamic displacement a simple ratio is used to relate the dynamic voltage measured for two turns (or 1.27mm) as used in the calibration as per Equation 5.1.

$$Displacement(dynamic) = \frac{Voltage(dynamic)}{Voltage(1.27mm)} 1.27mm \qquad \text{Equation 5.1}$$

A similar calibration process was conducted for Emu strain coil pairs in the coplanar positions. The aim was to measure strains in the horizontal position as well as vertical. However, it was later found that the horizontal strains were not large enough to determine a peak dynamic voltage above the electrical noise in the field trial. The effect of offset and tilt was not tested during calibration but it is recognised to have an effect (Janoo et al, 1999), see Section 5.6. Therefore, the coils were placed to ensure they were at thir correct positions, lying flat and vertically in line with other coils.

5.4 STRESS MEASUREMENT

The laboratory study focussed on the effect of stress on permanent strain. Relationships between permanent strain and stress from Repeated Load Triaxial tests (Chapter 3) were developed and used to predict the rut depth of the pavement as a whole in Chapter 7. The prime factor that will affect the amount of rutting calculated is the stress calculated in the pavement. Therefore, measurements of stress in the pavement can be compared to those calculated to ascertain if necessary reasons why predicted and actual rut depth were not the same.

Stresses within the pavement were measured using 300mm diameter *Vibrating Wire Pressure Cells* sourced from Soil Instruments (Figure 5.9). These pressure cells are primarily used to measure total pressures and stress distribution within embankments and dams. They were chosen because it was thought the large plate size will minimise any point loading effects that commonly occur in granular materials. Another advantage of this soil pressure cell is its low aspect ratio, thickness/diameter=0.03. Therefore, it is expected to have acceptable accuracy for measurement of dynamic stresses in soils, independent of the soil stiffness (Aksnes et al, 2002). Given the importance of stress in the prediction of permanent strain, three pressure cells were installed in each pavement section (*NI Good* and *NI Poor*). The aim was to obtain 3 stress measurements at the same pavement depth and section where at least one measurement was correct.

The manufacturer's calibration was used for the pressure cells. This involved powering the cell's input wire with 15 volts direct current and reading the voltage on the output wire for a series of dead weights placed on top of the cells. It was found that the following relationship could be applied to all cells even though the start or base voltage (where no additional loading is applied) was different, Equation 5.2.

$$S = 50\,(\Delta V) \qquad \text{Equation 5.2}$$

Where,

S = stress (kPa); and

ΔV = peak voltage (v) minus the start or base voltage or voltage change due to load.

5.5 INSTRUMENT LOCATIONS

The chosen array of the Emu strain coils to measure strain per transverse cross-section was based on arrays successfully used in the CAPTIF pavement test track located in Christchurch, New Zealand (Figure 4.7). Spacing of the 100mm diameter Emu strain coils was set to 150mm, therefore allowing a total of 4 layers of Emu strain coils in the 450mm design depth of aggregate. Emu strain coils were not installed in the subgrade as this consisted of large boulders. The "L" shaped stack of 3 Emu strain coils enabled measurement of horizontal strains in both longitudinal and transverse directions which are quite different. Further, the additional Emu strain coils allow for some redundancy in vertical strain measurements should any errors or faults occur.

Pressure cells were installed on top of the 2nd layer of granular material just before the final 150mm granular layer was placed. These pressure tranducers were placed in the outside wheel path (closest to kerb on left hand side) within 1 metre of each Emu strain coil array.

Figure 5.10 describes the layout of the Emu strain coils and pressure cells in each trial section (*NI Good* and *NI Poor*). As discussed in the following section the design spacing of the Emu strain coils (150mm) and thus depth was not achieved during construction and ranged from a spacing of 100 to 200mm.

5.6 CONSTRUCTION

Location of the field trial was on the access road into Ballyclare landfill site in Northern Ireland, UK. A requirement to use the site was to ensure traffic was not restricted. Therefore, construction of the road trial including instrumentation and sealing could only take place from Saturday 12pm to 6am Monday morning when the landfill is closed. The Contractor employed for the construction Tullyraine Quarries Ltd felt confident the job could be completed in this time period. In preparation the granular material *NI Good* and *NI Poor* (Table 3.1) was stockpiled at the site during the weeks leading up to construction.

Prior to construction all the instruments were labelled and placed in groups relating to cross-section position of the field trial. The field trial was clearly marked at 1 metre intervals using spray-paint and masonry nails on the kerb. Construction commenced at 12pm on Saturday 10 November 2001. The first task was to cut edges of the existing pavement at the position of the field trial. Next followed the excavator to remove the existing pavement and materials. The aim was to achieve a sloping excavated base where the design depth from the surface to the base of the excavated surface varied from 491 to 579mm. Further, the depth to the excavated base was calculated as being different either side in order to achieve a perfectly level excavated surface as a platform for the next three three 150mm layers of aggregate. However, the excavator bucket was 1000mm in height and combined with the large boulders being excavated it was impossible to control the depth excavated.

There was not time to measure the depth nor undertake a level survey of the base of the excavation. The excavated depth was, therefore, estimated to range from 600 to 900mm. Additional, aggregate was added and compacted to form the base for the first layer of Emu strain coils approximately 550mm from the surface. A plumb bob, 5m steel tape and cloth tape stretched across the pavement was used to place the instruments in their correct locations as shown in Figure 5.11. A small spirit level was used to ensure the emu coils were lying perfectly flat. Appendix B shows the detailed plans used for installing the instruments at their correct locations.

After the base was compacted, the next aggregate layer of approximately 150mm was added compacted and then instruments placed. This process was repeated for the next two layers. Sand was placed on the instruments to assist in placement and also over the cables for protection that were fed back to the nearest of the two junction boxes. There were over a hundred wires from instruments and although numbered it took several days after construction to sort through (Figure 5.12).

The final surface was a paver laid hot rolled asphalt. The depth was determined by ensuring the finished surface was level with the existing surrounding pavement. In an attempt to achieve a tapered variation in asphalt surface thickness the final aggregate layer depth was guided by a string line.

Due to the length of time required to install the instruments and time pressures imposed by the contractors, the supervision of achieving construction tolerances was minimal. Further, the design was unrealistic in terms of the ability to practically construct. Therefore, the target instrument spacing of 150mm was not achieved. However, as the Emu strain coils were calibrated over a full range of spacings this did not pose any difficulties in measurement, but perhaps only in later comparison of strain measurements.

The asphalt layer did not achieve the desired taper but was approximately 100mm thick. Tables 5.1 and 5.2 are a summary of the depth of each layer as determined after reading the instruments several weeks after construction. The thickness of the asphalt layer was determined by using a Emu strain coil on the surface to take a reading to the top Emu strain coil. Ten millimetres was subtracted from this measurement to determine the asphalt thickness as the top Emu strain coil was always pushed into the surface of the aggregate by this amount.

Table 5.1. Layer thicknesses achieved on inside wheel path (closest to curb).

	Layer thicknesses (mm)						
	[1]*NI Poor*			[1]*NI Good*			
Layer	5m	11m	16m	18m	23m	29m	Avg.
Asphalt	114	102	108	108	86	117	106
Top aggregate	138	131	107	162	179	154	145
Mid. aggregate	176	144	151	152	153	154	155
Bott. aggregate	143	158	155	-	161	122	148

1 Cross-section positions where instruments are installed (Appendix D).

Table 5.2. Layer thicknesses achieved on the outside wheel path.

	Layer thicknesses (mm)						
	[1]*NI Poor*			[1]*NI Good*			
Layer	5m	11m	16m	18m	23m	29m	Avg.
Asphalt	139	121	118	100	100	136	119
Top aggregate	132	117	115	-	146	156	133
Mid. aggregate	197	206	153	-	181	124	172
Bott. aggregate	221	151	107	175	144	185	164

1 Cross-section positions where instruments are installed (Appendix D).

Installation of the instruments was a success as most were in working order. The only exceptions were a few Emu strain coils at the 18m cross-section.

5.7 STRAIN AND STRESS MEASUREMENTS

5.7.1 Set Up

All the cables from the Emu strain coils and stress cells terminated at one of two junction boxes. The junction boxes were simply an alignment of plugs. Each plug was given the same number as the particular Emu strain coil or stress cell that was attached to it. Input plugs were wired to the measuring instruments and/or power supply so that these could be plugged into the appropriate cells for measurement.

Two Emu strain measuring units were used to take the measurements. This allowed a maximum of 6 Emu strain coil pair measurements. There were 48 Emu strain coil pairs and in order to obtain sufficient measurements at each Emu strain coil pair a total of 24 combinations of measurements were formulated. These combinations were such so that two charged Emu strain coils are never in close proximity to each other. For example, a configuration sometimes consisted of one vertical Emu strain coil pair in each of the 6 cross-sections (5, 11, 16, 18, 23 and 29m) where instruments were placed.

All 6 stress cells could be powered together with one 15 volt dc power supply. Thus, measurements of all 6 stress cells were undertaken simultaneously.

5.7.2 Data-logging

To measure stress and strain pulses generated by passing wheel loads a data logger was used. The data-logger used was a dataTaker DT800 which could record up to 12 channels of data at 500 times a second simultaneously in burst mode. The 12 channels were primarily used to take dynamic measurements from 6 Emu strain coil pairs and 6 stress cells. For each new combination of Emu strain coil pairs the channels used for the 6 stress cells were replaced with 6 static readings from the Emu strain coils. This enabled the spacing between the Emu strain coils to be recorded electronically.

The dataTaker DT800 data-logger is an external device that can record and hold data. A computer is used to send instructions to the dataTaker and transfer the data stored on the logger. For this project the instruction sent was written using the software supplied with the dataTaker DT800. The instruction sent was simply a one line programme to undertake a sampling burst for channels 1 to 12 at a clock speed of 8,000 hertz for a total of 4,000 samples. The result was a recording speed of 500 times a second for 8 seconds. Running this programme was triggered by clicking the “run” button in the dataTaker software on the computer. This was timed when the lorries front wheels first entered the trial section. Provided the lorries did not stop to queue for the weighbridge the 8 second burst was usually sufficient. Also increasing recording time would also result in a reduction in the measurement speed due to a limit in the maximum amount of data that can be recorded.

The dataTaker logger has the advantage that it operates with any computer. However, 4 minutes were required between measurements. After the 8 second measurement, the data logger cannot be operated for 2 minutes. This time is needed to enable the data stored on a buffer to be transferred to a more permanent memory system in the logger. Another 2 minutes is needed while the data stored on the logger is transferred to the computer. This meant that some passes of lorries could not be recorded. Therefore the time needed on site was longer to obtain sufficient number of measurements.

5.7.3 Measurements

Measurements of stress and strain were undertaken during the months of February, March and April 2002 and again in September 2002. A van was used to hold the computer, data logger, two Emu strain measuring units, and the 15 volt power supply for the pressure cells. A petrol powered generator placed several metres away from the van (to reduce electrical interference) was used to power the recording and measuring units. For each measurement of a passing lorry, the time, number of axles and type (single or dual tyred), and number plate were recorded. This information enabled the gross weight to be determined at the end of the day from records held at the weighbridge. The gross weight, number of axles and type were later used to estimate the weight for each passing wheel load.

It was known that each pass of a lorry represented a different wheel load. Further, this wheel load may not be directly over the instruments. Therefore, many measurements were taken with the hope that trends could be developed. For example, the vertical strain at the top, middle and bottom Emu strain coil pairs versus wheel load can be determined.

Examples of the raw voltage data recorded from one Emu strain coil strain pair and the 6 stress cells are shown in Figures 5.13 and 5.14 respectively. The raw voltage measurements from the coil strain pairs were interpreted using Microsoft Excel combined with a program written in Visual Basic. The program opened the raw data file and first applied a smoothing function through the data. This smoothing function is similar to a running average and takes the form as cited in UNISTAT Statistical Package manual, Equation 5.3:

$$V_{A(smoothed)} = SV_A + (1\text{-}S)V_{A\text{-}1(smoothed)} \qquad \text{Equation 5.3}$$

where,

$V_{A(smoothed)}$ = Resulting smoothed value at row A;

V_A = Value at row A;

V_{A-1} = Value at row A-1; and

S = Smoothing constant a value from 0 to 1.

Various smoothing constants were chosen with the aim of maximum smoothing with minimal distortion of the results. It was found that a value of 0.5 was suitable due to the large amount of noise in the data (Figure 5.13).

After the Emu strain coil data were smoothed the peaks in the data were found and reported into the summary spreadsheet. Peaks were found by checking that 40 values either side of the peak value were less in magnitude. The summary spreadsheet then processed these peaked voltages to determine the values of stress and strain. Lorry wheel weights were included and the results were stresses and strain values at a range of locations and wheel weights.

5.8 SURFACE DEFORMATION

A primary objective of this research project is permanent deformation/rutting. Therefore, the surface deformation of the field trial was monitored over time. The University of Nottingham's profiler was used to measure the transverse profile of the surface at 2m intervals in the longitudinal direction.

The profiler consists of a 2.5m beam resting on two feet with a LVDT attached to a small wheel (Figure 5.15). The LVDT is pulled along the beam with an electric motor and chain. As the LVDT transverses the pavement, the vertical displacement and horizontal position is reported via voltage readings. The same data logger as used for stress and strain was used to record the voltage readings every $1/10^{th}$ of a second.

Relationships between voltage and displacement are linear and these were determined in the laboratory. Voltage from several points of known horizontal displacement was recorded to determine the horizontal displacement relationship. The vertical displacement calibration was undertaken using blocks of known spacings measured with electronic callipers. It was found that the calibration curve for the horizontal displacement depended on the vertical displacement position. This effect was possibly due to the interference that the vertical voltage had on the horizontal voltage in the data logger as they had both the same earth. The relationships found for vertical and horizontal displacement are given in Equations 5.4 and 5.5.

$$D_{vert} = (0.001897)V_{vert} - 12.62 \qquad \text{Equation 5.4}$$

where,
D_{vert} = displacement in the vertical direction (mm) relative to the base level (0mm) of the LHS foot;
V_{vert} = Voltage measured from vertical output wire (mv).

$$D_{horiz} = mV_{horiz} + \mathrm{c} \qquad \text{Equation 5.5}$$

where,
D_{horiz} = displacement in the vertical direction (mm);
V_{horiz} = Voltage measured from horizontal output wire (mv);
$m = (-1.5e\text{-}08)V_{vert} + 0.16$;
$c = (-0.00046)V_{vert} + X$; and
X = 401.7mm for profiler placed up against curb on LHS in order that the 0mm is on top of the curb at the centre, this being the same reference used in level surveys and design drawings.

5.9 TRAFFIC

The field trial is located on a private access road into the landfill at Ballyclare, Northern Ireland. This trial is conveniently located just prior to the weighbridge where records are kept on the weight of every vehicle that passes. Truck axles (number and type) and weights were also recorded while undertaking measurements of stress and strain. All this information gave a complete picture of traffic loading on the trial with time. A majority of the lorries are waste collection vehicles with a single tyred front steering axle and two dual tyred axles at the rear. Other axle configurations were either: one single tyred front steering axle and only one dual tyred rear axle; or two single tyred front steering axles and two dual tyred rear axles.

From the number of axles, type and load as surveyed while measuring stress and strain a proportion of each axle load group was determined. This proportion was multiplied by the number of loads throughout the year as recorded at the weighbridge. The results of this analysis are shown in Figure 5.16 for single and dual tyred axle load numbers. It can be seen that the most common axle groups are 22.5kN (i.e. 20 to 25kN) for the single wheel load and 45kN (i.e. 40 to 50kN) for the dual tyred wheel load.

The total number of passes per year for all axles combined is almost 55,000. It is usual in pavement design that traffic loading is calculated as the number of Equivalent Standard Axles. An Equivalent Standard Axle (ESA, Equation 5.6) is one dual tyred wheel load of 40kN and is calculated using a power law function. Although the number of ESAs is not strictly needed as part of this more fundamental study, it does give a comparison to design loads on typical UK highways.

$$ESAs = Number\left[\frac{Axle\_load}{Std\_axle\_load}\right]^n \qquad \text{Equation 5.6}$$

where,

ESAs = Equivalent Standard Axles

Axle_load = actual axle load (kN);

Number = number of passes of the Axle_load;

Std_axle_load = 40kN for a single tyred axle or 80kN for a dual tyred axle; and n = the damage exponent such that the number of ESAs calculated is the number of passes with the Std_axle_load that is needed to cause the same damage to the pavement caused by passes with the Axle_load, in pavement design a value of 4 is assumed.

The origins of the damage law equation (Equation 5.6) for combining traffic into one type came from the AASHO (1962) road test which was conducted in the United States in the late 1950s using roads, vehicles and under a climate which bear little resemblance to those in use today. AASHO (1962) calculated a damage law exponent of 4 based on a comparison of the number of axle passes to reach the end of the pavement life between the reference axle and the axle load in question. The pavement end of life in the AASHO (1962) tests was defined by reaching a certain pavement serviceability index value which considers factors such as rut depth, roughness and cracking. Accelerated pavement tests in New Zealand on thin-surfaced unbound granular pavements investigating the appropriate value for the damage law exponent found it can vary from a value of 1 for strong pavements to a value of 6 for weak pavements (Arnold et al., 2004). Therefore, for this study it is quite likely a damage law exponent *n* of 4 may not be appropriate. A more appropriate approach when predicting rut depth (Chapter 7) is to calculate the rutting for each individual wheel load group (Figure 5.16) and add these together to determine the total rut depth as this negates the need to combine traffic using a arbitrary damage law equation.

From Equation 5.6 and using a damage exponent, n of 4 the number of ESAs per year is 88,200. Since pavement construction in November 2001 the total number of loads to the end of monitoring in August 2003 is estimated as 150,000 axles or 243,000 ESAs calculated using an exponent of 4.

5.10 RESULTS

5.10.1 Strain

There were many measurements of strain corresponding to a full range of wheel loads. It was hoped that strains in the two trial sections and individual cross-sections with supposedly different thicknesses of asphalt could be compared. However, there was significant scatter in the results and no differences could be found. Therefore, all the strain measurements were grouped together as either bottom, middle or top aggregate layer strains.

Measured strains versus wheel load were plotted for top, middle and bottom layer strains. The result was a wide scatter of points and no direct trends could be found. To improve the result the results were thinned by removing points below a cut-off linear function relating wheel load to strain. Obviously this did improve the result but over 70% of the measurements were excluded. It was assumed that often the wheel does not track perfectly over the strain cells and a different approach to analysis was adopted.

It was assumed that when the wheel tracked directly above the strain cells then the maximum reading should be obtained. Therefore, an approach could have been to use only the maximum strain value for a particular wheel load. However, there were many outliers with very high recorded strains, possibly due to electrical interference and problems with the Emu system. As an alternative, therefore, a line was drawn such that 90% of the recorded peak strain values fall below it (the "90% rule"). This 90% rule was based on the analogy that only approximately 10% (??? WHO SAYS???) of the wheel loads that pass over the pavement are directly over the coil pairs. Strain is significantly reduced for wheel loads that do not pass directly over the coil pairs. Thus the value of peak strain for which 90% of peak strain readings are smaller should still be associated with a wheel load directly over the Emu coil pair and not associated with an off-line whell load. Finite element analysis of the pavement for a range of wheel loads indicated the 90% rule resulted in a similar relationship between strain and wheel load as would have been obtained for an unaffected 100% strain reading set. Results of this analysis for the February 2002 and September 2002 Emu strain coil measurements are shown in Figures 5.17 and 5.18. Table 5.3 summarises the estimated measured strains for each Emu strain coil pair for a standard 40kN wheel load.

Table 5.3. Comparison of February 2002 and September 2002 measured strains.

	Micro-strain for 40kN wheel load	
Layer	**Feb 2002**	**Sept 2002**
Top	781	2614
Middle	367	787
Bottom	320	678

The September 2002 results are significantly higher as the dynamic measurement setting on the Emu system was set on *slow*, while it was set to *fast* for the February 2002 measurements. The *slow* setting is the correct setting for field measurements, although this was not known for the first set of measurements. A slow setting for dynamic readings holds maximum readings a little longer than the fast setting and thus allows the capture of the maximum strain resulting from a passing wheel.

5.10.2 Stress

The measured results from the stress cells were analysed in a similar manner to the strain measurements. It was found from finite element analysis (Chapter 6) that stress at the depth of the stress cells (250mm) varied linearly with load (Figure 5.19). The finite element analysis used the porous elasticity model (Table 3.6) and the Drucker-Prager yield line (Table 3.3) for the *NI Good* aggregate. Further, the magnitude of the load was varied by changing the load radius and keeping the contact stress constant (0.75MPa). As this analysis is essentially non-linear it is surprising that stress did vary linearly with load. It was assumed that the measured values should show the same relationship as those calculated where stress is equal to some constant multiplied by the wheel load.

Similar to how the measured strains were processed, it was assumed that the wheel load did not always pass directly over the stress cells. Therefore, a relationship between load and measured stress was found by placing a straight line through the origin with a slope such that 90% of the values lie underneath. Figure 5.20 shows the results for the February 2002 and September 2002 measurements. As can be seen the relationships are very similar and are close to those calculated from the finite element model (Figure 5.19). Table 5.4 compares the measured values of stress to those calculated from the finite element model for the 40kN wheel load.

Table 5.4. Comparison of measured stress to calculated for 40kN wheel load.

	Stress (kPa) for 40kN wheel load (Contact stress = 750kPa)		
Layer	**Measured**	**Calculated**	**Ratio**
Feb 2002	112	113	1.01
Sept 2002	118	113	0.95

5.10.3 Surface Deformation

The surface deformation was measured using the University of Nottingham profiler (Figure 5.15). This device was placed transversely at 2m intervals on the field trial. Two measurements were required to cover the full lane width of the field trial. Deformation was small on nearly all of the sections which often meant some difficulty in interpreting the results above the electrical noise.

Each cross-section result including both sides was analysed individually in a manual process with the aid of a spreadsheet. For each transverse profile plot an imaginary 2 metre straight edge was placed on top. The vertical position of each end of this straight edge was manually changed until the result looked as if a straight edge was placed on the road. Once the position of the straight edge was established the maximum distance to this straight edge was calculated. The result is a calculated rut depth for each measured transverse profile. An example transverse profile with a 2m straight edge is shown in Figure 5.21. This example is fairly typical with rutting calculated being less than 4mm and is not visible with the "eye".

Trends and magnitudes of rutting in all the cross-sections were similar. Therefore, the rut depths were averaged for the *NI Good* and *NI Poor* aggregate sections as plotted in Figure 5.22. Results show that minimal rutting has occurred and further shakedown/stable behaviour has nearly occurred. The rate of rutting is low at approximately 1mm per year (or per 88,000 ESAs) for both sections and thus shakedown Range A behaviour is likely for both sections.

5.11 DISCUSSION

The original aim of this field trial was to construct pavements such that the three shakedown ranges A, B and C would occur. It was found through linear elastic analysis that this could be achieved through different asphalt thicknesses (Figure 5.3). To assess the affect of asphalt thickness an ambitious design was proposed with the thickness of asphalt being tapered. An idea to ensure a tapered asphalt layer was to taper the excavated base such that the granular material was in equal layers and the final asphalt surface was level with the existing pavement. Further, many Emu strain coils were installed to enable differences in pavement response to be measured for different asphalt thicknesses. There were many factors against the design being achieved in the field mainly due to time pressures and consequently the intended design was not constructed. Contractors were employed on a lump sum basis and construction had to be completed in a Saturday afternoon and Sunday. Added to the time pressures was a major Irish football match starting at 1pm on the Sunday which all the contractors did not want to miss. Another factor that influenced the final pavement constructed was the subgrade which included large boulders, typically greater than 500mm in diameter, that affected the finished excavated depth. The final pavement constructed had a similar asphalt thickness of 100mm throughout but with Emu strain coils installed at a range of spacings.

Many weeks were spent collecting over a thousand measurements of stress and strain from passing lorries with the aim of determining representative measurements for each wheel load. Added to the difficulty was the fact that there were 48 Emu strain coil pairs not including those in the horizontal direction while only 3 to 6 pairs can be measured at one time. There was a significant amount of noise in the data and the post-processing time to pick out the maximum values was significant. Effectively no conclusions could be found from the measured strains and stresses in terms of effects of load, granular material and asphalt thickness. Although taking a line through the top 10% of measurements provided some salvation to the data.

It is recommended for future field trials is to have a crude/simple design that consists, for example, of two distinct asphalt thicknesses of say 50 and 150mm. Further, the amount of instrumentation should be limited to an amount where they can be all read in 5 runs or less; for this field trial 21 runs were needed to cover 90% of the Emu strain coil pairs. In addition, measurements of strain and stress should only be done for passes by a lorry employed for this purpose where several repeat runs of a known weight and speed can be undertaken.

Despite the shortcomings of this field trial the rut depth progression was accurately recorded and will be useful in validating models and methods used to predict rut depth and deformation behaviour.

5.12 SUMMARY

A field trial in Northern Ireland was constructed in two sections with two different granular materials (*NI Good* and *NI Poor*, Table 3.1). It was found from initial pavement analysis that asphalt thickness could affect the type of deformation behaviour that could be observed (i.e. Range A, B or C as defined in Section 2.11.2). Therefore the trial was designed with a tapered asphalt thickness with the aim that all three shakedown range behaviours maybe observed. However, construction pressures and difficulties resulted in only one asphalt thickness being utilised. Strain and stress gauges were installed in the pavement and measurements taken in two separate months. Results from the strain and stress measurements were varied with no obvious pattern with respect to wheel load or granular material type. Postulating that many of the insitu measurements would be too low due to the wheels being off centre in reference to the strain and stress gauges some interpretation with respect to load and pavement depth was made.

Despite the shortcomings of the field trial the progression of rut depth was accurately determined from transverse profile measurements. The average rut depth was 4mm with progression having stabilised to less than 1mm per year and it is predicted a shakedown Range A behaviour is most likely.

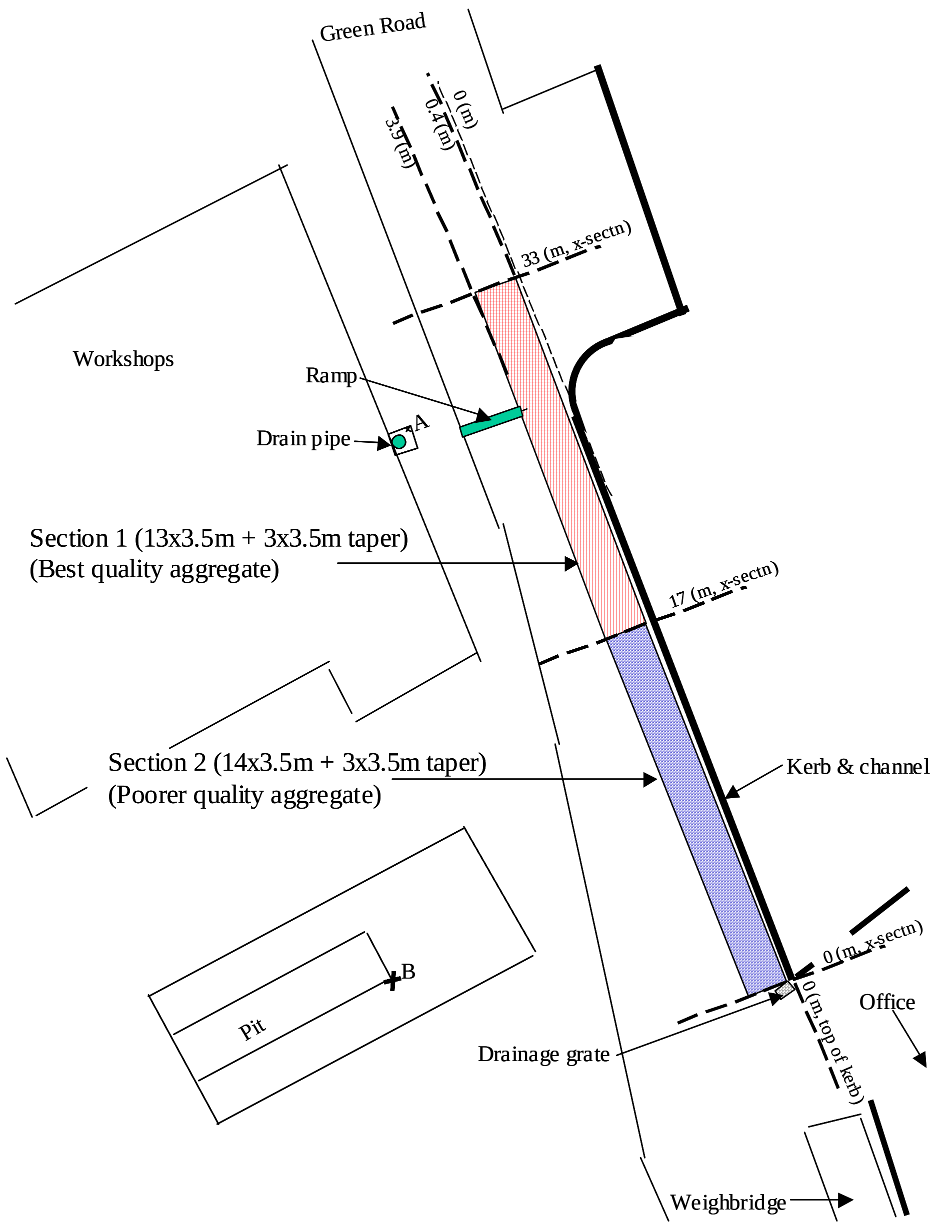

Figure 5.1. Field trial layout.

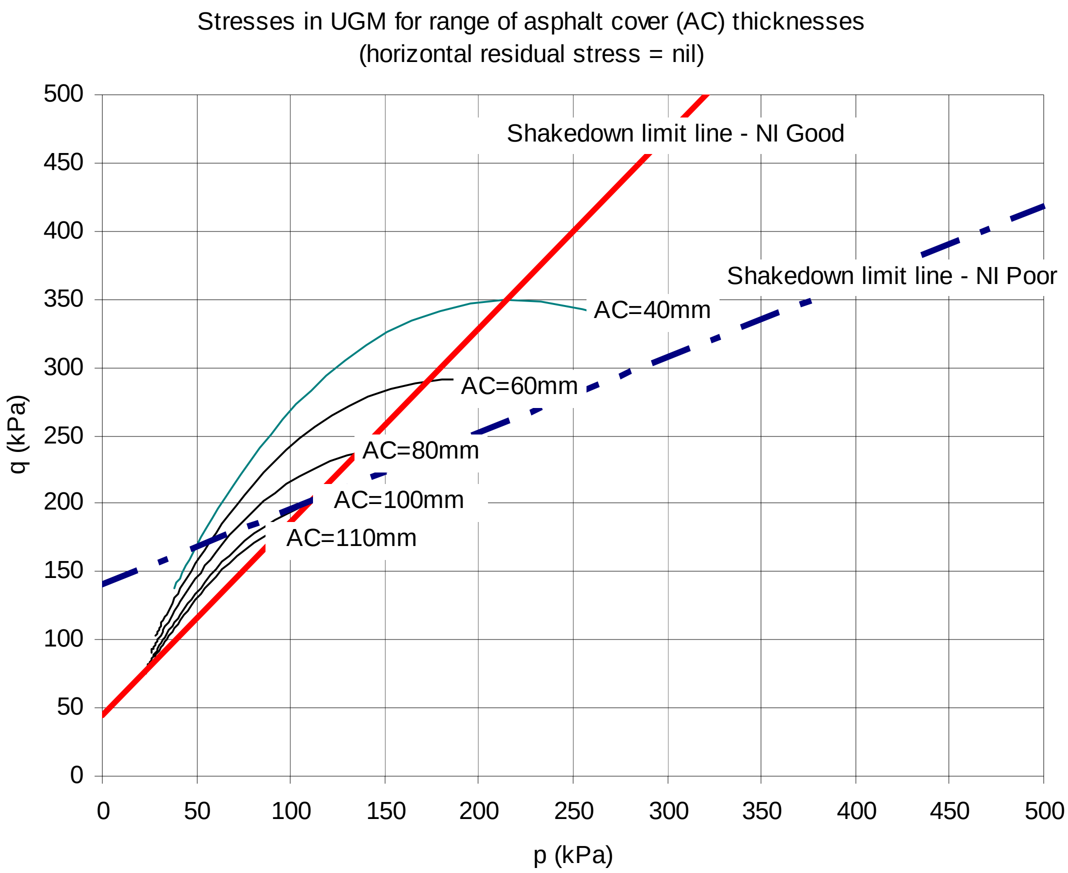

Figure 5.2. Stresses in the granular material caused by a contact tyre stress of 550kPa for a range of asphalt cover thicknesses, where horizontal residual stresses are assumed to be *nil*.

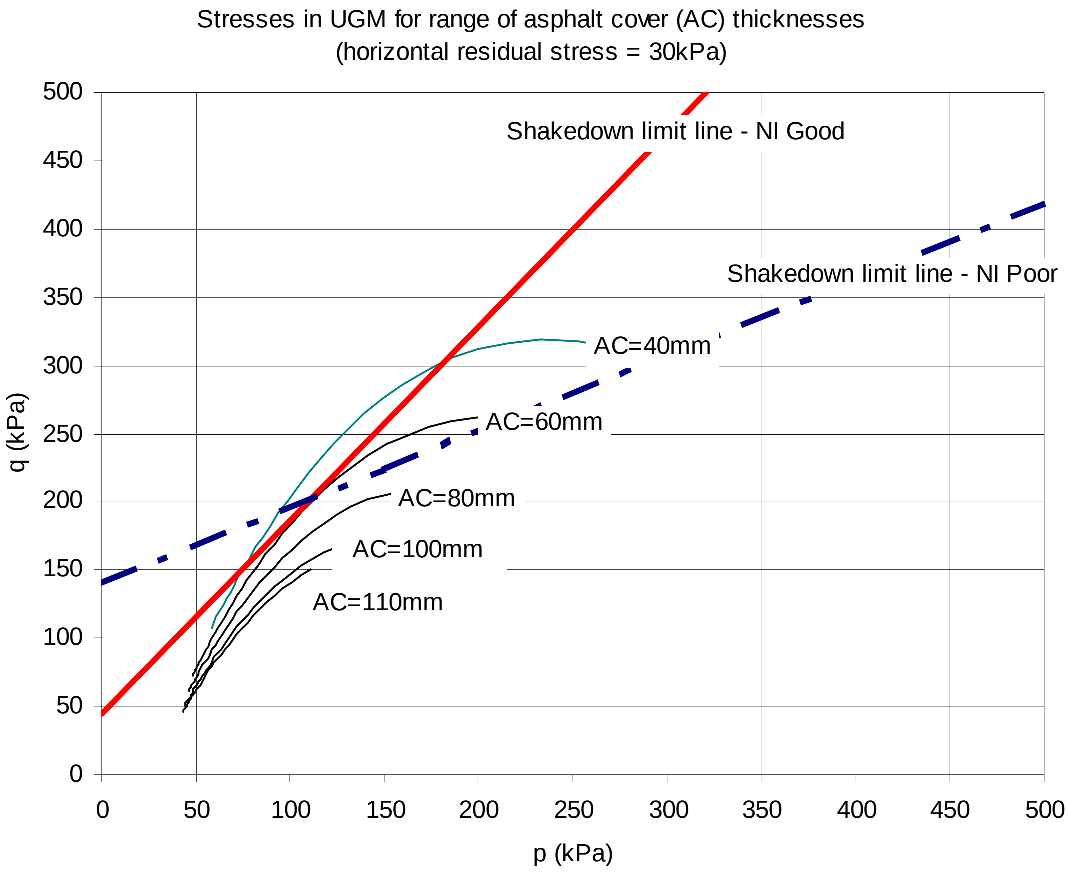

Figure 5.3. Stresses in the granular material caused by a contact tyre stress of 550kPa for a range of asphalt cover thicknesses, where horizontal residual stresses are assumed = 30 kPa.

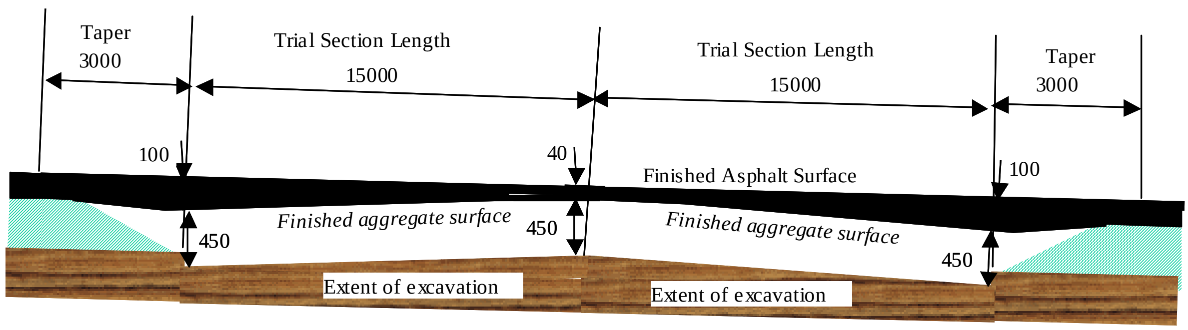

Figure 5.4. Field trial design longitudinal section.

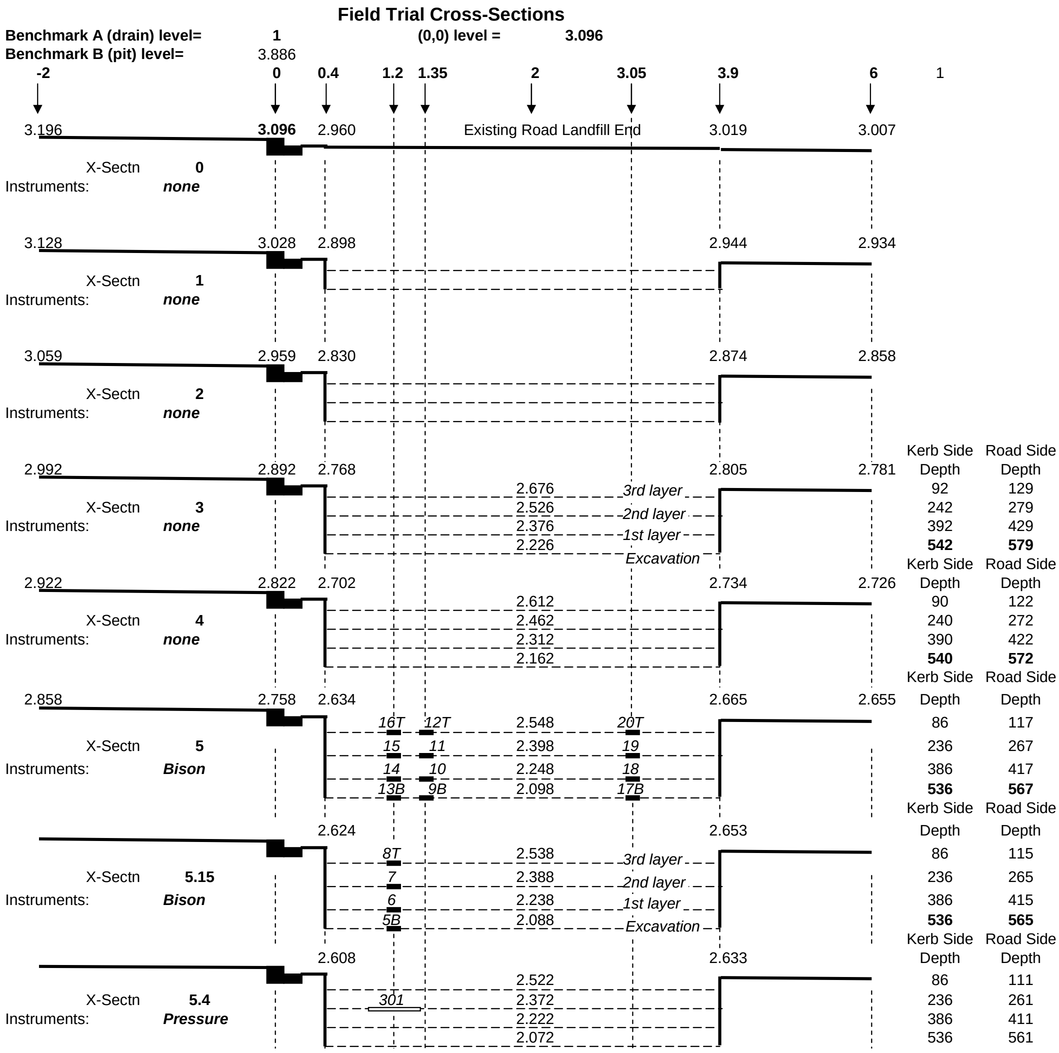

Figure 5.5. Cross-section setout information example.

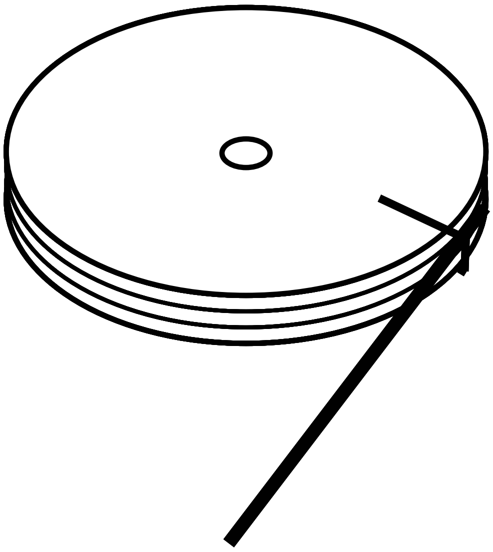

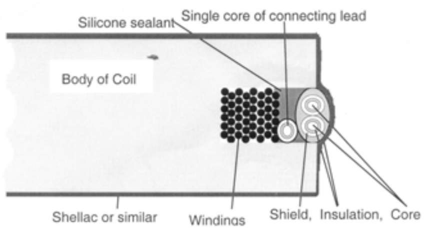

Figure 5.6. Emu strain coil.

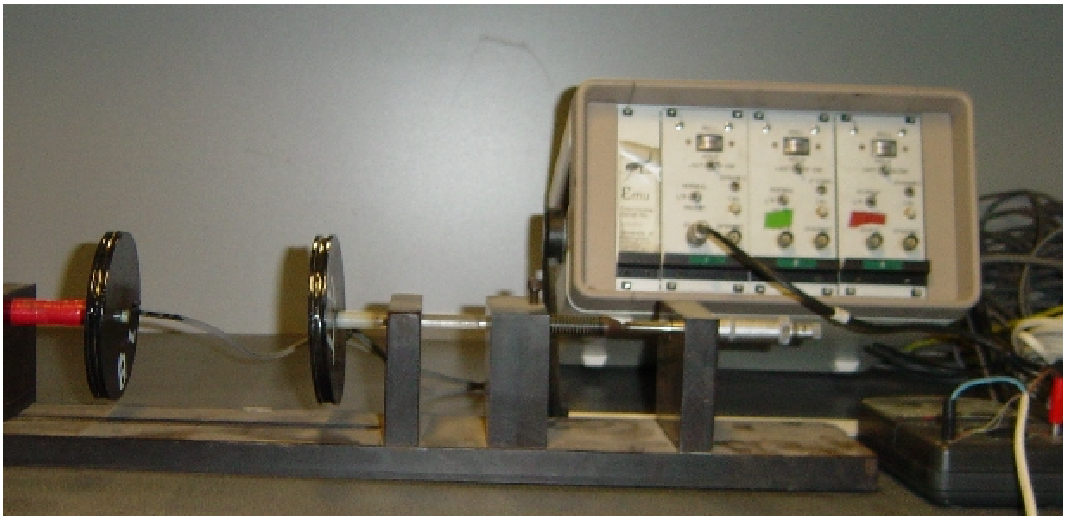

Figure 5.7. Emu strain coil calibration set up.

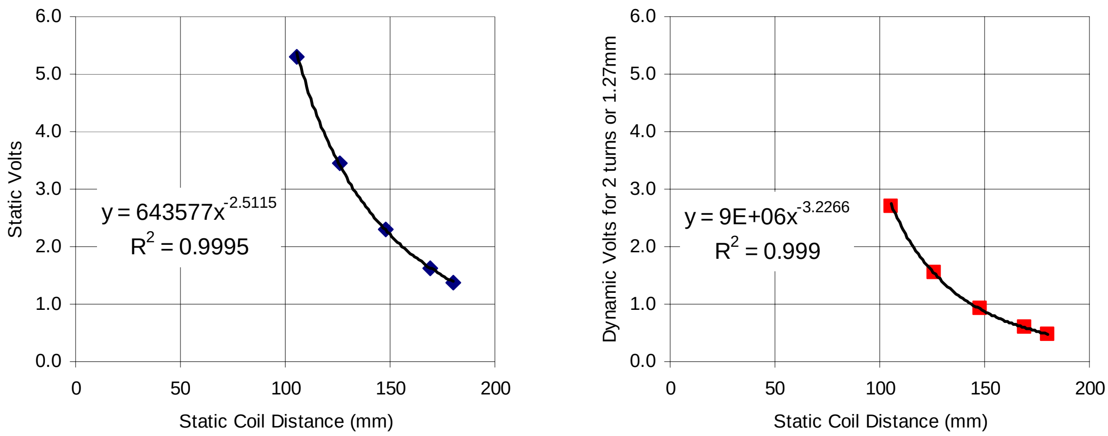

Figure 5.8. Typical calibration curves for Emu strain coil pairs.

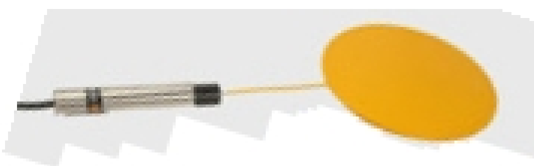

Figure 5.9. Vibrating Wire Pressure Cells.

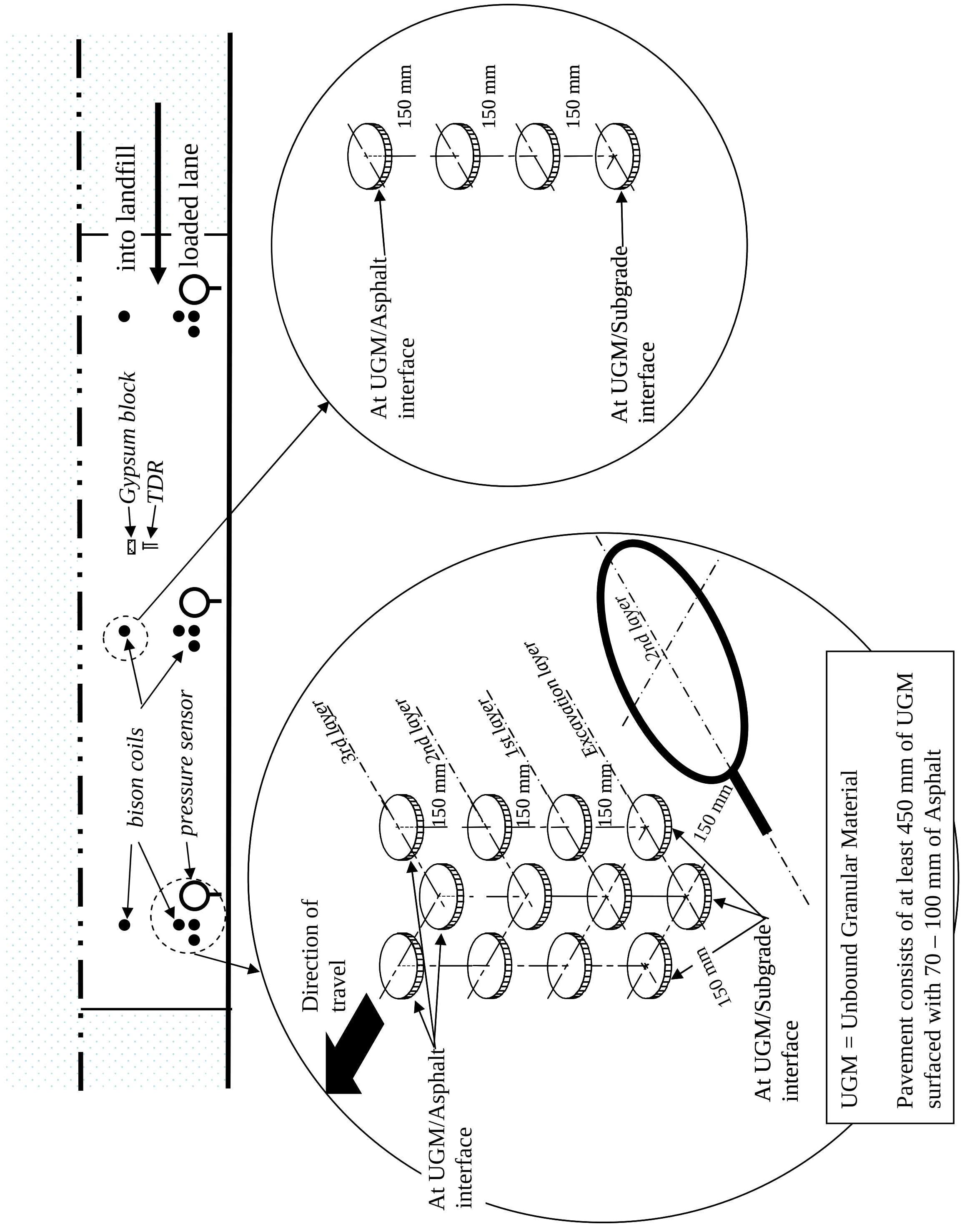

Figure 5.10. Field trial Emu strain coil and stress cell locations.

Figure 5.11. Emu strain coil installation.

Figure 5.12. Sorting instrument wires.

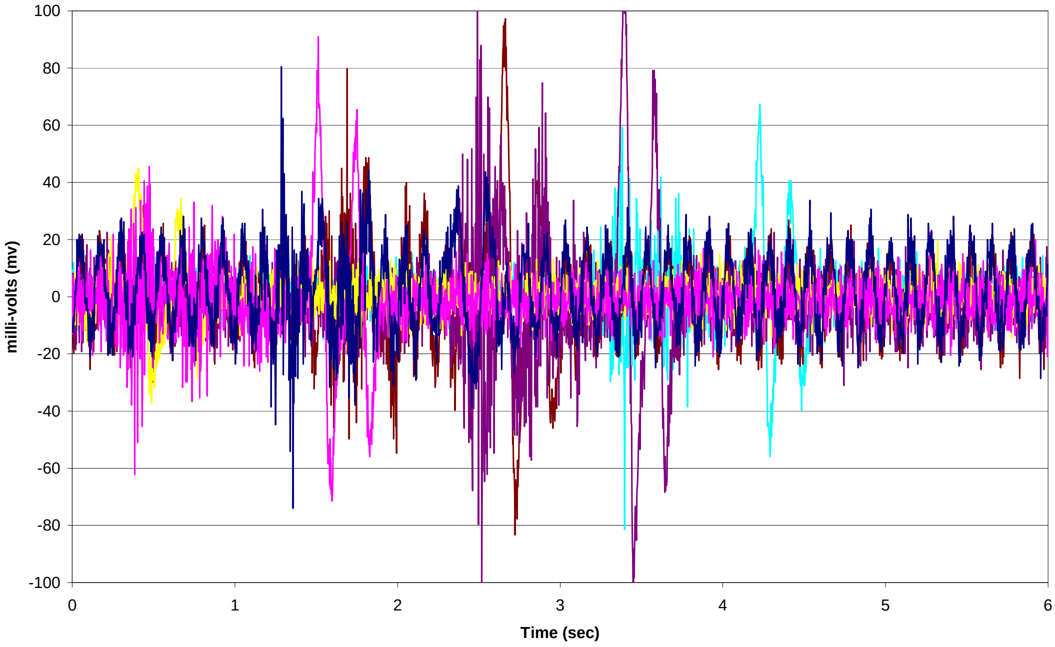

Figure 5.13. Typical Emu strain coil pair output.

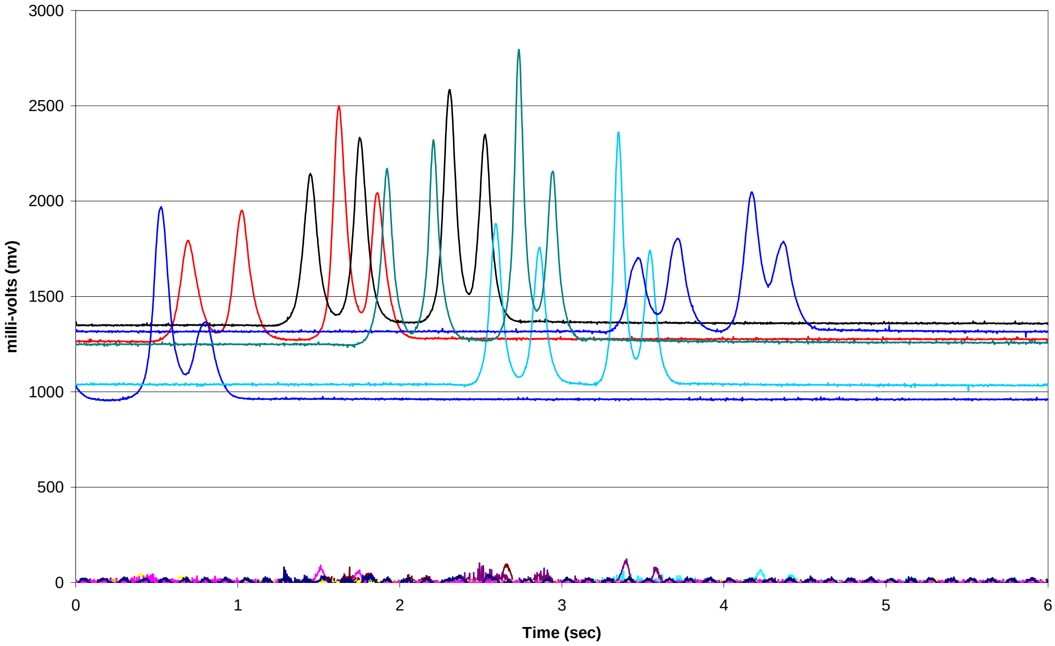

Figure 5.14. Typical output from stress cells.

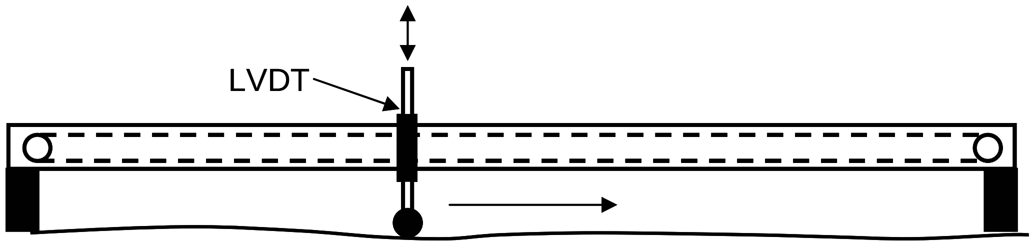

Figure 5.15. Transverse pavement surface profiler.

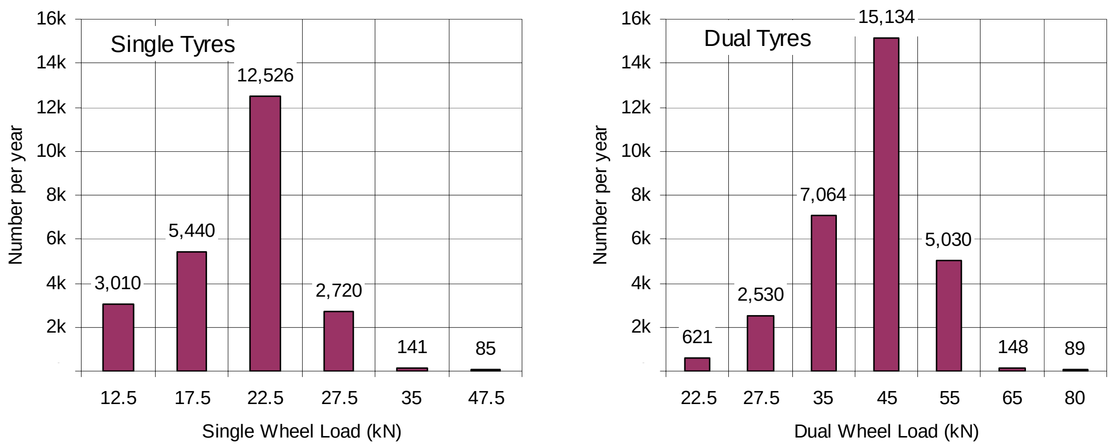

Figure 5.16. Half axle load distributions.

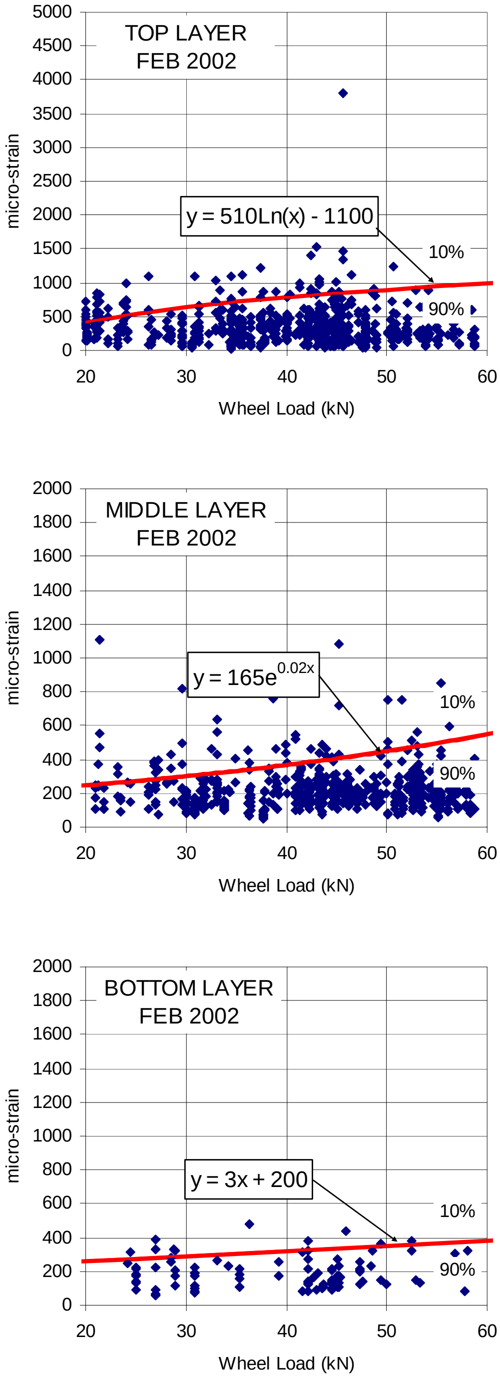

Figure 5.17. Strain results for February 2002 measurements.

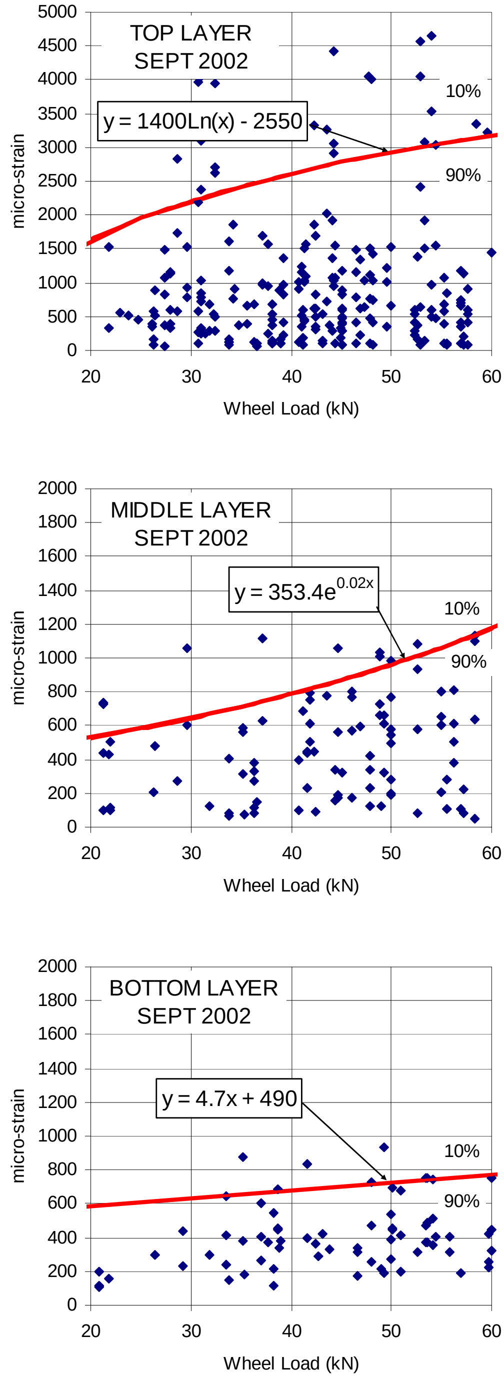

Figure 5.18. Strain results for September 2002 measurements.

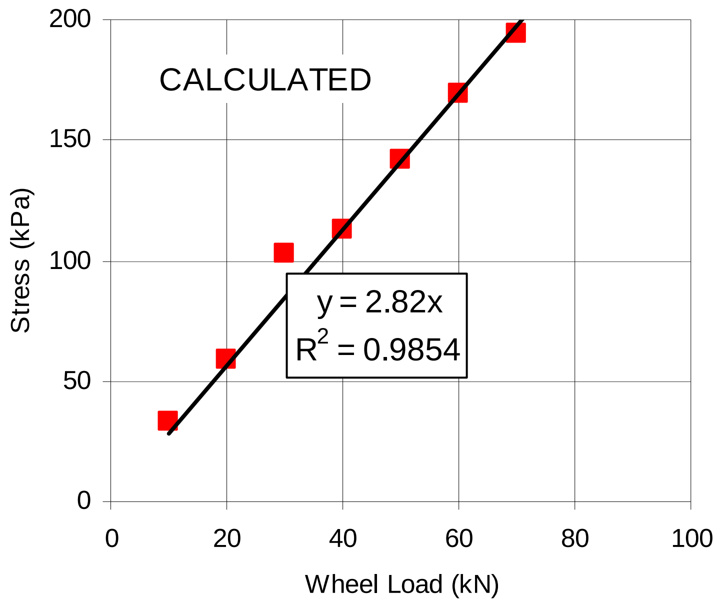

Figure 5.19. Calculated stress for various wheel loads at stress cell depth from finite element analysis.

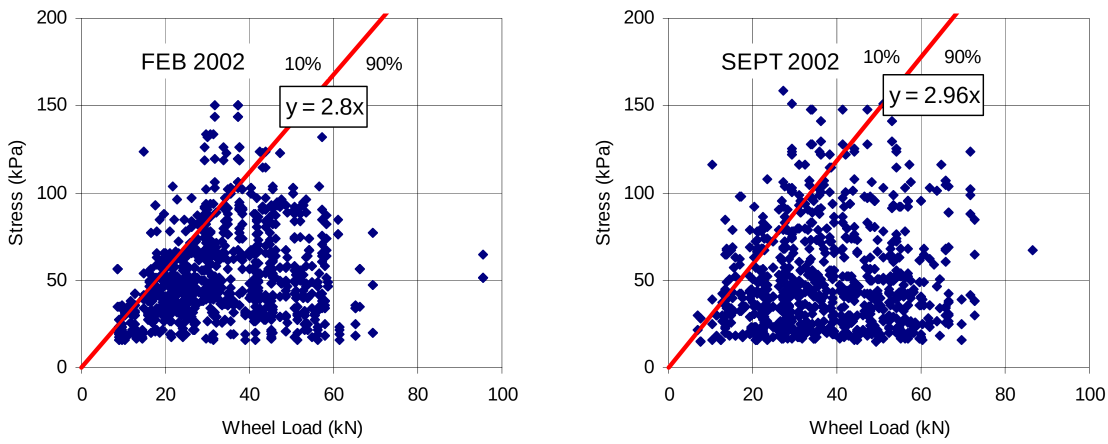

Figure 5.20. Measured stress during February and September 2002.

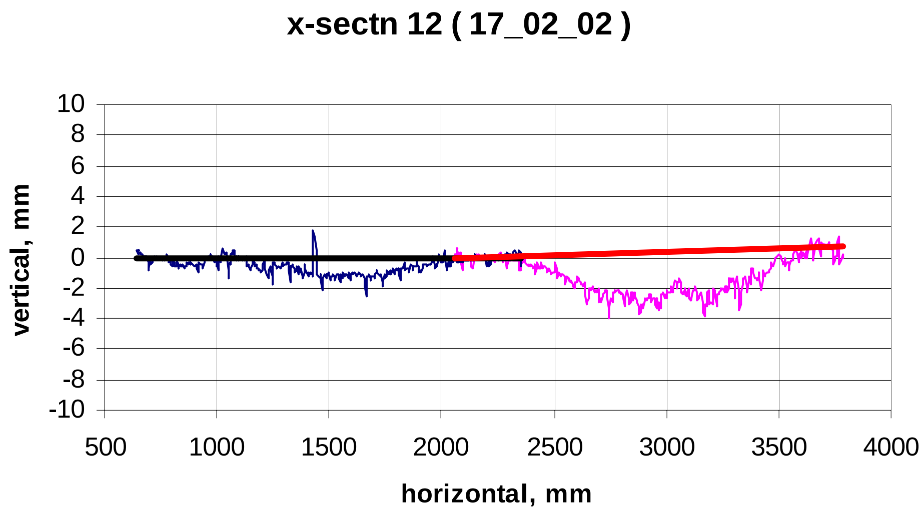

Figure 5.21. Transverse profile example with 2m straight edges to calculate rut depth.

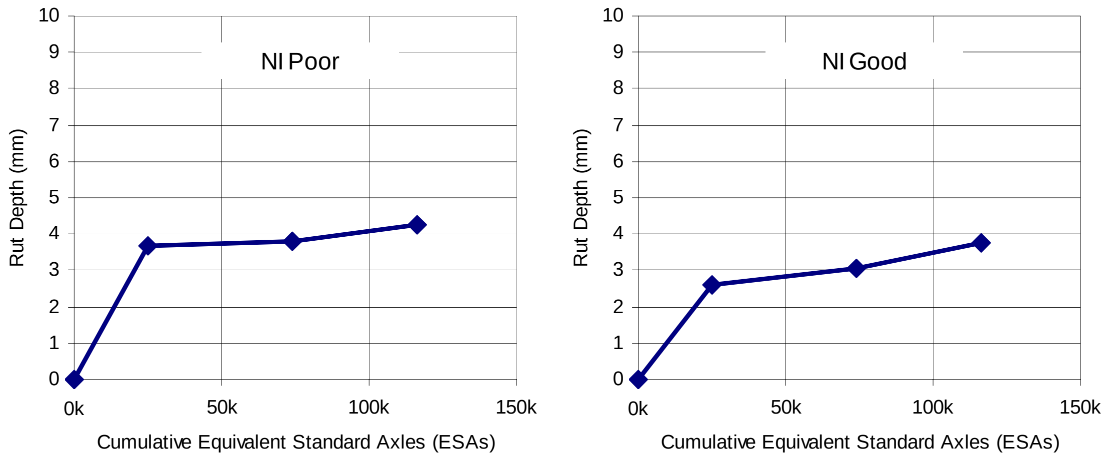

Figure 5.22. Rut depth progression for NI Poor and NI Good aggregate trials.

CHAPTER 6 FINITE ELEMENT MODELLING

6.1 INTRODUCTION

In the laboratory study (Chapter 3) Repeated Load Triaxial (RLT) permanent strain tests were conducted under a range of stress conditions on six granular materials and one subgrade soil (Table 3.1). An output from this study were boundaries defined by linear functions relating maximum mean principal stress, *p* to principal stress difference *q* (see stress invariants Section 2.4.3) that separated differences observed in permanent strain behaviour (i.e. either Range A, B or C defined in Section 2.11.2). Range A behaviour is considered ideal in terms of desirable performance of a granular material in a pavement as the permanent strain is asymptotic to a maximum value. The permanent strain boundaries found for a granular material in RLT tests could therefore provide a useful means of assessing expected performance in a pavement for design purposes. For example, the asphalt cover to a granular material could be increased until Range A behaviour is predicted to occur in the granular material. The commercial general finite element package (FEP) ABAQUS (1996) was therefore investigated for its ability to predict shakedown range behaviour of unbound materials utilised in a pavement.

Four pavements tested in the New Zealand accelerated pavement tests and two pavements in the Northern Ireland field trial were analysed in ABAQUS FEP. Material models available in ABAQUS were utilised to define shakedown range boundaries found for the materials tested in the laboratory study. Results were compared with these obtained in the actual pavement tests. From this comparison, criteria for the finite element model outputs were determined for the prediction of shakedown range behaviour. Finite element modelling is also undertaken on other wheel loads not tested to assess the effect on shakedown range prediction.

6.2 ABAQUS FINITE ELEMENT MODEL

6.2.1 Introduction

The ABAQUS/CAE commercial finite element package was selected to build the pavement model to predict shakedown range behaviour A, B or C (Section 2.11.2). It has a number of advantages:

a) is an advanced program,
b) it has excellent user interfaces for creating, submitting, monitoring, and evaluating results from finite element simulations,
c) it was available economically and immediately when needed,
d) was able to perform analyses of the pavements under consideration, and
e) incorporated a material model suitable for reproducing the behaviour of the granular material.

ABAQUS/CAE is divided into modules, where each module defines a logical aspect of the modelling process; for example, defining the geometry, defining material properties, and generating a mesh. Once the model is developed an input file is generated and then submitted to the ABAQUS/Standard solver. The solver performs the analysis and sends information to an output database. The results are then viewed in the Visualisation module of ABAQUS/CAE where specific reports on results can be generated as text files for further analysis in a spreadsheet. For models where only the material properties change then often the input file is more easily modified in a text editor rather than regenerated in ABAQUS/CAE.

ABAQUS does allow for the design of new material models although this is a complex process. Therefore, the existing models within the ABAQUS material library were utilised rather than develop new models for the purpose of pavement analysis. The geometry used for the pavement was kept simple and the resilient material models were those recommended in the ABAQUS manual. It was found that the form of the linear Drucker-Prager yield criterion (Section 2.9.3) available in ABAQUS matched the method of defining the shakedown range boundaries found in the laboratory study (Figure 3.15). Thus the shakedown range boundaries were defined as a pseudo-linear Drucker-Prager yield criterion.

6.2.2 Geometry and Boundary Conditions

Many researchers (Almeida 1986; Zienkiewicz 1989; Brunton & Almeida, 1992; Neves & Correia, 2003) define the geometry of the pavement as axisymmetric (Section 2.10.2) in finite element modelling (FEM). The main reason is the advantage of symmetry that significantly reduces the number of elements and thus computational effort. This is particularly important when complex non-linear resilient models are used, such as the Boyce model (Boyce, 1980). Therefore, the 2D axisymmetric model was used to model pavements for the purpose of predicting shakedown range behaviour. Also, as with most mechanistic design methods it was assumed there was full bonding between the asphalt, granular and subgrade layers.

Boundary conditions chosen were the same as used by researchers (Almeida 1986; Zienkiewicz 1989; Brunton & Almeida, 1992; Neves & Correia, 2003) where axisymmetric geometry is assumed. The vertical boundary provided free movement in the vertical direction while in the radial/outward direction was fixed. The boundary at the base is fixed vertically while movement in the radial direction is not restricted.

6.2.3 Porous Elasticity

A porous elasticity model is recommended in the ABAQUS manual for modelling the non-linear behaviour of soils. The porous elasticity model does not match those used by other researchers for modelling resilient behaviour (Dunlap, 1963; Pezo, 1993; Tam & Brown, 1988; Hicks, 1970; Uzan, 1985; Wellner and Gleitz, 1999; Brown and Hyde, 1975; Boyce, 1980; Hornych et al, 2002; Mayhew, 1983) but is considered adequate in the light of the main focus of the finite element modelling to predict permanent strain behaviour rather than resilient strains. Porous elasticity is described by Equations 2.24 and 2.25.

Most of the parameters of the porous elasticity model can be entered through the menu options in ABAQUS/CAE . However, the initial stress (p_0, Equation 2.28) and void ratio (e_0, Equation 2.28) porous elasticity parameters can only be added in the input file with the aid of a text editor.

6.2.4 Shakedown Behaviour Range Boundaries

ABAQUS has available a range of elasto-plastic models (Section 2.9) for defining the yield criteria of materials. The linear Drucker-Prager criterion (Section 2.9.3) is defined by a straight line in *p* (mean principal stress, Equation 2.2), *q* (principal stress difference, Equation 2.7) stress space (Equation 2.55). It was found in the laboratory study (Chapter 3) the shakedown range boundaries could be defined in the same way (Figure 3.15). Therefore, the shakedown range boundaries were defined as pseudo yield criteria in ABAQUS. As only one yield criterion is possible the shakedown range boundaries A/B and B/C are modelled in separate analyses. It was initially thought that if shakedown Range A/B boundary was used as the yield criterion and if no yielding occurred then it is safe to assume the shakedown Range A behaviour is likely. However, as found in later analysis, achieving nil yield is near impossible and criteria on the amount of yielding are required to define when shakedown Range A is likely to occur.

6.3 FEM OF PAVEMENT TESTS

A total of 4 pavement cross-sections tested in the New Zealand accelerated pavement tests (ID: 1, 2, 3 and 4 – Table 4.1) and 2 from the Northern Ireland field trial (Chapter 5) were modelled in ABAQUS finite element package. As described in Section 6.2 existing material models in ABAQUS were utilised with the purpose of predicting the shakedown range behaviour of the pavement.

6.3.1 Geometry

The pavement cross-sections consisted of 4 from the New Zealand accelerated pavement tests (ID: 1, 2, 3 and 4 – Table 4.1) and two from the Northern Ireland trials. Three cross-sections modelled from the New Zealand tests were designed to have the same asphalt and granular thickness (ID: 1, 2, 3 Table 4.1), but the as built pavement thicknesses reported in Arnold et al. (2001) were used in the finite element model. The two Northern Ireland trials were identical with the only variation being the aggregate type (*NI Poor* or *NI Good*). Table 6.1 summarises the cross-sections modelled along with the material types as defined in Table 3.1.

Table 6.1. Pavement cross-sections.

Layer:	Asphalt	Granular	Subgrade
	Thickness (mm)		
Pavement cross-section/ID (Table 4.1): 1	36	289	1200
2	31	282	
3	25	282	
4	90	200	
5	100	650	750
6	100	650	
	Material Types (Table 3.1)		
Pavement cross-section/ID (Table 4.1): 1	AC	*CAPTIF 1*	*CAPTIF Subgrade*
2		*CAPTIF 2*	
3		*CAPTIF 3*	
4		*CAPTIF 4*	
5		*NI Good*	*Soil & Rock*
6		*NI Poor*	

For each different geometry a new ABAQUS/CAE model was required. However, the models were very similar in terms of mesh density, loading, element type and boundary conditions. Figures 6.1, 6.2 and 6.3 show the typical models developed for the thin asphalt pavements at CAPTIF (cross-sections 1, 2 and 3, Table 6.1); the thick asphalt pavement at CAPTIF (cross-section 4, Table 6.1) and the Northern Ireland road trial (cross-sections 5 and 6, Table 6.1). These Figures also show how the loading of a dual tyred 40kN half axle load was approximated with a circular load with a radius of 130mm and thus a stress of 0.75 MPa. The model chosen was a simple 2 dimensional axisymmetric model with quadratic elements as described in Section 6.2.2.

6.3.2 Material Models – Resilient Behaviour

The resilient properties of the granular materials and the CAPTIF subgrade are defined by the porous elasticity model (Section 6.2.3). Parameters for the porous elasticity model were determined for each material in the laboratory study (Section 3.8.3) and are listed in Table 3.6.

Properties of the Asphalt (AC, Table 6.1) were assumed to be linear elastic with an elastic modulus of 3,000 MPa and a Poisson's ratio of 0.35. An elastic modulus of 2,000 MPa and Poisson's ratio of 0.35 was assumed for the subgrade being a mixture of large boulders and soil (*Soil & Rock*, Table 6.1). These assumed properties were based on typical values (Austroads, 1992) and some quick pavement analysis to assess whether or not the computed stresses and deflections are reasonable.

6.3.3 Material Models – Shakedown Range Boundaries and Residual Stress

The shakedown range boundaries A/B and B/C found in the laboratory study (Table 3.4) were defined as linear Drucker-Prager yield criteria (Section 2.9.3 and 6.2.4). For the linear Drucker-Prager model the ABAQUS general finite element package requires the yield surface to be defined as per the line plotted in Figure 2.17. The angle of the line, β, is inputted directly while the value of "d" the "q-intercept" (Figure 2.17) is not used. Instead a value on the yield line, σ_{0c}, is used. This value (σ_{0c}) is the yield stress where the confining stress is zero and is calculated using Equation 2.56 from the angle β and intercept d defining the linear yield surface/shakedown range boundary.

Prior to the calculation of linear Drucker-Prager parameters for the shakedown range boundaries defined by slope β and intercept d in Table 3.4 an adjustment was made to account for residual stress. As detailed in Section 2.4.6 residual stresses in the pavement that due to compaction, active earth pressure and confinement of the pavement layer are significant and should be considered. Linear elastic analysis during preliminary design of the Northern Ireland field trial highlighted the need for including a value for horizontal residual stress (see Section 5.2 and Figures 5.2 and 5.3). A value of 30kPa was considered appropriate as concluded in Section 2.4.6 and found to result in more realistic predictions of pavement performance (Figure 5.3). Inclusion of the 30kPa residual stress in linear elastic analysis estimates that a minimum asphalt thickness of 80mm should result in Range A behaviour for the *NI Good* (Table 3.1) material. This result is broadly confirmed by accelerated pavement tests where the section with 90mm of asphalt cover (ID 4: Table 4.1) resulted in Range A behaviour. Although the accelerated pavement test used a different granular material (CAPTIF 4), because they are both premium quality crushed rock, the performance should be approximately the same.

In linear elastic analysis undertaken in Section 5.2 the horizontal residual compressive stress of 30kPa was added to the horizontal stresses and the resulting p (mean principal stress, Equation 2.2) and q (principal stress difference, Equation 2.7) was calculated and compared with the shakedown range boundaries (Figure 5.3). This approach to applying the additional residual stress is suitable where pavement stresses have been imported into a spreadsheet. However, to avoid this step one method is to translate the shakedown boundaries by subtracting a 30 kPa horizontal stress. This has the effect of reducing p and increasing q and therefore increasing the value of the intercept of the shakedown boundaries while the slope remains unchanged. Thus, the effect is to increase the strength of the material similar to adding a 30kPa horizontal stress. An example of applying the 30kPa horizontal residual stress to the shakedown range boundaries is shown in Figure 6.4 for the CAPTIF 2 material.

The shakedown range boundaries listed in Table 3.4 were all translated by applying the 30kPa residual stress. This translation was undertaken to the three stress values found in the Repeated Load Triaxial tests used to define the boundary. After the three stress values were translated a new best fit line was fitted to the points which defined the new translated shakedown range boundaries that accounted for a 30kPa residual stress. Finally the, σ_{0c} value (Equation 2.56) needed by ABAQUS was calculated from the angle β and intercept d that defined the new translated shakedown range boundaries. Parameters for the translated shakedown range boundaries used in finite element modelling are summarised in Table 6.2.

Table 6.2. Shakedown range boundaries with 30kPa horizontal residual stress adjustment as used as Drucker-Prager yield criteria.

	Shakedown range boundary A-B plus 30kPa residual horizontal stress			**Shakedown range boundary B-C plus 30kPa residual horizontal stress**		
Material (Table 3.1)	*d (kPa)*	β *(°)*	σ_{0c} (Eqn. 2.52) (*kPa*)	*d (kPa)*	β *(°)*	σ_{0c} (Eqn. 2.52) (*kPa*)
NI Good	72	58	154	131	65	459
NI Poor	111	39	152	174	56	344
CAPTIF 1	91	48	144	129	61	324
CAPTIF 2	51	45	77	58	63	168
CAPTIF 3	90	54	166	106	65	372
CAPTIF 4	78	40	108	15	69	114
CAPTIF Subgrade	63	28	77	33	64	104

6.3.4 Shakedown Range Prediction

For each of the six pavement trials the shakedown range (A, B or C, Section 2.11.2) was predicted using the design information in Tables 6.1 and 6.2 and

Figures 6.1, 6.2, and 6.3. The wheel loading was approximated as a circular load of 40kN for cross-sections 1, 2, 3, 5 and 6 and 50kN for number 4 where these loads are the same load as in the pavement tests reported in Chapters 4 and 5. A uniform contact stress of 0.75MPa was assumed for all models. The shakedown range boundaries (Table 6.2) were defined in the ABAQUS FEM as Drucker-Prager yield criteria (Section 2.9.3). Two models were required the first model includes the shakedown Range A/B yield line. The second model uses the shakedown Range B/C yield line. Shakedown range was predicted by assessing the amount of plastic deformation to occur in each model. It was initially thought that if there was no plastic deformation then for the shakedown Range A/B yield line then a desirable shakedown Range A behaviour will occur. Similarly, for the shakedown Range B/C yield line model if there is no plastic deformation then premature failure or shakedown Range C should not occur. However, achieving nil plasticity is nearly impossible as trial FEM runs with very thick asphalt (250mm) cover still resulted in small amounts of plastic deformation. This is because the model will allow yielding in the aggregate to occur in order to ensure minimal tensile stresses in the unbound material. The yielding occurs at the base of the aggregate layer and is considered typical behaviour. Yielding results in lateral outward horizontal movement of the aggregate which is resisted by surrounding aggregate. The build-up of this resistance by the surrounding aggregates is, effectively, the build up of residual stresses. Therefore, a small amount of plastic deformation was considered acceptable. However, the exact amount defining whether shakedown Range A or B occurs is still to be determined.

Results showing regions where vertical plastic strain is occurring for the shakedown Range A/B analysis are shown in Figure 6.5. The scales are not identical and therefore a more direct comparison of the resulting plastic strains is summarised in Table 6.3. A similar analysis was undertaken using the shakedown Range B/C boundary yield line and results are shown in Table 6.4 and Figure 6.6.

Table 6.3. Plastic strains for shakedown Range A/B boundary yield line finite element analysis.

Cross-section (Table 6.1)	Total permanent vertical deformation (mm)			Plastic strains (μm/m)			
				Granular		Sub.	Gran.
	Total	Gran.	Sub.	*Depth (mm)*	Max Comp.	Max Comp.	Max Tensile
1	0.52	0.34	0.18	*108*	1567	2197	-235
2	0.97	0.66	0.32	*102*	2891	3678	-817
3	0.35	0.23	0.12	*96*	951	2484	-545
4	0.20	0.15	0.05	*90 (top)*	1017	1057	-5
5	0.07	0.07	-	*100 (top)*	450	-	-13
6	0.08	0.08	-	*100 (top)*	837	-	-30

Table 6.4. Plastic analysis of pavement tests for shakedown Range B/C boundary yield line.

Cross-section (Table 6.1)	Total permanent vertical deformation (mm)			Plastic strains (μm/m)			
				Granular		Sub.	Gran.
	Total	Gran.	Sub.	*Depth (mm)*	Max Comp.	Max Comp.	Max Tensile
1	0.12	0.09	0.03	*108*	430	163	-243
2	0.20	0.13	0.07	*102*	512	531	-552
3	0.10	0.06	0.04	*96*	236	412	-360
4	0.08	0.02	0.06	**290*	103	371	-202
5	0.02	0.02	-	*100 (top)*	193	-	-27
6	0.02	0.02	-	*100 (top)*	335	-	-15

* Plastic strain varied from 101 to 103 μm/m from top (90mm) to bottom (290mm) of cross-section 4.

The results shown in Tables 6.3 and 6.4 show a calculated permanent deformation. Permanent deformation should not be considered as a predicted rut depth. This is because the analysis is static and its purpose is to assess whether or not stresses within the pavement exceed the shakedown range boundaries. Assigning the shakedown range boundary as a yield line is a convenient means to assess whether or not there are regions in the pavement where the stresses meet or exceed the shakedown range boundary. Further, the maximum total deformation computed is only 0.20mm and thus does not resemble the rut depths that were actually measured in the pavement tests that were greater than 5mm.

Examining the results in terms of the extent the shakedown range boundaries have been exceeded, by way of yielding reported as plastic strains, does show to varying degrees some regions in the pavement will exhibit Range C behaviour. However, it is known from the pavement tests Range C behaviour which is effectively failure did not occur. For the first few thousand wheel passes it is observed the rutting increases rapidly before stabilising (Figure 4.20) and this could be considered as Range C behaviour occurring early in the pavements life. The pavement tests showed Range A behaviour occurred for the Northern Ireland trials (cross-sections 5 and 6, Table 6.1) and the New Zealand accelerated pavement test number 4 (ID: 4, Table 4.3), while the other tests exhibited Range B behaviour for the 40kN wheel load. Therefore, an initial estimate at a cut off plastic deformation defining the boundary between Range A and B behaviour could be 0.2mm as this is the value determined for cross section 4 (Table 6.3) that exhibited Range A behaviour in the pavement test (ID: 4, Table 4.1). It is important to note that this analysis using the shakedown range boundaries is aimed at predicting behaviour rather than magnitude. The magnitude of permanent deformation/surface rutting is predicted using a permanent strain model combined with a pavement stress analysis as in Chapter 7 *Permanent Deformation Modelling*.

6.4 PAVEMENT LOADING EFFECT

The CAPTIF 3 pavement trial was used in the finite element model to test the effect of changes in pavement loading on performance in terms of permanent deformation. A range of wheel loads and tyre contact stresses was chosen for analyses as detailed in Table 6.5. For each load type two finite element analyses were conducted: shakedown range boundaries A/B and B/C (Table 6.2).

Table 6.5. Load combinations modelled.

Wheel Load (kN)	Contact Stress (kPa)	Load Radius (mm)
20	750	92
30	750	113
40	750	130
50	750	145
60	750	160
40	350	191
40	550	152
40	750	130
40	950	116

These load combinations enabled the effects of either changing load or tyre contact stress had on the amount of deformation to occur for each shakedown range boundary/yield criterion. Results of theses changes are quantified in Table 6.6.

Table 6.6. Effect of pavement loading on permanent deformation and strain.

	Deformation (mm)			**Maximum strains in Granular material (bott.= bottom of granular = 307.mm)**					**Subgrade (max at top)**	
	Tot.	**Gran**	**Subg**	**Vol (μm/m)**	**Depth (mm)**	**Shear (μm/m)**	**Horiz (mm)**	**Depth (mm)**	**Vol (μm/m)**	**Shear (μm/m)**
A/B Stress=750kPa										
20kN (92mm)	0.13	0.13	0.00	-179	72	1425	0	72	-14	15
30kN (113mm)	0.23	0.17	0.06	-189	72	1570	85	72	-1857	1923
40kN (130mm)	0.38	0.22	0.16	259	bott.	1803	130	72	-2919	3022
50kN (146mm)	0.56	0.26	0.31	375	bott.	2124	146	119	-3877	4013
60kN (160mm)	0.76	0.30	0.47	485	bott.	2566	0	bott.	-4683	4850
A/B Load=40kN										
350kPa (191mm)	0.18	0.11	0.07	135	bott.	1064	191	72	-1756	1820
550kPa (152mm)	0.29	0.17	0.12	212	bott.	1466	152	72	-2458	2545
750kPa (130mm)	0.38	0.22	0.16	259	bott.	1803	130	72	-2919	3022
950kPa (116mm)	0.45	0.26	0.20	302	bott.	2117	116	72	-3291	3405
B/C Stress=750kPa										
20kN (92mm)	0.04	0.03	0.00	461	25	695	46	72	227	412
30kN (113mm)	0.06	0.04	0.02	519	48.5	757	113	72	465	848
40kN (130mm)	0.10	0.05	0.05	603	72	850	130	72	697	1269

50kN (146mm)	0.15	0.07	0.08	691	72	1026	0	bott.	881	1606
60kN (160mm)	0.19	0.08	0.11	837	bott.	1296	0	bott.	1020	1861
B/C Load=40kN										
350kPa (191mm)	0.06	0.03	0.03	463	25	582	191	25	481	878
550kPa (152mm)	0.09	0.04	0.04	535	48.5	733	152	72	617	1124
750kPa (130mm)	0.10	0.05	0.05	603	72	850	130	72	697	1269
950kPa (116mm)	0.12	0.06	0.05	661	72	950	116	72	760	1385

Table 6.7. Effect of halving the load or stress on total deformation.

	Reduction in deformation caused by:	
FE Analysis	**Halving Load**	**Halving Stress**
Shakedown A/B	67%	45%
Shakedown B/C	64%	35%

Figures 6.7 and 6.8 show the total vertical surface permanent deformation calculated for a range of load cases when using the shakedown boundaries A/B and B/C as yield lines in the finite element analysis. It is argued that if the total deformation calculated is nil then shakedown of the pavement is likely. For this thin surfaced CAPTIF 3 pavement there is a tendency towards nil deformation as the load is decreased. However, some total surface deformation is still calculated for the low 20kN load where the volumetric strains calculated for shakedown Range A/B (Table 6.6) would suggest otherwise. Volumetric strains for the 20kN and 30kN were all expansive in both the granular and subgrade layers. Therefore, it is likely that shakedown will occur for this pavement at wheel loads of less than 30kN with a tyre contact stress of 750kPa. Changing the contact stress does have a significant effect on the total deformation calculated for the shakedown Range A/B and B/C boundary case. Halving the contact stress will reduce the total deformation calculated by 45% and 35% for the shakedown Range A/B and B/C cases respectively.

It should be noted that these results relate to the CAPTIF 3 pavement test. Pavements of different layer thicknesses will likely result in different trends, particularly the effect of tyre contact stress. As the tyre contact stress effect is most noticeable at the surface, an unsealed unbound granular pavement will show a more marked effect with changes in tyre contact stress as compared with the CAPTIF 3 pavement.

6.5 SUMMARY

Finite element analysis was conducted on 4 pavement types tested in the New Zealand accelerated pavement tests (ID: 1, 2, 3 and 4: Table 4.1) and the 2 Northern Ireland field trials (Chapter 5) for the purpose of predicting the shakedown behaviour range (A, B or C defined in Section 2.11.2). The shakedown range boundaries A/B and B/C defined as linear functions of q (deviatoric stress) and p (mean principal stress) for the pavement materials in the laboratory study were defined as Drucker-Prager yield criteria in the ABAQUS finite element package. The shakedown range boundaries were translated, to account for the significant effect of horizontal residual stress due to compaction, before being defined in the finite element model (FEM) as yield criteria. The two shakedown range boundaries A/B and B/C were used in two separate finite element analyses as only one yield criterion could be defined. A non-linear porous elasticity model with parameters found from Repeated Load Triaxial tests was used to define the resilient properties of the granular and subgrade materials while linear elastic properties were assumed for the asphalt layer.

Results of the finite element analysis were plastic strains and total vertical deformation obtained for the two shakedown range boundaries A/B and B/C defined as yield criteria. The amount of plastic strains and total vertical deformation gives an indication of the amount of yielding that has occurred. Regions in the pavement that have yielded are considered locations where the stress level meets or exceeds the shakedown range boundary A/B or B/C. Based on results of New Zealand accelerated pavement tests and the Northern Ireland field trials, criteria on an acceptable amount of permanent deformation where shakedown Range A is likely were established. This limit on total vertical deformation was set at 0.20mm when shakedown range boundary A/B translated with a 30kPa horizontal residual stress was used as the yield criterion. However, this criterion is purely empirically based and is only valid for assumptions used in its derivation (e.g. porous elasticity, Drucker-Prager yield criterion, etc).

Finite element analysis utilising the shakedown range boundaries A/B and B/C was extended to a range of loads and contact stress. It was found that reduction in load and contact stress resulted in a reduction of the total amount of permanent deformation, where reducing the load had the greatest affect.

The method of finite element analysis used to predict shakedown range behaviour, utilised material models readily available in a commercial finite element model. Therefore, the method could be readily applied by pavement designers with access to a finite element model. However, the inability to predict a rut depth is a limitation particularly where a Range B response is predicted. Therefore, a method to predict rut depth has been developed and is presented in Chapter 7 *Permanent Deformation Modelling*.

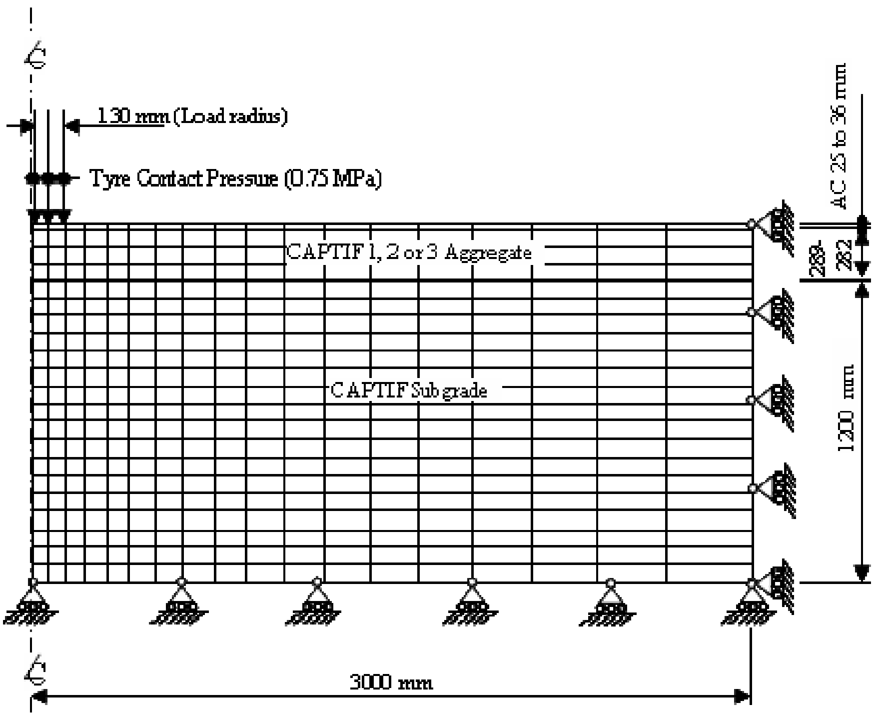

Figure 6.1. Finite element model for CAPTIF 1, 2 and 3 aggregate pavement tests.

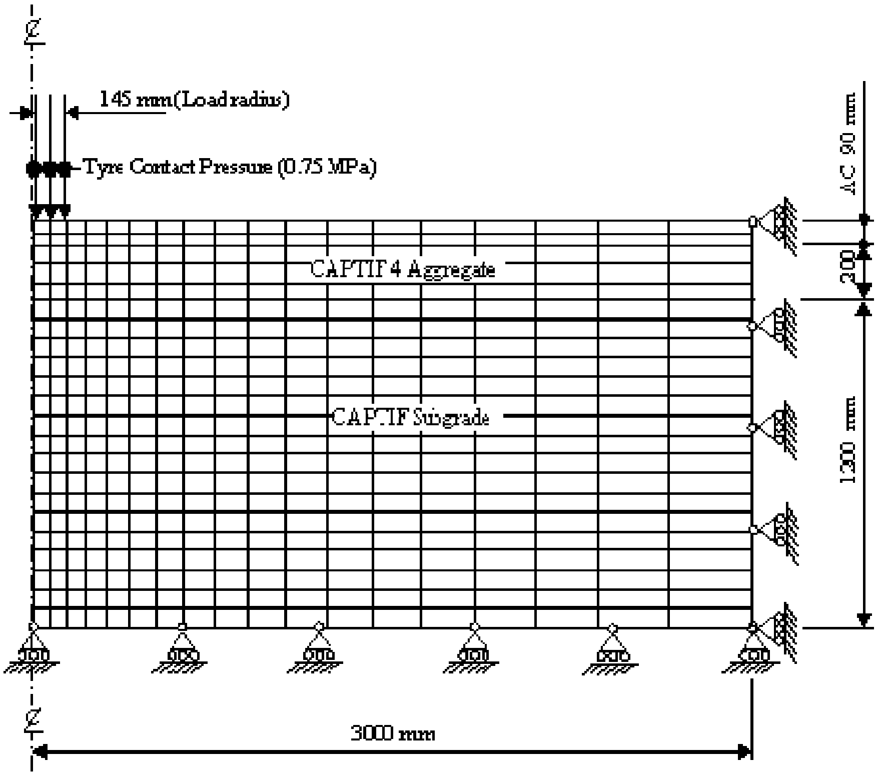

Figure 6.2. Finite element model for CAPTIF 4 aggregate pavement test.

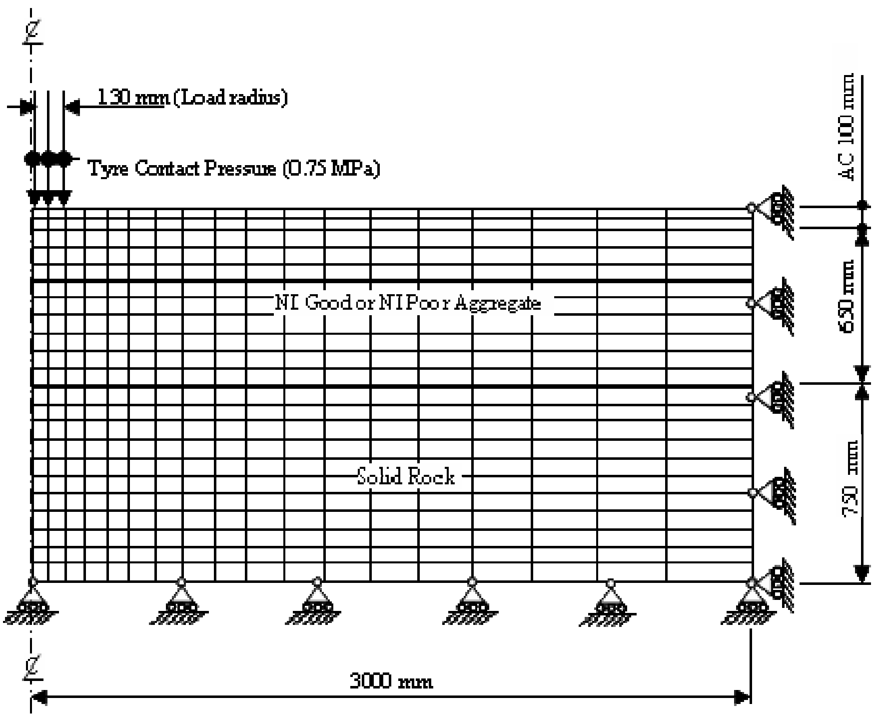

Figure 6.3. Finite element model for NI Good and NI Poor aggregate pavement tests.

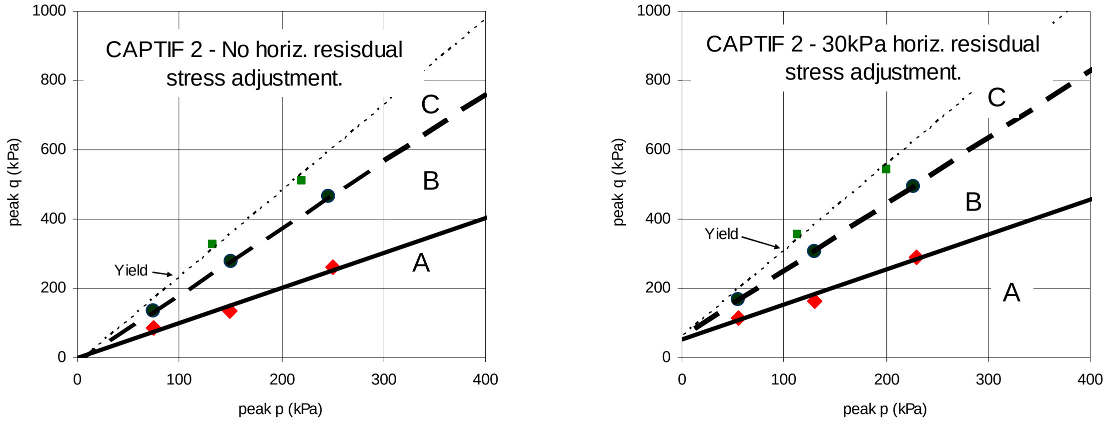

Figure 6.4. Effect on shakedown range boundaries with 30kPa horizontal residual stress added for CAPTIF 2 materials.

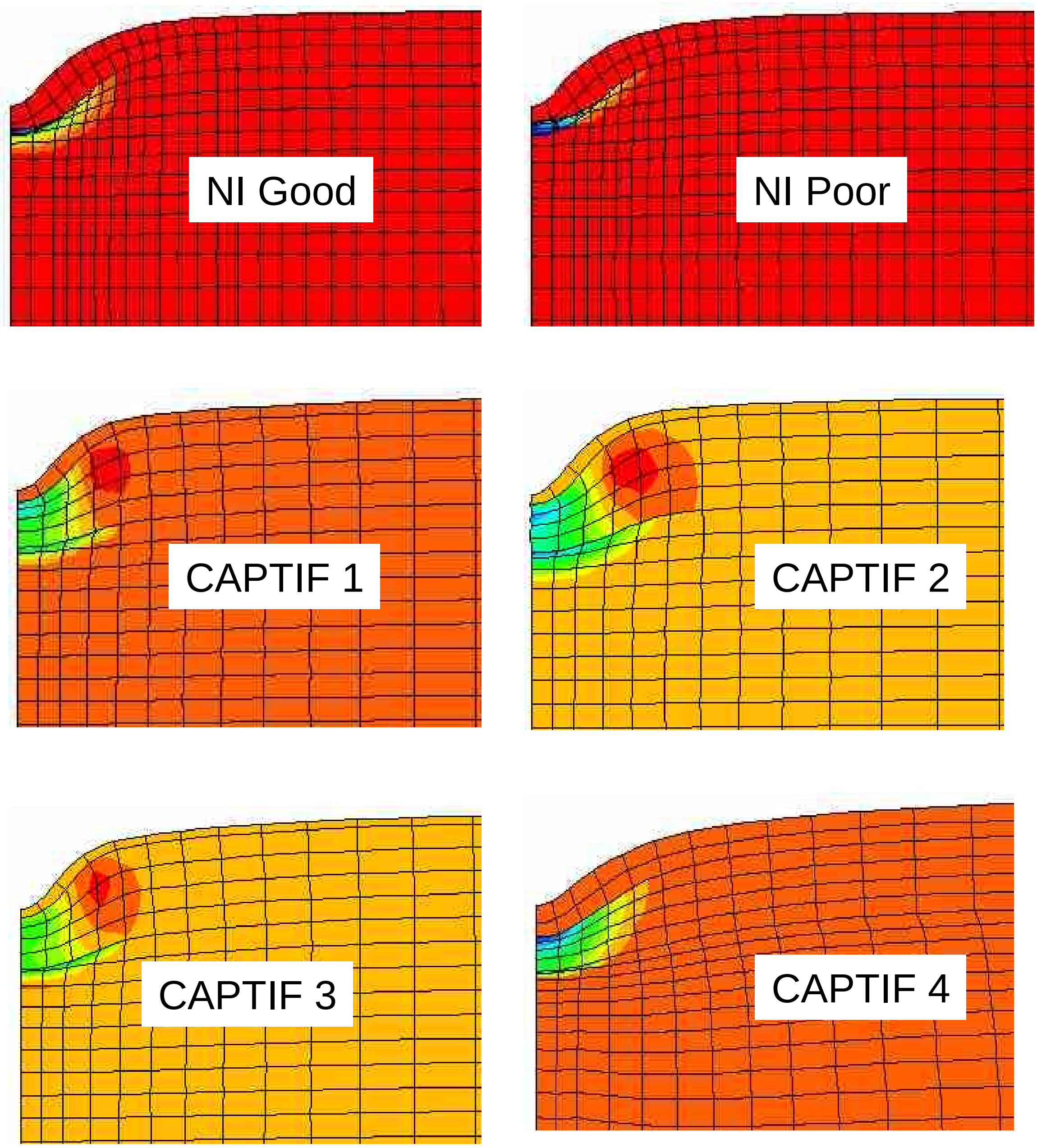

Figure 6.5. Regions of vertical plastic deformation for shakedown Range A/B boundary analysis (NB: scales are not the same and the red circles in CAPTIF 1, 2 and 3 are tensile or upwards).

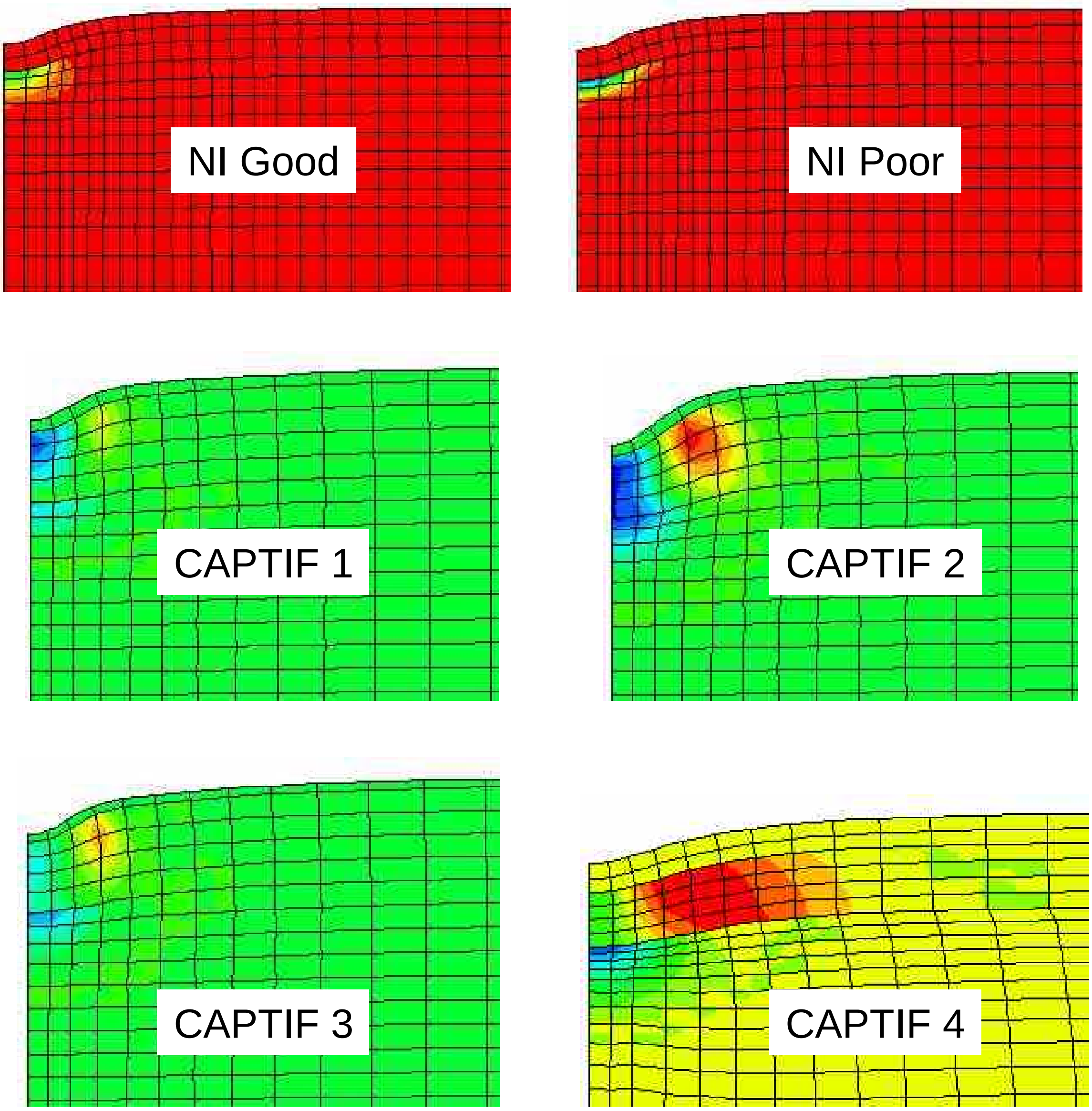

Figure 6.6. Regions of vertical plastic deformation for shakedown Range B/C boundary analysis (NB: scales are not the same and the red in CAPTIF 2, 3 and 4 are tensile or upwards strains).

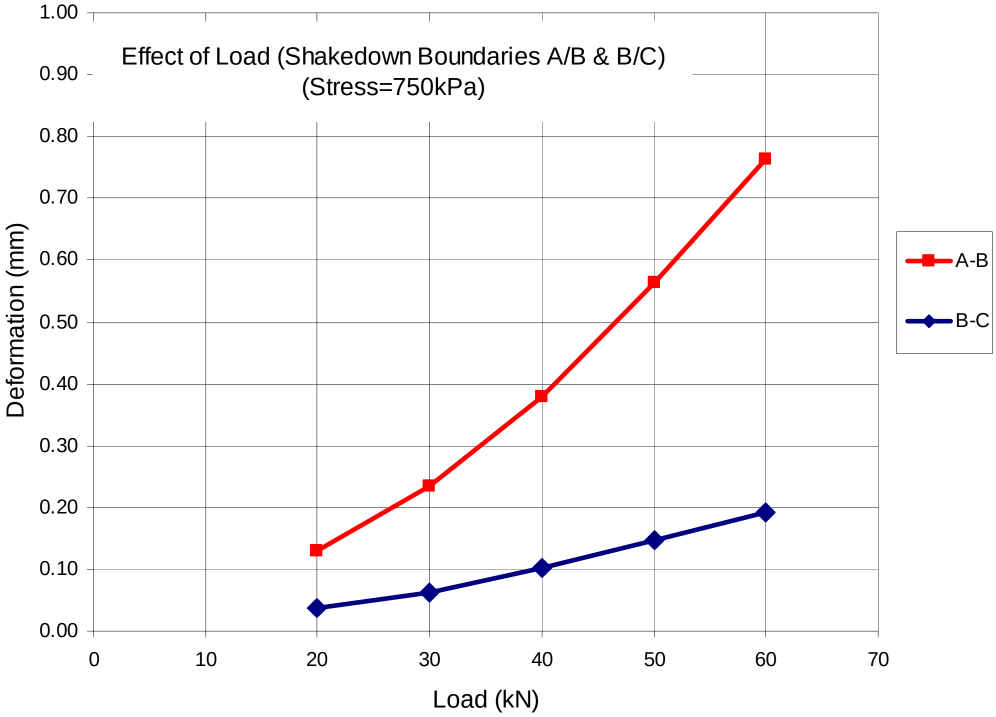

Figure 6.7. Permanent surface deformation calculated using shakedown range boundaries for a range of loads.

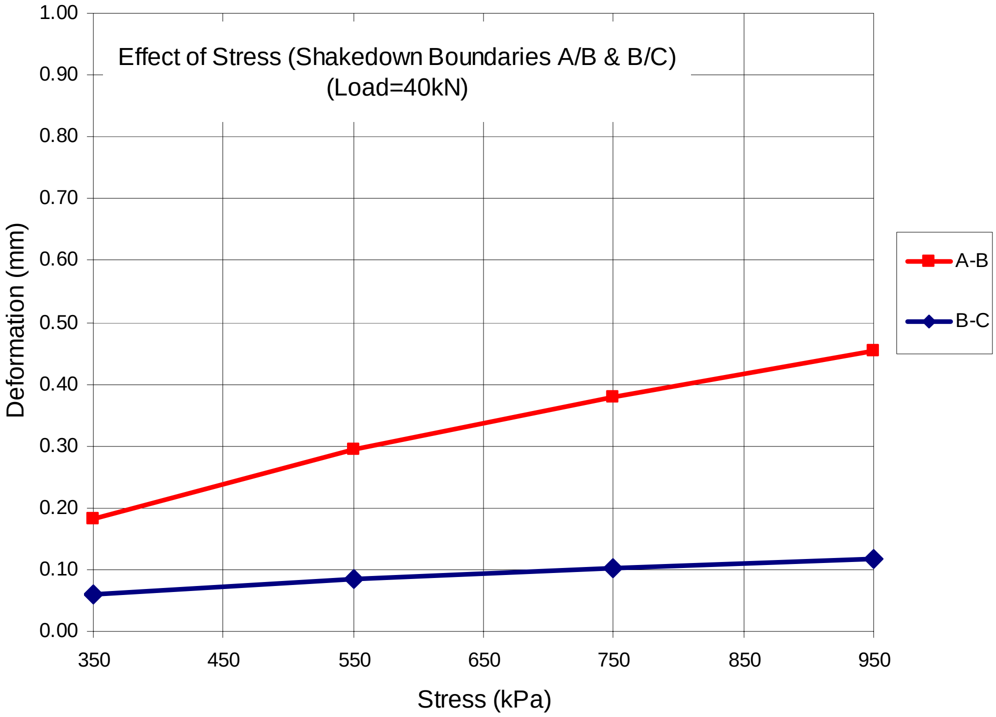

Figure 6.8. Permanent surface deformation calculated using shakedown range boundaries for a range of contact stresses

CHAPTER 7 MODELLING PERMANENT DEFORMATION

7.1 INTRODUCTION

In comparison to resilient behaviour, less research has been devoted to plastic response and permanent deformation development in granular materials. One of the reasons is the current pavement design procedures. The current underlying aim of pavement design is to keep vertical compressive resilient strains in the subgrade and tensile resilient strains in the asphalt below some critical value. Therefore, the load spreading or resilient characteristics of the granular material are important. However, the results from the New Zealand accelerated pavement tests (Chapter 4) show that the resistance to permanent deformation of the granular material has a significant effect on the amount of rutting. Further, good resilient characteristics do not necessarily mean good resistance to deformation, as found by Thom and Brown (1989).

Chapter 6 *Finite Element Modelling* explored the aspects of shakedown to pavement design. The concepts of shakedown have been utilised in terms of classifying observed behaviours of deformation in one of three possible ranges: A, B or C as defined in Section 2.11.2. In its simplest form of design, shakedown (Range A) will occur if stresses within the pavement fall below some critical value or boundary (e.g. Figure 5.3). Should shakedown Range A occur then the design is considered acceptable for resistance to permanent deformation. The number of load cycles is not considered in this approach and the magnitude of permanent strain is not calculated. This is because for a shakedown Range A response the amount of deformation is considered negligible and there will be a point where no further deformation will occur.

Achieving a shakedown Range A response usually requires thick asphalt covers to sufficiently reduce stresses from wheel loading to the granular and subgrade materials. For many countries and low volume roads it is uneconomical to use large thicknesses of asphalt cover. Therefore, a majority of pavements will exhibit to varying degrees shakedown Range B behaviour. This is where deformation will increase linearly with increasing load cycles. The number of load cycles thus becomes an important factor in design. Therefore, this chapter aims to develop a model fitted to permanent strain RLT test data and then apply this model to predict pavement rut depth for any given number of wheel loads.

There are three parts to this chapter, where the first two parts are the development of 1 parameter and 2 parameter models with respect to stress for the calculation of permanent strain using data obtained from Repeated Load Triaxial tests (Chapter 3). The third part involves the application of the 2 parameter model to predict the surface rut depth for pavement tests reported in Chapters 4 and 5.

The 1 parameter model developed is similar to existing models proposed by researchers (Table 2.1). A stress ratio that conveniently characterises both vertical and radial stresses as one value is used in the model and thus labelled as *1 Parameter Model*. It was found that the *1 Parameter Model* failed to adequately predict permanent deformation in Repeated Load Triaxial tests for some stress states where the differences between calculated and measured permanent strain was too large to ignore. Therefore, a more fundamental approach was taken to the development of a model to predict permanent strain rate from Repeated Load Triaxial tests. It involved considering two values of stress defining the vertical and radial components separately in an equation. This more fundamental approach utilises two stress values independently and thus is labelled as the *2 Parameter Model*. The *2 Parameter Model*, although more difficult to obtain the parameters, provided a better match to the measured Repeated Load Triaxial data, where adequate predictions were possible for all stress states tested, which was not the case for the *1 Parameter Model*.

The third part of this chapter utilises the *2 Parameter Model* to predict rut depth of pavement tests reported in Chapters 5 and 6. DEFPAV a simple finite element package specific for non-linear pavement analysis was used to calculate the axial and radial stresses at incremental depths under the centre of the wheel load. A permanent strain value from the *2 Parameter Model* is calculated at each depth increment where the stress level has been computed. Finally, permanent strain is integrated over the pavement depth and summed to obtain a prediction of surface rut depth. Predicted rut depth was compared to the measured rut depth in the pavement trials and reasons for possible differences is discussed.

7.2 EXISTING PERMANENT STRAIN MODELS

There are many models proposed by researchers that predict permanent strain with increasing number of load cycles and a full list is given in Table 2.1. These have been derived from Repeated Load Triaxial (RLT) test results and at first glance the resulting form of the model probably depended on the range of stresses tested in the RLT apparatus. Should these stresses be those that result in Range A type behaviour (Section 2.11.2) then Equations 2.34 and 2.40 (Paute et al. 1996), Equation 2.34 (Barksdale, 1972), Equation 2.35 (Sweere, 1990) would likely fit the data well as these tend towards an upper maximum permanent strain value. The Sweere equation can also fit most Range B type behaviour while the Wolff & Visser (1994) model (Equation 2.36) is well suited to Range B behaviour. The Wolf & Visser Equation is such that as *N* (load cycles) is large the resulting function is linear (i.e. $y=mx+c$). The Range C behaviour representing incremental collapse is not suited for modelling but rather could be useful as a stress boundary which should not be exceeded.

Lekarp and Dawson (1998) discarded all the previous models as they recognised that different permanent strain behaviours occur and proposed a different model. Their model (Equation 2.45) considers the length of the stress path and maximum stress ratio (q/p) to calculate the deformation for one particular load cycle case (N_{ref}).

7.3 1 PARAMETER MODEL DEVELOPMENT

7.3.1 Introduction

Results from Repeated Load Triaxial (RLT) tests showed a high dependence on stress level. Stress level in the RLT tests was characterised by stress invariants p and q (Section 2.4.3) when fully loaded (i.e. maximum values). This is convenient as many equations that predict permanent strain utilise the stress invariants p and q. Further, p and q are combined as one stress parameter being a form of stress ratio (e.g. q/p or $q/(p+p^*)$). One stress parameter instead of two allows greater ease of determining parameters for an equation to predict permanent strain and has been referred to as a *1 Parameter Model*. Based on a form of stress ratio and equations used by other researchers, a model that best fitted the RLT data in the laboratory study (Chapter 3) was proposed. The form of the proposed model was also influenced by considering the stress boundary between shakedown Range B (constant permanent strain rate) and shakedown Range C (failure) behaviour, as detailed in Table 3.4. As all of the RLT permanent strain tests were multi-stage and thus difficult to determine the amount of initial deformation, the permanent strain rate rather than the magnitude is considered.

7.3.2 Permanent Strain Rate

Utilising the rate of deformation is more appropriate for RLT multi-stage tests as it is unsure how permanent strain for each part of the multi-stage test should be added together. Presently, the sum of the permanent strains of all the previous tests, are added to the result. This will likely over-estimate the amount of deformation for example increasing the number of tests conducted prior to the stress level in question will lead to a higher magnitude of permanent strain. Also reviewing the RLT permanent strain results during the first 20,000 load cycles there is a "bedding in" phase until a more stable/equilibrium type state is achieved. It is argued that this equilibrium state is unaffected by differences in sample preparation and previous tests in the multi-stage tests. Therefore, relationships considering permanent strain rate were explored.

It was found that the scatter in results was reduced by using the secant rate of permanent strain between 25,000 and 50,000 load cycles in place of permanent strain magnitude when plotted against stress ratio (q/p). This rate of permanent strain was calculated in percent per 1 million load cycles. These units have some practical interpretation as a value of 5% per million load cycles can be related to 5mm of deformation occurring for a 100mm layer after 1 million loads. Further, as shakedown Range B is where deformation increases linearly with load cycles then this rate of permanent strain can be used to crudely predict the magnitude of deformation.

7.3.3 Initial Analysis

Various models were considered and in particular those that used stress level as a parameter. The ideal model should: predict the magnitude of deformation in relation to stress level; have a stress boundary; and be easy to use for routine pavement design. Initially, maximum stress ratio (q/p) was plotted against permanent strain rate between 25,000 and 50,000 load cycles as measured in the RLT apparatus. It was found that an exponential function ($y=ae^{bx}$, where $x=q/p$ and y=permanent strain rate) could be fitted to a majority of the results but there were significant outliers that could not be ignored. These outliers were points with the highest permanent strain rate but medium stress ratios. This suggests that maximum stress ratio alone is not an indicator of permanent strain rate.

Paute et al (1996, Equations 2.34 and 2.40) utilised a p^* parameter in the stress ratio while Lekarp and Dawson (1998, Equation 2.45) indirectly used the stress path length L. The p^* parameter is the value where the yield line intercepts the p-axis in p-q stress space (Figure 7.1). RLT permanent strain rate was then plotted against modified stress ratios $q/(p\text{-}p^*)$ and $(q/p)L$. This did reduce the number of outliers significantly. The best fit to the data was found when using the $q/(p\text{-}p^*)$ ratio with a exponential function ($y=ae^{bx}$, where $x=q/(p+p^*)$ and y=permanent strain rate). This was preferred as the stress path length L would impose some practical difficulties for use in pavement design. However, it was found the exponential function did not result in high enough permanent strain rates for cases close to yield/shakedown range boundary B/C (Table 3.4). Further, there is no limit to the stress ratio and stress ratios exceeding the yield criteria can still compute permanent strain rates.

7.3.4 1 Parameter Model Proposed

Based on the initial analysis the equation to calculate the parameter A in Paute et al (1996) Equation 2.44 looked promising. This equation only required one parameter to be calculated by regression (or curve fitting). The other two parameters m (slope ratio, Figure 7.1) and p^* (point where $q=0$, Figure 7.1) are determined from the yield line calculated from monotonic shear failure tests. Further, the hyperbolic function moves towards infinity for modified stress ratios close or equal to m. Hence, m the slope ratio of the yield line is a stress boundary. The equation used to fit the data is shown in Equation 7.1:

$$\varepsilon_p^r = \frac{\dfrac{q}{(p-p^*)}}{b\left(m - \dfrac{q}{(p-p^*)}\right)} \qquad \text{Equation 7.1}$$

where,

ε_p^r = Permanent strain rate after 25,000 load cycles (secant);

q = principal stress difference (Equation 2.7) and in this equation is the maximum value;

p = mean principal stress (Equation 2.4) and in this equation is the maximum value;

p^* = the value where the yield line intercepts the p-axis in p-q stress space (Figure 7.1);

m = slope ratio of the yield line in p-q stress space ($\tan\beta$, Figure 7.1);

b = regression parameter.

7.3.5 Fitting 1 Parameter Model to Permanent Strain Data

The model proposed to predict permanent strain rate (Equation 7.1) was fitted to the RLT test results for the 6 granular and 1 subgrade material (Table 3.1). This model relies on the slope ratio, m and intercept with the x-axis p^* parameters calculated from the yield line (Figure 7.1). Results from monotonic shear failure tests are affected by sample preparation and in particular compaction. Several test results were discarded as they fell well outside the failure criteria defined by the other two other tests. These outliers were also found to have compacted density outside the target density. Some tests were repeated with extra care to achieve the correct target densities and, thus the yield lines as shown in Figure 3.11 were derived. Therefore, it is expected that there is some error with the yield line parameters m and p^*. It was found that for the *NI Good*, *NI Poor*, *CAPTIF 3* and *4* granular materials (Table 3.1) using the boundary between shakedown Range B and C as the yield line for determining m and p^* parameters was best. The main reason was because the boundary for shakedown Range B and C fell outside the yield line for these aggregates. This suggests that the yield line is incorrect as it would be expected that under repeated loading the yield line would be less than that determined from monotonic shear failure tests. For high rates of repeated loading, stress states in excess of yield were possible (Theyse, 2002).

Figure 7.2 shows the results of fitting Equation 7.1 utilising the m and p^* parameters from the most appropriate of either the shakedown Range B/C boundary or the shear failure yield lines. There were usually 2 to 4 significant outliers and ignoring these gave a range of mean errors between measured and calculated (Table 7.1). For high modified stress ratios the fit to the data appears poor. Further, there were outliers that fell outside the yield line which suggests that the stress boundary could be extended.

Table 7.1. Parameters used for proposed model with yield line parameters that best fit the data excluding 2 to 4 outliers.

	Yield Line			Const.	Mean Error – excl. outliers		Mean Error – outliers	
Material (Table 3.1)	**Type**	**m**	**p*(MPa)**	**b**	**No.**	**ε_{pRate} (%/1M)**	**No.**	**ε_{pRate} (%/1M)**
NI Good	B/C	2.11	-0.028	3.8	16	1.6	4	3,351
NI Poor	B/C	1.90	-0.026	5.3	17	6.3	4	110
CAPTIF 1	Shear	2.08	-0.030	1.4	13	0.6	3	558
CAPTIF 2	Shear	2.48	0.007	0.74	12	2.7	3	162
CAPTIF 3	B/C	2.12	-0.016	10.8	15	0.3	4	277
CAPTIF 4	B/C	2.57	0.026	4.5	12	1.6	4	8,178
CAPTIF Subgrade	B/C	2.05	0.019	1.7	19	2.7	3	125

A majority of the data points fitted well to the permanent strain rate data. However, there were some significant outliers. In particular, the outlier of concern was for the test with the highest mean principal stress (i.e. p=0.250 MPa) and maximum vertical stress for each aggregate. This test had the highest permanent strain rate but the modified stress ratio ($q/(p+p^*)$) did not suggest that this should be the case. Therefore, the proposed model was refitted to the data points but this time allowing the yield line slope ratio, m, to change while the intercept, p^* was set to -0.10 MPa. Setting p^* to a higher negative value did ensure that the highest modified stress ratio ($q/(p-p^*)$) ranked the test with the highest mean principal stress and maximum vertical stress case as the highest strain rate. This resulted in an improved fit to the data as shown in Table 7.2. Generally there was one less outlier and the mean error was halved. Figure 7.3 plots the permanent strain rate data with the calculated values based on setting $p^* = -0.10$ *MPa*.

Table 7.2. Parameters found for proposed model (excluding 2 or 3 outliers) with *p=-0.10MPa and allowing *m* to change.**

	Best fit, m (p* fixed)		Const.	Mean Error – excl. outliers		Mean Error – outliers	
Material (Table 3.1)	**m**	**p*(MPa)**	**b**	**No.**	**ε_{pRate} (%/1M)**	**No.**	**ε_{pRate} (%/1M)**
NI Good	1.80	-0.1	2.352	17	0.4	3	5,087
NI Poor	1.53	-0.1	1.8	18	2.6	3	149
CAPTIF 1	1.50	-0.1	2.771	13	0.3	3	565
CAPTIF 2	1.80	-0.1	0.379	12	1.2	3	117
CAPTIF 3	1.75	-0.1	4.722	17	0.2	2	362
CAPTIF 4	1.78	-0.1	2.796	14	0.8	2	851
CAPTIF Subgrade	1.50	-0.1	1.571	20	0.9	2	146

7.3.6 Initial Permanent Strain

It appears that the model used to predict permanent strain rate by setting *p** to a value of -0.10 MPa is appropriate. However, the initial permanent strain that occurs in the first 25,000 load cycles is not considered. This initial permanent strain can be often a quarter the total permanent strain over the life of the pavement. Because this initial permanent strain occurs over such few load cycles it will be modelled as a single value of permanent strain at 25,000 load cycles. This single value can then be added to the permanent strain rate predicted for load cycles beyond 25,000.

The same form of the function used to predict permanent strain rate (Equation 7.1) was used to predict the permanent strain at 25,000 load cycles. Yield line slope ratio (*m*) parameter was the same as that found to predict permanent strain rate, where *p** was set equal to -0.10 MPa (Table 7.2). The equation to predict permanent strain after 25,000 load cycles thus becomes:

$$\varepsilon_{p(N=25k)} = \frac{\dfrac{q}{\left(p - p^*_{Rate}\right)}}{B\left(m_{Rate} - \dfrac{q}{\left(p - p^*_{Rate}\right)}\right)} \qquad \text{Equation 7.2}$$

where,

$\varepsilon_{p(N=25k)}$ = permanent strain after 25,000 load cycles;

q = principal stress difference and in this equation is the maximum value;

p = mean principal stress and in this equation is the maximum value;

p^*_{Rate} = the value of p^* used to predict permanent strain rate (i.e. p^* = -0.10 MPa);

m_{Rate} = slope ratio found to predict the permanent strain rate; and

B = regression parameter found as best fit the measured permanent strain data at 25,000 load cycles.

The regression parameter B was found by the best fit of Equation 7.2 to the measured permanent strain values after 25,000 load cycles. This resulted in a good fit to the data provided 2 or 3 outliers were excluded. Finally, the ratio of calculated permanent strain at 25,000 load cycles to permanent strain rate (tangentially from 25,000 to 50,000 loads) per 1 million load cycles was computed. It was found that this ratio was constant for all data points. Results of this analysis are summarised in Table 7.3 and plotted in Figure 7.4.

Table 7.3. Parameters used for proposed model to predict permanent strain at 25,000 load cycles with *p=-0.10MPa and *m* the same used to predict permanent strain rate (Table 7.2).**

	Strain rate parameters (Table 7.2)		Const (Eq. 7.2)	Mean Error – excl. outliers		Mean Error – outliers		Ratio of Calc. $\varepsilon_{pN=25,000}$ to $\varepsilon_{pRate}\times$(1M) *K*
Material (Table 3.1)	**m**	**p*(MPa)**	**B**	**No.**	ε_p **(%)**	**No.**	ε_p **(%)**	
NI Good	1.803	-0.1	13.06	17	0.08	3	351	0.32
NI Poor	1.530	-0.1	15.18	18	0.24	3	9	0.12
CAPTIF 1	1.504	-0.1	10.95	14	0.09	2	14	0.25
CAPTIF 2	1.803	-0.1	2.15	12	0.16	3	5	0.18
CAPTIF 3	1.748	-0.1	10.08	17	0.13	2	92	0.47
CAPTIF 4	1.778	-0.1	15.55	14	0.21	2	36	0.18
CAPTIF Subgrade	1.495	-0.1	6.18	17	0.11	3	8	0.25

7.3.7 Combined Model

It is convenient that the same parameters and model type could be used to predict both permanent strain rate from 25,000 to 50,000 load cycles and permanent strain after 25,000 load cycles. Also the ratio of calculated permanent strain at 25,000 load cycles and calculated permanent strain rate was constant for all points. This has allowed the combination of Equations 7.1 and 7.2 to predict the magnitude of permanent strain for any given stress level and number of load cycles greater than 25,000. The proposed function to predict permanent strain is thus:

$$\varepsilon_{p(N)} = \left(K + \frac{(N - 25{,}000)}{1{,}000{,}000}\right) \frac{\dfrac{q}{(p - p^*)}}{b\left(m - \dfrac{q}{(p - p^*)}\right)} \qquad \text{Equation 7.3}$$

where,

$\varepsilon_{p(N)}$ = cumulative permanent strain after N load cycles where N is greater than 25,000;

N = number of load cycles and not less than 25,000;

K = ratio of calculated cumulative strain to calculated permanent strain rate per 1 million load cycles (Table 7.3);

p^* = a constant and is recommended equal to -0.10 MPa;

m = regression constant and found as best fit to permanent strain rate data (Table 7.2);

q = principal stress difference and in this equation is the maximum value;

p = mean principal stress and in this equation is the maximum value;

b = regression constant and found as best fit to permanent strain rate data (Table 7.2).

7.3.8 Discussion

The *1 parameter model* developed (Equation 7.3) is linear and therefore suited only to cases where permanent strain is expected to be a shakedown Range B response as defined in Section 2.11.2. For low stress levels the model will calculate a low value of permanent strain and therefore it may suffice for expected Range A responses also.

There are some limitations of the model proposed as there were a few RLT tests that resulted in high permanent strains but the model predicted permanent strains up to 100 times less as seen in Figure 7.3 for the CAPTIF 1, 2, 3 and 4 materials. These RLT results that fell well outside the predictions are real test results and should not be considered merely as outliers but a result showing stress conditions where a significant amount of deformation can occur. It is therefore possible that Equation 7.3 could predict a low value of permanent strain at stress conditions that would cause significant amount of deformation within the pavement.

It may be considered an advantage of the model proposed (Equation 7.3) to predict the brittle behaviour observed to occur in RLT permanent strain tests where most of stress conditions tested permanent strain is low until such time as a stress limit is exceeded (shakedown range boundary B/C) where failure occurs. However, this brittleness of the prediction of permanent strain will cause some difficulties in application to predicting deformation with a pavement as modified stress ratios in excess of the limits posed by m in Equation 7.3 will result in a negative value for permanent strain.

7.4 2 PARAMETER MODEL

7.4.1 Introduction

As discussed the *1 parameter model* failed to compute an adequate permanent strain for some test stresses. Another limitation revealed by preliminary stress analysis of the New Zealand accelerated pavement tests using the finite element model DEFPAV (Snaith et al, 1980) did reveal modified stress ratios in excess of the limits posed by m in Equation 7.3, with the result a negative value of permanent strain being computed. Further, for modified stress ratios equal to m (Equation 7.3) a value cannot be computed as the result is infinite. The New Zealand accelerated pavement tests did not fail as the predictions would suggest. Therefore, a fresh approach was taken to this problem by developing a *2 parameter model* and was later utilised successfully in pavement stress analysis to predict surface rutting.

7.4.2 2 Parameter Model Development

Results from Repeated Load Triaxial tests showed a high dependence on stress level. The multi-stage RLT permanent strain tests were conducted by keeping the mean principal stress p constant while increasing deviatoric stress q for each new stage of the multi-stage test. Plots of maximum deviator stress, q versus permanent strain rate for each multi-stage test with mean principal stress, p constant does result in exponential relationships that fit well to the measured data

(Figure 7.5). This prompted an investigation of an exponential model that could determine the secant permanent strain rate from two values of maximum stress being *q* (deviatoric stress) and *p* (mean principal stress).

Regression analysis was undertaken on the CAPTIF 3 RLT test data with stress invariants *p* and *q* against the associated natural logarithm of the strain rate. The result was the first part (on the left of the subtraction sign) of Equation 7.4, while the part of Equation 7.4 being subtracted (i.e. on the right of the subtraction sign) was added on to ensure when deviatoric stress, *q* is zero the resulting permanent strain rate is also zero. Permanent strain rate is thus defined by Equation 7.4:

$$\begin{aligned} \varepsilon_{p(\text{rate or magn})} &= e^{(a)}\, e^{(bp)}\, e^{(cq)} - e^{(a)}\, e^{(bp)} \\ &= e^{(a)}\, e^{(bp)}\, (e^{(cq)} - 1) \end{aligned} \qquad \text{Equation 7.4}$$

where,

e = 2.718282

$\varepsilon_{p(\text{rate or magn})}$ = secant permanent strain rate or can be just permanent strain magnitude;

a, b & c = constants obtained by regression analysis fitted to the measured RLT data;

p = mean principal stress (MPa) (Equation 2.2); and

q = mean principal stress difference (MPa) (Equation 2.7).

For the purists it is recognised the units for Equation 7.4 are not balanced on either side. Therefore, stress invariants *p* and *q* in Equation 7.4 can be substituted by p/p_0 and q/q_0 respectively, where p_0 and q_0 are reference stresses. In the following analysis it can be assumed the reference stresses were taken as equal to 1MPa.

To determine the total permanent strain for any given number of load cycles and stress condition it is proposed that three values of permanent strain are added together (Equation 7.5). It was observed in the New Zealand Accelerated Pavement Tests (Chapter 4) that the permanent strain rates changed during the life of the pavements, different values being associated with the early, mid, late and long term periods of trafficking. Similarly RLT permanent strain tests showed changing permanent strain rates during their loading. After studying RLT and accelerated pavement test results and to limit the number of times Equation 7.4 is used to fit the RLT data, it was decided to break the RLT permanent strain data into four zones of different behaviour for use in calculating permanent strain at any given number of loads (*N*):

(i) Early behaviour (compaction important) – 0 – 25,000 loads.

The magnitude of permanent strain at 25,000 loads, being the incremental amount (ε_p(25k) incremental, Figure 7.6), is used because the cumulative amount in multi-stage tests over-estimates the permanent strain. Further, the magnitude of permanent strain is prone to errors due to factors such as sample preparation, compaction etc and thus keeping the magnitude of permanent strain separate at 25,000 was useful when predicting rut depth (Section 7.5.3) in terms of identifying where the errors occurred.

(ii) Mid term behaviour – 25k – 100k loads. The secant permanent strain rate between 25k and 100k loads is used.

(iii) Late behaviour - 100k – 1M loads. The secant permanent strain rate between 100k and 1M loads is used.

(iv) Long term behaviour - > 1M loads. The secant permanent strain rate between 1M and 2M loads is used as the permanent strain rate for all loads greater than 1M.

This assumes that the permanent strain rate remains constant after 1M loads and in effect decides on shakedown Range B behaviour. The approach is appropriate as the aim is to calculate rut depth for pavements with thin surfacings where Range B behaviour is predicted where the rate of rutting is linear. Further, assuming the permanent strain rate does not decrease after 1M loads is a conservative estimate compared with the assumption of permanent strain rate continually decreasing with increasing load cycles (ie. shakedown Range A behaviour).

Hence, four versions (four sets of constants) of Equation 7.4 are determined and used for describing the permanent strain behaviour at any given number of loadings as defined by Equations 7.5 to 7.12:

$$\varepsilon_{pN} = \varepsilon_{p25k} + \varepsilon_{p25k\_100k} + \varepsilon_{p100k\_1M} + \varepsilon_{p1M\_N} \qquad \text{Equation 7.5}$$

$$\varepsilon_{p25k} = e^{(a\,(25k))}\, e^{(b\,(25k)\,p)}\, (e^{(c\,(25k)\,q)} - 1) \qquad \text{Eqn 7.6}$$

$$\varepsilon_{p25k\_100k} = \varepsilon_{p25k\_100k(rate)} \times (100k\text{-}25k) \qquad \text{Eqn 7.7}$$

$$\varepsilon_{p25k\_100k(rate)} = (e^{(a\,(25k\_100k))}\, e^{(b\,(25k\_100k)\,p)}\, (e^{(c\,(25k\_100k)\,q)} - 1)) \qquad \text{Eqn 7.8}$$

$$\varepsilon_{p100k\_1M} = \varepsilon_{p100k\_1M(rate)} \times (1M\text{-}100k) \qquad \text{Eqn 7.9}$$

$$\varepsilon_{p100k\_1M(rate)} = (e^{(a\,(100k\_1M))}\, e^{(b\,(100k\_1M)\,p)}\, (e^{(c\,(100k\_1M)\,q)} - 1)) \qquad \text{Eqn 7.10}$$

$$\varepsilon_{p1M\_N} = \varepsilon_{p1M\_2M\,(rate)} \times (N\text{-}1M) \qquad \text{Eqn 7.11}$$

$$\varepsilon_{p1M\_2M\,(rate)} = (e^{(a\,(1M\_2M))}\, e^{(b\,(1M\_2M)\,p)}\, (e^{(c\,(1M\_2M)\,q)} - 1) \qquad \text{Eqn 7.12}$$

where,

ε_{pN} = total permanent strain for N wheel passes that are greater than 1 million (1M);

ε_{p25k} = permanent strain that occurs in the first 25,000 wheel loads ($\varepsilon_{p(25k)}$);

ε_{p25k_100k} = incremental permanent strain from 25,000 to 100,000 wheel loads;

ε_{p100k_1M} = incremental permanent strain that occurs from 100,000 to 1M wheel loads;

ε_{p1M_N} = incremental permanent strain that occurs from 1M to N wheel loads (N > 1M);

N = number of wheel loads;

$\varepsilon_{p25k\text{-}100k(rate)}$ = secant permanent strain rate from 25,000 to 100,000 loads;

$\varepsilon_{100k\text{-}1M(rate)}$ = secant permanent strain rate from 100,000 to 1M loads;

$\varepsilon_{1M\text{-}2M(rate)}$ = secant permanent strain rate from 1M to 2M loads, where it is assumed the permanent strain rate remains constant for all loads (N) >1M;

a (25k), b (25k), c (25k) = constants found by fitting 2 parameter model (Eqn. 7.6) to Repeated Load Triaxial (RLT) permanent strain magnitude at 25,000 loads ($\varepsilon_{p(25k)}$incremental, Figure 7.6);

a (25k_100k), b (25k_100k), c (25k_100k) = constants found by fitting 2 parameter model (Eqn. 7.8) to extrapolated RLT secant permanent strain rates calculated from 25,000 to 100,000 loads;

a (100k_1M), b (100k_1M), c (100k_1M) = constants found by fitting 2 parameter model (Eqn. 7.10) to extrapolated RLT secant permanent strain rates calculated from 100k to 1M loads;

a (1M_2M), b (1M_2M), c (1M_2M) = constants found by fitting 2 parameter model (Eqn. 7.12) to extrapolated RLT secant permanent strain rates calculated from 1M to 2M;

Equation 7.5 will result in a linear progression of rut depth with increasing load cycles for loadings greater than 1M. Thus the *2 parameter model* is suited to pavements where it is expected that Range B type behaviour (Section 2.11.2) will occur. As the permanent strain rates are derived from RLT test data for low testing stresses that resulted in a Range A behaviour very low permanent strain rates will be calculated. This in turn will result in a low rut depth and approximating a Range A behaviour of the pavement. It is currently assumed that the strain rate from 1M to 2M wheel passes will be valid for all loads in excess of 1M wheel passes. This is considered appropriate as the number of wheel passes in the pavement tests in New Zealand (Chapter 4) and Northern Ireland (Chapter 5) where rut depth will be predicted for comparison were all less than 1.7 million.

7.5 Predicting Pavement Rut Depth

7.5.1 Introductions

To predict the surface rut depth of a granular pavement from the *2 parameter model* (Equation 7.5) requires a series of steps. There are assumptions required in each step which significantly affects the magnitude of calculated rut depth. Steps and associated errors and assumptions are summarised below. The first five steps relate to the interpretation of RLT permanent strain tests as detailed in Figure 7.7, while the final three steps involve pavement stress analysis, calculations and validation required to predict surface rut depth of a pavement (Figure 7.8).

1. Repeated Load Triaxial Permanent Strain Tests

Many Repeated Load Triaxial permanent strain tests are undertaken at a range of testing stresses with the aim to cover the full spectra of stresses that are expected to occur in-service. However, as discussed in the literature review, the Repeated Load Triaxial apparatus only approximates actual stresses that occur in-service from passing wheel loads. For example, principal stress rotation (Section 2.6.3) and cyclic confining pressure/stresses are not replicated in the RLT tests. Thus errors are expected with the RLT tests, although their magnitude is unknown. As the effect of principal stress rotation and cyclic confining stresses increase the severity of the loading, it is expected that the RLT tests will under-estimate the magnitude of permanent strain.

2. Extrapolation of RLT Permanent Strain Test Data

The RLT permanent strain tests were undertaken for 50,000 loads due to time constraints with the necessity to undertake many tests at different stress levels. However, from a pavement design perspective 50,000 is probably less that 1% of the design loading. Therefore, all the RLT tests required extrapolation. The model fitted to the RLT data for the purpose of extrapolation has a significant effect on the magnitude of permanent strain and resulting rut depth predicted. As discussed in terms of shakedown range behaviours (Section 2.11.2) there are three possible trends in permanent strain with increasing load cycles (i.e. Range A, B or C). Range A behaviour advocates the permanent strain decreases with increasing load cycles and a power model of the form $\varepsilon_p = aN^b$ was used to replicate this behaviour for extrapolation. A linear extrapolation model replicates Range B behaviour, while Range C where failure occurs was not considered as RLT tests that lasted for 50,000 were expected to not suddenly fail.

The first method of extrapolation trialled was linear as it was considered to be a conservative approach. Further, the need to predict rut depth was for pavements where Range B behaviour is expected. However, assuming a linear projection of RLT data after 50,000 cycles based on the permanent strain rate from 25,000 to 50,000 cycles resulted in initial rut depths of the New Zealand pavement tests calculated in excess of 100mm, while the measured values were around 10mm. Thus, it was concluded that the linear extrapolation method after 50,000 was inappropriate. Therefore, the power model of the form $\varepsilon_p = aN^b$ was used for extrapolation.

The choice of extrapolation method has the most influence on the calculated rut depth and the model chosen for extrapolation requires knowledge of typical actual pavement behaviour.

3. Estimating the magnitude of permanent strain at 25,000 loads for multi-stage RLT permanent strain tests

Multi-stage RLT tests are advantageous in terms of the ability to reduce the number of RLT specimens required to cover the full spectra of loading stresses expected in-service. Although the secant permanent strain rates can be determined with confidence for each testing stress stage, the actual magnitude of permanent strain at 25,000 loads is difficult to determine. From the multi-stage RLT permanent strain test results, two values of permanent strain at 25,000 cycles are obvious. These two values are either the cumulative or incremental permanent strain at 25,000 cycles ($\varepsilon_{p(25k)}$cumulative or $\varepsilon_{p(25k)}$incremental, Figure 7.6). The cumulative permanent strain magnitude depends on the number of tests before it and thus considered not to be the true value. Therefore, the incremental value was used to estimate the permanent strain at 25,000 cycles. However, as the prior tests will result in further compaction of the specimen, it is expected the incremental permanent strain at 25,000 cycles to under-estimate the true value obtained where only one sample per testing stress is used.

4. Dividing the extrapolated RLT permanent strain rates into 4 different zones.

To limit the number of models needed, the extrapolated RLT data was divided into four zones. These zones are early, mid, late and long term as described in Section 7.4.2. The choice of zones will affect the calculated permanent strains between the zones as straight lines are used to join the zones rather than a curve/power law model. However, these series of straight lines for each zone all link up on actual points on the extrapolated RLT permanent strain data and therefore the errors are minimised especially for predicting deformations for loads in excess of 1M passes as the RLT curve is close to a straight line as assumed for the long term behaviour zone.

5. Fitting the four RLT permanent strain zones to the 2 parameter model to determine constants (a, b and c).

The 2 parameter model idealises the permanent strain rate in terms of stress defined by mean principal stress (*p*) and deviatoric stress (*q*). This model does not fit all the RLT data points and thus errors will result. However, most of the error relates to low permanent strain rate points, where its effect in final rut depth calculated is small. Section 7.5.2 details the accuracy of the 2 parameter model in fitting the permanent strain rates for the extrapolated RLT data.

6. Pavement stress analysis.

Steps 1 to 5 result in a model where for any number of loads and stress condition the permanent strain can be calculated. Stress is therefore computed within the pavement under a wheel load for use in the *2 parameter model* to calculate permanent strain. It is recognised from the literature (Section 2.7) and RLT tests the stiffness of granular and subgrade materials are highly non-linear. A non-linear finite element model, DEFPAV (Snaith et al., 1980) was used to compute stresses within the pavement. DEFPAV only approximated the non-linear characteristics of the granular and subgrade materials. Further, the horizontal residual confining stresses considered to occur during compaction of the pavement layers as discussed in Section 2.4.6 were assumed to be nil in the first analysis as the actual value is unknown, although its influence is significant on the calculated permanent strain. Therefore, during validation with actual pavement tests the horizontal residual stress is one value that was altered to improve rut depth predictions.

From the pavement stress analysis, the mean principal stress (p) and deviatoric stress (q) under the centre of the load are calculated for input into a spreadsheet along with depth for the calculation of rut depth. The calculated stresses have a direct influence on the magnitude of permanent strain calculated and resulting rut depth. Thus any errors in the calculation of stress will result in errors in the prediction of rut depth. Some errors in the calculation of stress from DEFPAV are a result of not considering the tensile stress limits of granular materials and the assumption of a single circular load of uniform stress approximating dual tyres that do not have a uniform contact stress (de Beer et al, 2002).

7. Surface rut depth calculation.

The relationships derived from the RLT permanent strain tests in steps 1 to 5 (Figure 7.7) are applied to the computed stresses in the FE analysis. Permanent strain calculated at each point under the centre of the load is multiplied by the associated depth increment and summed to obtain the surface rut depth.

8. Validation.

The calculated surface rut depth with number of wheel loads is compared with actual rut depth measurements from accelerated pavement tests in New Zealand (Chapter 4) and the Northern Ireland field trial (Chapter 5). This comparison determines the amount of rut depth adjustment required at 25,000 cycles while the long term slope of rut depth progression and, in part, the initial rut depth at 25,000 cycles is governed by the magnitude of horizontal stress added. An iterative process is required to determine the initial rut depth adjustment and the amount of horizontal residual stress to add, in order that the calculated surface rut depth matches the measured values.

7.5.2 Parameters from RLT Data (Permanent Strain)

Test data from multi-stage RLT permanent strain tests at each stress level were limited to 50,000 loading cycles (Chapter 3). The model (Equation 7.4) requires strain rates up to 1 million load cycles. To determine the secant permanent strain rate from 25,000 to 100,000 cycles (mid term), 100,000 to 1M cycles (late term), and 1M to 2M cycles (long term) the RLT cumulative permanent strain values were extrapolated to 2 million load cycles. The extrapolation method used a power model ($y = ax^b$) fitted to the measured RLT data and for some of the higher testing stresses a linear model as these models provided the best fit to the measured data. As discussed in Section 7.5.1 (Step 2) the chosen model for extrapolation has the most significant effect on computed rut depth and thus results from pavement tests and/or experience are required to determine the most appropriate model to use. It should be noted that dividing the RLT permanent strain data into four zones (Section 7.4.2) was to minimise the computational effort as for each zone new constants for the model (Equation 7.4) are required.

The first step is to individualise and extrapolate the permanent strain data for each stress level tested. Figure 7.9 shows the permanent strain results for the CAPTIF 1 material (Table 3.1) for the multi-stage test where mean principal stress, p=75kPa. After each new stress level is applied the loading count returns to zero and plots shown in Figure 7.10 are produced. These plots also show the best fit power curve used to extrapolate the data up to 2 million load cycles. For the final/highest testing stress and occasionally the one prior a linear fit was used for extrapolation where it resulted in a better fit to the data. After the data were individualised for all the three RLT multi-stage tests of p=75, 150 and 250 kPa, the deformation at 25,000; 100,000; 1M and 2M load cycles was determined. From these deformations the average permanent strain rates were calculated from 25,000 to 100,000, 100,000 to 1M and 1M to 2M cycles. Table 7.4 shows typical results with maximum testing stresses and associated permanent strain rates that were obtained for the *CAPTIF 3* material. This same process was applied to all the RLT permanent strain results for the five CAPTIF materials tested as listed in Table 3.1. Permanent strain rates for the *NI Good* and *NI Poor* materials were calculated for each stage of the multi-stage RLT permanent strain tests from 25,000 to 50,000, 50,000 to 100,000 and 100,000 to 1M load cycles as the pavement test sections had only 114k wheel passes. Parameters for Equations 7.5 to 7.12 are listed in Table 7.5.

Table 7.4. Permanent strain rates determined for the CAPTIF 3 material.

			Permanent strain rate	
CAPTIF 3			**25,000 to 100,000 cycles**	**100,000 to 1M cycles**
TEST (Appendix A)	***p* (MPa)**	***q* (MPa)**	**%per1M**	**%per1M**
1A	0.075	0.037	0.022	0.006
1B	0.075	0.135	0.170	0.030
1C	0.075	0.181	0.246	0.047
1D	0.075	0.204	0.378	0.445
2A	0.150	0.135	0.062	0.010
2B	0.150	0.274	0.295	0.085
2C	0.150	0.318	14.126	14.612
3A	0.250	0.375	0.191	0.073
3B	0.250	0.420	0.299	0.087
3C	0.250	0.469	0.673	0.299
3D	0.250	0.517	1.203	0.539
3E	0.250	0.562	3.465	1.806

Parameters for Equations 7.8, 7.10 and 7.12 were determined with the aid of SOLVER function in Microsoft Excel where the difference between measured and calculated was minimised. Excluded from the fit were the tests that failed prior to 50,000 load cycles, which was the last/highest stress level in each multi-stage test. Results where failure occurs do not follow the same trend as the other results due to significantly larger deformations and shear failure that occurs and this is a different mechanism of accumulation of permanent strain to the other test results. Constants for the *CAPTIF Subgrade* test results were obtained by excluding all the test results where the mean principal stress values were 0.250 MPa to improve the fit to the model. Excluding these test results with a mean principal stress of 0.250 MPa for the subgrade can be justified as pavement analysis shows at the subgrade soil level the mean principal stress is less than 0.150 MPa.

Model parameters for Equation 7.4 and the mean errors are listed in Table 7.5. Comparison between measured permanent strain rates and those calculated with Equations 7.4 with the constants listed in Table 7.5 are plotted in Figure 7.11, Figure 7.12, and Figure 7.13. Visually the model fits the data well, where the correct trend is shown being an increasing permanent strain rate with increasing deviatoric stress (q). Mean errors were generally less than 1%/1M which, when applied to rut prediction, give an equivalent error of 1mm per 100mm thickness for every 1 million wheel passes.

Table 7.5. Model parameters for calculation of permanent strain rate from Equation 7.4.

		Model Parameters (Equation 7.4) $\varepsilon_{rate} = e^{(a)}\, e^{(bp)}\, e^{(cq)} - e^{(a)}\, e^{(bp)}$			Mean error
Material	ε_{rate}	**a**	**b**	**c**	ε_{rate} (%/1M)
NI Good	$\varepsilon_{rate(25k\text{-}50k)}$	-0.772	-21.409	14.485	0.21
	$\varepsilon_{rate(50k\text{-}100k)}$	-1.085	-23.331	15.277	0.20
	$\varepsilon_{rate(100k\text{-}1M)}$	-4.142	-3.192	9.807	0.14
NI Poor	$\varepsilon_{rate(25k\text{-}50k)}$	-3.359	-51.175	38.679	0.21
	$\varepsilon_{rate(50k\text{-}100k)}$	-2.484	-51.971	37.363	0.58
	$\varepsilon_{rate(100k\text{-}1M)}$	-1.867	-63.175	19.965	0.39
CAPTIF 1	$\varepsilon_{rate(25k\text{-}100k)}$	-1.548	-18.937	14.993	0.22
	$\varepsilon_{rate(100k\text{-}1M)}$	-3.100	-13.578	12.203	0.10
CAPTIF 2	$\varepsilon_{rate(25k\text{-}100k)}$	-0.345	-9.732	10.548	0.77
	$\varepsilon_{rate(100k\text{-}1M)}$	-5.372	-12.507	20.768	0.47
CAPTIF 3	$\varepsilon_{rate(25k\text{-}100k)}$	-2.460	-19.956	15.197	0.13
	$\varepsilon_{rate(100k\text{-}1M)}$	-7.141	-12.761	19.283	0.09
CAPTIF 4	$\varepsilon_{rate(25k\text{-}100k)}$	-28.868	-27.061	70.421	0.03
	$\varepsilon_{rate(100k\text{-}1M)}$	-26.047	-17.251	60.272	0.03
CAPTIF Subgrade	$\varepsilon_{rate(25k\text{-}100k)}$	2.260	-22.602	9.036	0.04
	$\varepsilon_{rate(100k\text{-}1M)}$	0.842	-17.372	9.783	0.09

The rutting in the first 25,000 cycles was derived from the incremental permanent strain for each new stage of a multi-stage RLT permanent strain test ($\varepsilon_{p(25k)incremental}$, Figure 7.6). This incremental amount is expected to under-estimate the amount of rutting in the first 25,000 cycles as the sample has already received some additional compaction from the previous tests in the multi-stage tests. Another approach considered was to use the cumulative permanent strain at 25,000 cycles which included the permanent strain that has occurred in the previous stages of a multi-stage test ($\varepsilon_{p(25k)incremental}$, Figure 7.6). However, preliminary analysis to predict rutting using the cumulative permanent strain resulted in rut depths of the order of 100mm and therefore this approach was discounted. Parameters for Equation 7.4 to calculate the amount of permanent strain in the first 25,000 load cycles are listed in Table 7.6 and plotted against measured RLT values in Figure 7.14. These parameters were determined from incremental permanent strains at 25,000 determined from the multi-stage RLT permanent strain tests.

Table 7.6. Model parameters for calculation of permanent strain for the first 25,000 load cycles from Equation 7.4.

	Model Parameters (Equation 7.4) $\varepsilon_{p(25,000)} = e^{(a)} e^{(bp)} e^{(cq)} - e^{(a)} e^{(bp)}$			**Mean error**
Material (Table 3.1)	**a**	**b**	**c**	ε_p **(%)**
NI Good	-3.474	-25.732	16.745	0.04
NI Poor	-4.290	-73.977	48.286	0.03
CAPTIF 1	-4.369	-13.052	14.410	0.03
CAPTIF 2	-0.616	-14.472	8.026	0.08
CAPTIF 3	-8.763	-13.166	18.360	0.04
CAPTIF 4	5.262	-166.979	60.888	0.07
CAPTIF Subgrade	0.401	-20.243	4.479	0.01

The fit of Equation 7.4 appears adequate to the permanent strain values after 25,000 load cycles with the mean error < 0.10%. Therefore, this would suggest that the model could be used to predict the magnitude of permanent strains rather than the rate. However, permanent strain rate was modelled as it is expected because of multi-stage RLT permanent strain tests the true magnitude of permanent strain is not known. Therefore, this error in magnitude was singled out for the permanent strain after 25,000 load cycles and permanent strain rates are used to predict the permanent strain for other load cycles.

7.5.3 Pavement Analysis

The *2 Parameter Model* provided a good fit to the Repeated Load Triaxial data as shown in Section 7.5.2. However, this model is of little use unless it can be utilised in pavement analysis to predict the surface rut depth attributable to the granular and subgrade materials. Therefore, the *2 Parameter Model* was used to predict the surface rut depth of the pavement tests reported in Chapters 4 and 5. Key inputs for the model are stress invariants p and q and thus DEFPAV (Snaith et al., 1980) a finite element program was used to calculate these stresses under a wheel load. A permanent strain value is calculated from the *2 Parameter Model* at each depth increment where the stress level has been computed. Rut depth is the permanent strain integrated over the pavement depth and summed. Predicted rut depth was compared to the measured rut depth in the pavement trials and reasons for possible differences are discussed.

The finite element package DEFPAV (Snaith et al., 1980) was chosen for pavement analysis due to its simplicity and the ability to model the non-linear resilient properties of granular and subgrade soils. DEFPAV assumes an axisymmetric finite element model (Section 2.10.2). Non-linear resilient properties are input in tabular form of resilient modulus versus stress level defined as either: major principal stress (σ_1); mean stress (p); deviatoric stress (q); or minor principal stress (σ_3). The choice of the stress level used to define the resilient modulus depends on the fit to the triaxial data. Plots of resilient modulus versus the different stress levels found that the fit was better with mean stress.

Tabular data to define the resilient modulus with respect to mean stress were found from the RLT tests results. Resilient properties of the materials have been already deduced in terms of the k-θ model (Equation 2.27, Hicks 1970) with parameters listed in Table 3.5. This model uses bulk stress, being the sum of the principal stresses or three times the mean stress as required by DEFPAV. Resilient moduli were calculated from the k-θ model and parameters from Table 3.5 for a range of bulk stresses/mean stresses for input into DEFPAV as listed in Table 7.7.

Table 7.7. Resilient properties for input into DEFPAV finite element model.

Mean Stress (kPa)	Resilient Moduli (MPa)						
	NI Good	NI Poor	CAPTIF 1	CAPTIF 2	CAPTIF 3	CAPTIF 4	CAPTIF Subgrade
25	**247**	**283**	**190**	**89**	**408**	**59**	**91**
50	**302**	**333**	**256**	**151**	**423**	**113**	**128**
100	**368**	**391**	**345**	**257**	**439**	**218**	**181**
150	**414**	**430**	**411**	**351**	**448**	**319**	**221**
250	**479**	**485**	**511**	**520**	**461**	**517**	**284**

Ten New Zealand accelerated pavement tests (NZ APTs) (ID: 1, 1a, 1b, 2, 2a, 2b, 3, 3a, 3b, 4: Table 4.1) and two Northern Ireland pavement tests were modelled in DEFPAV (cross-sections 5 & 6: Table 6.1). Two wheel loads were modelled in DEFPAV for the NZ APTs (except number 4, Table 4.1) being a 40kN and either 50 or 60kN as detailed in Table 4.2. For the number 4 pavement test (Table 4.1) a 50kN wheel load was modelled being the same as the wheel load used in the test. For the Northern Ireland pavement tests a standard 40kN half axle load was used for both cross-sections. Tyre contact stress was assumed equal to 750 kPa. Properties for the asphalt layer were assumed as linear elastic with a resilient modulus of 3000 MPa and a Poisson's ratio of 0.35, which are considered typical values (Austroads, 1992). Poisson's ratios for the granular and subgrade materials were assumed as 0.35 and 0.45 respectively as recommended in the Austroads pavement design guide (Austroads, 1992).

Principal stresses were computed using DEFPAV for the full range of pavements and loads reported in Chapters 4 and 5 and the 21 analyses are identified by the matrix of loading and cross-section identifications in Table 7.8. The principal stresses under the centre of the load at depth increments of 25mm were imported into a text file and used in a spreadsheet to compute the mean principal stress, p (Equation 2.4) and principal stress difference q (Equation 2.7) as these were needed to compute permanent strain rate using the *2 Parameter Model* (Equation 7.4).

Table 7.8. Cross-section and loading identification for pavement analysis.

Cross-section	Load = 40kN	Load = 50kN	Load = 60kN
Table 4.1:			
1	1: 40kN	1: 50kN	
1a	1a: 40kN		1a: 60kN
1b	1b: 40kN		1b: 60kN
2	2: 40kN	2: 50kN	
3	3: 40kN	3: 50kN	
3a	3a: 40kN		3a: 60kN
3b	3b: 40kN		3b: 60kN
4		4: 50kN	
Table 6.1:			
5	5: 45kN[1]		
6	6: 45kN[1]		

1: 45kN is the most common weight passing over the Northern Ireland field trial.

7.5.4 Rut Depth Prediction

Calculated stresses from DEFPAV for the 21 different pavement analyses listed in Table 7.8 were imported into a spreadsheet for the calculation of surface rutting. Surface rutting was calculated for various number of wheel loads being 25,000, 50,000, 100,000, 1.0M, 1.4M and 1.7M. Equation 7.5 was used to calculate the permanent strain at depth increments where stress was calculated. Rut depth was calculated as the sum of the permanent strain multiplied by an associated thickness/depth increment.

As discussed it is expected the value of permanent strain after the first 25,000 wheel loads will be inaccurate due to the value being derived from RLT multi-stage tests (Figure 7.6). However, it is hoped the trend in rut depth progression (i.e. slope) predicted will be the same as that measured as this is derived from longer term steady state response in the RLT permanent strain tests.

Residual horizontal stresses were recognised as being important and should be considered in pavement analysis (Section 2.4.6). However, the value chosen for the residual horizontal stresses is arbitrary and preliminary analysis found the choice of value had a significant influence on the predicted rut depth, namely in terms of rut depth progression or the slope of the predicted rut depth with loading cycles. Therefore, for the first analysis the residual horizontal stresses were not added and assumed to be nil.

Results of predicted rut depth, measured rut depth and a best fit predicted rut depth are shown in Figure 7.15 to Figure 7.20. The best fit rut depth shown is an adjusted original predicted rut depth by an amount of rutting added to the rut depth at 25,000 and if necessary some horizontal residual stress added in order to obtain a near perfect match between predicted and measured rut depth. Values of rut depth added at 25,000 and horizontal stress needed to obtain a near perfect fit of predicted to the measured rut depth are listed in Table 7.9. Obviously the lower in magnitude the adjustments (Table 7.9) are then the better the fit of the original method where an additional rut depth was not added and the horizontal residual stresses are nil. Previously, it has been argued that residual stresses of 30kPa are present in the aggregate and subgrade soils and this residual stress should be included in the computation of the stress distribution. However, in order that the predicted rut depth matched the measured values from the pavement tests the horizontal stresses were kept, in most cases, as nil. Reasons for not requiring the addition of a 30kPa residual stress are discussed in Section 8.4.2.

Table 7.9. Adjustments required to obtain best fit of calculated to measured rut depth.

	Adjustments to obtain fit to measured rut depth.		
Test ID (Table 4.1 & 6.1)	Rut depth added @ 25,000 (mm)	Horizontal residual stress (kPa)	Figure
1: 40kN	-1.4	17	7.15
1: 50kN	0.6	0	
1a: 40kN	-1.6	17	
1a: 60kN	0.0	0	
1b: 40kN	-3.5	17	
1b: 60kN	-3.3	0	
2: 40kN	-2.6	250	7.16
2: 50kN	-1.1	200	
3: 40kN	1.1	0	7.17
3: 50kN	0.9	0	
3a: 40kN	2.2	0	
3a: 60kN	4.3	0	
3b: 40kN	1.3	0	
3b: 60kN	5.9	0	
4: 50kN	6.3	50	7.18
5: 45kN	1.9	0	7.19
6: 45kN	0.9	0	7.20

The predicted rut depths for the New Zealand accelerated pavement tests were examined further (IDs 1 to 4) to determine the relative contributions of rutting from the subgrade and granular materials. This was not necessary for the Northern Ireland trials (ID 5 and 6) as the subgrade was not modelled plastically as this was solid rock material being a characteristic of the site. Table 7.10 shows the relative contributions of rutting for the subgrade and granular materials. As can be seen for the Test Sections 3, 3a, and 3b only 12 to 16% of the rutting could be attributable to the granular material (CAPTIF 3, Table 3.1). Test Section 4 showed most of the rutting could be attributable to the subgrade (96%). Another point with Test Section 4 is after 100,000 loads there was no additional rutting predicted to occur in the granular material (CAPTIF 4, Table 3.1), where the rut progression was a result of subgrade rutting only. Predicted rut depths for Test Section 1 showed that between 40 to 50% of the rut depth was attributable to the granular material (CAPTIF 1). Trenches in the New Zealand accelerated pavement tests revealed over 50% of the surface rut depth was attributed to the granular materials, which was only predicted to occur in Test Section 1. A possible reason for this is errors in RLT testing, particularly in the initial deformation at 25,000 cycles which is unknown due to multi-stage RLT tests (Figure 7.6).

Table 7.10. Rut depths attributable to aggregate and subgrade in NZ APTs.

	Rut Depth @ 100k				Rut Depth @ 1M			
	A	S	A	S	A	S	A	S
ID	(mm)	(mm)	%	%	(mm)	(mm)	%	%
1: 40kN	3.2	1.5	69	31	6.1	5.2	54	46
1: 50kN	3.3	1.8	64	36	6.2	6.6	48	52
1a: 40kN	3.2	1.5	69	31	6.1	5.2	54	46
1a: 60kN	3.0	2.2	58	42	5.8	8.2	41	59
1b: 40kN	4.6	2.0	70	30	8.3	7.6	52	48
1b: 60kN	4.3	2.7	61	39	8.0	11.2	42	58
2: 40kN	8.6	1.8	82	18	105	7.0	94	6
2: 50kN	8.1	2.3	78	22	85	9.3	90	10
3: 40kN	0.2	1.2	14	86	0.6	4.1	12	88
3: 50kN	0.3	1.4	16	84	0.7	5.0	13	87
3a: 40kN	0.2	1.2	14	86	0.6	4.1	12	88
3a: 60kN	0.4	1.6	18	82	0.9	5.8	13	87
3b: 40kN	0.4	1.5	20	80	0.8	5.4	13	87
3b: 60kN	0.8	2.0	29	71	1.5	7.8	16	84
4: 50kN	0.4	2.3	14	86	0.4	10.0	4	96

For Test Section 2, the predicted rut depth was over 90mm with most of this being due to the granular material (CAPTIF 2, Table 3.1) of 96% (Table 7.10). This is not an error as the RLT permanent strain tests for the CAPTIF 2 material have the greatest amount of deformation. This was expected for the CAPTIF 2 material as this had 10% clay fines added to purposely weaken the material. However, the result of the New Zealand accelerated pavement test (APT) was a surprise as it performed as well as the other test sections with good quality aggregates with nil clay fines. Clay fines will increase the sensitivity to moisture, thus slight differences in moisture from insitu and that tested in the RLT apparatus will have a significant effect on the amount of permanent strain. Therefore, the moisture content in the pavement test could have been less than that tested in the RLT apparatus, and the CAPTIF 2 material therefore being stronger in-situ.

Overall the predictions of rut depth are good, particularly the trends in rut depth progression with increasing loading cycles (i.e. this relationship is sensibly the same for actual and predicted measurements in 11 out 17 analyses). Adjustment of up to a few millimetres to the predicted rut depth at 25,000 cycles is generally all that is needed to obtain an accurate prediction of rut depth. This was expected as the actual magnitude for the first 25,000 loads is difficult to estimate, it being unknown whether the value is the cumulative or incremental value of permanent strain (Figure 7.6). The method adopted was to take the incremental value of permanent strain at 25,000 cycles, which is considered to be a low estimate. This is the case for pavement Test Sections 3, 3a and 3b which all used the CAPTIF 3 granular material and for Test Sections 4, 5 and 6 where an additional amount of rutting was added to coincide with the measured values in the pavement test (Table 7.9). The opposite occurs for the Test Sections 1, 1a, and 1b which all used the CAPTIF 1 material.

From the predicted rut depths for the test sections using CAPTIF 1 material (Figure 7.15), it can be seen the trend in rut depth progression is accurately predicted for the heavier wheel loads of 50kN and 60kN. The trend was not accurately predicted for the lighter wheel loads of 40kN, although a small horizontal residual stress of 17kPa was all that was needed to obtain an accurate prediction. Trends in rut depth progression were determined accurately for all wheel loads for those test sections using the CAPTIF 3 material (3, 3a and 3b, Figure 7.17). This result suggests the RLT testing and consequential fit to the 2parameter model (Equation 7.4) has an influence as the trend in results is specific to the material types used.

For Test Sections 4, 5 and 6 with thicker asphalt cover of 90 and 100mm it was generally felt predictions were not as good as the other test sections with only 25mm cover of asphalt. Stresses are lower in the granular and subgrade materials which in turn reduces the magnitude of permanent strain predicted with Equation 7.5. Prediction of low permanent strains from low testing stresses in the RLT apparatus were found to be less accurate as although the mean error appears low at say 0.2% this could mean a 100% difference between the predicted and measured value. Generally, the predicted permanent strains at low stress levels were less than those actually measured in the RLT apparatus. This was found to affect the calculation of permanent strains in the granular materials being very small in Test Sections 4, 5 and 6. In fact after 100,000 there was virtually nil (<0.001%) increase in permanent strain predicted in the granular materials. Therefore, the model could be signalling a Range A behaviour (Section 2.11.2) in these granular materials with asphalt cover greater than 90mm.

The objective of the method employed to predict rut depth was primarily for the case where Range B behaviour is likely (Section 2.11.2). Thus, as seen from Equation 7.5 the model was devised to predict a constant rate of increase in rut depth as assumed in the model used for extrapolating RLT results past 1M loads, which is characteristic of a Range B response. Results of the analysis comparing predicted rut depths with actual measured values shows that predictions are good with those pavements with thin asphalt cover as a Range B response occurs. However, predictions are not so good with those pavements with thick asphalt covers but rather a Range A response is indicated to occur as permanent strains do not accumulate with increasing loads after 100,000.

7.6 SUMMARY

Two methods are presented for modelling permanent strain with respect to stress from Repeated Load Triaxial tests. The first method is based on models used by other researchers where the radial and axial stresses are combined as a stress ratio and was therefore referred to as a *1 Parameter Model*. An asymptotic *1 Parameter Model* being an adaptation of the Paute et al (1996) model was found to fit the RLT results the best, and in particular being able to provide a stress limit where failure occurred (i.e. permanent strain is calculated to be infinite). However, the *1 Parameter Model* calculated very low permanent strains at some testing stresses where high permanent strain occurred in the RLT test. Another problem with the *1 Parameter Model* was that when applied to predict rut depth, it often computed negative (expansive) permanent strains as the stress ratios found from pavement analysis exceeded the stress boundary.

To resolve the inadequacies found with the *1 Parameter Model* a *2 Parameter Model* was developed. This *2 Parameter Model* requires stress to be defined by two independent variables being the stress invariants p (mean principal stress) and q (deviatoric stress). The *2 Parameter Model* fitted the RLT test results well showing the same trend in measured RLT values where, for a constant mean principal stress, as the deviatoric/axial stress increases the permanent strain increases exponentially. Parameters for the *2 Parameter Model* were found for permanent strain at 25,000 load cycles and permanent strain rates from 25,000 to 100,000, 100,000 to 1M and 1M to 2M load cycles as measured in RLT tests. The *2 Parameter Model* was then applied to predict rut depth for 17 different pavement tests reported in Chapters 4 *New Zealand Accelerated Pavement Tests* and 5 *Northern Ireland Field Trial*. It was found that the trend in rut depth progression was accurately predicted for 11 out of the 17 tests. Further, adjusting the rut depth predicted at 25,000 wheel passes by up to a few millimetres resulted in an accurate prediction of rut depth for these 11 tests where the rut depth progression was accurately predicted. It was expected that the prediction of the magnitude of rutting for the first 25,000 loads would be inaccurate due to the nature of multi-stage permanent strain tests where the previous stage tests affect the magnitude or permanent strain compared with testing on a new sample. Predictions of rutting for pavement tests with thick asphalt cover of 90 and 100mm were poor. For these pavements the permanent strain rates in the granular materials calculated to occur from 100,000 to 1M load cycles were fractions of a percent and too low to register as additional rutting (i.e. < 0.01mm). Thus the model predicts a Range A response rather than an accurate magnitude of permanent strain.

It is recognised that the RLT test only approximates the real loading condition in a pavement. In particular, the confining stress is not cycled and the principal stresses are not rotated. Despite, these limitations the *2 Parameter Model* for the prediction of permanent strain derived from RLT tests resulted in adequate predictions for rut depth. One of the reasons for this is residual horizontal stresses although recognised to occur were assumed to be nil. Tests with the hollow cylinder apparatus that do rotate the principal stresses will result in higher permanent strains than the RLT apparatus for the same testing stress. Thus, residual horizontal stresses would need to be assumed if predicting rut depth from permanent strain models derived from tests like the hollow cylinder apparatus.

Should the *2 Parameter Model* with parameters from RLT tests be used in practice, then it is recommended to assume the horizontal residual stresses are nil and 5mm should be added to the initial rut depth calculated at 25,000 loads as this should lead to a conservative estimate of rut depth.

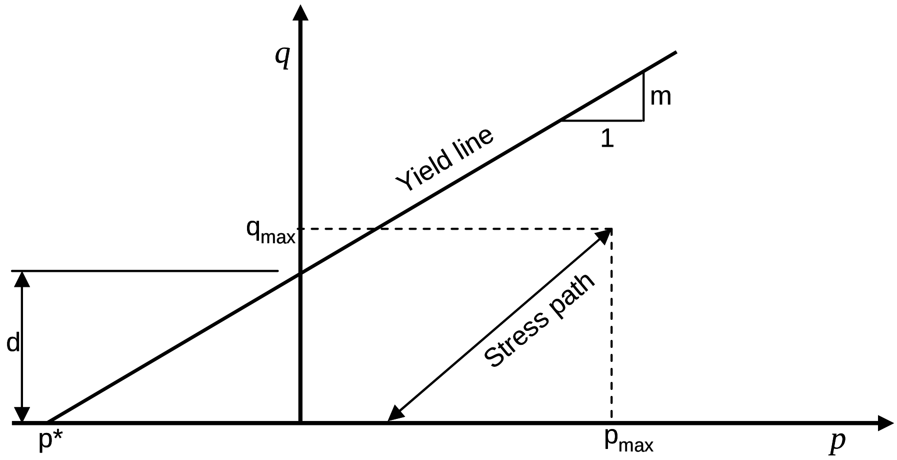

Figure 7.1. Illustration of parameters used in proposed model.

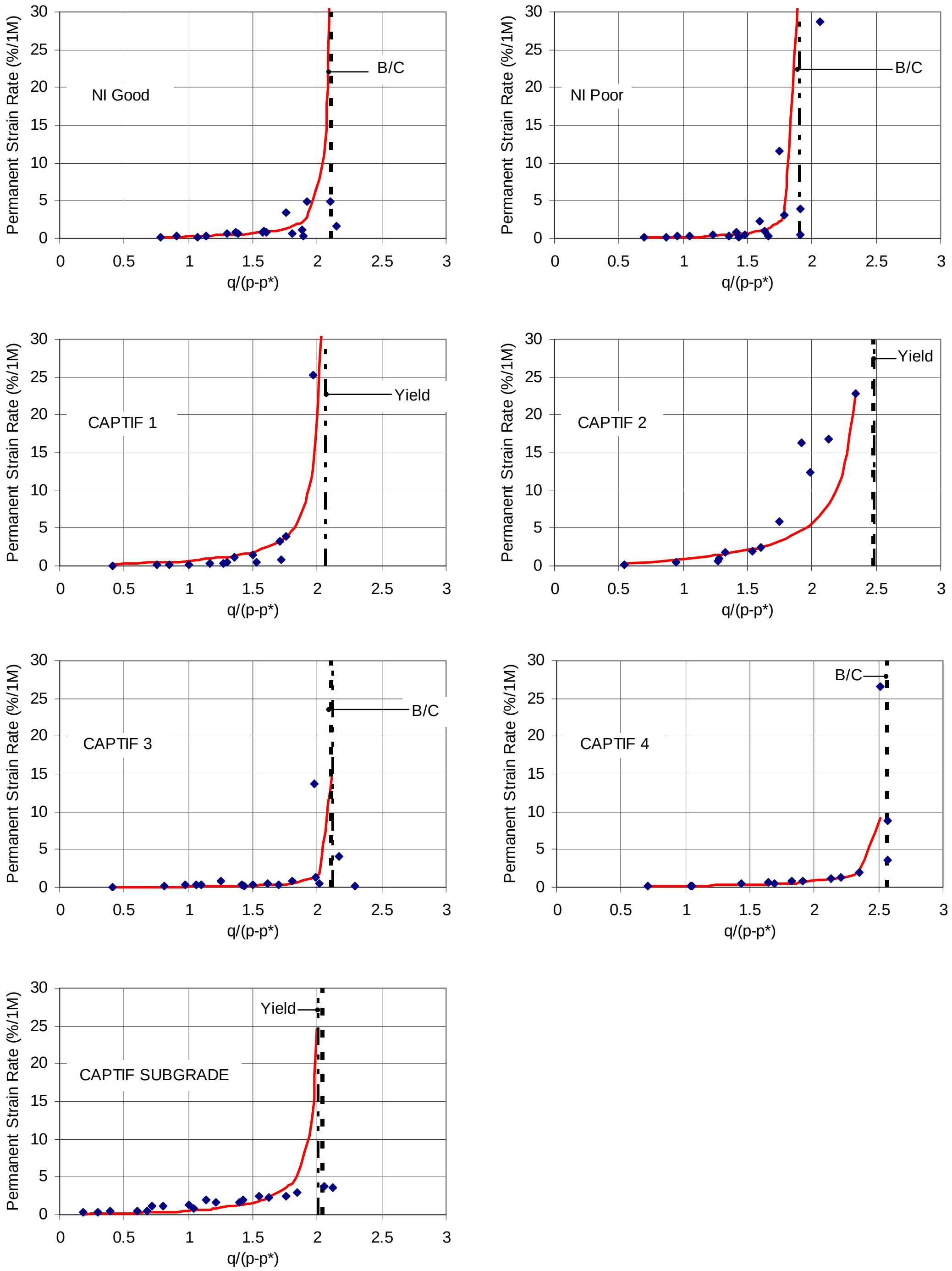

Figure 7.2. Fitting model to data points using parameters from yield line or shakedown Range B/C boundary.

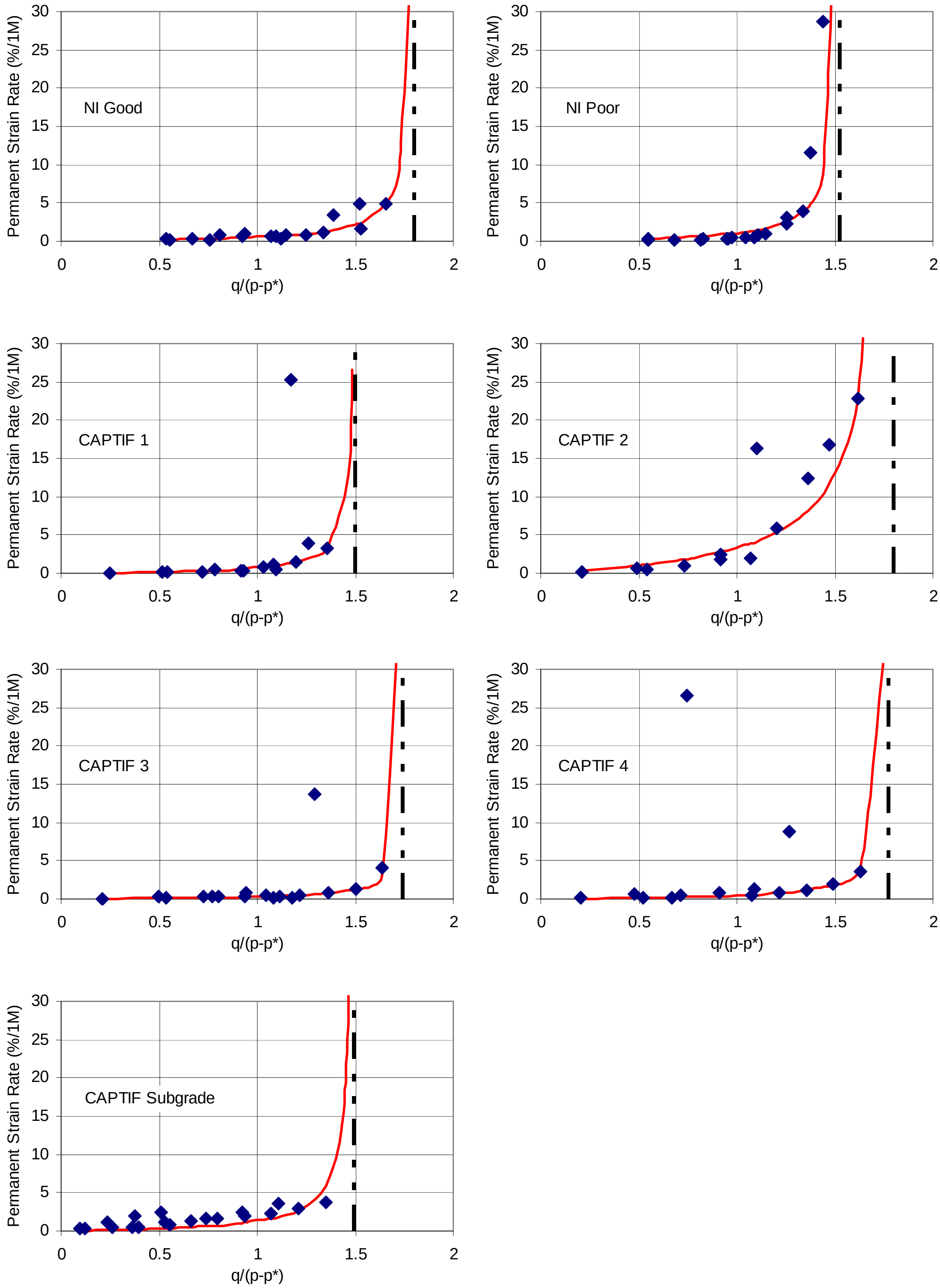

Figure 7.3. Fitting permanent strain rate model to data points using best fit parameters with p* = -0.10 MPa.

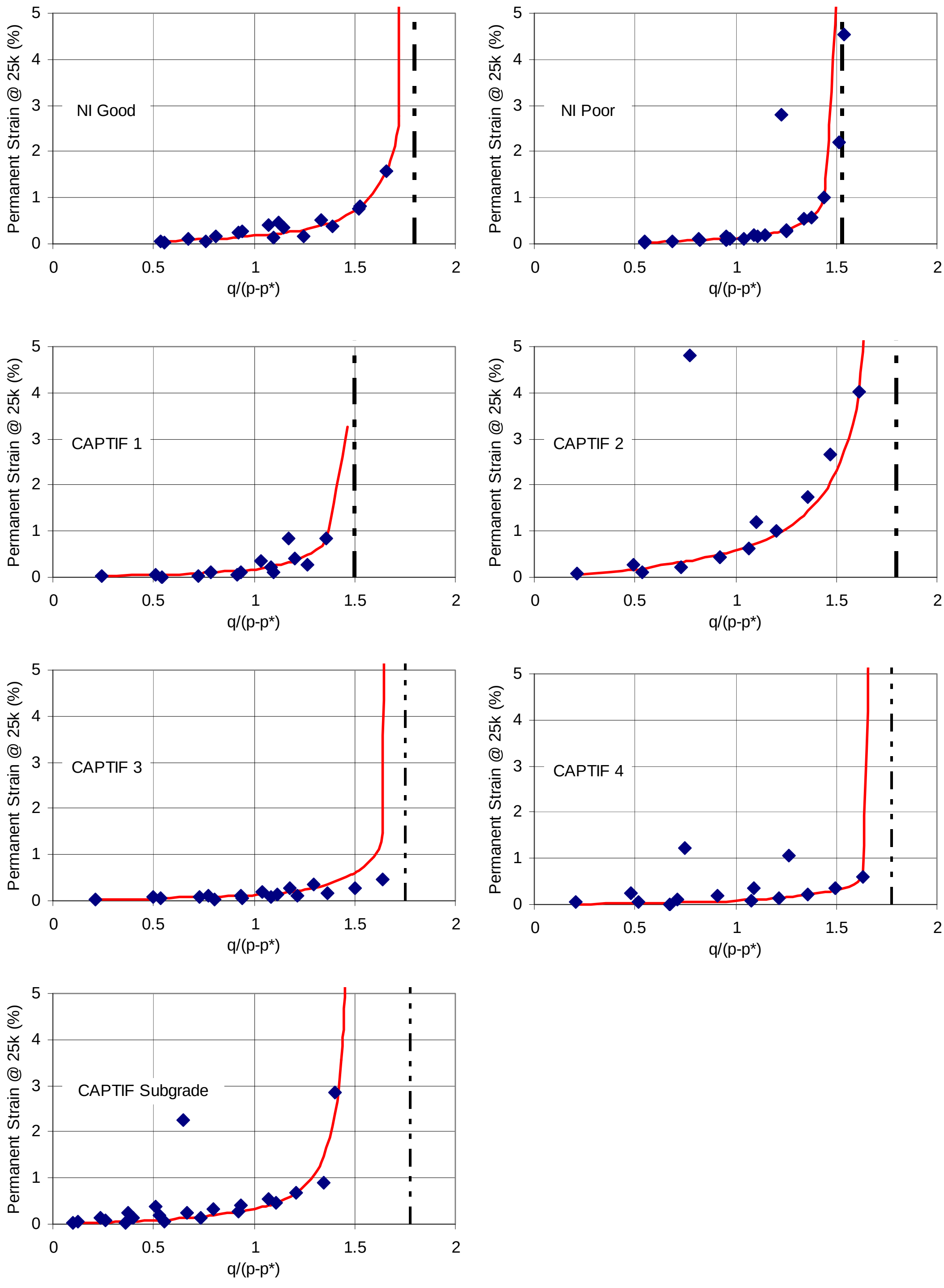

Figure 7.4. Fitting permanent strain model at 25,000 load cycles to data points using parameters from permanent strain rate model with p* = -0.10 MPa.

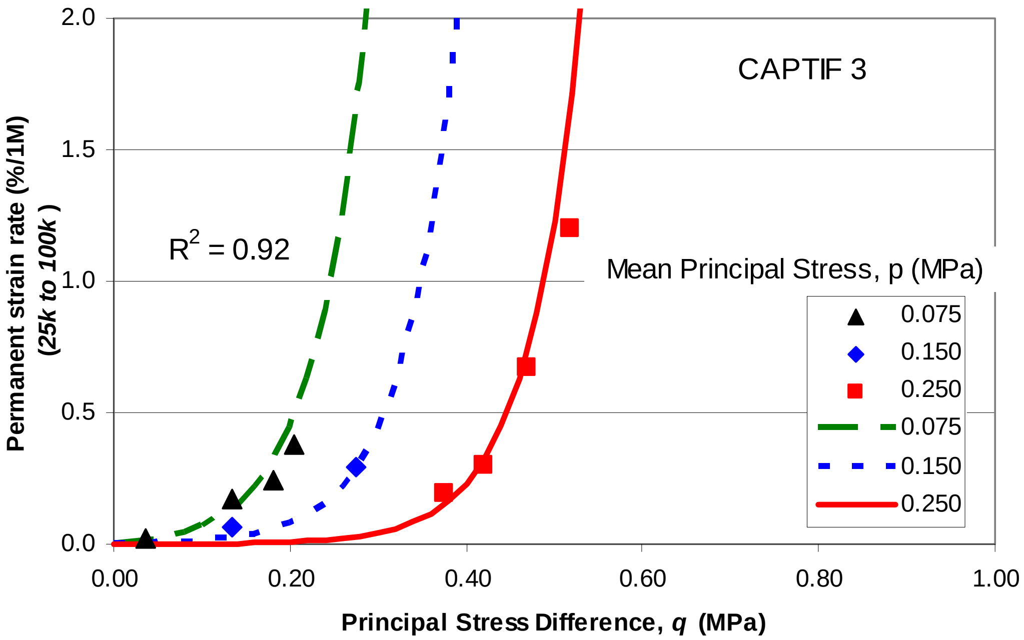

Figure 7.5. Example plot showing how exponential functions fit measured data for individual multi-stage tests.

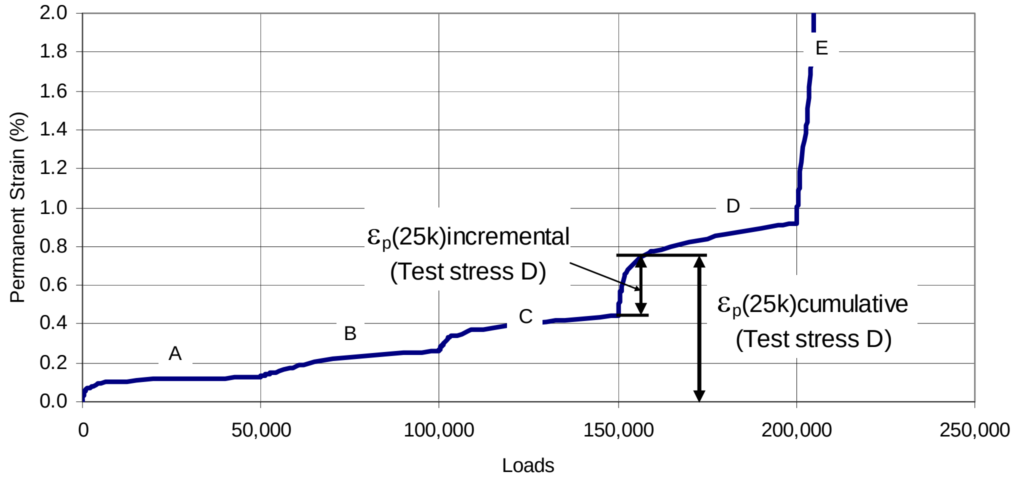

Figure 7.6. The difference between incremental and cumulative permanent strain at 25,000 load cycles for each testing stress.

RLT tests

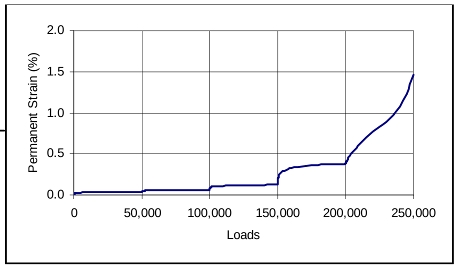

RLT Extrapolation
(to *N* of interest)

(i) 0 to 25k; (ii) 25k to 100k; (iii) 100k to 1M; and (iv) >1M

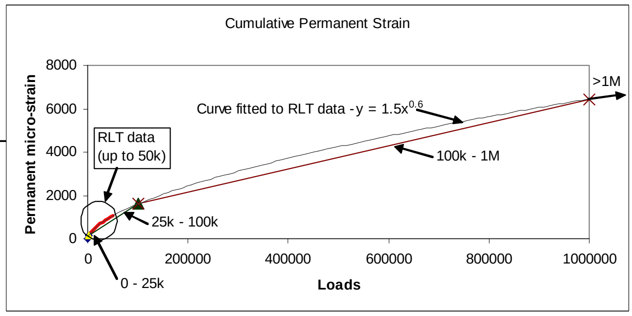

Tabulate RLT permanent strain rates with test stress

Material	Testing stress		Permanent strain	Permanent strain rate (tangential)		
TEST	*p*	*q*	25k (magnitude)	25k – 100k	100k – 1M	>1M
-	-	-	-	-	-	-
-	-	-	-	-	-	-

Fit data to Two parameter model Eqn 7.10:
$\varepsilon_{rate} = e^{(a)}\, e^{(bp)}\, e^{(cq)} - e^{(a)}\, e^{(bp)}$

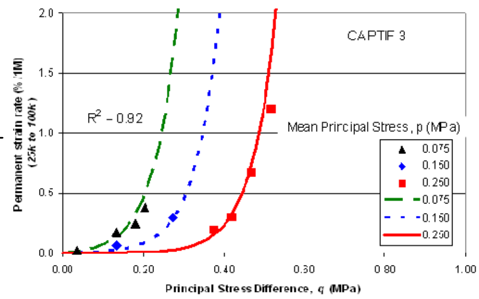

Eqn 7.4	Permanent strain	Permanent strain rate (tangential)		
Constants	25k (magnitude)	25k – 100k	100k – 1M	>1M
a	-	-	-	-
b	-	-	-	-
c	-	-	-	-

Figure 7.7. Interpretation of RLT permanent strain tests for modeling permanent strain with respect to stress and number of loads.

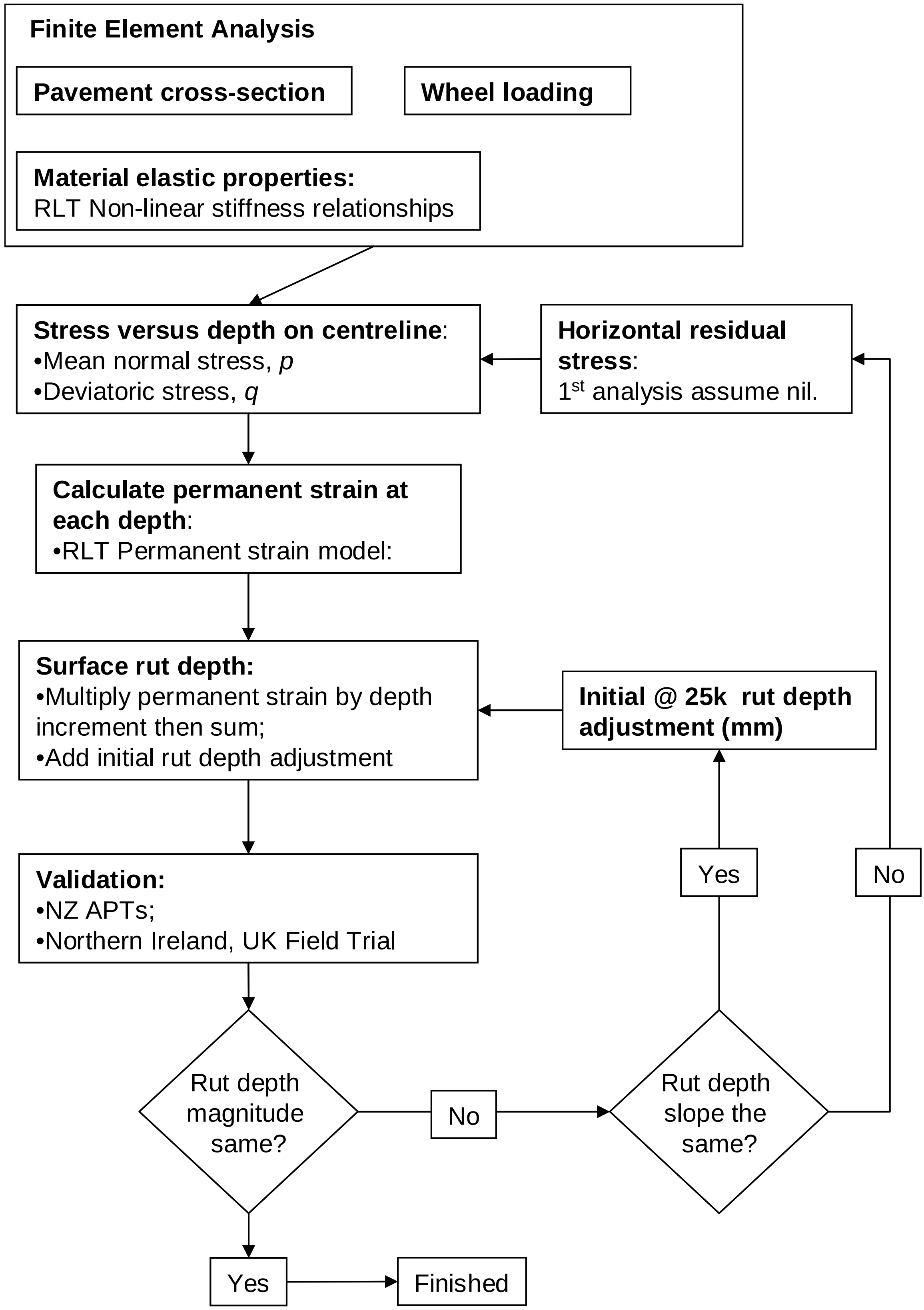

Figure 7.8. Methodology for calculation of rut depth and validation.

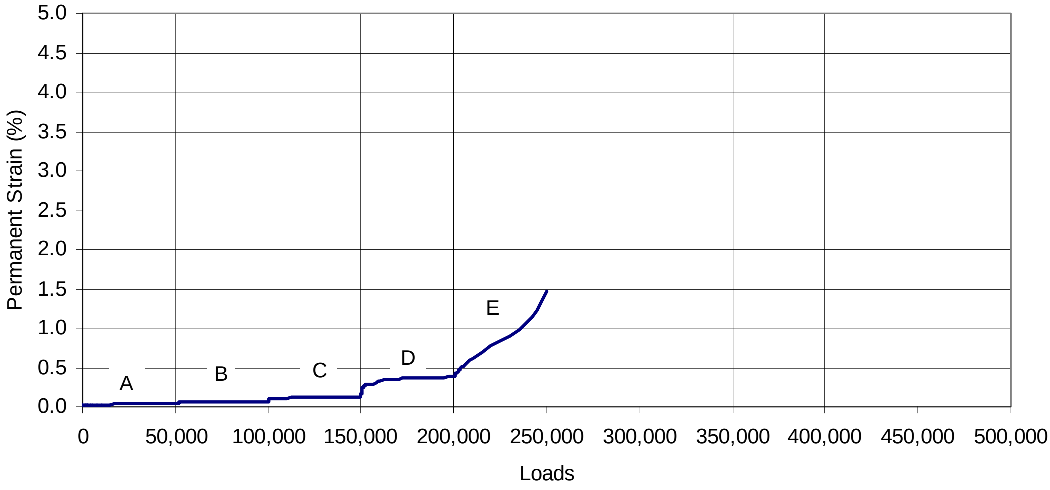

Figure 7.9. RLT permanent strain result for CAPTIF 1 material, Test 1 - p=75kPa (see Appendix A for stress levels).

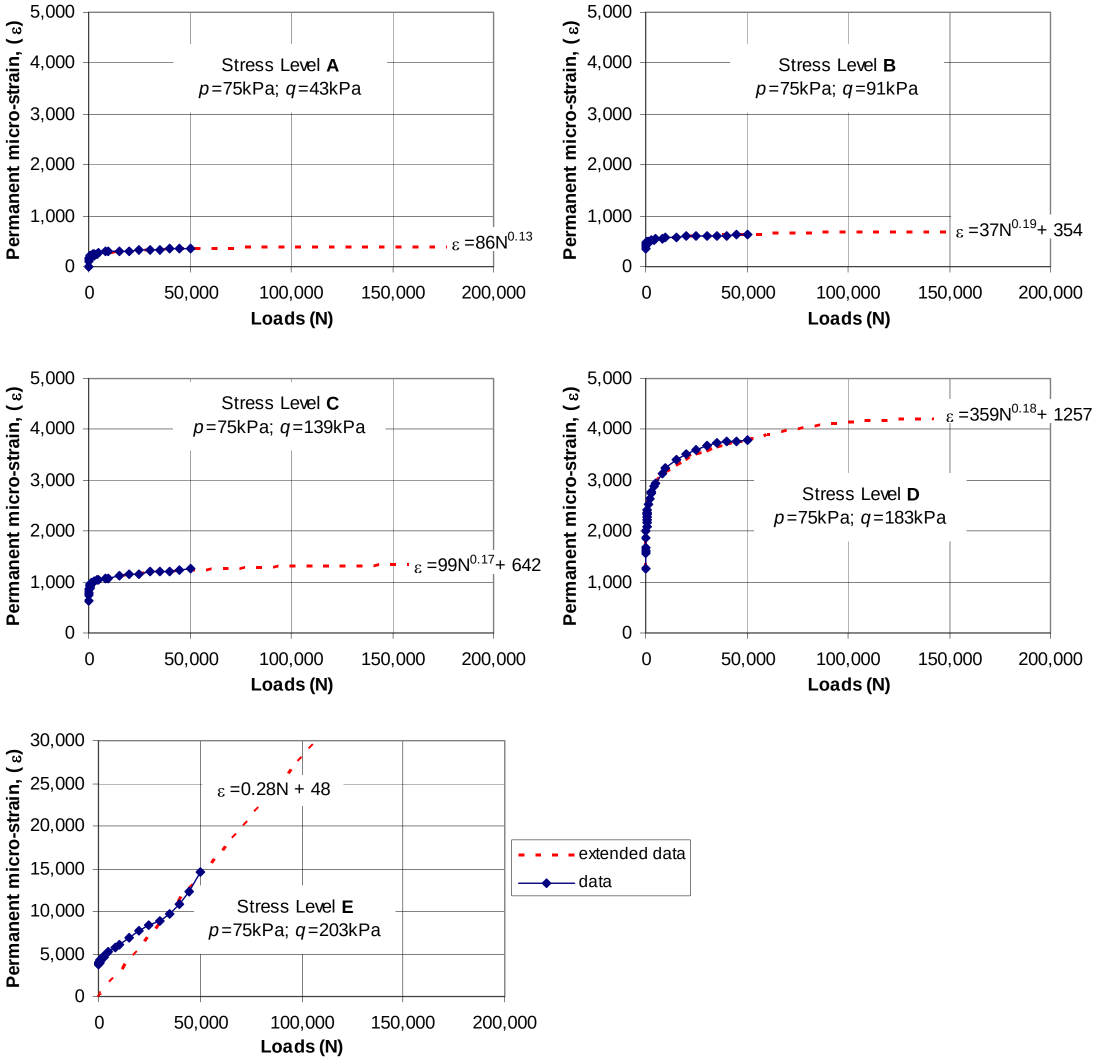

Figure 7.10. Individualised permanent strain results for CAPTIF 1 material – (Test 1 - p=75kPa).

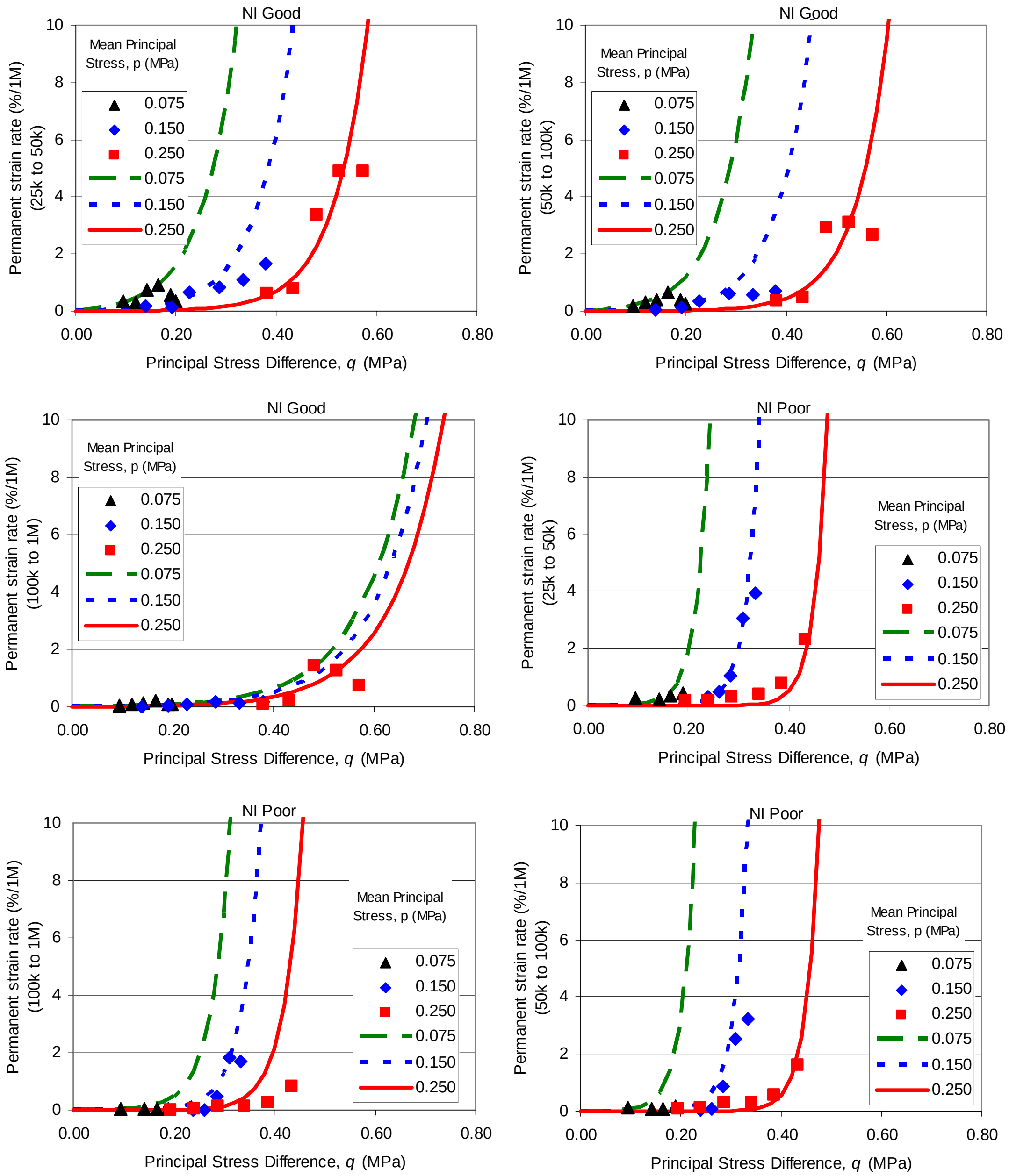

Figure 7.11. Measured permanent strain rate compared with predicted from model (Equation 7.4) for NI Good and NI Poor materials.

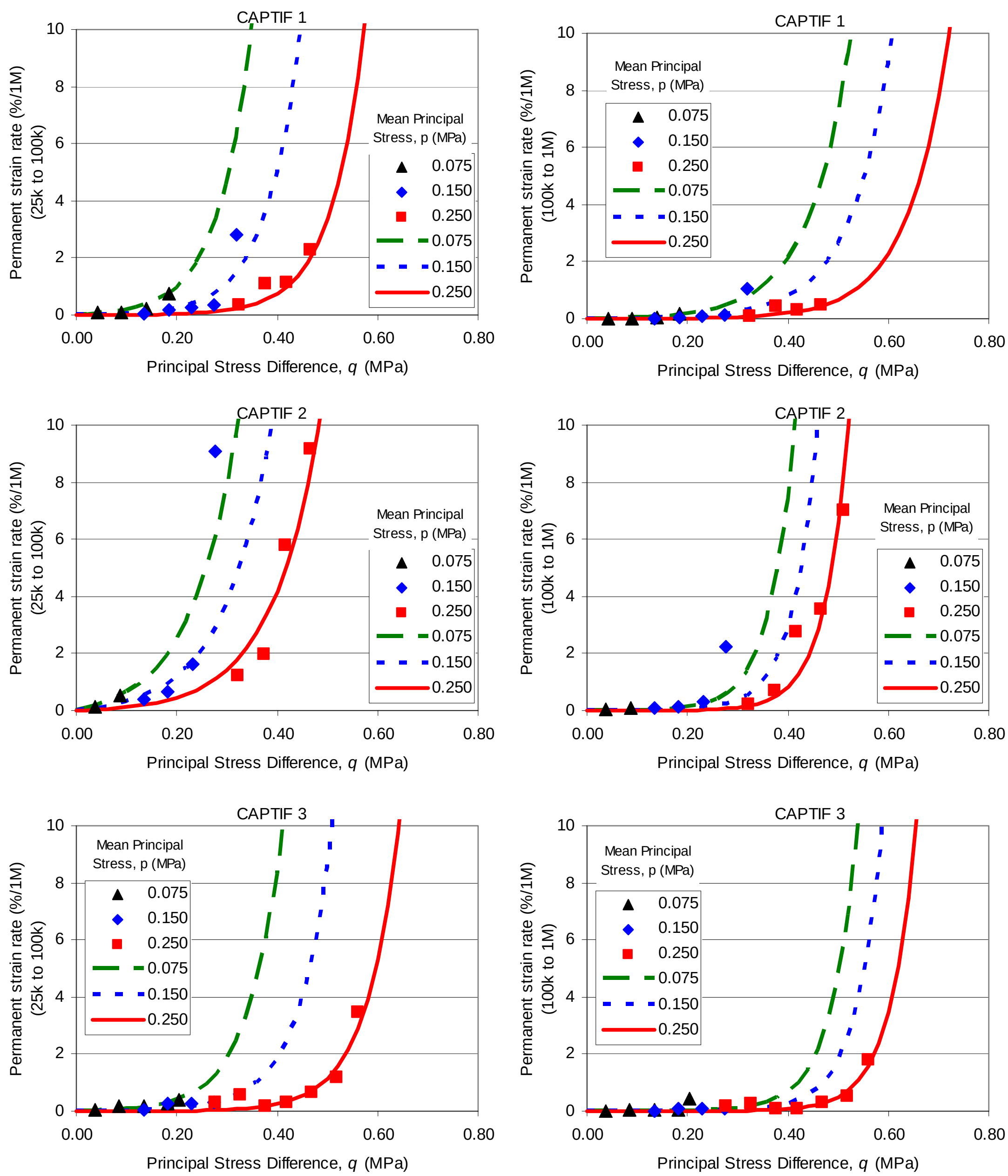

Figure 7.12. Measured permanent strain rate compared with predicted from model (Equation 7.4) for CAPTIF 1, CAPTIF 2, and CAPTIF 3 materials.

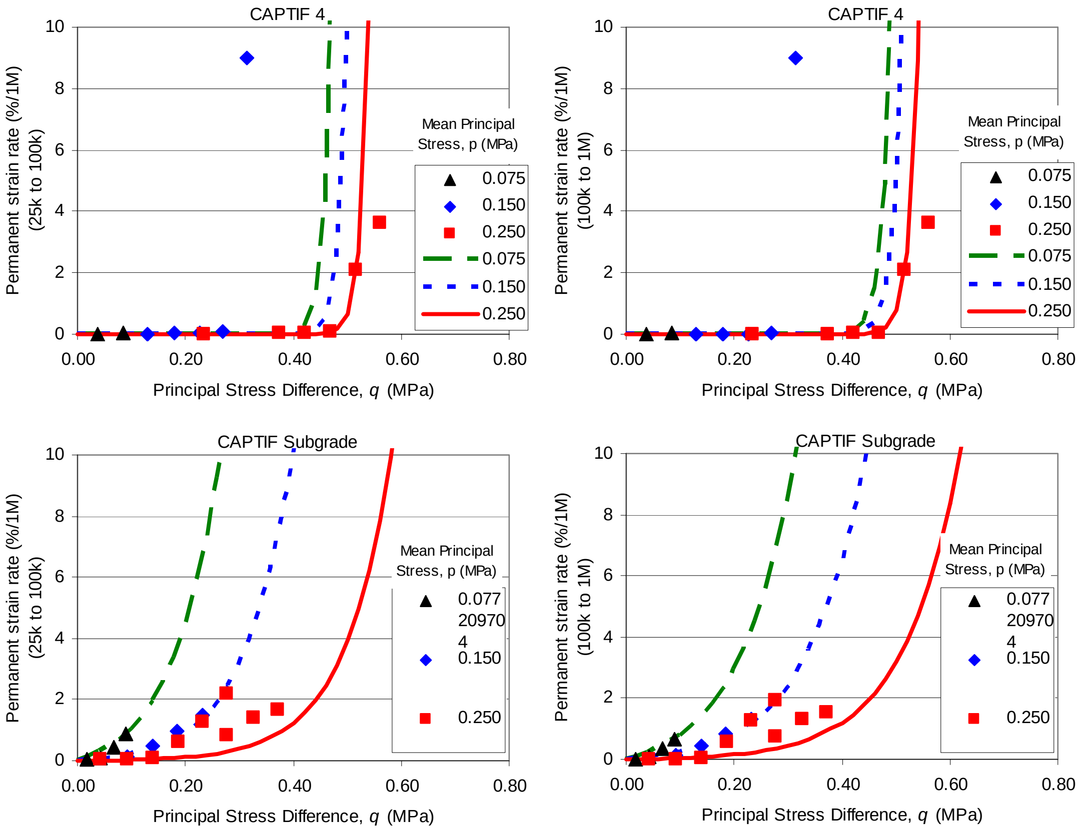

Figure 7.13. Measured permanent strain rate compared with predicted from model (Equation 7.4) for CAPTIF 4 and CAPTIF Subgrade materials.

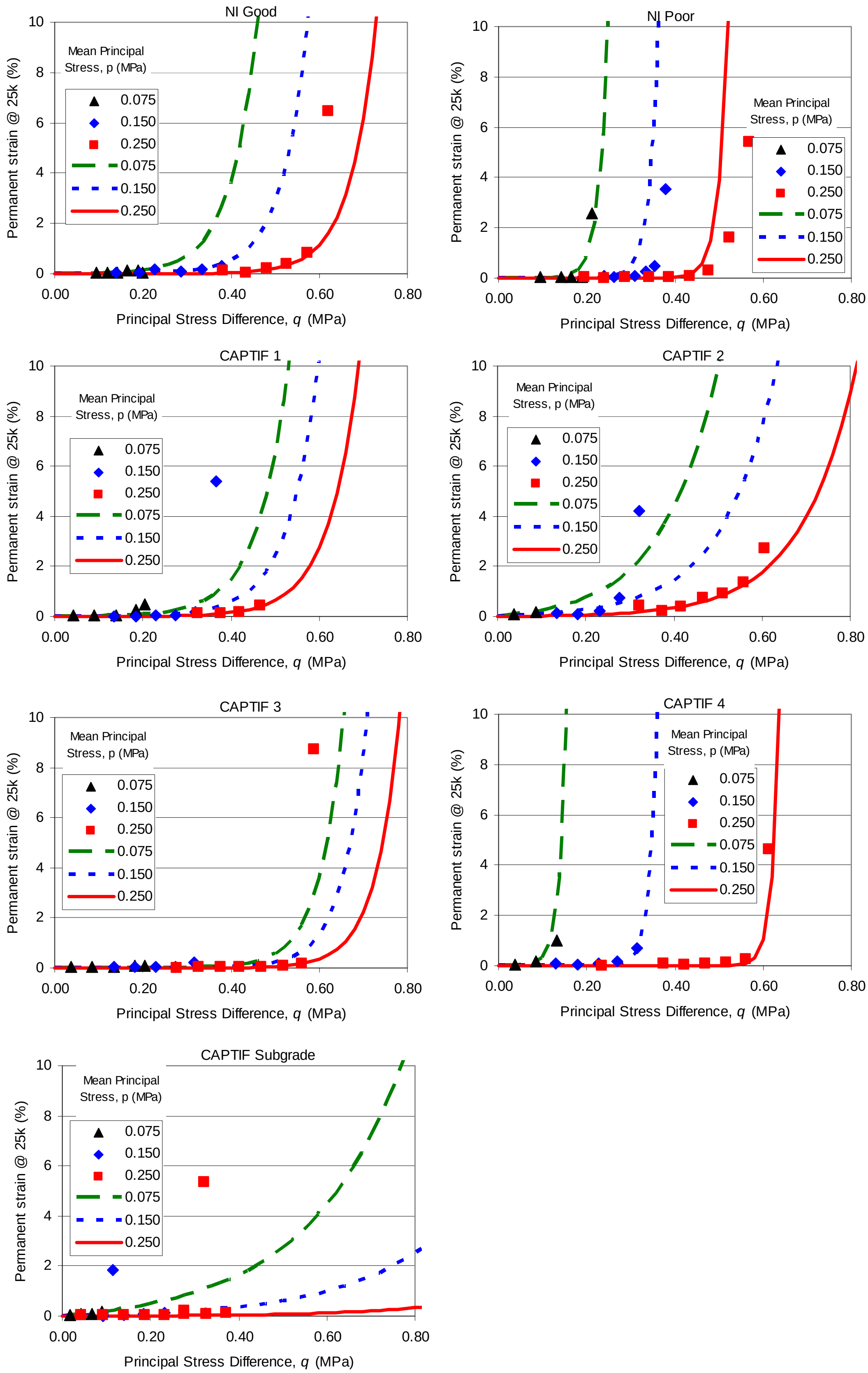

Figure 7.14. Measured permanent strain @ 25,000 compared with predicted from model (Equation 7.4).

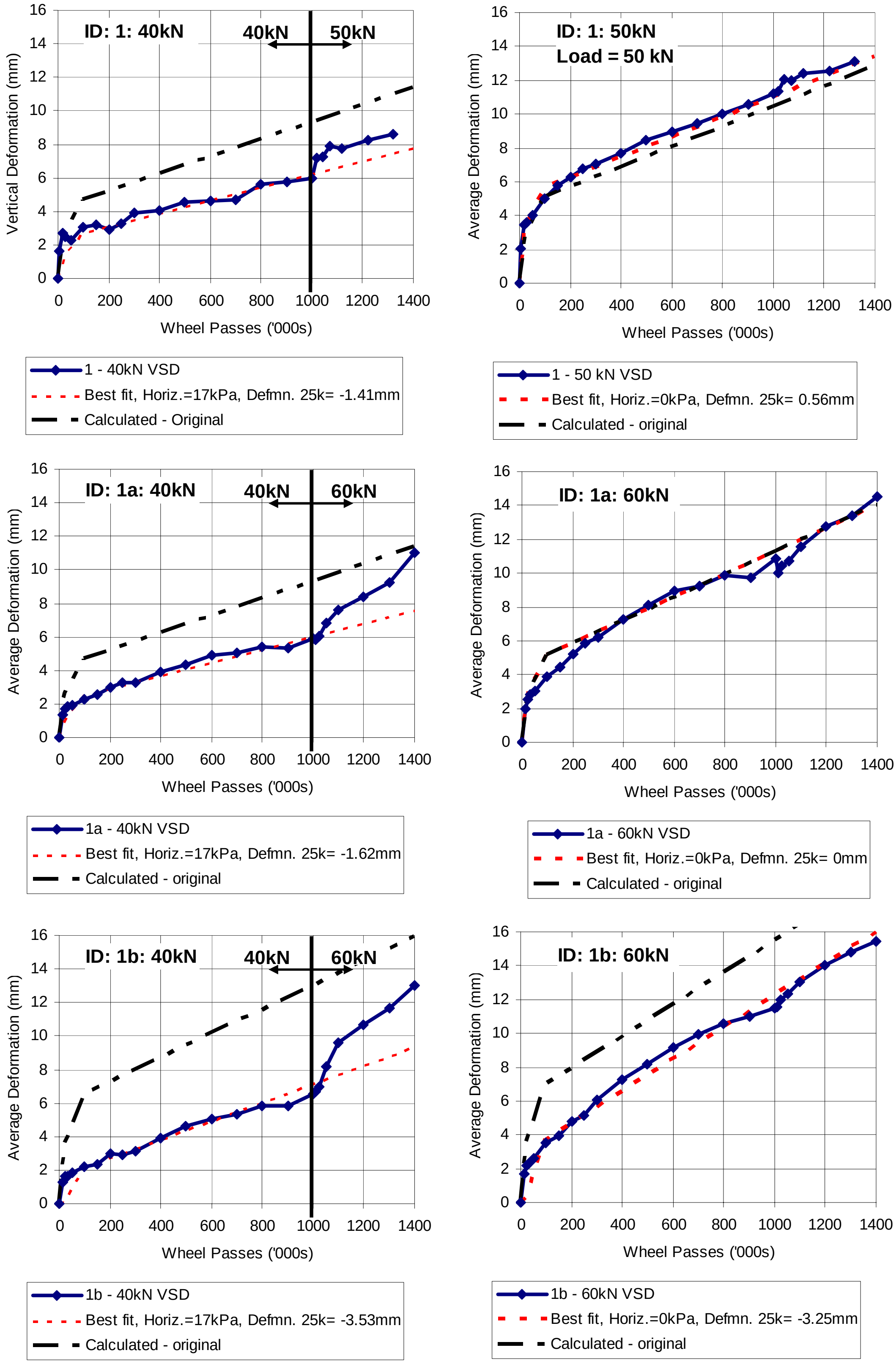

Figure 7.15. Predicted compared with measured rut depth for cross-sections 1, 1a and 1b (Table 7.8).

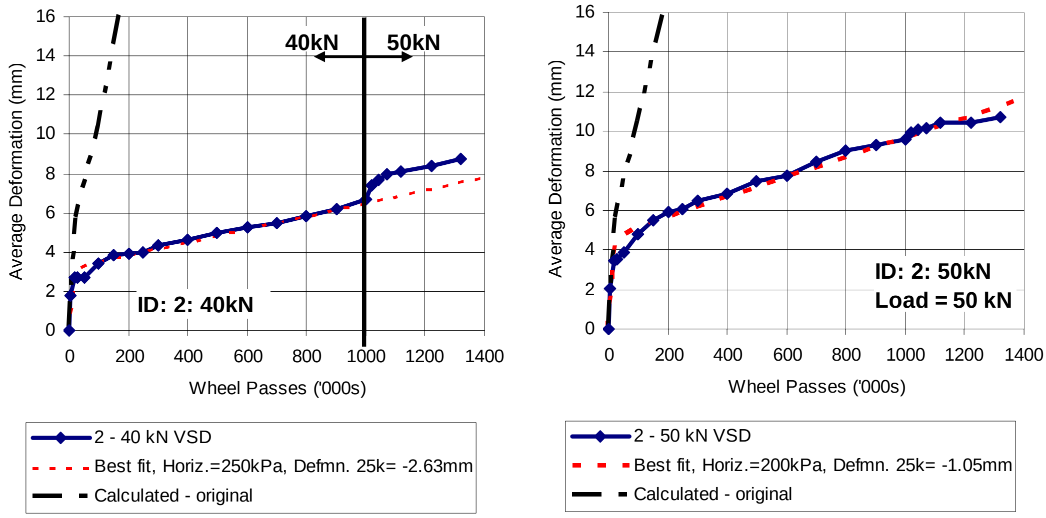

Figure 7.16. Predicted compared with measured rut depth for cross-section 2 (Table 7.8).

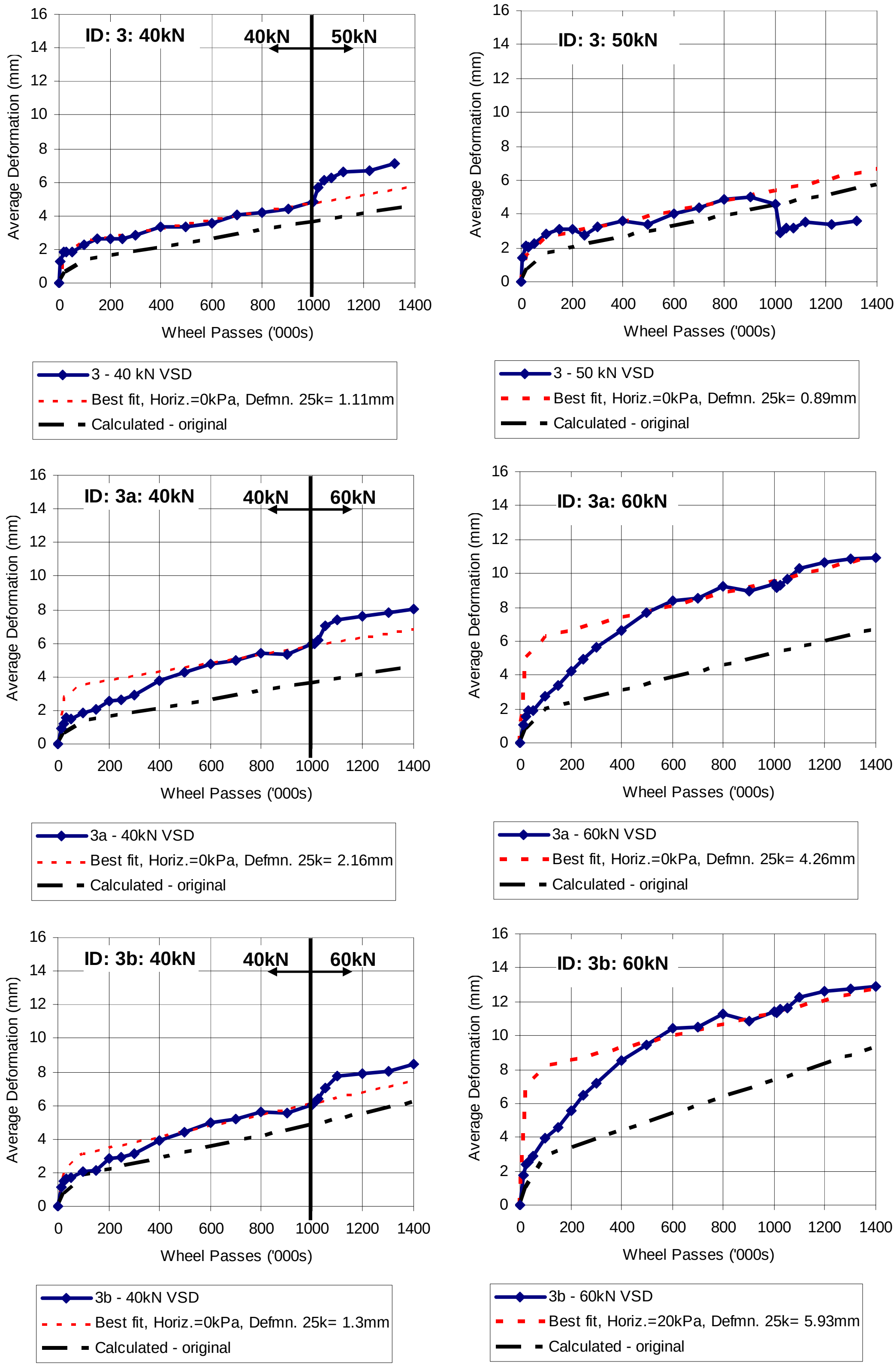

Figure 7.17. Predicted compared with measured rut depth for cross-sections 3, 3a and 3b (Table 7.8).

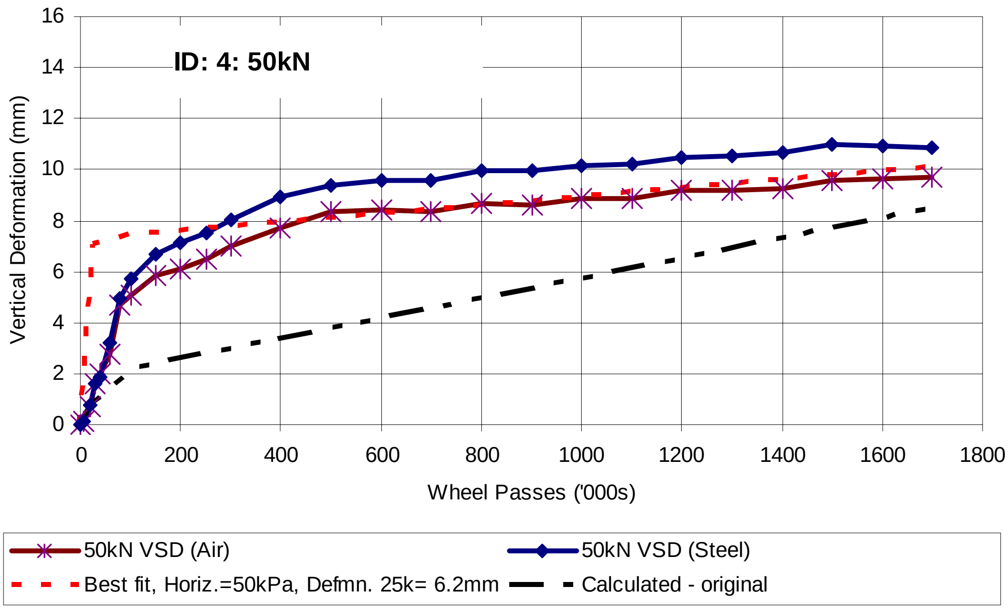

Figure 7.18. Predicted compared with measured rut depth for cross-section 4 (Table 7.8).

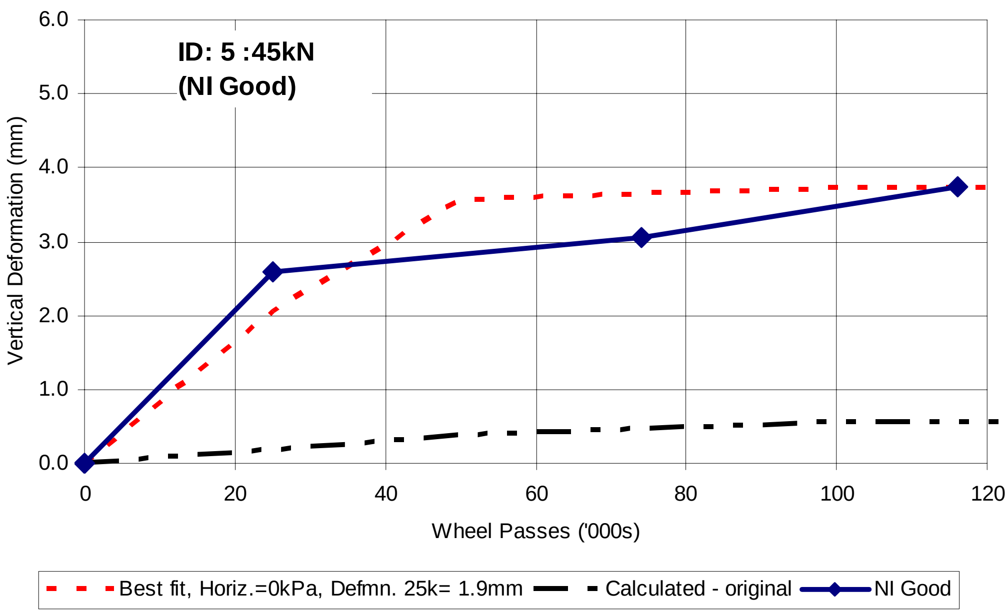

Figure 7.19. Predicted compared with measured rut depth for cross-section 5 (Table 7.8).

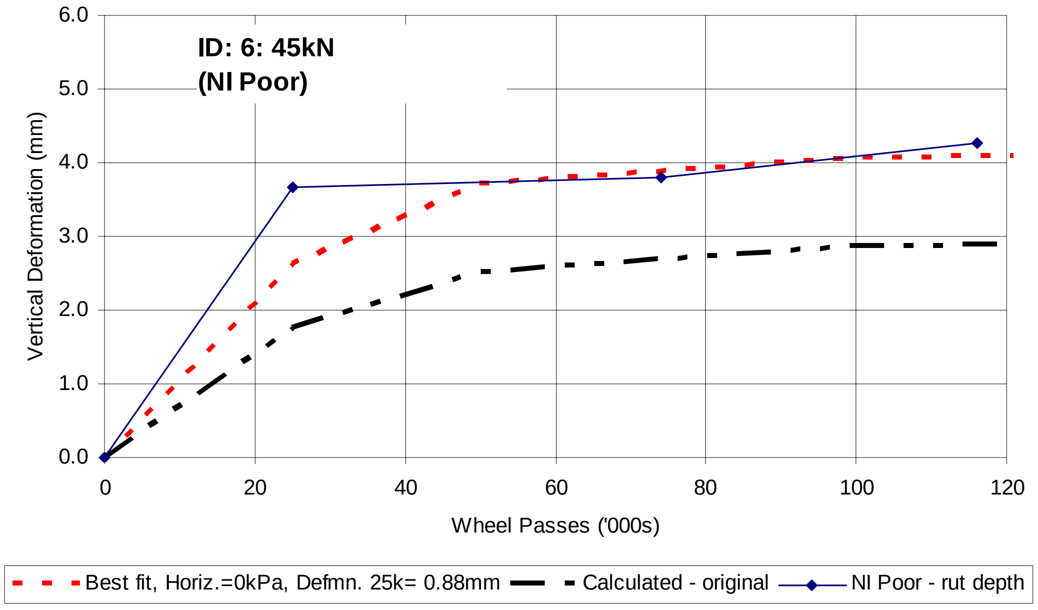

Figure 7.20. Predicted compared with measured rut depth for cross-section 6 (Table 7.8).

CHAPTER 8 DISCUSSION

8.1 INTRODUCTION

This thesis has introduced the concept of considering the plastic behaviour of granular and subgrade materials from the Repeated Load Triaxial (RLT) apparatus to predict rutting behaviour or magnitude of a pavement. Predicting rutting relates directly to the duration of pavement life, as pavement failure is due to excessive cracking and/or surface deformation or rutting. Comparing this to current methods of design, which are based on formulae utilising resilient strains at critical locations within the pavement, enables a calculation of the pavements life (Section 2.2.2). Current methods of design encourage the use of materials with greater resilient moduli because these reduce the resilient strains and thus increase pavement life according to the formulae.

The methods of predicting rutting behaviour and magnitude introduced in this thesis, on the other hand, encourage the use of materials with high permanent deformation resistance to increase the pavement life. Greater or comparable resilient moduli of granular materials do not always result in greater or comparable permanent deformation resistance. An example of this was found for the analysis of test pavement 2 in Chapter 7 (Table 7.8). Test pavement 2 utilised the *CAPTIF 2* material where the resilient moduli was comparable to the other granular materials and certainly higher than the *CAPTIF 4* material (Table 7.7). The permanent strains were the highest and, as a consequence, the predicted rut depth was in excess of 80mm for 1 million wheel passes (Table 7.10). *CAPTIF 2* material (Table 3.1) was contaminated with 10% by mass of silty clay fines to deliberately produce a poor quality granular material, so the 80mm predicted rut was no surprise. However, under existing methods of pavement design where resilient modulus is important, resilient analysis of a pavement with the *CAPTIF 2* granular material would not alert the designer to any potential rutting problems. Highways Agency specification for granular base material would likely reject the *CAPTIF 2* granular material, on the grounds of too many plastic fines.

Material specifications do ensure a granular material has sufficient permanent deformation resistance. Therefore, material specifications must be used in conjunction with current pavement thickness design methods that do not consider deformation resistance but, rather, resilient characteristics. A limitation of material specifications is apparent when considering the use of new alternative materials such as those derived from recycled materials. Often this new material will not pass the specification and thus be rejected, which could result in the loss of economic and environmental benefits. A method that relies on the plastic characteristics of a material which predicts rutting behaviour and magnitude (as used in Chapters 6 and 7 respectively) has many applications. One application is the ability to predict pavement performance in terms of rutting for the assessment of the suitability of using an alternative material (eg. from recycled sources). Should the predicted performance in terms of rutting be unacceptable then the pavement cross-section can be changed to accommodate the alternative material. For example, the asphalt cover thickness can be increased and/or the alternative material can be demoted to deeper in the pavement. Both these options will reduce the traffic induced stresses on the alternative material.

8.2 APPLICATIONS

Three applications of predicting rutting behaviour (Chapter 6) and rut depth (Chapter 7) in pavement design are investigated further. The first assesses the ability to determine the optimum asphalt cover thickness where shakedown Range A behaviour occurs in the granular and subgrade materials using the finite element method devised in Chapter 6. The second application compares the predictions of rutting behaviour (i.e. shakedown range prediction, Chapter 6) and rut depth (Chapter 7) with the lives for several standard UK Highways Agency flexible pavement designs. For the third application a methodology is discussed for using the rut depth prediction method, proposed in Chapter 7, for the assessment of alternative granular material suitability for use in the pavement instead of premium quality unbound granular base and sub-base material.

8.2.1 Effect of Asphalt Cover Thickness on Shakedown Range Behaviour

The onset of rutting can be minimised in the subgrade and granular materials by increasing the thickness of asphalt cover. Increasing asphalt cover will reduce the stress on the subgrade and granular materials, which in turn will reduce traffic induced rutting. Two methods have been utilised in this thesis for the assessment of rutting in granular and subgrade materials. Finite element modelling in Chapter 6 used either shakedown range boundaries A/B or B/C as Drucker-Prager yield criteria to predict the expected shakedown range behaviour (Range A, B or C defined in Section 2.11.2) of the pavement as a whole. Chapter 7 presented a methodology to predict the actual rut depth of the pavement for a given number of wheel loads. Both these approaches were derived from permanent strain data obtained from the Repeated Load Triaxial (RLT) tests on granular and subgrade materials.

The finite element method (Chapter 6) was used to predict the rutting behaviour of pavements in terms of shakedown Ranges A, B or C and can be used to design the asphalt cover thickness. The asphalt cover thickness is increased until nearly all the stresses are below the shakedown Range A/B boundary limit. Shakedown Range A response is considered ideal as if this occurs the rutting is minimal and the rate of rutting decreases with increasing load cycles. Further, a shakedown Range A response does not depend on the number of wheel passes as there is theoretically a point where no further deformation occurs. To assess this design approach, finite element analysis was undertaken on pavements with a range of asphalt cover thicknesses and the amount of surface rutting reported as an indication of the extent of stresses exceeding the shakedown Range A/B boundary.

For the purpose of evaluating the design method utilising the shakedown Range A/B boundary, all 6 granular materials (Table 3.1) were analysed in the finite element model with a range of asphalt cover thicknesses. The granular and subgrade thicknesses modelled were the same as used for the 1, 2 and 3 pavement tests (Table 4.1). The shakedown Range A/B boundary lines for the granular and subgrade materials were defined in the model as Drucker-Prager linear yield criteria (Table 6.2). Results of this finite element analysis are given in Table 8.1 and the total amount of yielding (deformation) versus asphalt thickness is plotted in Figure 8.1.

The results of using the shakedown Range A/B boundary as a Drucker-Prager yield criterion between the different granular materials all show similar results. At least 100mm of asphalt cover is needed before shakedown Range A behaviour is likely (i.e. rut depth/vertical deformation <0.2mm being an appropriate criterion determined in Chapter 6). Also for an asphalt cover of 100mm, plastic deformation in the subgrade ceases. Therefore, the subgrade deformation behaviour with respect to stress is the main factor that governs the shakedown range behaviour type (ie. either A, B or C). Utilising the shakedown Range A/B boundary as a yield line does not aim to predict the amount of surface deformation as number of loads are not considered. This method of finite element analysis gives an indication of how much the insitu stresses exceed the shakedown Range A/B stress boundary.

A vertical deformation limit of 0.2mm was found to be an appropriate value for defining when shakedown Range A occurs, determined from the results of pavement tests as reported in Chapter 6. This limit appears to be supported when reviewing Figure 8.1 as 0.2mm is approximately the inflexion point after which the additional benefit of increasing asphalt cover is reduced.

Table 8.1. Plastic finite element analysis with linear shakedown Range A/B boundary yield line.

AC Cover (mm)	Vertical deformation (mm)			Plastic strains (μm/m)			
				Granular		Sub.	Gran.
	Total	Gran.	Sub.	*Depth (mm)*	Max Comp.	Max Comp.	Max Tensile
NI Good: 0	0.55	0.20	0.35	275	1133	3897	-793
50	0.23	0.15	0.08	96	674	1785	-211
100	0.06	0.06	0.00	100	447	0	-37
150	0.02	0.02	0.00	150	303	0	-15
200	0.01	0.01	0.00	200	203	0	-4
NI Poor: 0	1.16	0.60	0.56	275	3308	5365	-1885
50	0.32	0.27	0.05	96	1544	1467	-71
100	0.08	0.08	0.00	100	828	0	-42
150	0.02	0.02	0.00	150	518	0	-26
200	0.00	0.00	0.00	200	314	0	-27
CAPTIF 1: 0	0.84	0.40	0.44	275	2148	4550	-1314
50	0.31	0.24	0.06	96	1204	1664	-106
100	0.08	0.08	0.00	100	708	0	-19
150	0.03	0.03	0.00	150	461	0	-24
200	0.01	0.01	0.00	200	298	0	-17
CAPTIF 2: 0	1.76	0.84	0.91	275	3938	6900	-4425
50	0.57	0.41	0.16	96	1768	2372	-213
100	0.16	0.16	0.00	100	893	0	-19
150	0.06	0.06	0.00	150	579	0	-15
200	0.03	0.03	0.00	200	390	0	-9
CAPTIF 3: 0	0.52	0.21	0.30	275	1234	3632	-704
50	0.21	0.15	0.05	96	714	1564	-142
100	0.06	0.06	0.00	100	466	0	-19
150	0.02	0.02	0.00	150	314	0	-11
200	0.01	0.01	0.00	200	207	0	-15
CAPTIF 4: 0	1.69	0.85	0.84	275	4324	6736	-3683
50	0.48	0.38	0.10	96	1789	2020	-101
100	0.11	0.11	0.00	100	902	0	-26
150	0.04	0.04	0.00	150	574	0	-21
200	0.01	0.01	0.00	200	372	0	-25

8.2.2 UK Pavement Design Examples

Three pavements were chosen from the Highways Agency pavement design manual (2001) for analysis using the shakedown range boundary approach (Chapter 6) and rut depth prediction (Chapter 7). The thicknesses of these pavements were determined from the design chart given for a flexible pavement over a subgrade with a CBR (California Bearing Ratio) of 5% (Figure 8.2 after Figure 3 Pavement Design, The Highways Agency, 2001). Each pavement had 225mm of granular material with asphalt thicknesses of 120, 190 and 285mm representing design lives of 0.1, 1 and 10 msa (million standard axles) respectively. A standard axle was modelled as a 40kN circular wheel load with a contact stress of 750kPa.

8.2.2.1 Shakedown Range Prediction

The three standard cross-sections were analysed using the same finite element method used in Chapter 6 to predict the shakedown behaviour range. For each cross-section, finite element analysis was undertaken to model the two shakedown range boundaries defining stress limits between shakedown Ranges A and B. Material properties for the granular material were the same as those derived for the *NI Good* granular material (Chapter 6). This granular material complies with the UK Highways Agency's specification for aggregate and is regularly used on highway projects in Northern Ireland. Properties for the subgrade with CBR (California Bearing Ratio) of 5% were estimated from the multi-stage Repeated Load Triaxial permanent strain tests for the CAPTIF Subgrade (CBR=11%) as RLT results were not available for a subgrade soil with a CBR of 5%. It was assumed that for a constant confining stress the permanent strain in the RLT test will be the same for a material if the ratios of CBR and cyclic major principal stress (σ_1) are the same. Therefore, each RLT major principal stress (i.e. σ_1) for the CAPTIF subgrade was multiplied by 5/11, being the ratio of the two CBR values, and the stress invariants p and q (Section 2.4.3) were recalculated. Shakedown range boundaries were then determined for the subgrade material based on the adjusted/reduced stress invariants p and q.

Determining the properties of a subgrade soil with a CBR of 5% was based purely on engineering judgement. Therefore, to further investigate the implications of this research on current pavement design procedures, it is recommended Repeated Load Triaxial tests on a subgrade soil with a CBR of 5% be undertaken in a similar testing regime as in the laboratory study in Chapter 3.

Results of the finite element analysis in terms of total surface, aggregate and subgrade deformation are summarised in Table 8.2. Figure 8.3 plots the trend in deformation results predicted from the finite element analysis using the shakedown Range A/B boundary as the Drucker-Prager yield criterion. Determining when shakedown Range A behaviour occurs is judgemental, but based on the result of other pavement tests a deformation criterion of 0.2mm was assigned as a maximum limit in Chapter 6. Therefore, asphalt cover of 120mm for 0.1 msa (million standard axles) could be considered sufficient to ensure a shakedown Range A behaviour and thus unnecessary to increase the pavement thickness above this value for larger traffic volumes. However, a more conservative approach to ensure a shakedown Range A response is to consider the asphalt cover needed when the plastic strains within the subgrade material are nil, and in the granular material are nearly nil. This more conservative criterion occurs when the asphalt cover is 285mm as required for 10 msa. Applying the more conservative approach in practice would set a maximum limit of asphalt cover of 285mm for all design traffic loading and thus save on asphalt cover requirements for design traffic in excess of 10 msa.

Table 8.2. Finite element results for UK Highway Agency Pavement designs with shakedown Range A/B boundary as yield criterion.

UK Design x-sectn		Vertical Deformation (mm)			Plastic strains (μm/m)		
					Granular		Sub.
Asphalt (mm)	Traffic (msa)	Total	Gran.	Sub.	*Depth (mm)*	Max Comp.	Max Comp.
120	0.1	0.13	0.05	0.08	*345 (bott)*	1124	960
190	1	0.03	0.02	0.01	*190 (top)*	168	346
285	10	0.002	0.002	0.00	*285 (top)*	30	0

8.2.2.2 Rut Depth Prediction

The methodology to predict the pavement rut depth attributable to the granular and subgrade layers detailed in Chapter 7 was applied to four standard UK Highway Pavement designs for 0.1, 1, 10 and 80 msa as per Figure 8.2. As used to predict shakedown range behaviour (Section 8.2.2.1) the pavement consisted of asphalt over the *NI Good* granular material on a subgrade of CBR=5%. Constants for the 2 parameter model (Equations 7.4 and 7.5) which calculates permanent strain from stress were unchanged for the *NI Good* granular material (Tables 7.5, 7.6 and 7.7). Determining the 2 parameter model constants for a subgrade of CBR=5% involved multiplying the major principal stress (σ_1) in the permanent strain results for the *CAPTIF Subgrade* material (CBR=11%) by the CBR ratio (i.e. 5/11) and then recalculating stress invariants p and q (Section 2.4.3). Constants were then determined by fitting the model to the adjusted p (mean principal stress) and q (deviatoric stress) values for the permanent strains measured for the *CAPTIF Subgrade* material.

The current method to predict permanent strain from the 2 parameter model is to assume constant permanent strain rates for various load increments. Load increments used in the prediction of rut depth in Chapter 7 were 25,000 to 100,000, 100,000 to 1M and then 1M to 2M cycles. UK design examples were up to 80 msa (million standard axles). Therefore, to extend the permanent strain predictions to 80 msa or more it was assumed the same permanent strain rate from 1M to 2M would apply to all wheel passes in excess of 1M. Assuming a constant permanent strain rate after 1M wheel passes may be a conservative estimate as it is likely for low stresses that the permanent strain rate would decrease with increasing load cycles. However, the RLT permanent strain tests were only for 50,000 loads and extrapolating the results beyond 2 Million loads was dangerous considering the true long term trend in material behaviour is unknown. Further, when investigating the current UK pavement design procedures a conservative approach to rut depth prediction is more appropriate.

As in Chapter 7 the finite element package DEFPAV was used to model the four UK Highway pavements with asphalt covers of 120, 190, 285 and 390mm over 225mm of granular material on top of a subgrade with a CBR of 5%. Principal stresses computed at depth increments directly under the load centre were imported into a spreadsheet where the 3D model was applied to calculate permanent strain at each depth increment. Permanent strain was integrated over the associated depth increment and summed to obtain a surface rut depth for as many loads as needed until a rut depth of 25mm was obtained. A nominal 5mm was added to the rut depth calculated to account for expected inaccuracies in estimating the permanent strain for the first 25,000 loads from multi-stage tests as recommended from results in Chapter 7. Results of rut depth prediction for each cross-section are plotted in Figure 8.4. The end of pavement life was assumed to occur when a rut depth of 25mm occurred. Predicted end of life in relation to asphalt cover is compared with the end of life from the UK Highways Agency's design chart (Figure 8.2) as shown in Figure 8.5. Predicted end of life due to rutting is related to asphalt cover in a linear function with a near perfect fit. This is in contrast with the end of life predicted by the UK Highways Agency where the life in terms of asphalt cover is not related by a linear function. For asphalt covers less than 390mm the UK Highway Agency predicts a shorter life by factors ranging from 5.4 to 200 (Table 8.5).

Table 8.3. Comparison of predicted life with standard UK Highway Agency Designs (Figure 8.2).

Asphalt Cover over 225mm Granular on CBR=5% Subgrade. (mm)	Predicted Life Based on 2 Parameter (Equation 7.5) (msa – *million standard axles*)	Predicted Life from UK Highway Agency Chart (Figure 8.2) (msa)	Ratio of Predicted Life compared with UK Highway Agency
120	20	0.1	200
190	35	1	35
285	54	10	5.4
390	75	80	0.9

Interestingly the life predicted for the asphalt cover of 390mm is nearly the same as in the UK Highway Agency design chart (Figure 8.2). Perhaps this result is just coincidental or perhaps they should be the same. It is possible that for the pavements with asphalt cover < 300mm, the life is shortened due to the tensile fatigue life of the asphalt layer and thus the end of life is a result of cracking rather than rutting. The predicted life based on rut depth calculation does not consider cracking but rutting only. Should this have been the case for the development of the UK Highways Agency's design chart then predicted lives would be nearly the same for all asphalt depths.

Another point relating to predicted rut depth is that only a fraction of the rut depth at the surface is due to rutting in the granular layer as nearly all of the rutting is attributable to the weak subgrade soil (CBR=5%). In fact if the nominal 5mm added to the first 25,000 wheel passes is ignored, only 1mm of rutting of the remaining 20mm occurred in the granular material. Analysis in Chapter 7 also found that for asphalt thicknesses > 90mm the rut depth is governed solely by the subgrade after 100,000 wheel passes. Therefore, given the importance of the subgrade in terms of predicting the rut depth, the fact that the subgrade properties for a material with a CBR=5% were estimated does question the reliability of the predicted rut depth for the UK Highways Agency designs. Nevertheless, an important result for asphalt thicknesses over 90mm is the rutting is primarily attributed to the subgrade materials. This result supports Dormon and Metcalf

(1965) assumption that rutting is a result of vertical compression in the subgrade, although the modelling found, for large granular depths with thin covers of asphalt, that most of the rutting occurs in the granular material.

Prediction of rut depth came from a model that assumes shakedown Range A (Section 2.11.2) does not occur, but rather that a constant permanent strain rate results after 1 million wheel passes. Therefore, it is likely that the estimates of rut depth are conservative. Further, the assumption of a constant permanent strain rate after 1 million wheel passes will never predict a shakedown Range A response, regardless of how thick the asphalt cover is used. However, shakedown Range A behaviour could be assumed to occur when the predicted life is in excess of 200 M wheel passes in terms of rutting. This could occur for strong subgrades, greater depth of granular material and thick asphalt cover.

8.2.3 Material Assessment

A key application of a method to predict rut depth from Repeated Load Triaxial (RLT) tests is its ability to assess the suitability of alternative materials to replace traditional premium quality crushed rock aggregate. Permanent strain RLT testing at a range of stresses is a key component for material assessment via rut depth prediction. The results from the RLT tests are used to derive parameters for a model to calculate permanent strain from any given stress level (Equation 7.5). Pavement analysis is then undertaken to determine the stresses under the load. The calculated stresses are used in the model to calculate the permanent strain, which is then integrated over the depth increment and summed to obtain a rut depth. It was shown that prediction of rut depth progression was accurate most of the time when comparing the results of actual pavement tests. Therefore the rut depth prediction methodology can be used with some confidence when predicting the expected performance of a pavement utilising an alternative material.

Evaluating an alternative material by way of predicting rut depth in a pavement cross-section as intended for its use, is a more robust and “fit for purpose” method of assessment compared to more simpler methods. A simple approach (although not recommended) for material assessment is to undertake a permanent strain RLT test at one particular stress level on both the premium quality crushed rock aggregate typically used for highways and an alternative material. Should the RLT results for the alternative material show the same or less permanent strain than the premium aggregate then the alternative material can be classed as acceptable in terms of deformation resistance. There are two disadvantages of using the simpler “one RLT test” approach. The first is that performance at all stress conditions present in the pavement are not considered. Second, should the alternative material not be as good as the premium aggregate there is not scope to assess the suitability to use the material where stresses in the pavement are lower. For instance, use as a lower sub-base or under thicker asphalt cover. Apart from the lack of flexibility in material assessment with the simpler approach, there is a danger that although the alternative material may show sufficient permanent strain resistance at one set of stress levels, it may in fact fail at another set of stress levels that occur within the pavement.

It is recommended to use the rut depth prediction method for material assessment as detailed in Chapter 7. The method of shakedown range prediction in Chapter 6 is approximate for RLT tests of only 50,000 cyclic loads. For this small number of loads it is uncertain whether or not the ideal condition shakedown Range A will actually occur. Further, Range B condition is often predicted, in which case the permanent strain rate is constant and the magnitude of the rut depth is dependent the number of wheel passes. Also it was found that shakedown Range A was defined when the permanent strain rate was very low. This very low permanent strain rate would predict a small rut depth for traffic volumes of say 2 million standard axles (msa) but a significant rut depth will result for traffic volumes of 80 msa. Rut depth prediction methodology encompasses all shakedown ranges. It also considers the number of wheel loads so that high design traffic volumes of 80 msa are catered for, as well as lower traffic volumes where a more efficient “fit for purpose” pavement design can be found.

There are several steps proposed for the assessment of alternative materials. It is recommended that the same assessment be applied to a standard premium quality aggregate complying with the appropriate material specification to enable a benchmark to be established on the amount of rutting acceptable. Further, there are many different methods used to calculate stresses within a pavement and variations in Repeated Load Triaxial apparatuses. Therefore, it is important to compare alternative materials with pavement designs of known performance when standard materials are used. The steps are:

1. Establish density and moisture content for RLT permanent strain tests;
2. Undertake multi-stage RLT permanent strain tests (number of samples and testing stresses);
3. Determine *2 Parameter Model* constants for permanent strain (Equation 7.5) and resilient properties from RLT tests;
4. Trial design pavement cross-section;
5. Stress analysis of pavement design;
6. From the stress analysis, predict the rut depth using the *2 Parameter Model* with parameters for the good quality premium aggregate and add 5mm to the calculated rut depth to account for post-compaction effects due to traffic and difficulty in determining the initial amount of deformation in multi-stage tests;
7. If necessary, determine an appropriate level of horizontal residual stress to be added to the stresses calculated in the pavement in order to obtain a reasonable prediction of rut depth when the premium quality material is used (provided the design cross-section will provide the required life based on current pavement design standards);
8. Use the *2 Parameter Model* found from RLT testing for the alternative material and the horizontal residual stress determined in step 7. Apply this to the stress analysis in step 5 and calculate the rut depth, with 5mm added as discussed in step 6;
9. If the rut depth calculated in step 8 is below an acceptable value the pavement design and alternative material are acceptable. Acceptable rut depth is the same as that determined for the premium quality aggregate for the very first cross-section assessed and should comply with current pavement design procedures;

10. If rut depth is not acceptable in step 9 then change the design cross-section, for example increasing the asphalt cover thickness, and re-do steps 5, 8 and 9 or reject the material;
11. Before final acceptance of the alternative material consideration is required on the expected long term durability of the material, for example weathering and crushing resistance as required in existing material specifications.

8.3 FINITE ELEMENT MODELLING

The finite element analysis undertaken in Chapter 6 shows that the shakedown range boundaries determined from the laboratory study can be easily accommodated in the ABAQUS finite element package. Shakedown range boundaries can be defined as linear Drucker-Prager yield criterion with a 30kPa horizontal residual stress adjustment. Results of the finite element analysis are plastic strains showing regions in the pavement that have yielded.

Interpreting the results of the finite element analysis in terms of expected shakedown range behaviour is difficult. The intended interpretation was a simple "yes" there were plastic strains (yielding), or "no" there were not any plastic strains (nil yielding) that occurred within the pavement. If there was no plastic strain/yielding in the pavement materials then it could be safely assumed that all of the stresses computed in the pavement fall within the shakedown range boundary. Thus, if the shakedown range boundary was A/B, then for no plastic strains a Range A behaviour would be predicted for the pavement. This approach was taken in the preliminary design of the Northern Ireland field trial where linear elastic analysis was undertaken to compute stresses for a range of asphalt thicknesses, which were then compared with the shakedown range boundaries (see Figure 5.3). However, achieving no plastic strains with the finite element analysis is nearly impossible. This is because the finite element model will allow yielding in the aggregate to occur in order to ensure minimal tensile stresses in the unbound material. Therefore, criteria in terms of maximum allowable plastic strain, which were summed in terms of total permanent deformation at the surface, were developed.

Shakedown Range A was defined to occur when the maximum permanent vertical deformation is less than 0.20mm, as calculated with the yield criterion being the shakedown range boundary A/B, with a 30kPa horizontal residual stress added. The vertical deformation limit was determined by empirical means, where shakedown Range A response was observed for pavement test number 4 (Table 4.1) and a vertical deformation of 0.20mm was computed in the FEM. Therefore, the criterion is valid only where the model assumptions are the same (i.e. porous elasticity, ABAQUS, linear Drucker-Prager yield criterion, 30kPa horizontal residual stress added to the shakedown Range A/B criterion).

A limitation in the finite element method presented is that the magnitude of permanent deformation/rutting is not calculated. Rather, the deformation calculated is simply an indication of the amount of pavement area that has stresses that met or exceeded the shakedown range boundary/yield criterion. The inability to predict a rut depth is a limitation because unless the asphalt thickness is greater than 100mm it is likely a Range B response will be predicted. Range B response is not failure but rather a constant rate of rutting which, unlike Range A behaviour, the magnitude of rutting is affected by the number of wheel passes. Therefore, a method to predict rut depth has been developed and was presented in Chapter 7 *Permanent Deformation Modelling*.

8.4 MODELLING PERMANENT DEFORMATION

8.4.1 1 Parameter Model

A *1 Parameter Model* was developed (Equation 7.3) based on models proposed by other researchers, namely Paute et al (1996). This model predicts a linear rate of rutting for the cases where shakedown Range B response is likely. For low stress levels the model will calculate a low value of permanent strain and therefore it may suffice for expected Range A responses also. There are some limitations of the model proposed. For instance there were a few RLT tests that resulted in high permanent strains but the model predicted permanent strains up to 100 times less than the actual measured values. The RLT results that fell well outside the predictions are real test results and could not be considered merely as outliers. They are a result showing stress conditions where a significant amount of deformation can occur. However, it may be considered that an advantage of the *1 Parameter Model* proposed (Equation 7.3) is that it caters well for the brittle behaviour observed to occur in RLT permanent strain tests where, for most of stress conditions tested, permanent strain is low until such time as a stress limit is exceeded (shakedown range boundary B/C) where failure occurs. However, this brittleness of the prediction of permanent strain will cause some difficulties in application as modified stress ratios in excess of the limits posed by *m* in Equation 7.3 will result in a negative value for permanent strain.

8.4.2 2 Parameter Model

The *2 Parameter Model* to predict permanent strain from any given stress condition was derived from Repeated Load Triaxial tests. Results of using this *2 Parameter Model* to predict rutting were better than expected as there are many differences to loading in the Repeated Load Triaxial (RLT) apparatus than what actually occurs within a material in a real road. Constant confining stresses were used in the RLT tests while in the pavement the confining stresses would be cycled in conjunction with the vertical stresses from passing wheel loads. Further in a real pavement the principal stresses rotate as discussed in Section 2.6.3. Details of the stress path were not required from the RLT test as the model only required stress invariants p and q in the fully loaded state or maximum values.

Permanent strain relationships derived from tests which better simulated loading conditions like the hollow cylinder apparatus (Section 2.5.3) which rotates the principal stresses would result in higher permanent strain for the same fully loaded stress as in the RLT apparatus. Although a test like the hollow cylinder apparatus better simulates real loading conditions, it is likely the rut depth will be over-estimated. This will be the case when the residual horizontal residual stresses are assumed to be nil. As discussed in Section 2.4.6 horizontal residual stresses are unlikely to be nil and can be significant. Predicting rut depth from constant confining RLT tests the horizontal stresses were assumed to be nil, because the actual value of horizontal residual stresses is not known and assuming nil residual stresses led to adequate predictions of rut depth. Should a value of 30kPa be assumed as the residual horizontal stresses then rutting will be under-estimated with models derived from RLT tests at constant confining stress but it is likely to be more accurately predicted with the higher permanent strain tests from a hollow cylinder apparatus. Therefore, in a “roundabout” way the lower permanent strains found from constant confining RLT tests are compensated for in pavement analysis when the horizontal residual stresses are assumed to be nil.

Predicting rutting is more accurate for Range B type behaviour where the long term rutting response is a constant rate of rutting with increasing wheel loads. For pavements with asphalt cover of 90mm stresses are reduced significantly and the calculated permanent strains in the granular material are very small and therefore the relative error is higher. Often the permanent strain rate calculated after 100,000 wheel loads was too small to register being only fractions of one percent. Therefore, for pavements with thick asphalt covers the prediction of rutting should be limited to predicting a Range A type response, where the permanent strain rate is continuously decreasing.

8.5 PREDICTING SHAKEDOWN RANGE A

Reviewing results of Table 8.1 shows that for a asphalt cover of greater than 100mm over 275mm of granular material on a subgrade CBR of 11% shakedown Range A behaviour should occur. Shakedown Range A behaviour is where the rate of rutting is decreasing with increasing load cycles to a point where no further rutting will occur. Pavement Test Section 4 (Chapter 7) with 90mm of asphalt cover confirms, at least for 1.7 million wheel passes, that shakedown Range A behaviour is occurring. However, can confidence in Range A behaviour occurring be extended to design traffic loads up to 80 msa (million standard axles) which can be the case as indicated by the UK Highway Agency's design chart (Figure 8.2)? The answer is possibly not as, although the rate of rutting of 0.5mm per 1 million passes is considered very low as observed for pavement Test Section 4 (Chapter 7) after 1 million wheel passes (and thus assigned as Range A behaviour), after another 78 million wheel passes the rut depth will increase by 39mm! This same analogy can be applied to the permanent strain Repeated Load Triaxial (RLT) results used to define the shakedown Range A/B boundary. When the small permanent strain observed within the limited number of 50,000 load cyclesis increased to allow for 80 million loads then a significant amount of permanent strain may be predicted.

It is unsure whether or not shakedown Range A behaviour will in fact occur as predicted for an asphalt cover of 285mm on a UK Highways Agency road with design traffic of say 80 msa (million standard axles). This is because the shakedown Range A/B boundary is based on Repeated Load Triaxial tests for only 50,000 load cycles being approximately 1/1600th of the total wheel passes for a design traffic loading of 80 msa. Therefore, the shakedown Range A/B boundary is based on testing stresses where it appears the permanent strain rate is decreasing within the short 50,000 loading history. It is unsure whether or not the permanent strain rate will in fact decrease to a point where no further permanent strain will occur or reach a point where the permanent strain rate is constant. Even if the permanent strain rate is small for a testing stress and assigned a shakedown Range A behaviour response this small permanent strain when multiplied 80 million times (being the design traffic load) can often result in a significant rut depth.

8.6 ELASTIC BEHAVIOUR

Elastic properties in terms of modulus and Poisson's ratio have been used in pavement analysis for the calculation of stress. The stress calculated was then used in permanent strain models for the prediction of rut depth. Rut depth predicted was compared to the measured values in the New Zealand (Chapter 4) and Northern Ireland field trials (Chapter 5). Results of this comparison confirmed that rut depth could be predicted for a majority of cases and thus the assumptions used in the analysis are adequate. However, when comparing elastic strains computed in the pavement analysis with those measured insitu a different story is told. Elastic strains computed were less than half those measured in the New Zealand CAPTIF pavement tests. This result commonly occurs in pavement analysis of CAPTIF pavements (Steven, 2004). It is observed that the subgrade constructed insitu at CAPTIF behaves as a spring with very low stiffness. Therefore, high deflections and strains result, although these high deformations are nearly fully recoverable. Thus, the subgrade has a low stiffness insitu but still a relatively high resistance to deformation. Some of the higher strains measured insitu are a result of longer and more complex stress paths that occur insitu. In pavements the confining pressure is cycled and principal stresses rotates with each passing wheel load. The elastic properties of the subgrade obtained in the Repeated Load Triaxial tests were from simple shorter stress paths where the confining pressure was constant and the principal stresses were not rotated. As the loading in the RLT apparatus is less severe, higher stiffnesses are obtained than those that occur insitu.

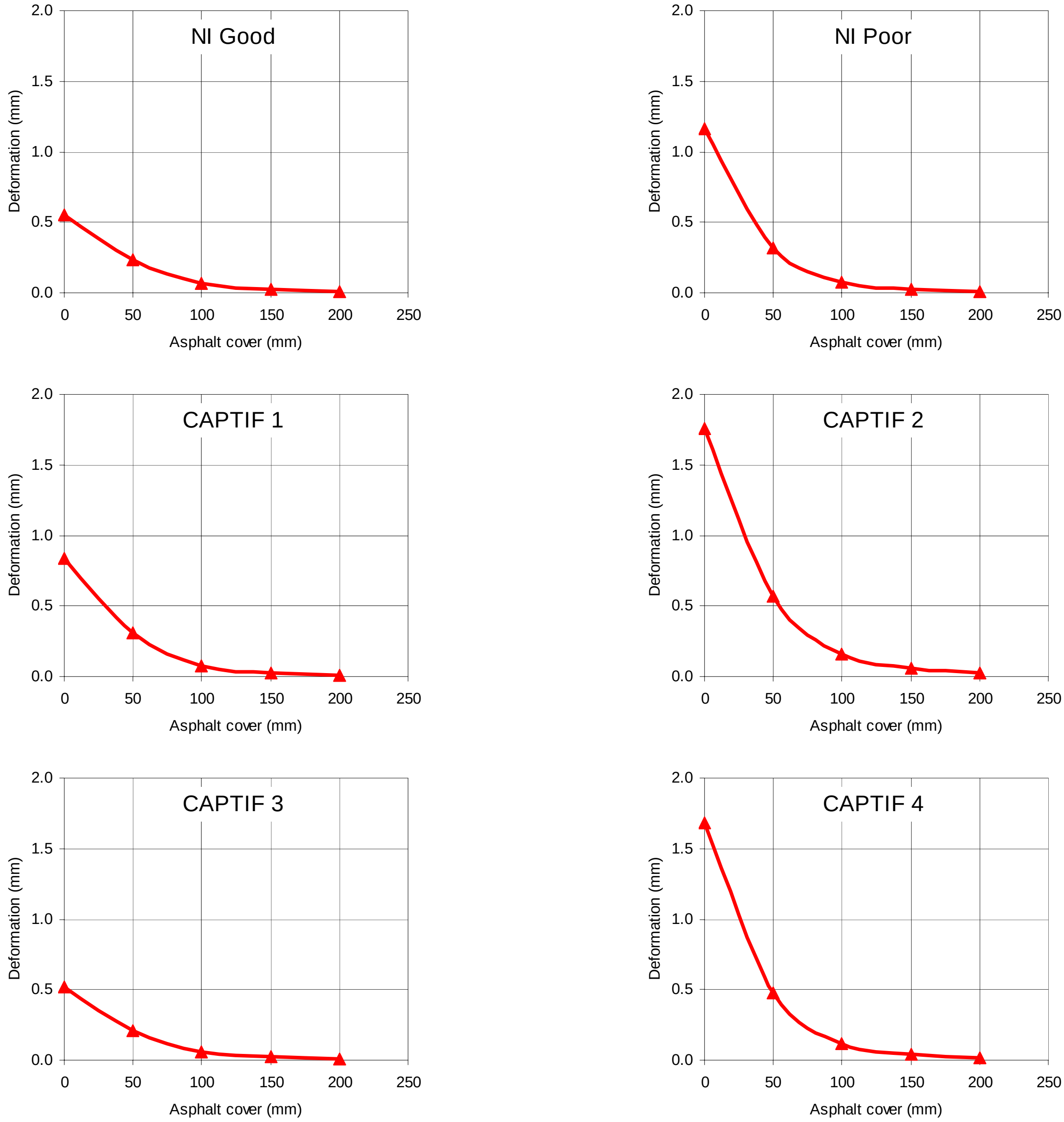

Figure 8.1. Surface deformation from plastic finite element analysis with linear shakedown Range A/B boundary yield line.

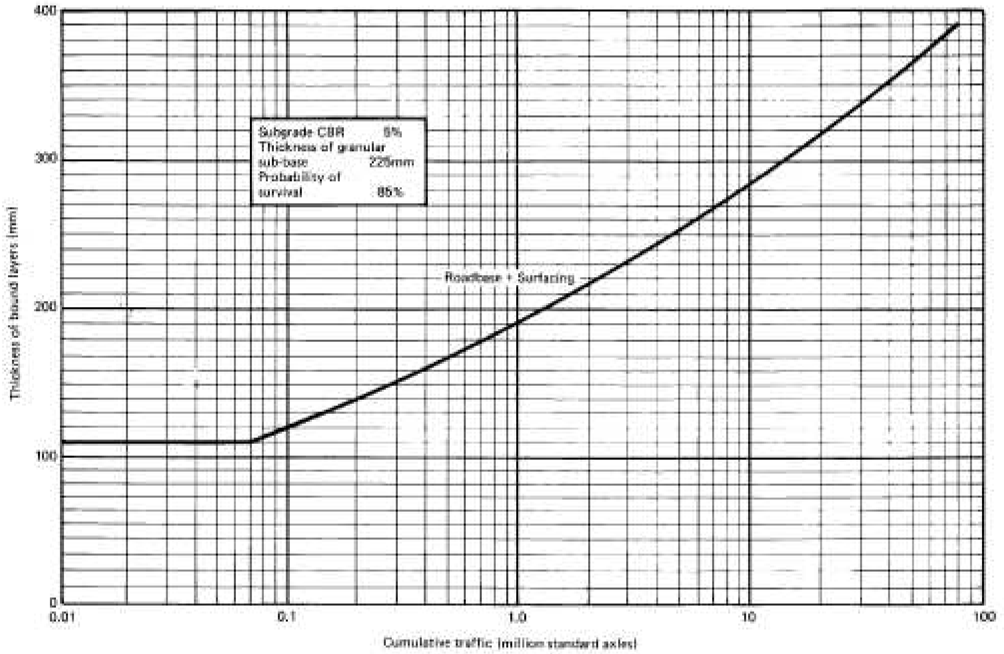

Fig. 3 Design curve for roads with bituminous roadbase

Figure 8.2. UK Higway Agency Pavement Thickness Design Curve (after Figure 3, Pavement Design, The Highways Agency, 2001).

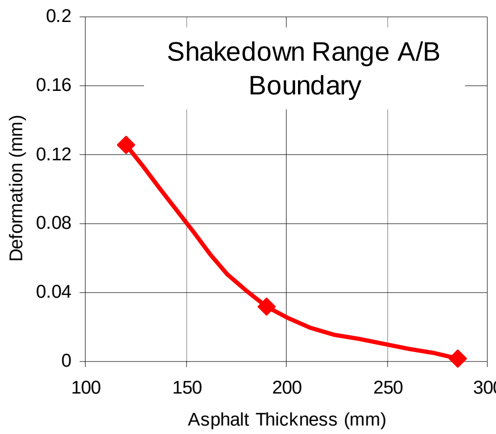

Figure 8.3. Finite element analysis results of UK Highway Agency pavements of asphalt over 225mm granular on subgrade of CBR=5%.

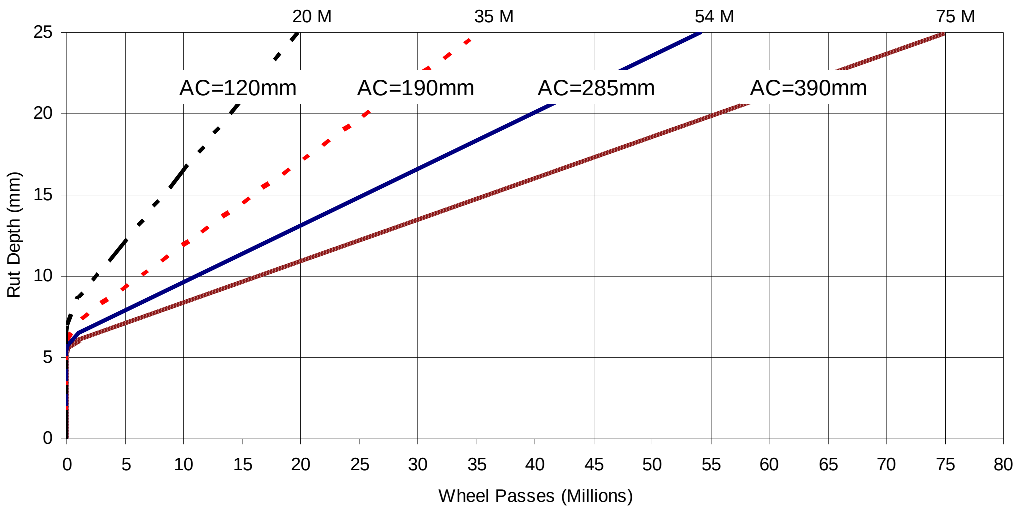

Figure 8.4. Rut depth prediction for standard UK Highway pavement designs.

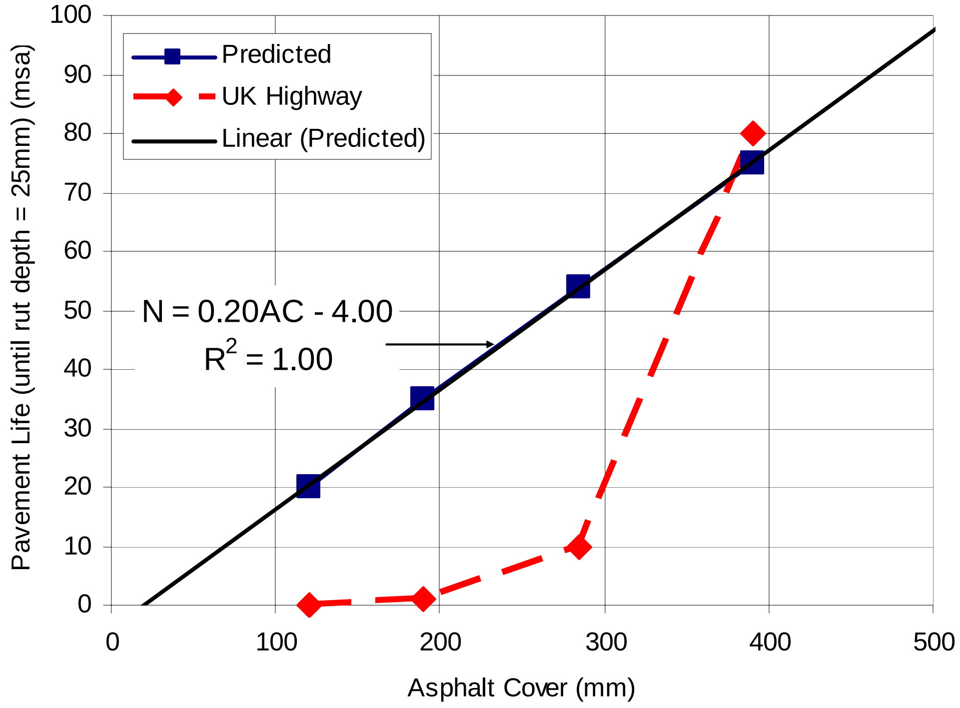

Figure 8.5. Trend predicted in number of wheel passes until end of life for various asphalt cover thicknesses compared with UK Highway requirements.

CHAPTER 9 SUMMARY, CONCLUSIONS AND RECOMMENDATIONS

9.1 SUMMARY

9.1.1 General

The rutting of granular pavements was studied by examining the permanent deformation behaviour of granular and subgrade materials used in a Northern Ireland, United Kingdom pavement field trial and accelerated pavement tests at CAPTIF (Transit New Zealand's test track) located in Christchurch New Zealand. Repeated Load Triaxial (RLT) tests at many different combinations of confining stress and vertical cyclic stress for 50,000 loading cycles were conducted on the granular and subgrade materials. Moisture content was not varied in the RLT tests, although it was recognised that the resulting permanent strain depends on moisture content. However, the aim of the RLT tests was to obtain relationships between permanent strain and stress level. These relationships were later used in finite element models to predict rutting behaviour and magnitude for the pavements tested in Northern Ireland and the CAPTIF test track. Predicted rutting behaviour and magnitude were compared to actual rut depth measurements during full scale pavement tests to validate the methods used.

9.1.2 Repeated Load Triaxial Testing

The aim of the Repeated Load Triaxial tests was to obtain relationships between permanent strain, number of loads and stress level. To cover the full spectra of stresses found in pavement analysis with only three samples, multi-stage RLT permanent strain tests were developed and utilised (Figure 9.1). Relationships between permanent strain behaviour in terms of shakedown behaviour ranges and permanent strain rate stress level could be found from multi-stage RLT permanent strain tests. Shakedown range behaviours defined by Dawson and Wellner (1999) are:

- Shakedown Range A – Decreasing Permanent Strain Rate;
- Shakedown Range B – Constant Permanent Strain Rate;
- Shakedown Range C – Increasing Permanent Strain Rate and Failure.

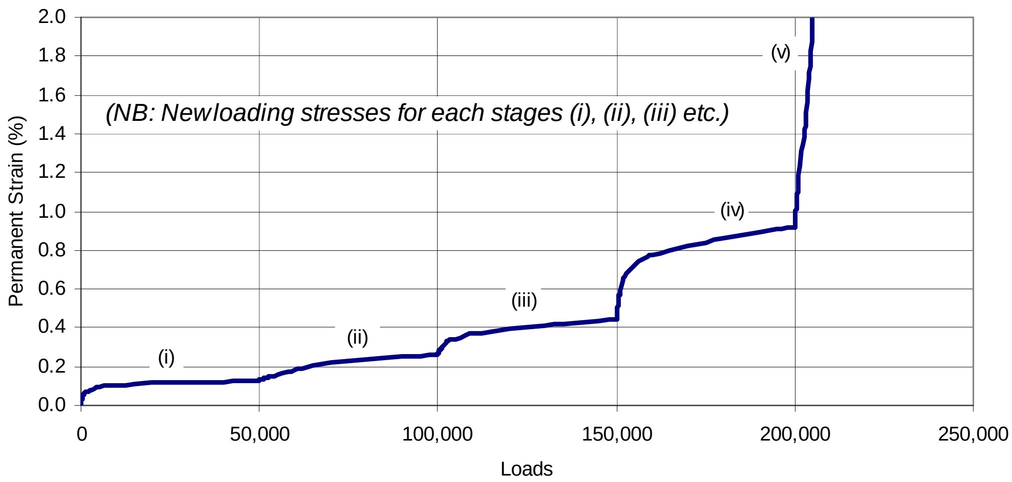

Figure 9.1. Example result from multi-stage Repeated Load Triaxial (RLT) permanent strain tests.

The shakedown Ranges A, B and C could be defined by linear stress boundaries in p (mean principal stress) and q (principal stress difference) stress space as shown in Figure 9.2. These plots show that for a given value of cyclic vertical stress the resulting shakedown range behaviour depends on the level of confining stress which affects the mean principal stress (p).

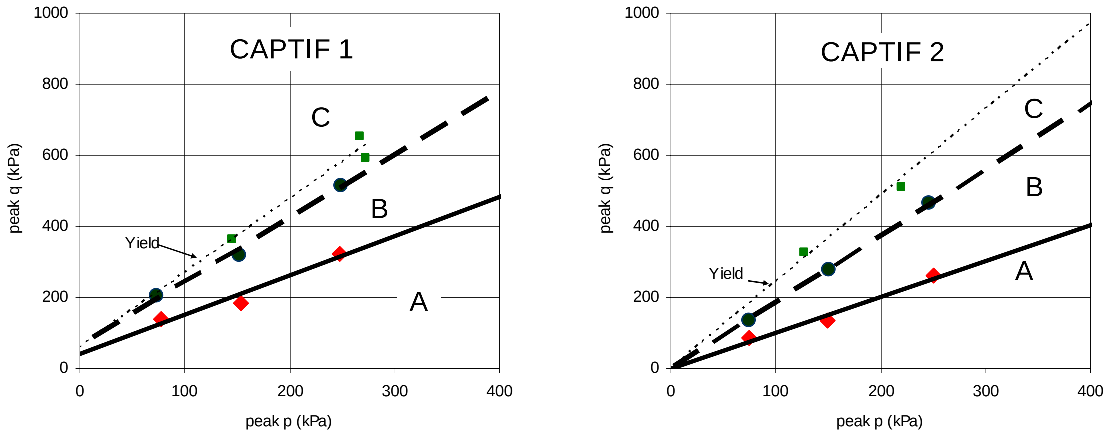

Figure 9.2. Shakedown range stress boundaries defined in *p* (mean principal stress) - *q* (principal stress difference) stress space.

Further analysis of the RLT permanent strain rate (secant) data with respect to stress found a *1 Parameter Model* (Equation 7.3) and repeated below (Equation 9.1) could fit most of the data. However, there were a few levels of stress where failure occurred in the RLT test but the *1 Parameter Model* predicted a low permanent strain rate. Therefore, a *2 Parameter Model* was developed (Equation 7.4) and is repeated below (Equation 9.2). It was found the *2 Parameter Model* fitted the RLT permanent strain rate data well (Figure 9.3) and was later utilised in models to predict surface rut depth.

$$\varepsilon_{p(N)} = \left(K + \frac{(N - 25{,}000)}{1{,}000{,}000}\right) \frac{\dfrac{q}{(p - p^*)}}{b\left(m - \dfrac{q}{(p - p^*)}\right)} \qquad \text{Equation 9.1}$$

$$\varepsilon_{p(\text{rate or magn})} = e^{(a)}\, e^{(bp)}\, e^{(cq)} - e^{(a)}\, e^{(bp)}$$

$$= e^{(a)}\, e^{(bp)}\, (e^{(cq)} - 1) \qquad \text{Equation 9.2}$$

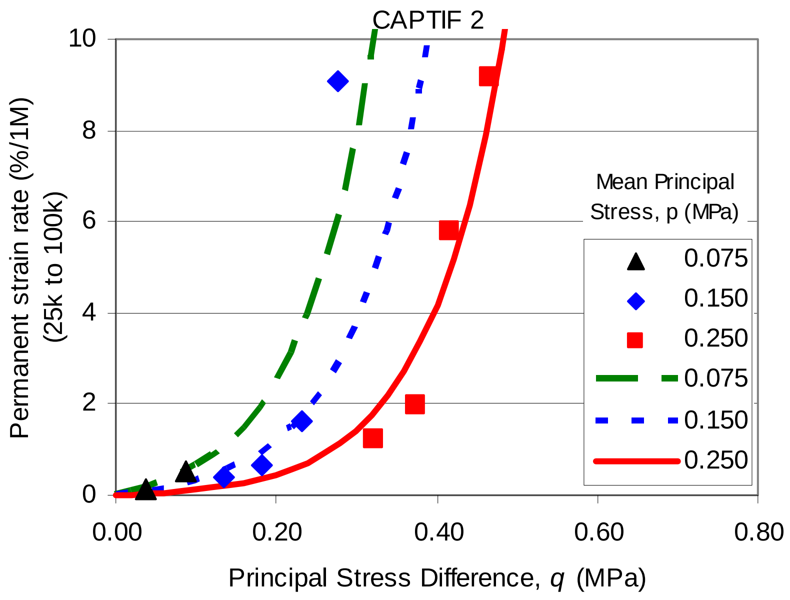

Figure 9.3. Example showing, 2 parameter model (Equation 9.2) fitted to RLT permanent strain rate data for CAPTIF 2 aggregate.

9.1.3 New Zealand Accelerated Pavement Tests

Results from Transit New Zealand's accelerated pavement testing facility (CAPTIF) over the past 6 years were analysed. Pavement tests for at least 1 million loads included a total of 8 different asphalt surfaced granular pavements at two different loads (i.e. different loads on each wheel path at the circular test track) where the asphalt surface thickness was 25mm for 7 sections, while 1 section had an asphalt thickness of 90mm. A total of 4 aggregates and 1 subgrade were used in the tests.

9.1.4 Northern Ireland Field Trial

A pavement trial was constructed on an access road to Ballyclare landfill in Northern Ireland, UK. The field trial had approximately 100mm of asphalt cover over 650mm of granular material on a solid rock subgrade. This trial was instrumented with strain and stress gauges although the measured results were varied and difficult to determine stresses and strains that represented different wheel loads and locations within the pavement. Despite the shortcomings of the field trial the progression of rut depth was accurately determined from transverse profile measurements. The average rut depth was 4mm with progression having stabilised to less than 1mm per year and it is predicted a shakedown Range A behaviour is most likely.

9.1.5 Predicting Rutting Behaviour

Finite element analysis was conducted on pavements tested at CAPTIF (NZ APT) and the Northern Ireland field trials for the purpose of predicting the shakedown behaviour range (A, B or C). It was found the shakedown range boundaries A/B and B/C defined as linear functions of q (deviatoric stress) and p (mean principal stress) for the pavement materials in the laboratory study were defined as Drucker-Prager yield criteria in the ABAQUS finite element package. However, it was necessary to translate the shakedown range boundaries by adding 30kPa horizontal residual stress assumed to occur during compaction of the pavement, before being defined in the finite element model (FEM) as yield criteria.

Results of the finite element analysis were plastic strains and total vertical deformation obtained for the two shakedown range boundaries A/B and B/C defined as yield criteria. The amount of plastic strains and total vertical deformation gives an approximate indication of the amount of yielding that has occurred. Regions in the pavement that have yielded are considered locations where the stress level meets or exceeds the shakedown range boundary A/B or B/C. Based on results of New Zealand accelerated pavement tests and the Northern Ireland field trials 0.20mm was derived as a suitable limit for the amount of permanent deformation where shakedown Range A is likely.

The finite element analysis used simple material models and a readily available commercial finite element model to predict shakedown range behaviour. Therefore, the method could readily be applied by pavement designers with access to a finite element model. However, the inability to predict a rut depth is a limitation.

9.1.6 Predicting Rut Depth

To predict rut depth of the pavements tested at CAPTIF and the Northern Ireland field trials a series of steps was required. The first step was to extrapolate the RLT permanent strain tests to the number of load cycles of interest. Generally, the load cycle of interest was 1 million (being the same as that tested at CAPTIF). The extrapolation method has the most significant effect on the rut depth calculated and it was found that assuming a power law model resulted in predicted rut depths close to those measured during the pavement trials. A linear extrapolation resulted in calculated rut depths of the order of 100mm while the measured rut depths were around 10mm and thus the linear extrapolation was discounted. After extrapolation the *2 Parameter Model* (Equation 7.4) was fitted to secant permanent strain rates from 0 to 25,000, 25,000 to 100,000, 100,000 to 1M and 1M to 2M load cycles as extrapolated from measured RLT test permanent strain results. These loading increments were found to match the trend in rut depth observed to occur in the pavement tests.

DEFPAV, an axisymmetric finite element model, was used to determine stresses within the pavement for 17 different pavement tests reported in Chapters 4 *New Zealand Accelerated Pavement Tests* and 5 *Northern Ireland Field Trial*. The *2 Parameter Model* (Equation 7.4) was then applied to stresses calculated within the pavement to determine permanent strain at 25,000, 100,000, 1M and 2M wheel loads. Permanent strains calculated under the load centre were multiplied by their associated depth increment and summed to obtain a surface rut depth at the various numbers of wheel passes. It was found that the trend (long term tangential rate of rutting) in rut depth progression was accurately predicted for 11 out of the 17 tests, while the magnitude of rut depth predicted for these 11 tests was within 3mm of the measured values. Predictions of rutting for pavement tests with thick asphalt covers of 90 and 100mm were poor. For these pavements the permanent strain rate in the granular materials calculated to occur from 100,000 to 1M load cycles was a small fraction of one percent and too low to register as additional rutting (i.e. < 0.01mm). Thus the model predicts a Range A response rather than an accurate magnitude of permanent strain.

9.2 CONCLUSIONS

9.2.1 Repeated Load Triaxial Testing

The following conclusions were found from the laboratory study:

- To ensure consistent RLT specimens it was found necessary to separate granular material into various size fractions and later re-mix to the defined particle size distribution;

- Vibrating hammer compaction tests resulted in differences between maximum dry density and optimum moisture content for different materials, which are due to many factors such as: the source rock solid density, inter particle friction, PSD and fines content, further:

    - The granular materials with higher fines contents, being CAPTIF 2 and CAPTIF 3, do result in the highest density due to the fact that the fines will fill the small void spaces between the stones;

    - The lowest maximum dry density obtained for the NI Good material is due to the solid rock having the lowest density.

- Results of the monotonic shear failure tests show relatively high angles of internal friction for all materials, where for every 1 kPa increase in confining stress the incremental rise in deviatoric stress, until failure, is nearly 2 kPa;

- Apparent cohesion is seen in all materials except CAPTIF 2 and CAPTIF 4 and is due to the matrix suction and strong particle interlock with crushed rock materials;

- CAPTIF 2 material which is the same as CAPTIF 1 but with 10% by mass of silty-clay fines added showed a higher friction angle than CAPTIF 1, while the opposite would be expected due to the lubricating effect of silty-clay fines on the stones;

- The CAPTIF Subgrade material being a silty-clay had a friction angle of 44 degrees, being within 2 degrees of several granular materials;

- Multi-stage RLT permanent strain tests at a range of stress conditions proved an efficient means to cover the full spectra of stresses expected to occur in a pavement under wheel loading;

- Results from the RLT permanent strain tests could be categorised into one of three possible long term (i.e. after 30,000 load cycles) shakedown Ranges: A (decreasing strain rate); B (constant permanent strain rate); and C (increasing permanent strain rate);

- Plotting the fully loaded testing stresses in *p* (mean principal stress) -*q* (deviatoric stress) stress space with each point labelled with either shakedown Range A, B and C, it was found that:

    - A stress boundary existed in *p* (mean principal stress) – *q* (deviatoric stress) stress space between the various shakedown ranges and the A/B and B/C boundary could be defined by linear functions;

- The shakedown Range B/C boundary plotted close to the yield line (obtained from monotonic shear failure tests) while the shakedown Range A/B boundary had a gradient much lower than the B/C boundary (approximately half);

- The shakedown Range B/C boundary was similar for all the materials ranging from a silty-clay subgrade, a granular material contaminated with fines to premium quality crushed rock, which suggests parameters obtained from failure or near failure conditions do not adequately distinguish between the strength of the various materials;

- The shakedown Range A/B boundary was better able to distinguish between expected performance in terms of resistance to deformation for all the materials;

- The silty-clay soil (CAPTIF Subgrade) and the granular material contaminated with silty-clay fines, which exhibited the highest permanent strains, resulted in the flattest slope for the linear function defining the shakedown Range A/B boundary;

- The k-θ model that relates resilient modulus with bulk stress showed a poor fit to the measured RLT data, although the goodness of fit varied depending on material;

- CAPTIF 2 material, with the highest magnitude of permanent strain compared to the other granular materials, resulted in the highest stiffness as determined from the k-θ model; this suggests that stiffness alone is a poor indicator of expected performance, in–pavement, of a granular material;

- Parameters for the porous elasticity model, as recommended for use in the ABAQUS finite element package later used in Chapter 6, were obtained, although the fit to the measured data was poor, due to:

    - the testing stresses chosen were such that for several tests (3 to 10) that although the maximum deviatoric stress, q increased the maximum mean principal stress, p remained constant, thus the volumetric strain calculated from the porous elasticity model would remain the same regardless of changes in q.

9.2.2 New Zealand Accelerated Pavement Tests

- Range B behaviour (where the long term deformation rate remains nearly constant) was assigned to nearly all the pavement tests with 25mm asphalt cover;

- Two tests at a 60kN load with the CAPTIF 3 material used in the 2003 trial produced Range A behaviour, although this result is questionable because the wheel path for the lighter load of 40kN resulted in Range B behaviour;

- Range A behaviour was assigned to the pavement test with 90mm asphalt cover;

- Reviewing the Emu strain coil static spacings at regular loading intervals for the 2001 tests shows that 40 to 60% of the surface deformation can be attributed to the granular material;

- Peak deflections in general did not change during the testing of the pavements up to 1.4 million wheel passes;

- Insitu measurements of stress and strain in the subgrade soil showed a gradual increase with increasing wheel passes;

- Insitu strains measured in the granular materials tended to decrease with increasing wheel passes indicating a stiffening of these materials, possibly due to tighter interlock being developed and/or build up of lateral residual stresses increasing the confinement;

- Results of calculating insitu stiffnesses for the 2001 tests show all the granular materials to be highly non-linear with respect to stress;

- Excavated trenches at the end of 2001 tests show that over half the surface deformation can be attributed to the granular materials.

9.2.3 Northern Ireland Field Trial

- The pavement could not be constructed to achieve the intended design pavement depths;

- There was significant scatter in insitu measurements of stress and strain such that differences due to axle load could only be approximated by using the upper 90th percentile values;

- The progression of rut depth was accurately determined from transverse profile measurements.

- The average rut depth was 4mm with progression having stabilised to less than 1mm per year and it is predicted a shakedown Range A behaviour is most likely.

9.2.4 Predicting Rutting Behaviour

- For the purpose of predicting the shakedown behaviour range (A, B or C) for the pavement as a whole, the shakedown range boundaries A/B and B/C found for the pavement materials in the laboratory study could be readily defined as Drucker-Prager yield criteria in the ABAQUS finite element package;

- Horizontal residual stresses built up during compaction of the granular layers could be easily be accommodated by translating the shakedown range boundary defined as a yield criteria with ABAQUS;

- A horizontal residual value of 30kPa (identified in the literature review as being an appropriate value) was found to give a realistic prediction of shakedown range behaviour for the pavement trial sections modelled;

- The amount of plastic strains and total vertical deformation computed in the finite element model gives an indication of the amount of yielding that has occurred;

- Regions in the pavement that have yielded are considered locations where the stress level meets or exceeds the shakedown range boundary A/B or B/C;

- Based on results of New Zealand Accelerated Pavement Tests and the Northern Ireland field trials an acceptable amount of total permanent deformation where shakedown Range A is likely was established as 0.20mm;

    - The deformation limit of 0.20mm is purely empirically based and is only valid for assumptions used in its derivation;

- A reduction in wheel load had a greater effect on reducing the total deformation than a reduction in the contact stress;

- Prediction of shakedown range behaviour of the pavement as a whole could easily be accomplished utilising material models readily available in a commercial finite element model;

- Predicting shakedown range behaviour provides a methodology to determine the minimum asphalt cover requirements to ensure a stable shakedown Range A response;

9.2.5 Predicting Rut Depth

1 Parameter Model

- An asymptotic *1 Parameter Model* being an adaptation of the Paute et al (1996) model was found to fit the RLT results the best compared to those 1 Parameter Models proposed by other researchers, and in particular it was able to provide a stress limit where failure occurred (i.e. permanent strain is calculated to be infinite), however:

- The *1 Parameter Model* was proved to be inadequate as, for some test stresses, very low permanent strains were calculated whereas the measured values in the RLT test were high permanent strains;

- The *1 Parameter Model* could not be applied to predict rut depth as the pavement analysis computed stress ratios that exceeded the stress boundary, resulting in a negative (expansive) permanent strains being calculated;

2 Parameter Model

- A *2 Parameter Model* relating permanent strain as a function of two independent variables, being the stress invariants p (mean principal stress) and q (deviatoric stress), could be fitted adequately to all RLT test results;

- The *2 Parameter Model* showed the same trend as that obtained from the RLT tests where, for a constant mean principal stress, as the deviatoric/axial stress increases the permanent strain increases exponentially;

- To predict the permanent strain for up to 1.4 M wheel load cycles the *2 Parameter Model* could be fitted to extrapolated RLT data;

- The axisymmetric finite element program DEFPAV (Snaith et al., 1980) could compute principal stresses at depth increments directly under the load for later use with the *2 Parameter Model* to compute permanent strain;

- Rut depth of the pavement could be computed by summing the deformations calculated at each depth increment found from the *2 Parameter Model* applied to the stresses determined from the pavement analysis;

- For predicting rut depth for the field trials it was necessary to extrapolate the RLT permanent strain results using a power law model since this gave the best fit to the measured data along with the most accurate predictions of rut depth;

- It was found that the trend in rut depth progression (long term rate of rutting) was accurately predicted for 11 out of the 17 pavement tests reported in this thesis;

- Adjusting the rut depth predicted at 25,000 wheel passes by up to a few millimetres resulted in an accurate prediction of rut depth for these 11 tests, i.e. where the rut depth progression was accurately predicted;

- Predictions of rutting for pavement tests with thick asphalt cover of 90 and 100mm were poor; for these pavements the permanent strain rate in the granular materials calculated to occur from 100,000 to 1M load cycles was a fraction of one percent and too low to register as additional rutting (i.e. < 0.01mm);

- It is concluded that the *2 Parameter Model* derived from RLT permanent strain tests can be utilised in analysis of pavements with thin asphaltic layers to calculate the rut depth for any given number of load cycles. However, the chosen method of extrapolation of the RLT permanent strain results has a significant effect on the resulting rut depth and the power law model used for extrapolation gave the most accurate prediction of rut depth.

9.3 RECOMMENDATIONS

This thesis has presented and validated a method to predict the rut depth of a granular pavement. In particular the method proved more accurate in predicting rut depth for pavements with thin surfacings. Current pavement design methods for a thin surfaced granular pavement use an empirical relationship between vertical resilient strain on top of the subgrade and pavement life in terms of number of passes of an Equivalent Standard Axle (ESA). This current design method is a indirect method of predicting pavement performance. Variations in aggregate strength in terms of rutting resistance cannot be evaluated using current design methods. For example, recycled and alternative materials that do not meet material specifications cannot be evaluated with current design procedures and, thus, are often rejected by road controlling authorities. However, the method developed to calculate rut depth from RLT permanent strain tests is a fundamental design method and directly predicts performance in terms of rut depth. This design method allows for the prediction of performance for a range of materials regardless of compliance to a specification. Further, the ability to predict rut depth allows the determination of the best performing aggregates so that these can be targeted for higher traffic roads where the highest rut resisting aggregates are needed. In addition, the benefits of modifying aggregates with small quantities of cement type binders in terms of an increase in rut resistance can be evaluated. It is therefore recommended that the method developed in this thesis for predicting rut depth be examined for its use by road controlling authorities for the following applications:

- to evaluate the use of alternative and recycled materials that do not meet existing specifications;

- to rank granular materials used for pavement base material in terms resistance to rutting and use this ranking to group the granular materials into those applicable for low, medium and high traffic intensities;

- to evaluate the rut resisting beneficial properties that are possible when adding small quantities of cement type binders to granular materials and thus to identify these modified materials as suitable for the highest traffic roads.

Recommendations for future research:

- One key factor that affects permanent deformation is moisture content and its effect should be investigated by further RLT tests on the same materials;

- Development of a multi-stage RLT test in which a minimum number of tests is conducted while still having the ability to determine the model parameters. This will reduce the cost of conducting RLT tests and thus be more readily considered by road controlling authorities;

- Further research is needed to test the ability to predict the in-service performance in terms of rutting of non-standard materials, such as those from recycled sources;

- The ABAQUS Finite Element Model used in this thesis was an approximation where it is empirically based, therefore, research is required to develop more appropriate material models that can simulate the build up of residual stresses due to the yielding of the aggregate.

REFERENCES

AASHO (1962). The AASHO Road Test: Proceedings of a Conference: Special Report 73. Highway Research Board. National Academy of Sciences, National Research Council, Washington DC, USA.

AASHTO. (1978). Standard specifications for transportation materials and methods for sampling and testing. Part 2. Methods for sampling and testing. American Association of State Highway and Transportation Officials (AASHTO), Washington, D.C. USA.

AASHTO. (1994). Resilient modulus of unbound granular base/sub-base materials and subgrade soils – SHRP Protocol P46. American Association of State Highway and Transportation Officials, Standard T294-94, Washington DC, USA.

ABAQUS Theory Manual Version 5.6 (1996).

Airey, G. Collop, A. Dunhill, S. (2002). A constitutive material modelling methodology for asphalt mixtures. Ninth International Conference on Asphalt Pavements, August 17-22, 2002, Copenhagen Denmark. Volume 1: 6-1. International Society for Asphalt Pavements.

Akou, Y. Heck, J.V. Kazai, A. Hornych, P. Odéon, H. Piau, J.M. (1999). Modelling of flexible pavements using the finite element method and a simplified approach. Unbound Granular Materials – Laboratory testing, in-situ testing and modelling. Edited by A. Gomes Correia, Technical University of Lisbon. Proceedings of an International Workshop on Modelling and Advanced Testing for Unbound Granular Materials Lisbon 21-22 January 1999.

Aksnes, J. Hoff, I. Mork, H. (2002). Measurement of edge effects on pavements with thin asphalt surfacing. Ninth International Conference on Asphalt Pavements, August 17-22, 2002, Copenhagen Denmark. Volume 1: 10-5. International Society for Asphalt Pavements.

Allen, J. (1973). The effect of non-constant lateral pressures of the resilient response of granular materials, PhD thesis, University of Illinois at Urbana-Champaign, Urbana, Ill.

Almeida, J. R. de. (1986). Structural Analysis of Rigid Pavements by the Finite Element Method. MSc Thesis, Technical University of Lisbon (in Portuguese).

Almeida, J. R. de. (1993). Development and validation of a finite element code for pavement analysis. Flexible Pavements. Edited by A. Gomes Correia, Technical University of Lisbon. Proceedings of the European Symposium Euroflex 1993, Lisbon, Portugal 20-22 September 1993.

Amedeus (2000). AMADEUS: Advanced Models for Analytical Design of European Pavement Structures. RO-97-SC.2137. Project Funded By The European Commission Under The Transport Rtd Programme Of The 4th Framework Programme

Anderson and Collins, I.F. (1995). "Plane strain stress distributions in discrete and blended coated solids under normal and sliding contact." *Wear* 185, pp. 23-33.

ANSYS (2002). User's Manual-revision 6.1. Swanson Analysis Systems, Inc., Huston, PA, USA.

Antunes M. L. (1993): Avaliação da capacidade de carga de pavimentos utilizando ensaios dinâmicos (Pavement bearing capacity evaluation using dynamic tests) PhD thesis, LNEC/Technical University of Lisbon, October 1993. *(cited in Amedeus, 2000).*

Arnold, G. Sharp, K. Steven, B. (1999). Towards the Development of a Cooperative Research Program Involving ALF and CAPTIF. Transfund New Zealand, Wellington, New Zealand.

Arnold, G. Alabaster, D. Steven, B. de Pont, J. (2003). Effect on Pavement Wear of an Increase in Mass Limits for Heavy Vehicles – Stage 3. Transfund New Zealand, Wellington, New Zealand.

Arnold, G. Dawson, A. Hughes, D. & Robinson, D. (2002). The application of shakedown approach to granular pavement layers. Ninth International Conference on Asphalt Pavements, August 17-22, 2002, Copenhagen Denmark. International Society for Asphalt Pavements.

Arnold, G. (2000). Performance based specifications for road construction and materials. UNBAR 5. University of Nottingham, UK.

Arnold, G. Alabaster, D & Steven, B. (2004). Damage law exponents for thin surfaced granular pavements. UNBAR 6. University of Nottingham, UK.

Arnold, G. Alabaster, D. Steven, B. (2001). Prediction of pavement performance from repeat load triaxial tests on granular materials Transfund New Zealand Research Report.

Arnold, G., Steven, B., Alabaster, D., Fussell, A. (2004a). Effect on pavement surfacing wear of an increase in mass limits for heavy vehicles – Part 3. Transfund New Zealand Research Report. In press.

Arnold, G., Steven, B., Alabaster, D., Fussell, A. (2004b). Effect on pavement wear of an increase in mass limits for heavy vehicles – concluding report. Transfund New Zealand Research Report. In press.

Australian Standards. (1995). Determination of the resilient modulus and permanent deformation of granular unbound materials. Standards Australia, AS 1289.6.8.1. Australia.

AUSTROADS. (1992). Pavement Design: A Guide to the Structural Design of Road Pavements. AUSTROADS, Sydney 1992.

Barksdale, R. D. (1972). Laboratory evaluation of rutting in basecourse materials. Proc., 3rd Int. Conf. on the Struct. Design of Asphalt Pavements, London, 161-174.

Barksdale, R. D. (1991). *The aggregate handbook*. National Stone Association, Washington, D.C.

Basma, A & Al-Suleiman, T. (1991). Climatic considerations in new AASHTO flexible pavement design. Journal of Transportation of Engineering, Vol 117, No. 2, ASCE, USA.

Becker, A.A. (2004). An Introductory Guide to Finite Element Analysis. Series Editor, Roger C. Baker. Professional Engineering Publishing Limited, London and Bury St Edmunds, UK.

Bonaquist, R. F., and Witczak, M. W. (1997). ‘‘A comprehensive constitutive model for granular materials in flexible pavement structures.’’ Proc., 8th Int. Conf. on Asphalt Pavements, Vol. 1, 783–802.

Boulbibane, M. and Weichert, D. (1997). “Application of shakedown theory to soils with non associated flow rules.” *Mechanics Research Communications*, Vol. 24, No. 5, pp. 516-519.

Boulbibane, M. and Collins, I.F. (1999a). A geomechanical analysis of unbound pavements based upon shakedown theory. University of Auckland, 1999.

Boyce, J. R. (1976). The behaviour of granular material under repeated loading. PhD Thesis, University of Nottingham, UK.

Boyce, J. R. (1980). A non-linear model for the elastic behaviour of granular materials under repeated loading. Proc., Int. Symp. on Soils under Cyclic and Transient Loading, Swansea, UK. 285–294.

Brown, S. F., and Pell, P. S. (1967). ‘‘An experimental investigation of the stresses, strains and deflections in a layered pavement structure subjected to dynamic loads.’’ Proc., 2nd Int. Conf. Struct. Des. of Asphalt Pavements, 487–504.

Brown, S. F. (1996). 36th Rankine Lecture: Soil Mechanics in Pavement Engineering, Géotechnique, Vol. 46, No. 3, 1996, pp 383-426.

Brown, S. F., and Hyde, A. F. L. (1975). Significance of cyclic confining stress in repeated-load triaxial testing of granular material. Transp. Res. Rec. 537, Transportation Research Board, Washington, D.C., 49–58.

Brunton, J. M. & Almeida, J. R. (1992). Modelling material non-linearity in a pavement backcalculation procedure, Transp. Res. Record No. 1377, Transportation Research Board, Washington, DC, 99-106.

BS 1377-4: (1990). Soils for civil engineering purposes. Compaction-related tests (AMD 8259) (AMD 13925). BS 1377-4:1990. BSI.

BS 812-105.2:(1990) Methods for determination of particle shape, elongation index of coarse aggregate. BSI

Burmister, D. M. (1945). The general theory of stresses and displacements in layered systems, Journal of Applied Physics, Vol. 16(2), pp. 89-96; Vol. 16(3), pp. 126-127; Vol. 16(5), pp. 296-302.

Cebon, D. (1999). Handbook of vehicle-road interaction. Swets & Zeitlinger, Lisse, Netherlands.

CEN (2004). Unbound and hydraulically bound mixtures – Test methods – Part 7: Cyclic load triaxial test for unbound mixtures. European Committee for Standardisation, No. prEN 13286-7, Brussels, Belgium.

Chan, F. W. K. (1990). Permanent deformation resistance of granular material layers in pavements. PhD Thesis, University of Nottingham, UK.

Chen, W.-F. (1994). Constitutive equations for engineering materials, Elsevier, New York.

Chen, W.-F. and D. J. Han. (1988). Plasticity for structural engineers, Springer-Verlag, New York.

Craig, R. F. (1992). Soil Mechanics – Fifth edition. Department of Civil Engineering, University of Dundee, UK. Published by Chapman and Hall, London, UK.

Croney, D. (1952). The movement and distribution of water in soils, Geotechnique 5, No. 1, 1-16.

Croney, D. & Coleman, J. D. (1952). The estimation of the vertical moisture distribution with depth in unsaturated cohesive soils, Road Note No. 1709, DSIR, HMSO.

Croney, D., Croney, P. (1991). The design and performance of road pavements. Second Edition, Published by McGraw Hill International. Maidenhead, UK.

Dawson, A. R., Thom, N. H., and Paute, J. L. (1996). ‘‘Mechanical characteristics of unbound granular materials as a function of condition.’’ Flexible Pavements, Proc., Eur. Symp. Euroflex 1993, A. G. Correia, ed., Balkema, Rotterdam, The Netherlands, 35–44.

Dawson A R and Wellner F. (1999). Plastic behavior of granular materials, Final Report ARC Project 933, University of Nottingham Reference PRG99014, April 1999.

de Beer, M. Fisher, C. Jooste, F. J. (2002). Evaluation of non-uniform tyre contact stresses on thin asphalt pavements. Ninth International Conference on Asphalt Pavements, August 17 – 22, 2002, Copenhagen, Denmark.

de Pont, J., Steven, B., Alabaster, D., Fussell, A. 2001. Effect on pavement wear of an increase in mass limits for heavy vehicles. Transfund New Zealand Research Report No. 207. 55pp.

de Pont, J., Steven, B., Alabaster, D., Fussell, A. 2002. Effect on pavement wear of an increase in mass limits for heavy vehicles – Stage 2. Transfund New Zealand Research Report No. 231. 50pp.

de Pont, J. J. (1997). OECD DIVINE Project - Element 1. Longitudinal Pavement Profiles. Research Report 708, Industrial Research Limited, Auckland.

de Pont, J. J., and Pidwerbesky, B. (1995). The Impact of Vehicle Dynamics on Pavement Performance. Fourth International Heavy Vehicle Weights and Dimensions Symposium, Ann Arbor, Michigan, 323-332.

de Pont, J. J., Pidwerbesky, B. D., and Steven, B. D. (1996). The Influence of Vehicle Dynamics on Pavement Life. Fourth Engineering Foundation Conference on Vehicle-Infrastructure Interaction, San Diego.

Desai, C. S. and H. J. Siriwardane, 1984, Constitutive laws for engineering materials; with emphasis on geologic materials, Prentice Hall, Englewood Cliffs, New Jersey.

Dodds A, Logan T, McLachlan M & Patrick J, 1999, Dynamic Load Properties of New Zealand Basecourse, Transfund New Zealand, Wellington, New Zealand.

Dormon, G.M., and Metcalf, C.T. (1965). Design Curves for Flexible Pavements Based on Layered System Theory, Highway Research Record 71, Highway Research Board, Washington, D.C., 1965, pp. 69 83.

Drucker and Prager (1952) – Cited in Chen (1975).

Duncan, J.M. & Seed, R.B. (1986). Compaction induced earth pressures under K_o conditions. Proceedings ASCE. Vol. 112, No. 1, pp. 1-23.

Duncan, J. M., Monismith, C. L. & Wilson, E. L. (1968). Finite element analysis of pavements, Highway Res. Record No. 228, Highway Research Board, Washington, DC, 18-33.

Dunlap, W. A. (1963). ‘‘A report on a mathematical model describing the deformation characteristics of granular materials.’’ Tech. Rep. No. 1, Proj. 2-8-62-27, Texas Transp. Inst., Texas A&M University, College Station, Texas.

Gillett, S. (2003). Accuracy in mechanistic pavement design consequent upon unbound material testing. PhD Thesis, University of Nottingham, UK.

Guezouli, S. Elhannani, M. Jouve, P. (1993). NOEL: A non linear finite element code for road pavement analysis. Flexible Pavements. Edited by A. Gomes Correia, Technical University of Lisbon. Proceedings of the European Symposium Euroflex 1993, Lisbon, Portugal 20-22 September 1993.

Harichadran R.S., Baladi G.Y. and Yeh M.S. (1989): Development of a computer programme for design of pavement systems consisting on bound and unbound materials. FHWA-MI-RD-89-02. Michigan State University, Department of Civil Engineering, East Lansing, Michigan 48824, 1989.

Harvey, J.T. and L. Popescu. (2000). Rutting of Caltrans Asphalt Concrete and Asphalt-Rubber Hot Mix Under Different Wheels, Tyres and Temperatures – Accelerated Pavement Testing Evaluation, Pavement Research Center, Institute of Transportation Studies, University of California, Berkeley, January 2000.

Haynes, J. G., and Yoder, E. J. (1963). Effects of repeated loading on gravel and crushed stone base course materials used in the AASHO Road Test. Hwy. Res. Rec. 39.

Hicks, R. G. (1970). Factors influencing the resilient properties of granular materials, PhD thesis, University of California, Berkeley, Berkeley, Calif.

Hicks, R. G., and Monismith, C. L. (1971). Factors influencing the resilient properties of granular materials. Highway Research Record 345, 15-31. Highway Research Board. Washington, DC.

Highways Agency (2001). Pavement Design – HD 26/01 – Volume 7, Section 2, Part 3 – Design Manual for Roads and Bridges. The Highways Agency, UK.

Hoff, I. Nordal, S. Nordal, R. (1999). Constitutive model for unbound granular materials based on hyperelasticity. Unbound Granular Materials – Laboratory testing, in-situ testing and modelling. Edited by A. Gomes Correia, Technical University of Lisbon. Proceedings of an International Workshop on Modelling and Advanced Testing for Unbound Granular Materials Lisbon 21-22 January 1999.

Hornych, P. Kerzrého, J. (2002). Prediction of the behaviour of a flexible pavement using finite element analysis with non-linear elastic and viscoelastic models. Ninth International Conference on Asphalt Pavements, August 17-22, 2002, Copenhagen Denmark. International Society for Asphalt Pavements.

HMSO, 1994, Design manual for roads and bridges, Vol 7, HD 25/94, Part 2, Foundations.

Hyde, A. (1974). Repeated Load Triaxial testing of soils. PhD Thesis, University of Nottingham, UK.

Jacobs, M.M.J., A.H. de Bondt, A.A.A. Molenaar, and P.C. Hopman. 1992. Cracking in Asphalt Concrete Pavements. Proc. on 7th International Conference on the Structural Design of Asphalt Pavements. 1:89-105.

Janoo, V. Irwin, L. Knuth, K. Dawson, A. Eaton, R. (1999). Use of inductive coils to measure dynamic and permanent pavement strains. Proc. Accelerated Pavement Testing International Conference, Reno, Nevada, October 18-20, 1999.

Johnson K L. (1986). Plastic flow, residual stresses and shakedown in rolling contact. Pro-ceedings of the 2nd International Conference on Contact Mechanics and Wear of Rail/Wheel Systems, University of Rhode Island, Waterloo Ontario 1986.

Jouve, P., Martinez, J., Paute, J. L., and Ragneau, E. (1987). ‘‘Rational model for the flexible pavement deformations.’’ Proc., 6th Int. Conf. on Struct. Des. of Asphalt Pavements, Vol. 1, 50–64.

Jouve, P. Guezouli, S. (1993). Comparison and harmonized development of some finite element programs. Flexible Pavements. Edited by A. Gomes Correia, Technical University of Lisbon. Proceedings of the European Symposium Euroflex 1993, Lisbon, Portugal 20-22 September 1993.

Karasahim, M. Dawson, A. (2000). Anisotropic characteristics of granular material. The Proceedings of the UNBAR5 Symposium, June 21-23, 2000. Department of Civil Engineering, University of Nottingham, UK.

Khedr, S. (1985). ‘‘Deformation characteristics of granular base course in flexible pavement.’’ Transp. Res. Rec. 1043, Transportation Research Board, Washington, D.C., 131–138.

Kinder, D. F., Lay, M.G. (1988). Review of the fourth power law. Australian Road Research Board ARRB Internal Report MR 000-248.

Kolisoja, P. (1997). Resilient deformation characteristics of granular materials, PhD thesis, Tampere University of Technology, Publ. No. 223, Tampere, Finland.

Korkiala-Tanttu, L. Laaksonen, R. Törnqvist, J. (2003). Effect of the spring and overload to the rutting of a low-volume road. HVS-Nordic-research. Helsinki

2003. Finnish Road Administration. Finnra Reports 22/2003. 39 p. + app. ISSN 1457-9871, ISBN 951-803-052-9, TIEH 3200810E.

Lashine, A.K., Brown, S.F., and Pell, P.S. (1971). Dynamic properties of soils. Report No. 2 Submitted to Koninklijke/Shell Laboratorium, Department of Civil Engineering, University of Nottingham, UK.

Lay, M. (1984). Handbook Of Road Technology, Volume 1 Planning and Pavements. Gordon and Breach Science Publishers.

Lekarp F. (1997). Permanent deformation behaviour of unbound granular materials; Licentiate Thesis, Kungl Tekniska Högskolan, Sweden.

Lekarp, F., and Dawson, A. (1998). Modelling permanent deformation behaviour of unbound granular materials. Construction and Building Materials., 12(1), 9-18.

Lekarp, F., Isacsson, U., & Dawson, A. (2000). State of the Art – II: Permanent strain response of unbound aggregates. American Society of Civil Engineers (ASCE), Journal of Transportation Engineering. Volume 126, Issue 1, Jan/Feb 2000, pp. 76-83.

Lentz, R. W., and Baladi, G. Y. (1981). ‘‘Constitutive equation for permanent strain of sand subjected to cyclic loading.’’ Transp. Res. Rec. 810, Transportation Research Board, Washington, D.C., 50–54.

Little, P. H. (1993). The design of unsurfaced roads using geosynthetics, Dept. of Civil Engineering, University of Nottingham.

Long, F. Govindjee, S. Monismith, C. (2002). Permanent deformation of asphalt concrete pavements: development of a nonlinear viscoelastic model for mix design and analyses. Ninth International Conference on Asphalt Pavements, August 17-22, 2002, Copenhagen Denmark. International Society for Asphalt Pavements.

MCHW1 (2004). Manual of Contract Documents for Highway Works. Specification for highway works, Volume 1. Highways Agency, UK.

Maree, J.H. 1978. Ontwerpparameters vir Klipslag in Plaveisels. (Design Aspects for Crushed Stone in Pavements). M Eng. Thesis, University of Pretoria, Republic of South Africa.

Maree, J. H., Freeme, C. R., Van Zyl, N. J., and Savage, P. F. (1982). The permanent deformation of pavements with untreated crushed stone bases as measured in heavy vehicle simulator tests. Proc., 11th ARRB Conf., Part 2, 16–28.

Mayhew, H. C. (1983). Resilient properties of unbound road base under repeated triaxial loading. Lab. Rep. 1088, TRRL, Crowthorne, U.K.

Mohammad, F. Collop, A. Brown, S. (2003). The effects of surface cracking on primary responses in a flexible pavement structure. ASCE *in print*.

Morgan, J.R. (1966). The response of granular materials to repeated loading. Proc., 3rd Conf., ARRB, 1178-1192.

Muhammad N. Hadi, S. Bodhinayake,. B. (2003). Non-linear finite element analysis of flexible pavements, Advances in Engineering Software, Volume 34, Issues 11-12, December 2003, Pages 657-662

National Roads Board (1989): State Highway Pavement Design and Rehabilitation Manual. Transit New Zealand (formerly National Roads Board) Wellington, New Zealand.

Neves, J. Correia, A. (2003). Influence of Non-Linear Behaviour of Unbound Granular Materials on Pavement Reinforcement Design. MAIRPAV '03. 3rd Symposium on Maintenance and Rehabilitation of Pavements and Technological Control, July 7-10, 2003.

Niekerk, A. Scheers, J. Muraya, P. Kisimbi,A. 2000. The effect of compaction on the mechanical behaviour of mix granulate basecourse materials and on pavement performance. Unbound aggregates in roads - Proceedings of the international symposium, UNBAR 5, Nottingham, UK, 21-23 June 2000, pp 125-136.

Oloo, S.Y. , Fredlund, D.G. and Gan, J.K.M. (1997). “Bearing capacity of unpaved roads.” Can. Geotech. J. 34, pp. 398-407.

Pappin, J. W. (1979). Characteristics of granular material for pavement analysis. PhD Thesis, University of Nottingham, UK.

Paute, J. L., Jouve, P., Martinez, J., and Ragneau, E. (1988). ‘‘Mode`le de calcul pour le dimensionnement des chausse´es souples.’’ Bull. de Liaison des Laboratoires des Ponts et Chausse´es, 156, 21–36 (in French). *(cited in Lekarp et al. 2000)*.

Paute, J. L., Hornych, P., and Benaben, J. P. (1996). Repeated Load Triaxial testing of granular materials in the French network of Laboratories des Ponts et Chaussées. Flexible Pavements, Proc., European Symp. Euroflex 1993, A. G. Correia, ed., Balkema, 53-64.

Pezo, R. F. (1993). ‘‘A general method of reporting resilient modulus tests of soils—A pavement engineer’s point of view.’’ 72nd Annu. Meeting of the TRB.

Pidwerbesky, B. D. (1995). Accelerated Dynamic Loading of Flexible Pavements at the Canterbury Accelerated Pavement Testing Indoor Facility. Transportation Research Record, 1482, pp 79-86.

Pidwerbesky, B. D. (1996). Fundamental Behaviour of Unbound Granular Pavements Subjected to Various Loading Conditions and Accelerated Trafficking. PhD Thesis, University of Canterbury, Christchurch, New Zealand.

Raad, L. A. M. and J. L. Figueroa, (1980), Load response of transportation support systems, Transportation Engineering Journal, ASCE, Vol. 106(TE1), pp. 111-128.

Raad, L., Weichert, D. and Najm, W. (1988). "Stability of multilayer systems under repeated loads." *Transportation Research Record*, No. 1207, pp. 181-186.

Raad, L., Weichert, D. and Haidar, A. (1989a). "Analysis of full-depth asphalt concrete pavements using shakedown theory." *Transportation Research Record*, No. 1227, pp. 53-65.

Raad, L., Weichert, D. and Haidar, A. (1989b). "Shakedown and fatigue of pavements with granular bases." *Transportation Research Record*, No. 1227, pp. 159-172.

Raymond, G.P. & Williams, D.R. (1978). Repeated Load Triaxial tests on a dolomite ballast. Journal of Geotechnical Engineering Division, ASCE, 104(7), 1013-1029.

Scarpas, A, Al-Khoury, R, Gurp, CAPM & Erkens, SMJG. (1997). Finite Element Simulation of Damage Development in Asphalt Concrete Pavements, Eighth International Conference on Asphalt Pavements, Volume 1 Proceedings. University of Washington, Seattle, Washington pp673-692.

Scarpas, A & Blaauwendraad, J, 1998, Experimental Calibration of a Constitutive Model for Asphaltic Concrete, Proceedings of the Euro-C Conference on the Computational Modelling of Concrete Sturctures, Badgastein, Oostenrijk, 31 March - 3 April.

Schelt, W. van. Vos, E. Galjaard, P.J. Hendriks, M. P. (1993). The non-linear elastic model of Boyce: An evaluation of the model in the FEM-program DIANA. Flexible Pavements. Edited by A. Gomes Correia, Technical University of Lisbon. Proceedings of the European Symposium Euroflex 1993, Lisbon, Portugal 20-22 September 1993.

Seed, H. B., Mitry, F. G., Monismith, C. L., and Chan, C. K. (1967). Prediction of flexible pavement deflections from laboratory repeated load tests.'' NCHRP Rep. No. 35, National Cooperative Highway Research Program.

Selig, E. T. (1987). Tensile zone effects on performance of layers systems. Geotechnique, Vol. XXXVII, No. 3, pp. 247-354.

Semmelink C.J. and de Beer M. (1995). Rapid determination of elastic and shear properties of road building materials with the K-mould. The Proceedings of the UNBAR4 Symposium, July 17-19, 1995. Department of Civil Engineering, University of Nottingham, UK.

Semmelink, CJ, Jooste, FJ & de Beer, M. (1997). Use of the K-mould in determination of the elastic and shear properties of road materials for flexible pavements. 8th Int. Conf. on Asphalt Pavements, August, Seattle, Washington, USA.

Sharp R and Booker J. (1984). Shakedown of pavements under moving surface loads, pp. 1-14, ASCE Journal of Transportation Engineering, No 1, 1984.

Sharp, R.W. (1985). "Pavement design based on shakedown analysis." *Transportation Research Record*. 1022, pp. 99-107.

Shaw P. S. (1980). Stress-Strain Relationships for Granular Materials under Repeated Loading. PhD Thesis, Department of Civil Engineering , University of Nottingham, UK.

Snaith, M.S., McMullen, D., Freer-Hewish, R.J. and Shein, A. (1980). Flexible pavement analysis. Contracted Report to Sponsors, European Research Office of the U.S. Army.

Sowers, G. F. Robb, A.D. Mullis, C.H. & Glenn, A.J. (1957). The residual lateral pressures produced by compacting soils. Proceedings 4th International Conference on Soil Mechanics and Foundation Engineering, London, UK. Vol. 2, pp. 243-247.

Stewart, H. E., Selig, E. T. & Norman-Gregory, G. M. (1985). Failure criteria and lateral stresses in track foundations, Transp. Res. Record No. 1027, Transportation Research Board, Washington, DC, 59-64.

Steven, B (2004). PhD Thesis. University of Canterbury, Christchurch, New Zealand. In press.

Sweere, G. T. H. (1990). Unbound granular bases for roads. PhD thesis, University of Delft at Delft, the Netherlands.

Tam, W. A., and Brown, S. F. (1988). ‘‘Use of the falling weight deflectometer for in situ evaluation of granular materials in pavements.’’ Proc., 14th ARRB Conf., Vol. 14, Part 5, 155–163.

Terzaghi, K., Peck, R.B., and Mesri, G. (1996). Soil mechanics in engineering practice, 3rd ed., John Wiley & Sons, New York.

Theyse, H. Kekwick, S. Kleyn, E. (1999). Development of a Long-Term Accelerated Pavement Testing Programme and Structural Design Models - Paper I-1. Proc. Accelerated Pavement Testing International Conference, Reno, Nevada, October 18-20, 1999.

Theyse, H. L. (2002). Stiffness, Strength, and Performance of Unbound Aggregate Material: Application of South African HVS and Laboratory Results to California Flexible Pavements. University of California Pavement Research Center, July 2002.

Thom, N. H., and Brown, S. F. (1987). Effect of moisture on the structural performance of a crushed-limestone road base. Transp. Res. Rec.1121, Transportation Research Board, Washington, D.C., 50–56.

Thom, N.H. (1988). Design of road foundations. PhD Thesis, University of Nottingham, UK.

Thom, N. H., and Brown, S. F. (1988). The effect of grading and density on the mechanical properties of a crushed dolomitic limestone. Proc., 14th ARRB Conf., Part 7, 94–100.

Thom, N.H., and Brown, S. F., (1989). The mechanical properties of unbound aggregates from various sources. Proceedings of the Third International Symposium on Unbound Aggregates in Roads, UNBAR 3, Nottingham, United Kingdom, 11-13 April 1989.

Thom, N. & Dawson, A. (1996). The permanent deformation of a granular material modelled using hollow cylinder testing. Flexible Pavements, Gomes Correia (ed.). 1996 Balkema, Rotterdam.

Thom, N. H., Choi, Y-K., and Collop, A.C. (2002). Top-down cracking, damage and hardening in practical flexible pavement design. Ninth International Conference on Asphalt Pavements, August 17-22, 2002, Copenhagen Denmark. Volume 1: 10-1. International Society for Asphalt Pavements.

Thompson, M. R. and R. P. Elliot, 1985, ILLI-PAVE Based response algorithms for design f conventional flexible pavements, Transportation Research Record 1043, Transportation esearch Board, National Research Council, Washington, D. C., pp. 50-57.

Thompson, M. R, 1987, ILLI-PAVE based full depth asphalt concrete pavement design procedure, Proceedings, Sixth International Conference on Structural Design of Asphalt Pvements, Vol. 1, pp. 13-22.

Thompson, M. Gomez-Ramirez, F. Bejarano, M. (2002). ILLI-PAVE based flexible pavement design concepts for multiple wheel heavy gear load aircraft. Ninth International Conference on Asphalt Pavements, August 17-22, 2002, Copenhagen Denmark. Volume 1: 10-1. International Society for Asphalt Pavements.

TNZ M/4. (2002). Specification for basecourse aggregate (TNZ M/4). Transit New Zealand, Wellington New Zealand.

TNZ B/2. (1997). Construction of Unbound Granular Pavement Layers. Transit New Zealand, Wellington New Zealand.

TRL, 1993, A guide to the structural design of bitumen-surfaced roads in tropical and sub-tropical countries, RN31, Draft 4th Edition.

Tutumluer, E. Seyhan, U. (2000). Effects of fines content on the anisotropic response and characterisation of unbound aggregate bases. The Proceedings of the UNBAR5 Symposium, June 21-23, 2000. Department of Civil Engineering, University of Nottingham, UK.

Uzan, J. (1985). Characterisation of granular material. Transport Research Record No. 1022. Transport Research Board, Washington DC, USA. pp. 52-59.

Veverka, V. (1979). Raming van de spoordiepte bij wegen met een bitumineuze verharding. De Wegentechniek, 24(3), 25–45 (in Dutch). *(cited in Lekarp et al. 2000).*

Wardle L. J. (1980). Program CIRCLY, A Computer Program for the Analysis of Multiple Complex Loads on Layered Anisotropic Media.

Wellner, F. Gleitz, T. (1999). Stress-strain behaviour of granular materials. Unbound Granular Materials – Laboratory testing, in-situ testing and modelling. Edited by A. Gomes Correia, Technical University of Lisbon. Proceedings of an International Workshop on Modelling and Advanced Testing for Unbound Granular Materials Lisbon 21-22 January 1999.

Werkmeister, S. (2003). Permanent deformation behaviour of unbound granular materials in pavement constructions. PhD Thesis, Technical University of Dresden, Germany.

Werkmeister, S. Numrich, R. Wellner, F. (2000). Resilient and permanent deformation of unbound granular materials. The Proceedings of the UNBAR5 Symposium, June 21-23, 2000. Department of Civil Engineering, University of Nottingham, UK.

Werkmeister, S. Dawson, A. Wellner, F. (2001). Permanent deformation behaviour of granular materials and the shakedown concept. Transportation Research Board, 80th Annual Meeting, Washington D.C. January 7-11, 2001.

Wolff. H., and Visser, A. T. (1994). Incorporating elasto-plasticity in granular layer pavement design. Proc., Inst. Of Civil Engineers Transp., No. 105, 259-272.

Wong, S.K. and Kapoor, A. (1996). "The effect of hard and stiff overlay coatings on the strength of surfaces in repeated sliding." *Tribol. Int*., 29(8), pp. 695-702.

Wong, S.K., Kapoor, A. and Williams, J.A. (1997). "Shakedown limits on coated and engineered surfaces." *Wear* 203-204, pp. 162-170.

Yu, H.S. and Hossain, M.Z. (1998). "Lower bound shakedown analysis of layered pavements using discontinuious stress fields." Computer Methods in Applied Mechanics and Engineering, Vol. 167, pp. 209-222.

Zienkiewicz, O. C, and Taylor, R. L. 1989. The Finite Element Method. 4th Edition, McGraw-Hill.

APPENDIX A.

REPEAT LOAD TRI-AXIAL STRESS PATHS, PERMANENT STRAIN RESULTS AND SHAKEDOWN CLASSIFICATION BOUNDARIES

Stress Paths (kPa) – *NI Good (Test 1, p=75kPa)*							
	$p={}^1/_3(\sigma_1+2\sigma_3)$		${}^1q = \sigma_1-\sigma_3$		$\sigma_1=q+\sigma_3+{}^2k$		${}^3\sigma_3$
A	45	76	0	95	51	146	42
B	37	77	0	119	45	164	33
C	29	76	0	142	36	178	25
D	21	76	0	166	31	196	16
E	14	77	0	190	24	214	9
F	11	77	0	199	21	220	6
G	4	75	0	212	11	223	0

1. q = cyclic vertical load (kPa).
2. k = top platen weight and minimum vertical load.
3. σ_3 = cell pressure (kPa).

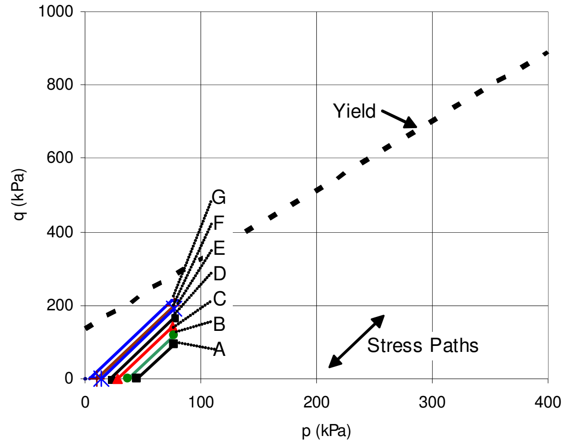

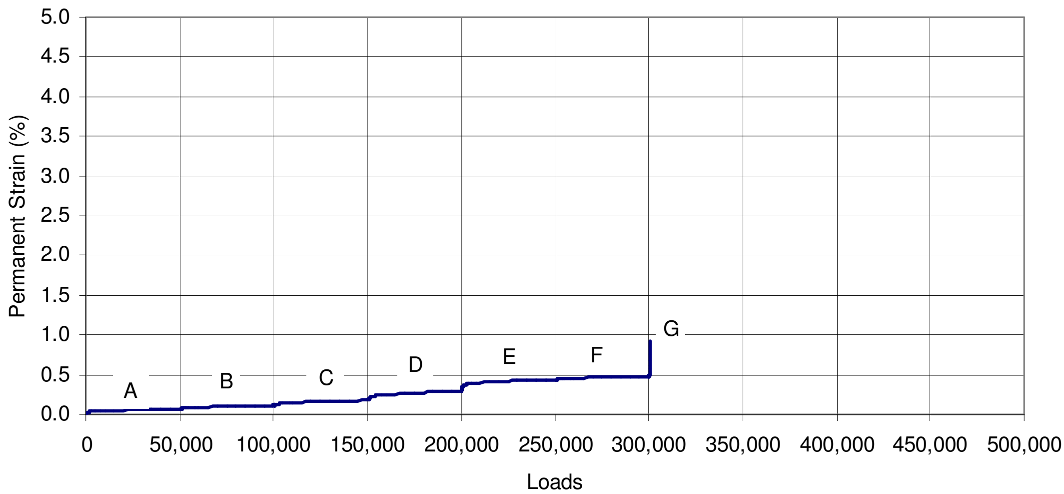

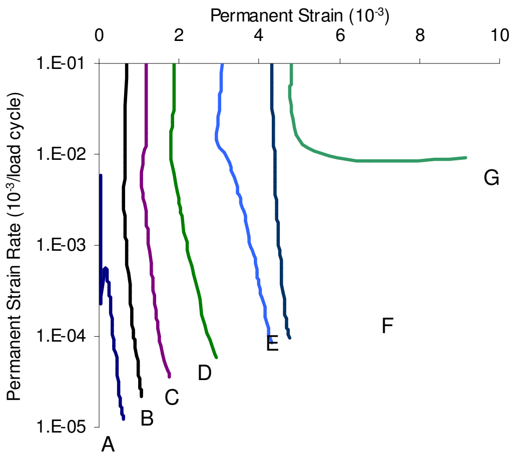

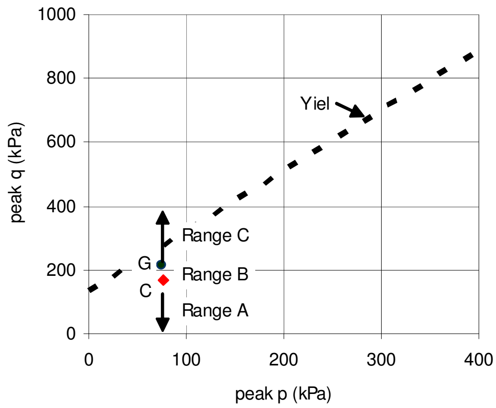

Figure A.1. RLT Permanent strain, stress paths, results, and shakedown range boundaries (NI Good - Test 1 - p=75kPa).

Stress Paths (kPa) – *NI Good (Test 2, p=150kPa)*								
	$p={}^{1}/_{3}(\sigma_1+2\sigma_3)$		${}^{1}q=\sigma_1-\sigma_3$		$\sigma_1=q+\sigma_3+{}^{2}k$		${}^{3}\sigma_3$
A	103	150	0	139	111	250	99
B	88	151	0	191	96	287	84
C	71	147	0	228	79	307	67
D	54	150	0	286	63	349	50
E	38	150	0	334	48	382	34
F	22	149	0	380	33	413	17
G	6	149	0	427	18	446	1

1. q = cyclic vertical load (kPa).
2. k = top platen weight and minimum vertical load.
3. σ_3 = cell pressure (kPa).

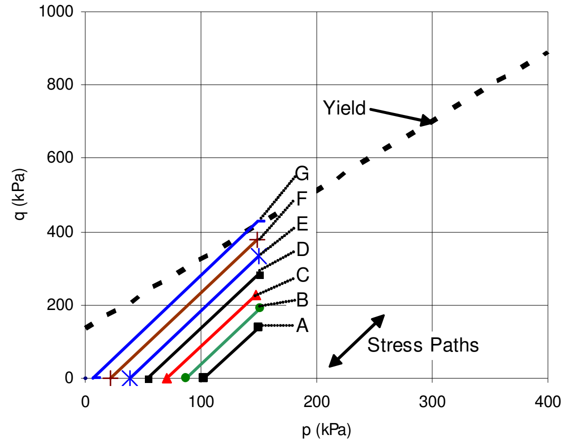

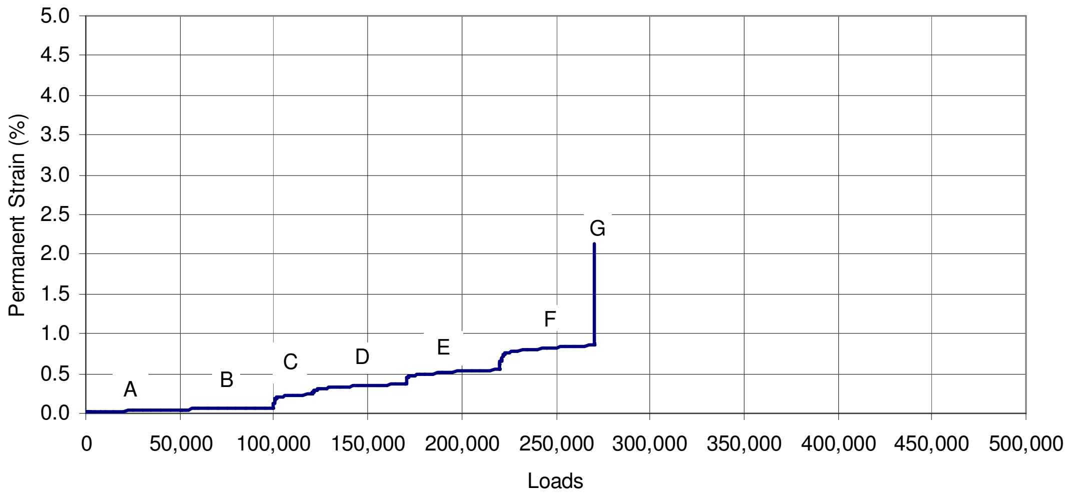

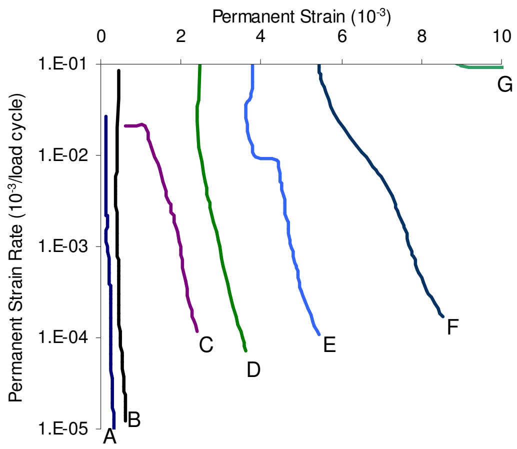

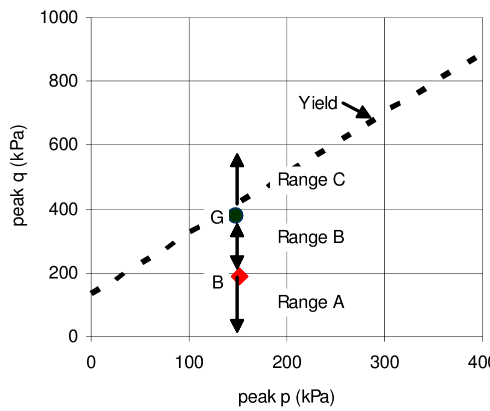

Figure A.2. RLT Permanent strain, stress paths, results, and shakedown range boundaries (NI Good - Test 2 - p=150kPa).

Stress Paths (kPa) – *NI Good (Test 3, p=250kPa)*							
	$p={}^{1}/_{3}(\sigma_1+2\sigma_3)$		${}^{1}q = \sigma_1 - \sigma_3$		$\sigma_1=q+\sigma_3+{}^{2}k$		${}^{3}\sigma_3$
A	120	247	0	381	128	509	116
B	103	247	0	433	110	543	99
C	86	247	0	482	94	576	82
D	70	246	0	526	77	604	67
E	54	245	0	572	62	634	50
F	38	245	0	621	47	668	33

1. q = cyclic vertical load (kPa).
2. k = top platen weight and minimum vertical load.
3. σ_3 = cell pressure (kPa).

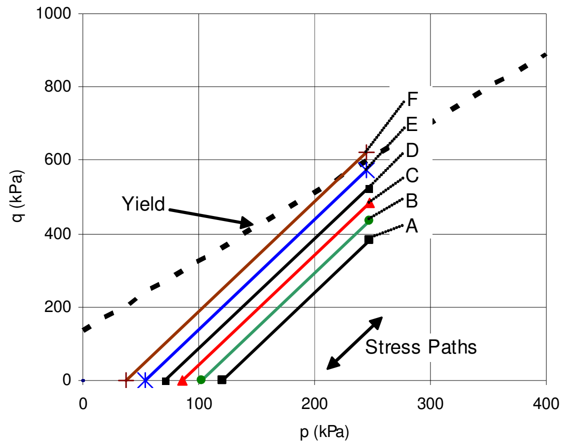

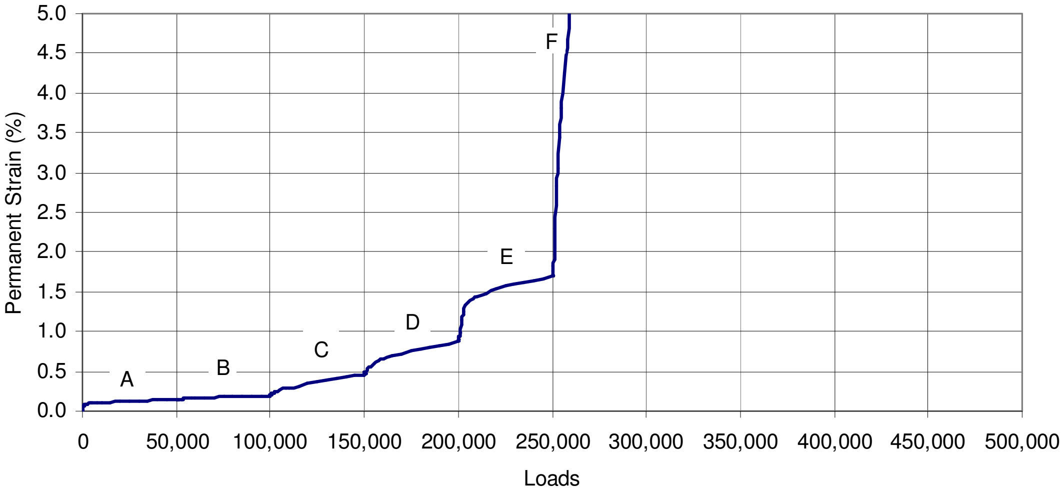

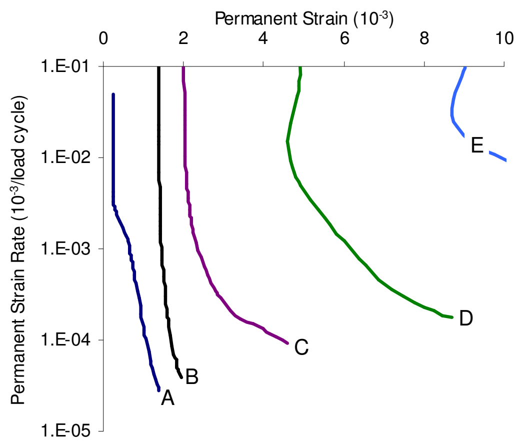

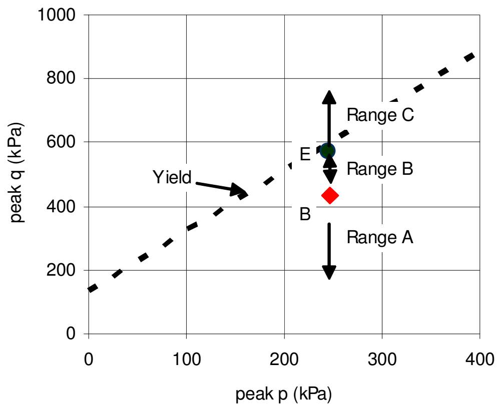

Figure A.3. RLT Permanent strain, stress paths, results, and shakedown range boundaries (NI Good - Test 3 - p=250kPa).

Stress Paths (kPa) – *NI Poor (Test 1, p=75kPa)*							
	$p={}^{1}/_{3}(\sigma_1+2\sigma_3)$		${}^{1}q=\sigma_1-\sigma_3$		$\sigma_1=q+\sigma_3+{}^{2}k$		${}^{3}\sigma_3$
A	41	72	0	94	42	136	41
B	26	73	0	142	28	170	25
C	19	74	0	166	24	190	16
D	10	73	0	189	15	204	8
E	2	72	0	211	7	218	0

1. q = cyclic vertical load (kPa).
2. k = top platen weight and minimum vertical load.
3. σ_3 = cell pressure (kPa).

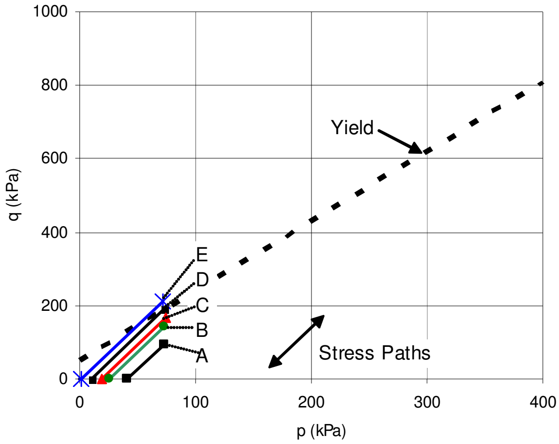

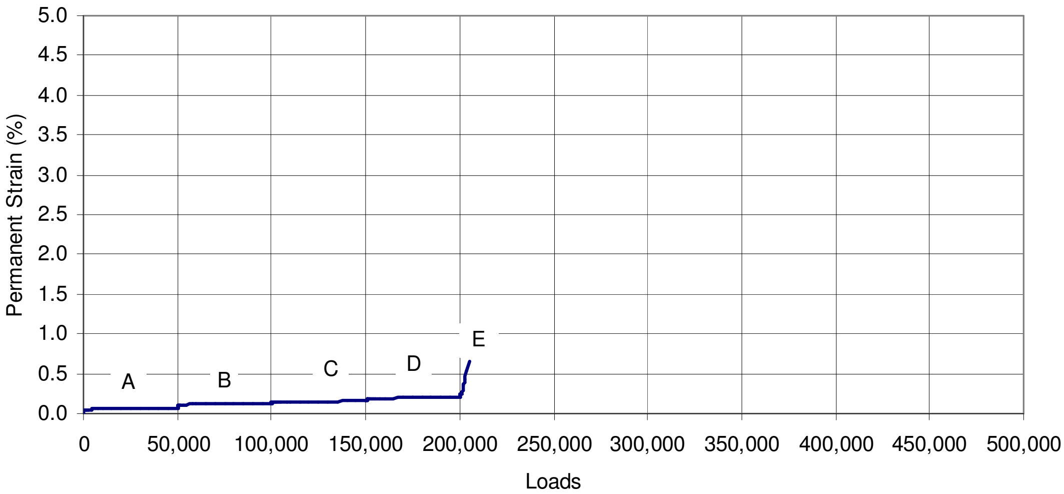

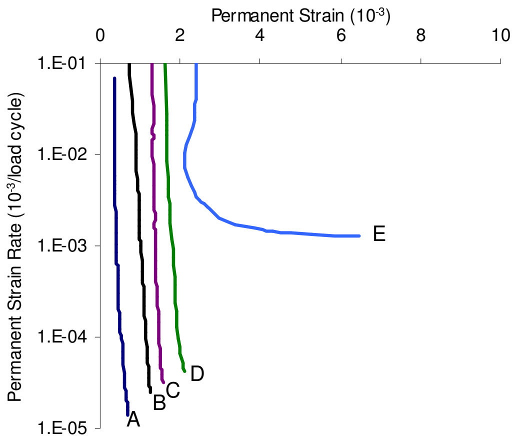

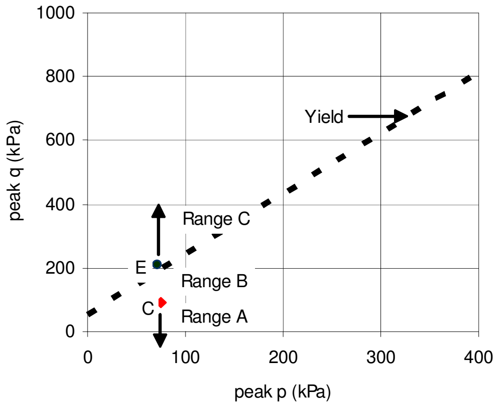

Figure A.4. RLT Permanent strain, stress paths, results, and shakedown range boundaries (NI Poor - Test 1 - p=75kPa).

Stress Paths (kPa) – *NI Poor (Test 2, p=150kPa)*							
	$p={}^1/_3(\sigma_1+2\sigma_3)$		${}^1q=\sigma_1-\sigma_3$		$\sigma_1=q+\sigma_3+{}^2k$		${}^3\sigma_3$
A	70	149	0	238	77	315	67
B	63	150	0	261	72	333	58
C	53	148	0	285	61	346	50
D	44	147	0	310	49	358	42
E	38	149	0	333	46	378	34
F	28	146	0	353	34	387	25
G	20	146	0	379	25	404	17

1. q = cyclic vertical load (kPa).
2. k = top platen weight and minimum vertical load.
3. σ_3 = cell pressure (kPa).

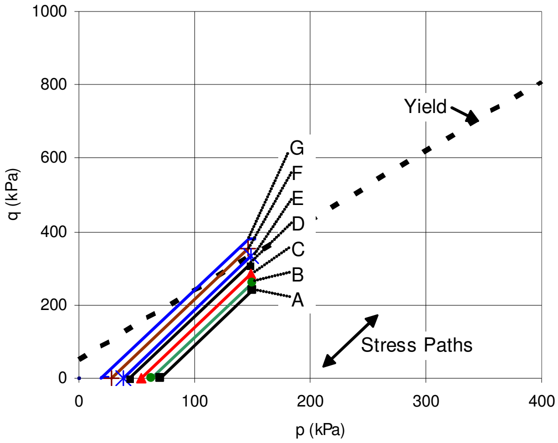

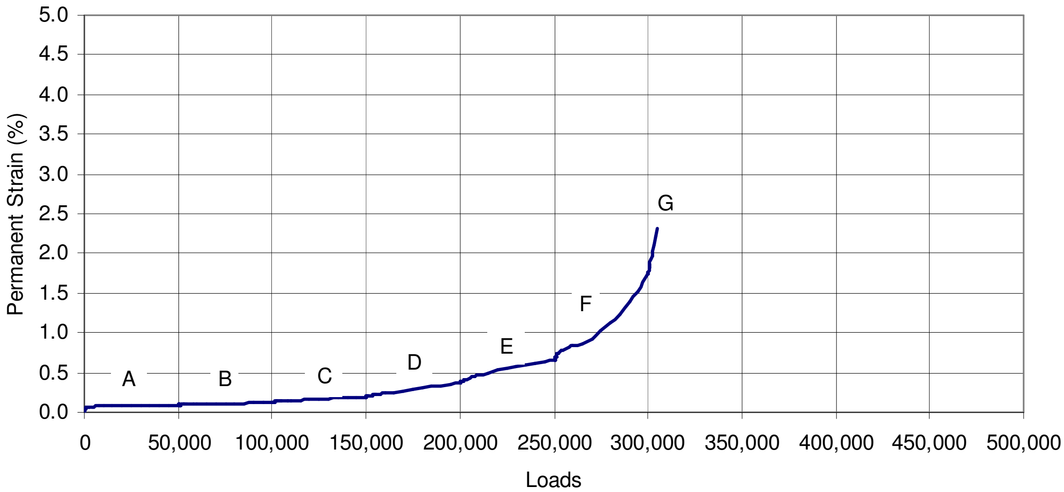

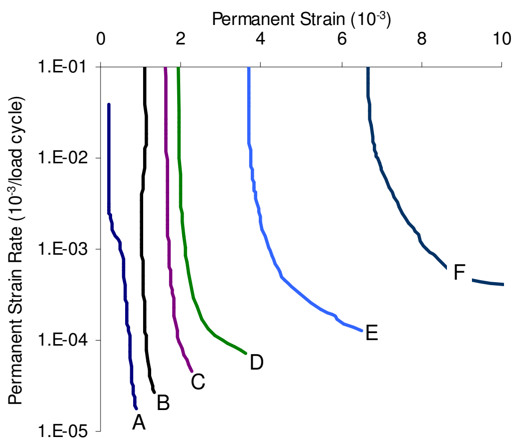

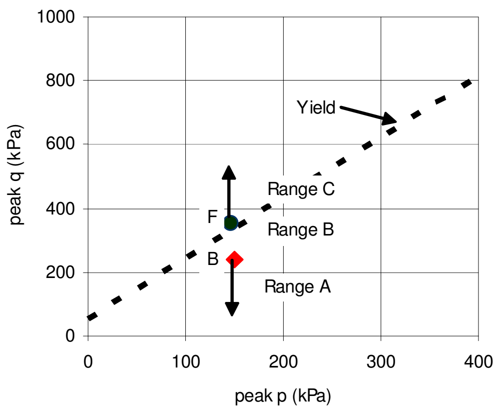

Figure A.5. RLT Permanent strain, stress paths, results, and shakedown range boundaries (NI Poor - Test 2 - p=150kPa).

Stress Paths (kPa) – *NI Poor (Test 3, p=250kPa)*							
	$p={}^1/_3(\sigma_1+2\sigma_3)$		${}^1q=\sigma_1-\sigma_3$		$\sigma_1=q+\sigma_3+{}^2k$		${}^3\sigma_3$
A	187	252	0	193	195	388	184
B	171	251	0	240	178	418	167
C	153	249	0	288	158	446	150
D	137	251	0	341	145	486	134
E	120	249	0	387	125	512	117
F	102	246	0	434	106	541	99
G	88	246	0	476	96	573	83
H	72	246	0	524	81	605	67
I	54	243	0	567	62	629	50

1. q = cyclic vertical load (kPa).
2. k = top platen weight and minimum vertical load.
3. σ_3 = cell pressure (kPa).

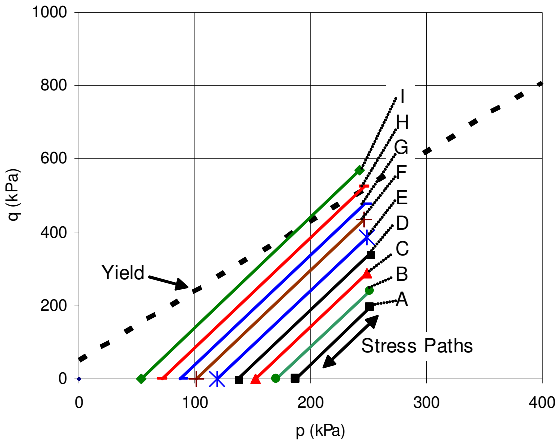

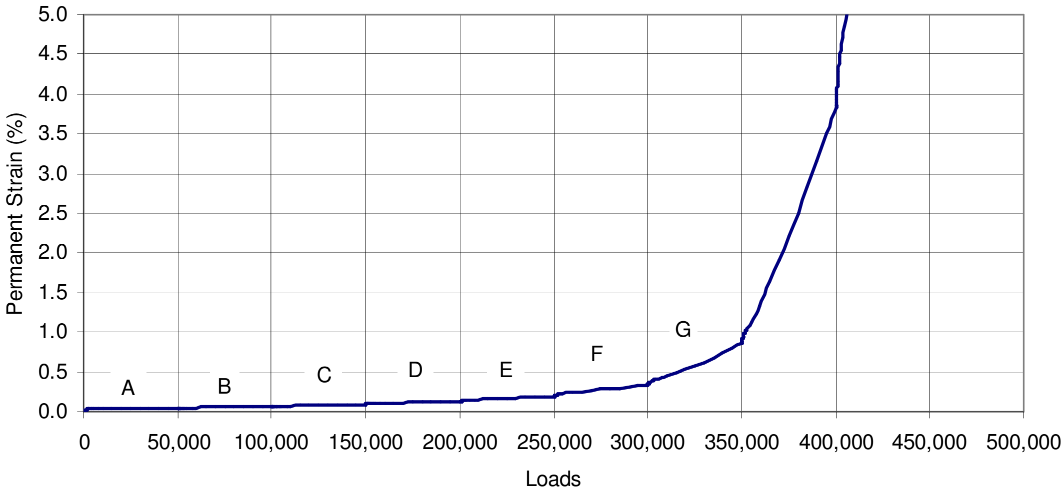

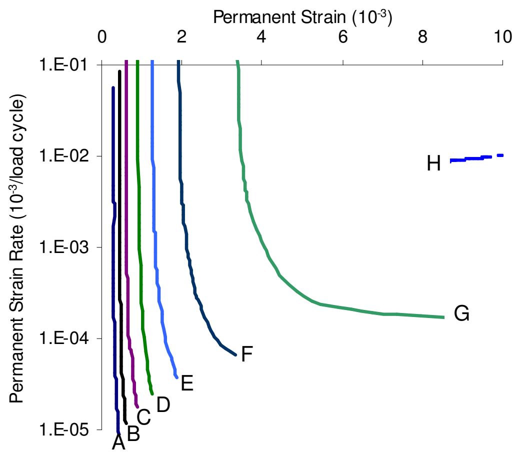

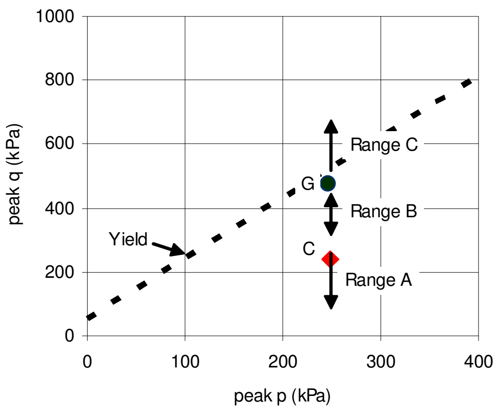

Figure A.6. RLT Permanent strain, stress paths, results, and shakedown range boundaries (NI Poor - Test 3 - p=250kPa).

Stress Paths (kPa) – *CAPTIF 1 (Test 1, p=75kPa)*							
	$p={}^1/_3(\sigma_1+2\sigma_3)$		${}^1q=\sigma_1-\sigma_3$		$\sigma_1=q+\sigma_3+{}^2k$		${}^3\sigma_3$
A	62	76	0	43	69	112	58
B	47	77	0	91	55	145	43
C	31	77	0	139	40	179	27
D	16	77	0	183	26	209	11
E	6	73	0	203	17	220	0

1. q = cyclic vertical load (kPa).
2. k = top platen weight and minimum vertical load.
3. σ_3 = cell pressure (kPa).

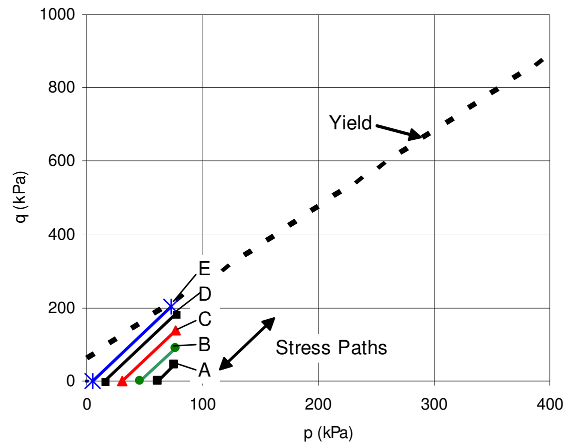

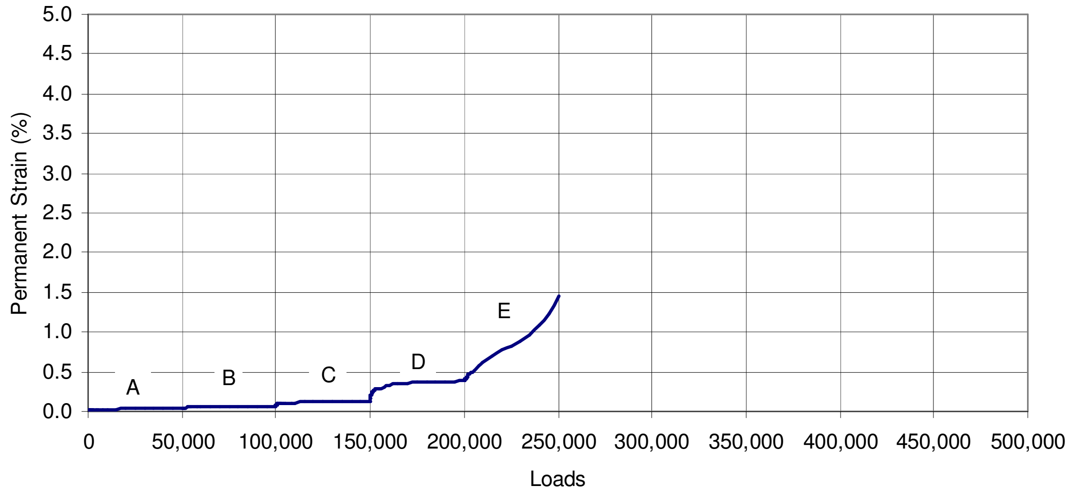

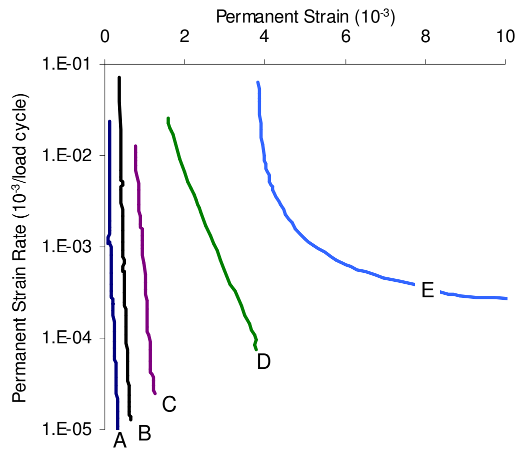

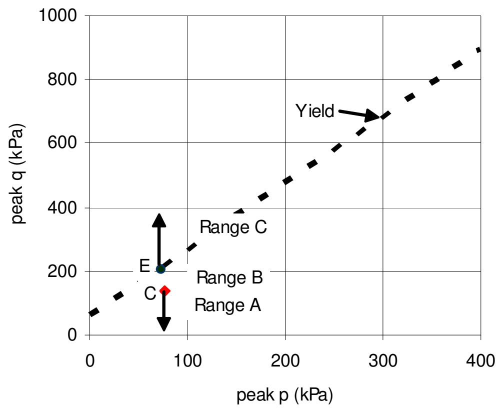

Figure A.7. RLT Permanent strain, stress paths, results, and shakedown range boundaries (CAPTIF 1 - Test 1 - p=75kPa).

Stress Paths (kPa) – *CAPTIF 1 (Test 2, p=150kPa)*							
	$p={}^{1}/_{3}(\sigma_1+2\sigma_3)$		$^{1}q = \sigma_1-\sigma_3$		$\sigma_1=q+\sigma_3+{}^{2}k$		$^{3}\sigma_3$
A	104	149	0	135	111	247	100
B	93	154	0	183	101	284	88
C	74	151	0	229	83	313	70
D	59	150	0	274	69	343	54
E	46	152	0	319	58	376	40
F	29	151	0	367	42	409	22

1. q = cyclic vertical load (kPa).
2. k = top platen weight and minimum vertical load.
3. σ_3 = cell pressure (kPa).

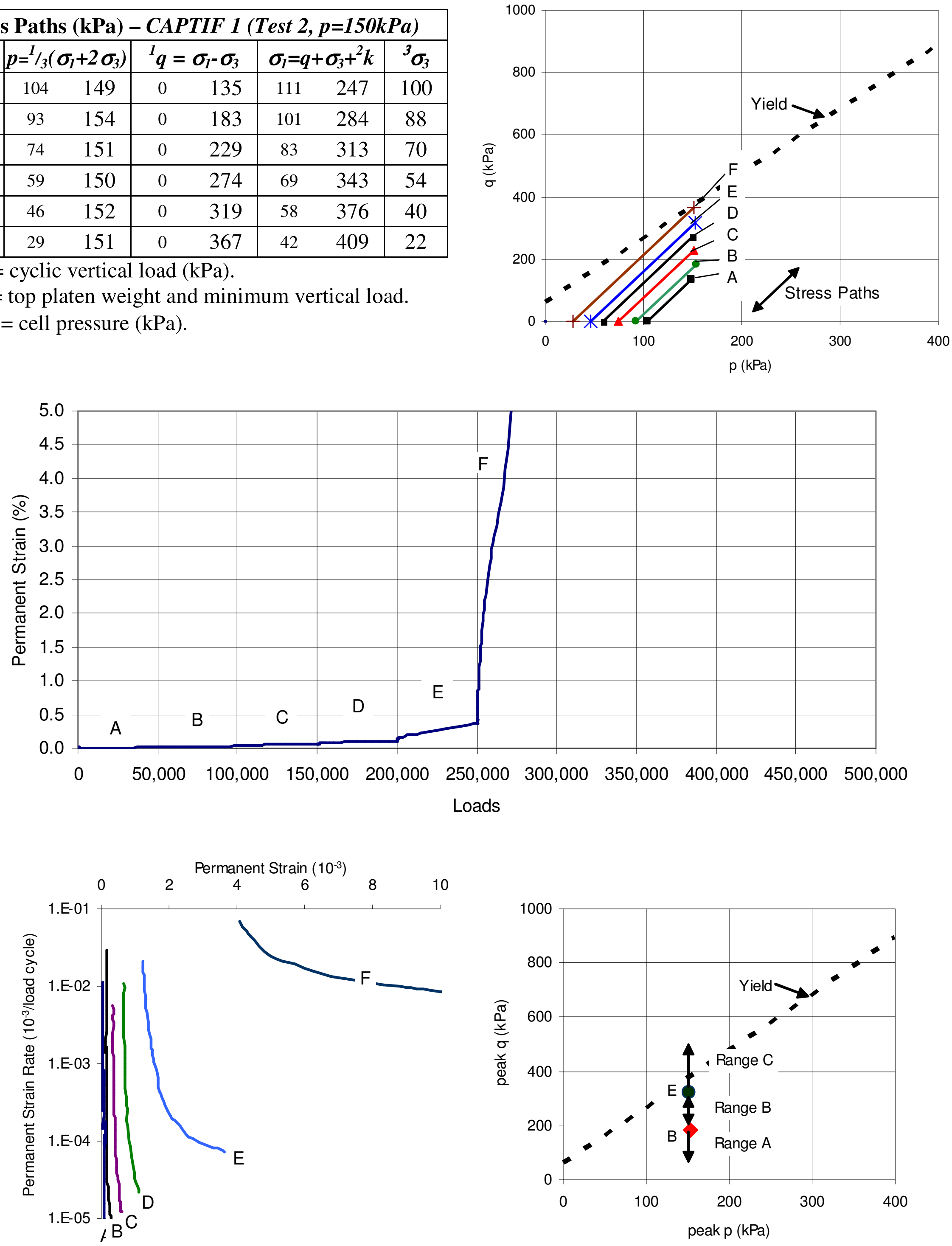

Figure A.8. RLT Permanent strain, stress paths, results, and shakedown range boundaries (CAPTIF 1 - Test 2 - p=150kPa).

Stress Paths (kPa) – *CAPTIF 1 (Test 3, p=250kPa)*							
	$p={}^{1}/_{3}(\sigma_1+2\sigma_3)$		${}^{1}q=\sigma_1-\sigma_3$		$\sigma_1=q+\sigma_3+{}^{2}k$		${}^{3}\sigma_3$
A	139	247	0	324	149	473	134
B	122	247	0	376	130	506	118
C	110	250	0	419	119	538	105
D	88	243	0	465	98	563	83
E	78	249	0	515	90	604	72

1. q = cyclic vertical load (kPa).
2. k = top platen weight and minimum vertical load.
3. σ_3 = cell pressure (kPa).

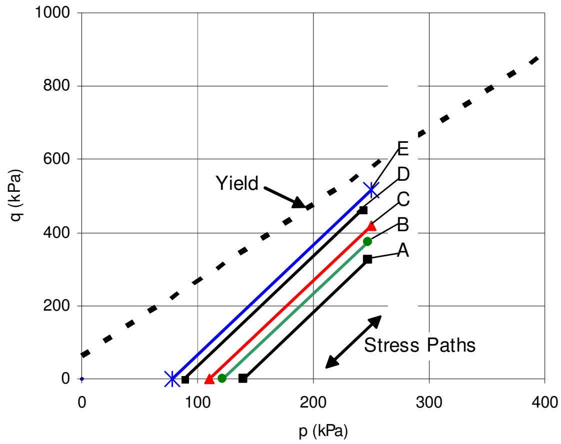

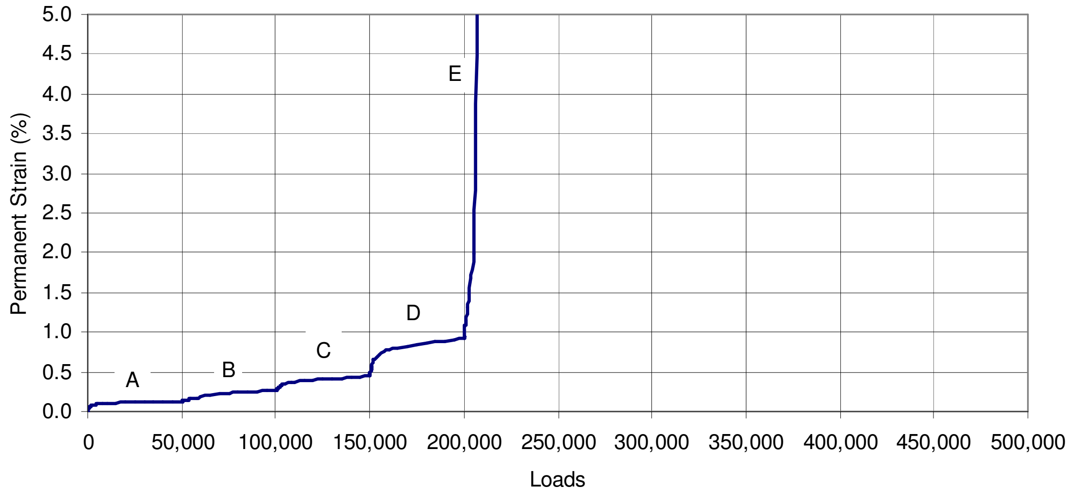

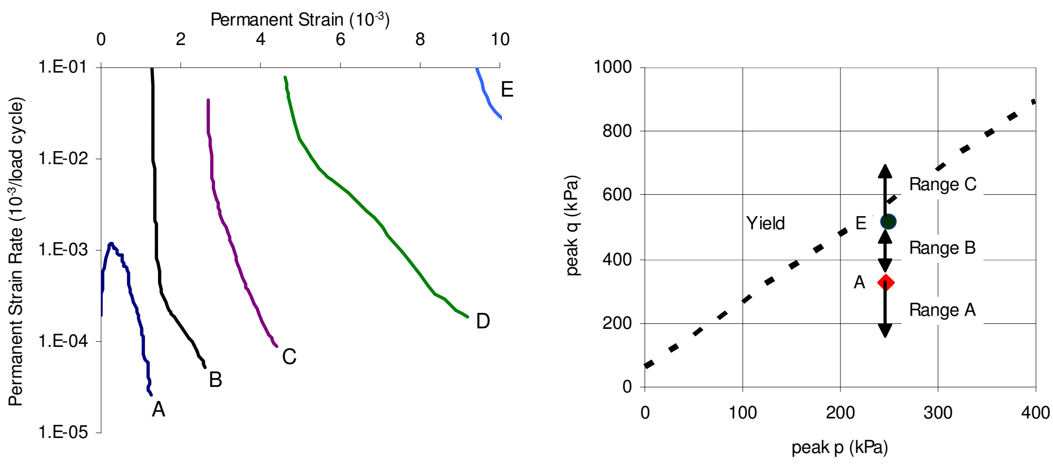

Figure A.9. RLT Permanent strain, stress paths, results, and shakedown range boundaries (CAPTIF 1 - Test 3 - p=250kPa).

Stress Paths (kPa) – *CAPTIF 2 (Test 1, p=75kPa)*							
	$p = {}^1/_3(\sigma_1 + 2\sigma_3)$		${}^1q = \sigma_1 - \sigma_3$		$\sigma_1 = q + \sigma_3 + {}^2k$		${}^3\sigma_3$
A	63	75	0	37	72	108	58
B	46	75	0	86	56	142	42
C	30	75	0	136	40	176	25

1. q = cyclic vertical load (kPa).
2. k = top platen weight and minimum vertical load.
3. σ_3 = cell pressure (kPa).

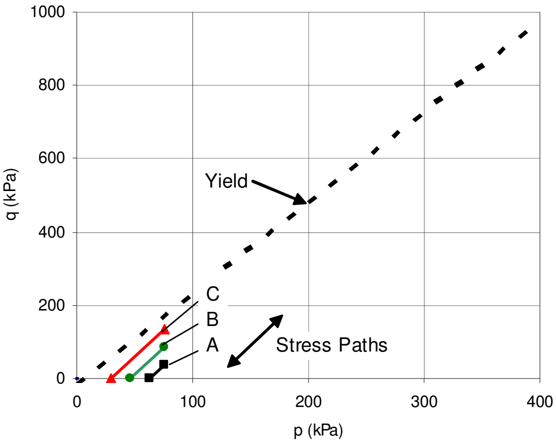

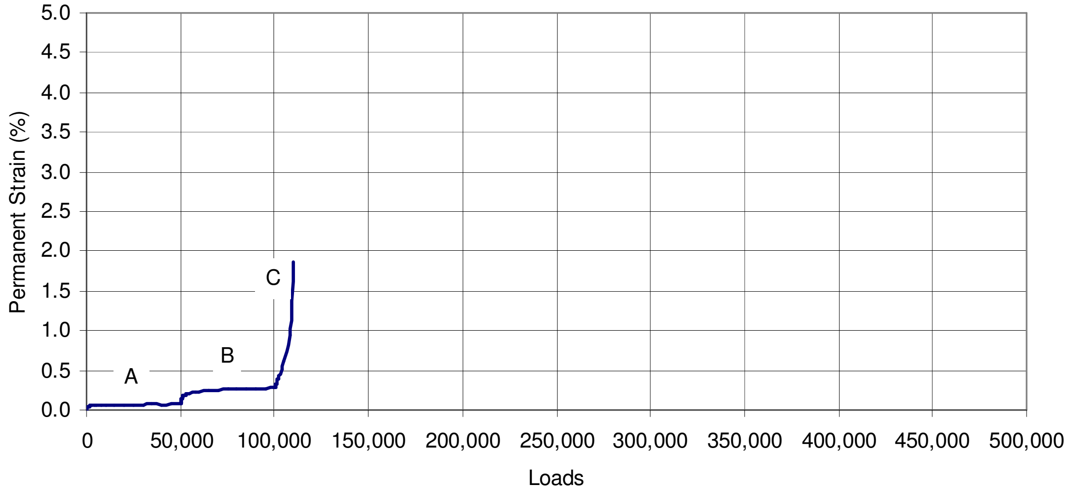

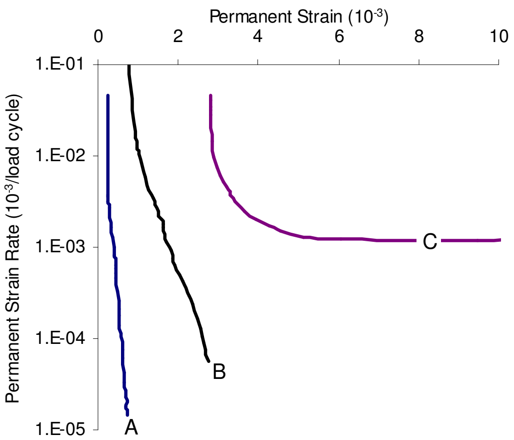

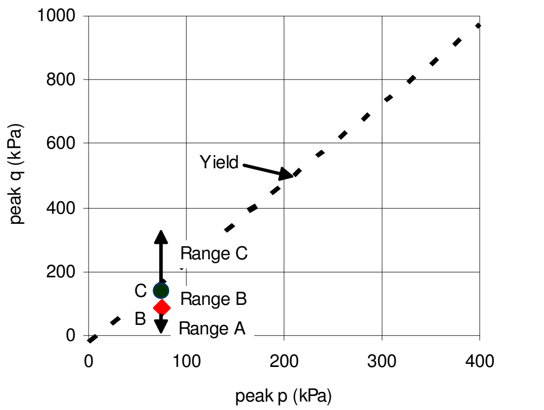

Figure A.10. RLT Permanent strain, stress paths, results, and shakedown range boundaries (CAPTIF 2 - Test 1 - p=75kPa).

Stress Paths (kPa) – *CAPTIF 2 (Test 2, p=150kPa)*							
	$p={}^{1}/_{3}(\sigma_1+2\sigma_3)$		${}^{1}q=\sigma_1-\sigma_3$		$\sigma_1=q+\sigma_3+{}^{2}k$		${}^{3}\sigma_3$
A	105	150	0	135	114	249	100
B	89	150	0	183	98	281	83
C	74	151	0	231	83	314	67
D	59	151	0	276	69	345	50
E	43	150	0	321	54	375	33

1. q = cyclic vertical load (kPa).
2. k = top platen weight and minimum vertical load.
3. σ_3 = cell pressure (kPa).

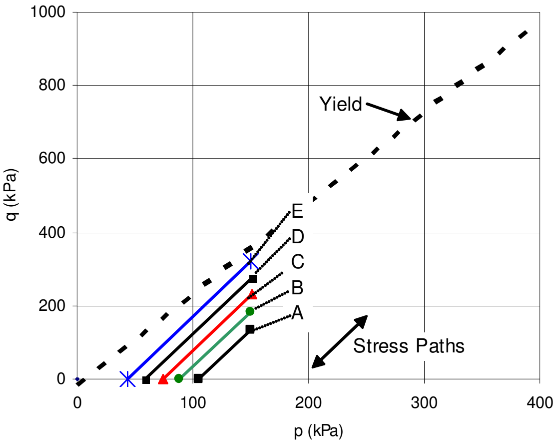

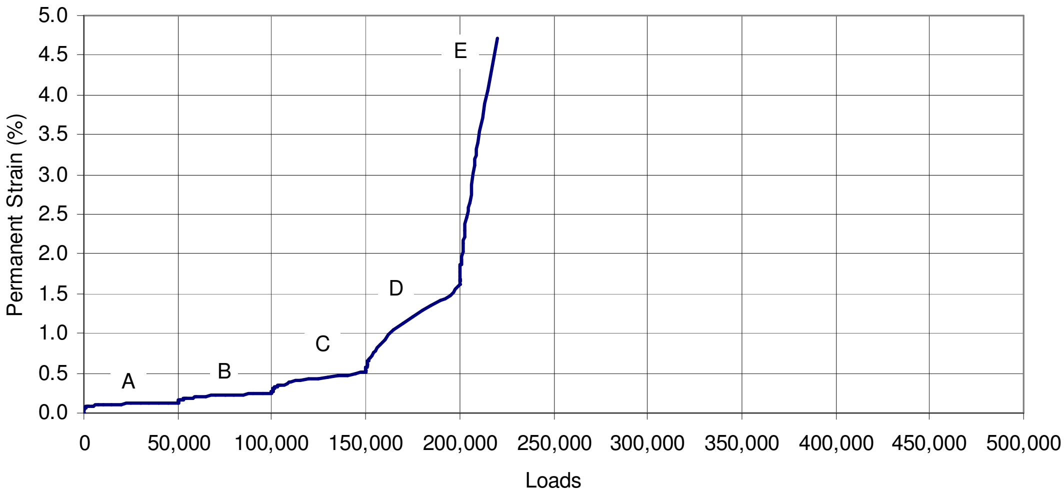

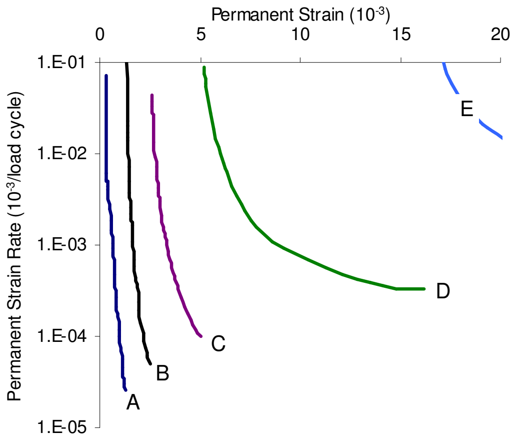

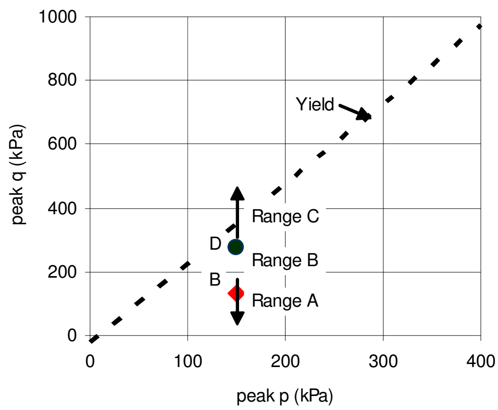

Figure A.11. RLT Permanent strain, stress paths, results, and shakedown range boundaries (CAPTIF 2 - Test 2 - p=150kPa).

Stress Paths (kPa) – *CAPTIF 2 (Test 3, p=250kPa)*							
	$p={}^{1}/_{3}(\sigma_1+2\sigma_3)$		[1] $q = \sigma_1-\sigma_3$		$\sigma_1=q+\sigma_3+$[2]k		[3] σ_3
A	142	249	0	321	155	476	136
B	125	250	0	374	137	511	119
C	107	246	0	416	120	536	100
D	87	242	0	465	102	567	79
E	77	247	0	510	93	602	69
F	59	246	0	559	77	636	51
G	45	248	0	607	63	670	36

1. q = cyclic vertical load (kPa).
2. k = top platen weight and minimum vertical load.
3. σ_3 = cell pressure (kPa).

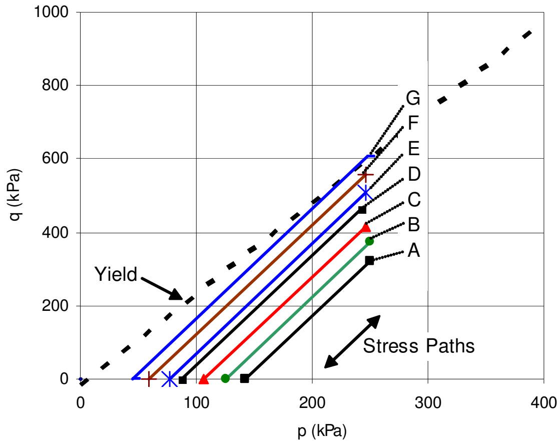

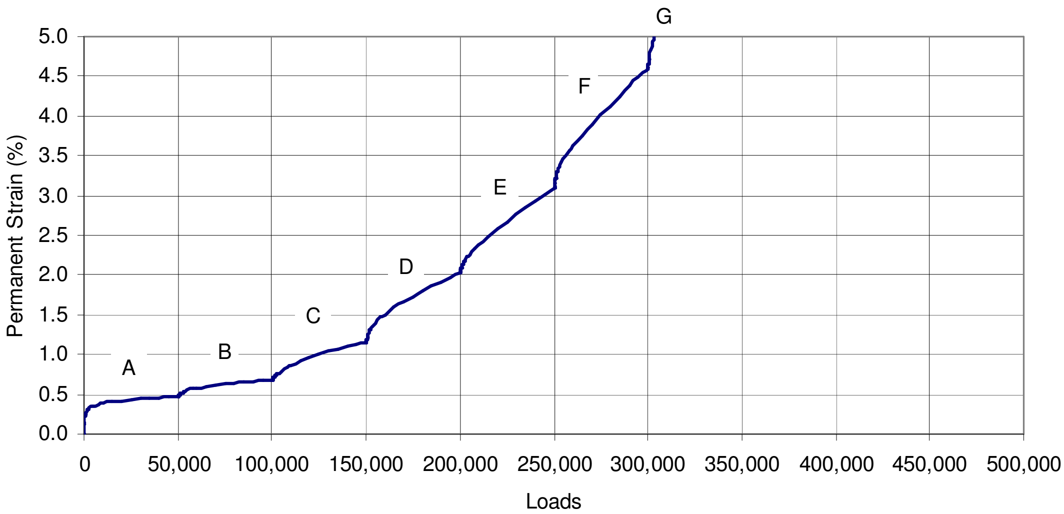

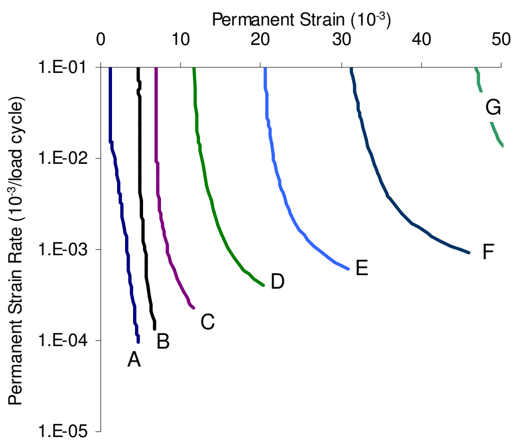

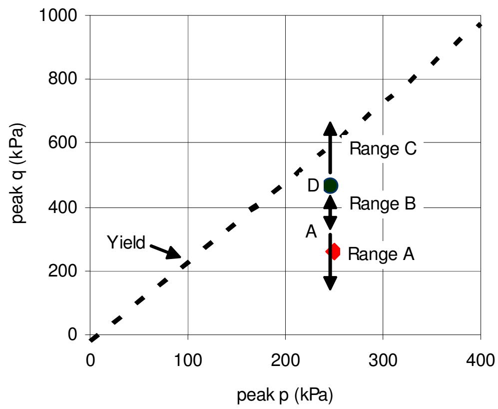

Figure A.12. RLT Permanent strain, stress paths, results, and shakedown range boundaries (CAPTIF 2 - Test 3 - p=250kPa).

Stress Paths (kPa) – *CAPTIF 3 (Test 1, p=75kPa)*							
	$p={}^1/_3(\sigma_1+2\sigma_3)$		[1] $q = \sigma_1 - \sigma_3$		$\sigma_1=q+\sigma_3+$[2]k		[3] σ_3
A	60	72	0	37	66	103	57
B	44	72	0	86	51	137	40
C	29	74	0	135	38	172	25
D	14	74	0	181	23	205	9
E	5	73	0	204	16	220	0
F	6	73	0	202	17	219	0

1. q = cyclic vertical load (kPa).
2. k = top platen weight and minimum vertical load.
3. σ_3 = cell pressure (kPa).

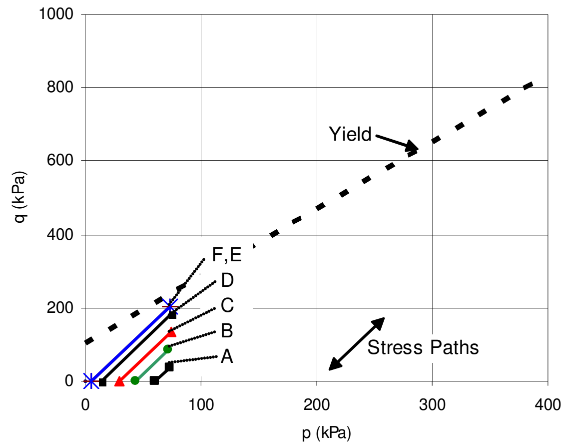

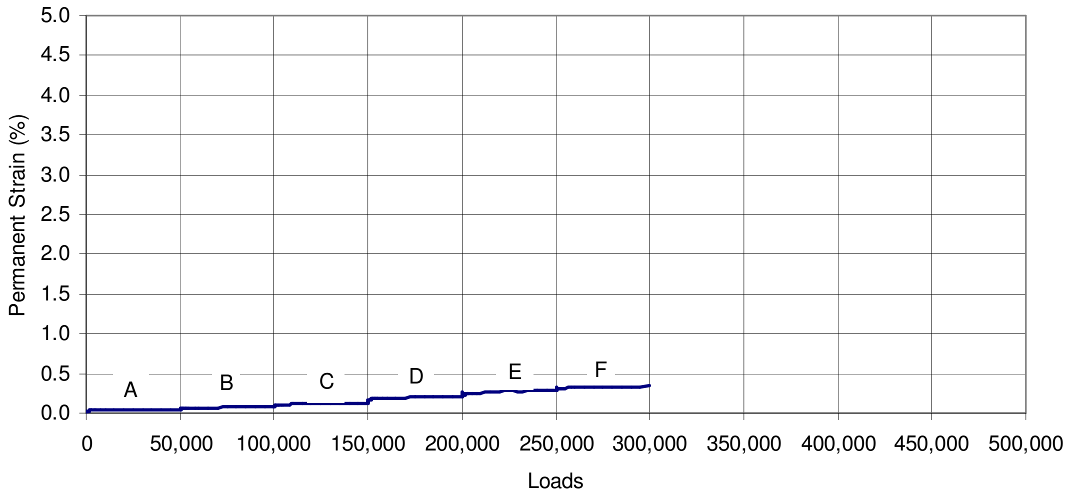

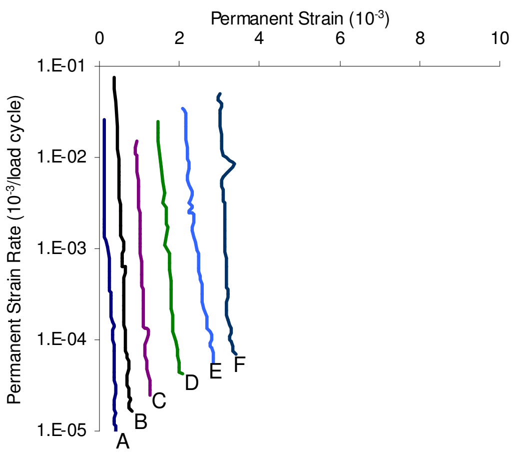

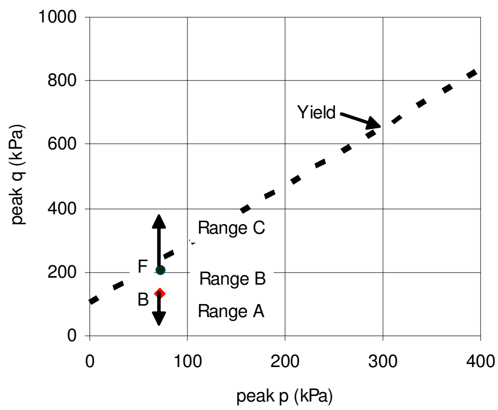

Figure A.13. RLT Permanent strain, stress paths, results, and shakedown range boundaries (CAPTIF 3 - Test 1 - p=75kPa).

Stress Paths (kPa) – *CAPTIF 3 (Test 2, p=150kPa)*							
	$p={}^{1}/_{3}(\sigma_1+2\sigma_3)$		[1] $q = \sigma_1 - \sigma_3$		$\sigma_1=q+\sigma_3+$[2]k		[3] σ_3
A	106	151	0	135	114	249	103
B	90	151	0	183	98	282	86
C	70	147	0	230	79	309	66
D	54	146	0	274	65	339	49
E	39	145	0	318	52	369	33
F	24	146	0	365	38	403	17

1. q = cyclic vertical load (kPa).
2. k = top platen weight and minimum vertical load.
3. σ_3 = cell pressure (kPa).

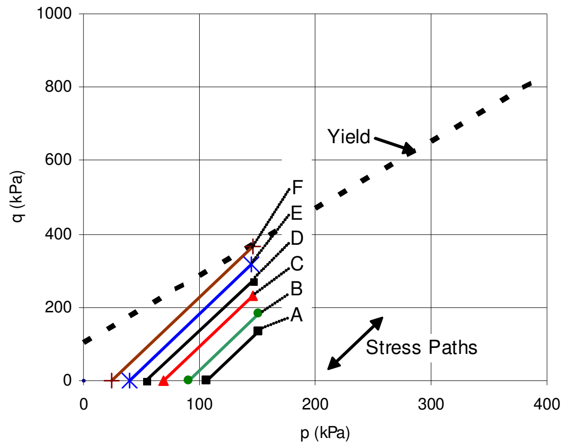

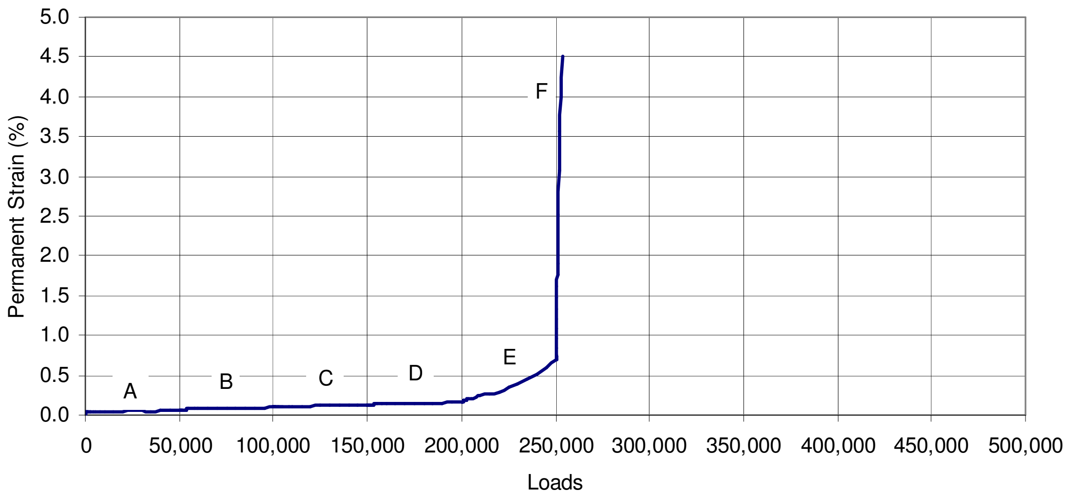

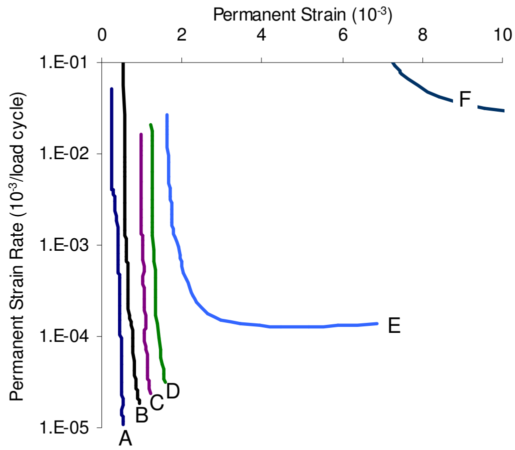

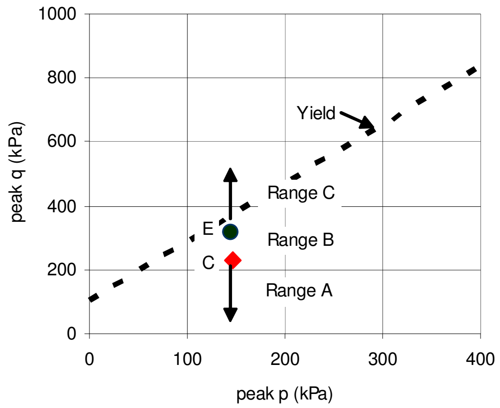

Figure A.14. RLT Permanent strain, stress paths, results, and shakedown range boundaries (CAPTIF 3 - Test 2 - p=150kPa).

Stress Paths (kPa) – *CAPTIF 3 (Test 3, p=250kPa)*							
	$p={}^1/_3(\sigma_1+2\sigma_3)$		[1] $q = \sigma_1-\sigma_3$		$\sigma_1=q+\sigma_3+$ [2] k		[3] σ_3
A	153	246	0	278	162	440	149
B	137	246	0	327	145	472	133
C	121	246	0	375	129	504	117
D	105	244	0	420	114	533	100
E	88	244	0	469	97	566	83
F	72	244	0	517	82	599	67
G	56	243	0	562	67	629	50
H	40	236	0	587	54	642	33

1. q = cyclic vertical load (kPa).
2. k = top platen weight and minimum vertical load.
3. σ_3 = cell pressure (kPa).

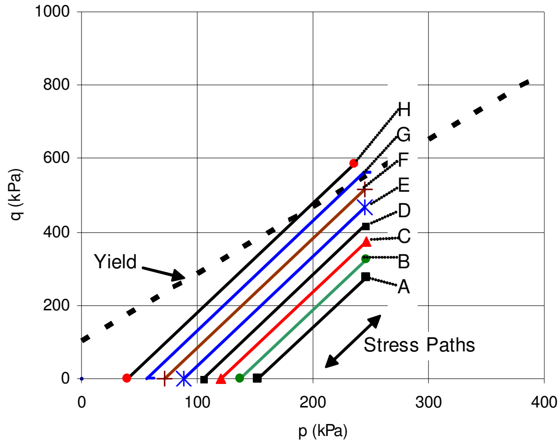

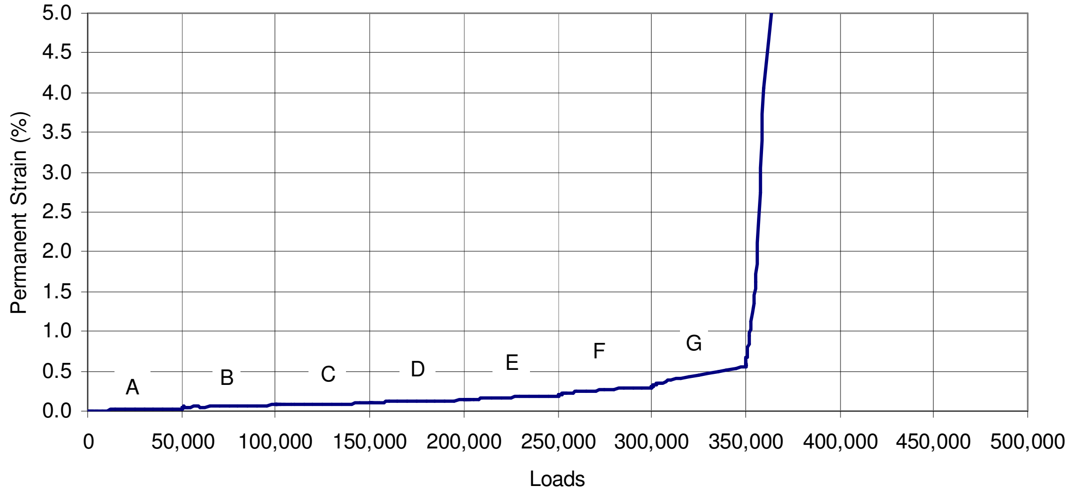

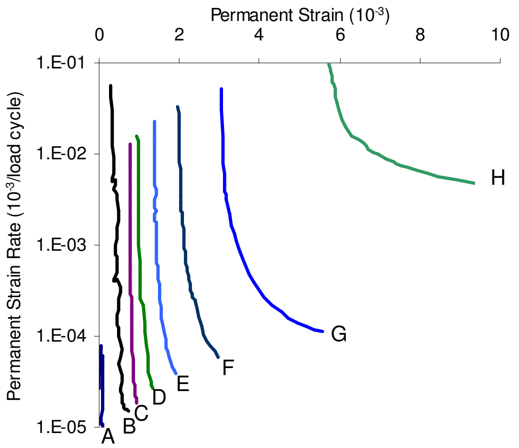

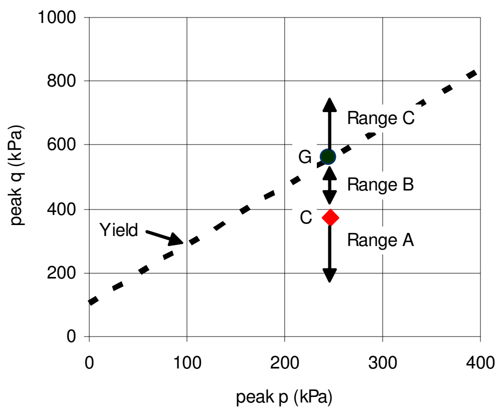

Figure A.15. RLT Permanent strain, stress paths, results, and shakedown range boundaries (CAPTIF 3 - Test 3 - p=250kPa).

Stress Paths (kPa) – *CAPTIF 4 (Test 1, p=75kPa)*								
	$p={}^1/_3(\sigma_1+2\sigma_3)$		${}^1q = \sigma_1-\sigma_3$		$\sigma_1=q+\sigma_3+{}^2k$		${}^3\sigma_3$
A	65	77	0	36	70	107	58
B	49	77	0	85	56	140	42
C	34	79	0	133	41	174	25

1. q = cyclic vertical load (kPa).
2. k = top platen weight and minimum vertical load.
3. σ_3 = cell pressure (kPa).

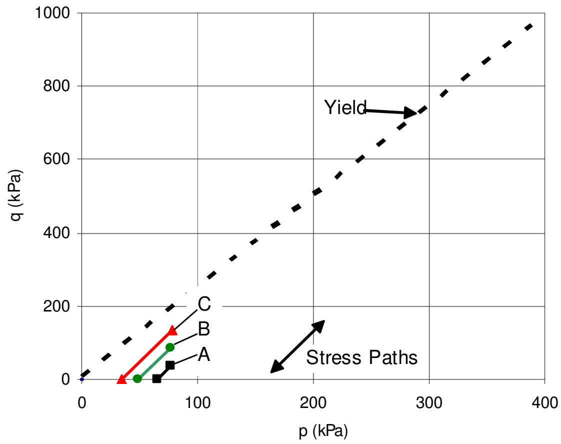

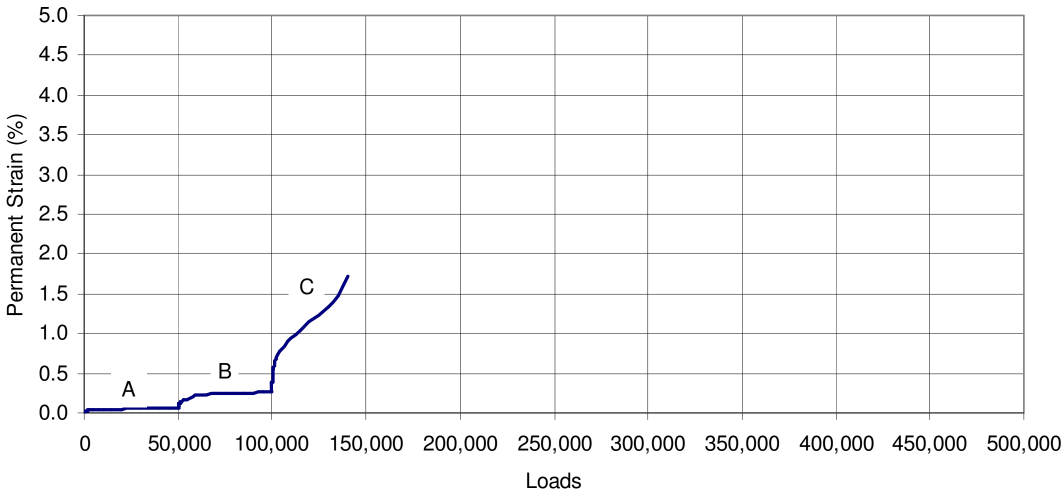

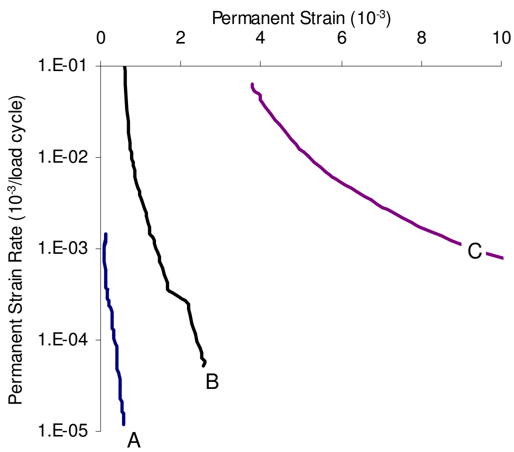

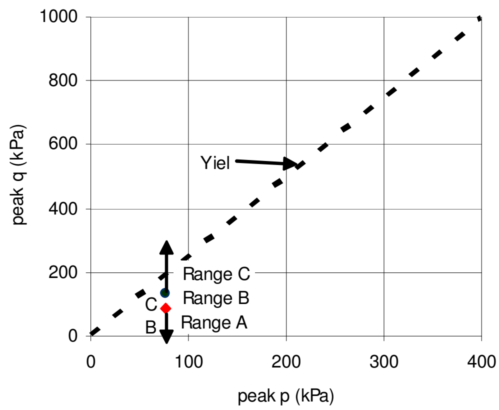

Figure A.16. RLT Permanent strain, stress paths, results, and shakedown range boundaries (CAPTIF 4 - Test 1 - p=75kPa).

Stress Paths (kPa) – *CAPTIF 4 (Test 2, p=150kPa)*								
	$p={}^1/_3(\sigma_1+2\sigma_3)$		${}^1q=\sigma_1-\sigma_3$		$\sigma_1=q+\sigma_3+{}^2k$		${}^3\sigma_3$
A	107	150	0	130	114	244	100
B	91	151	0	179	97	276	83
C	74	150	0	227	82	309	67
D	58	148	0	270	67	337	50
E	43	148	0	314	55	369	33
F	30	151	0	363	40	403	17

1. q = cyclic vertical load (kPa).
2. k = top platen weight and minimum vertical load.
3. σ_3 = cell pressure (kPa).

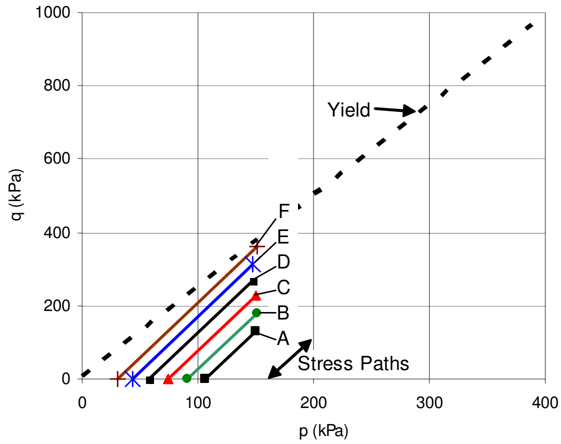

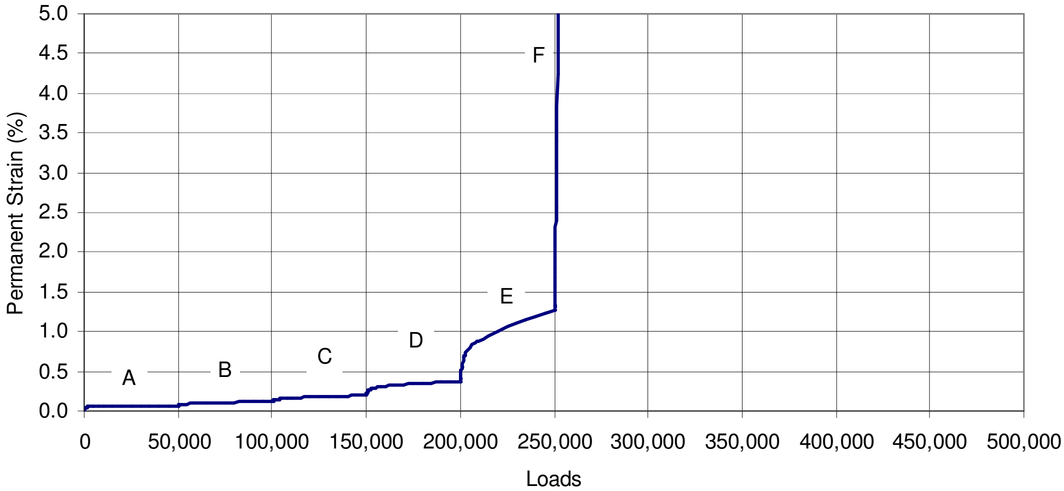

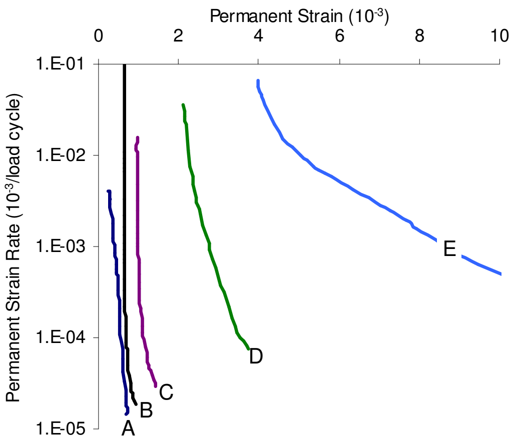

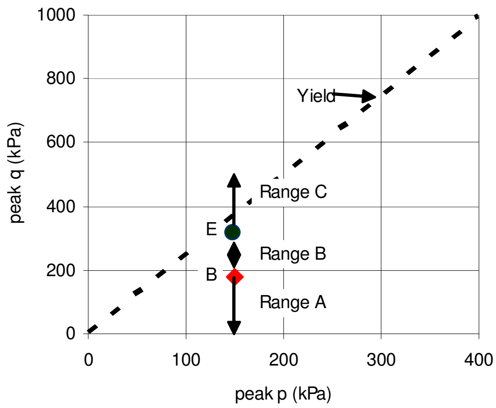

Figure A.17. RLT Permanent strain, stress paths, results, and shakedown range boundaries (CAPTIF 4 - Test 2 - p=150kPa).

Stress Paths (kPa) – *CAPTIF 4 (Test 3, p=250kPa)*								
	p=[1]/[3](σ_1+2σ_3)		[1]$q = \sigma_1 - \sigma_3$		$\sigma_1 = q + \sigma_3 +$[2]$k$		[3]σ_3
A	142	249	0	321	155	476	136
B	125	250	0	374	137	511	119
C	107	246	0	416	120	536	100
D	87	242	0	465	102	567	79
E	77	247	0	510	93	602	69
F	59	246	0	559	77	636	51
G	45	248	0	607	63	670	36

1. q = cyclic vertical load (kPa).
2. k = top platen weight and minimum vertical load.
3. σ_3 = cell pressure (kPa).

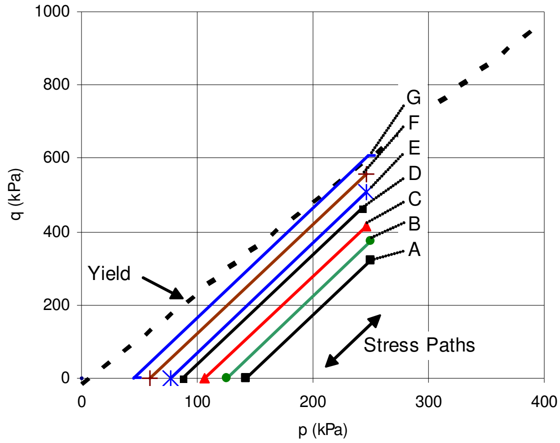

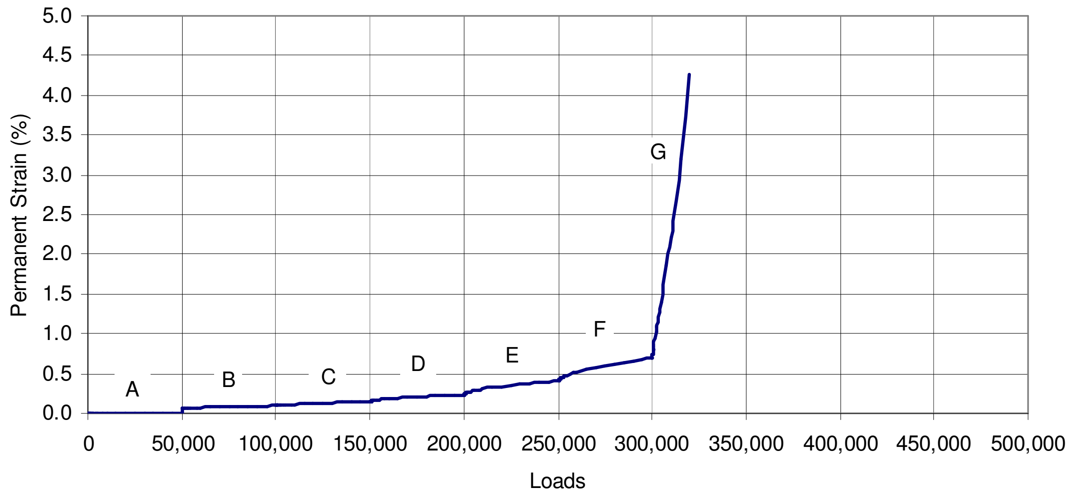

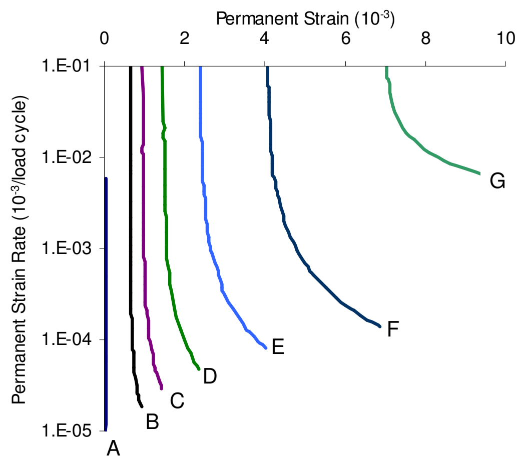

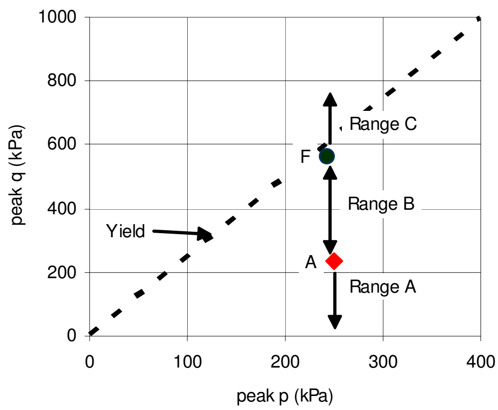

Figure A.18. RLT Permanent strain, stress paths, results, and shakedown range boundaries (CAPTIF 4 - Test 3 - p=250kPa).

APPENDIX B.

NORTHERN IRELAND FIELD TRIAL INSTRUMENT LOCATIONS.

Instrumentation Layout – Excavation (QUB Road Trial – Ballyclare)

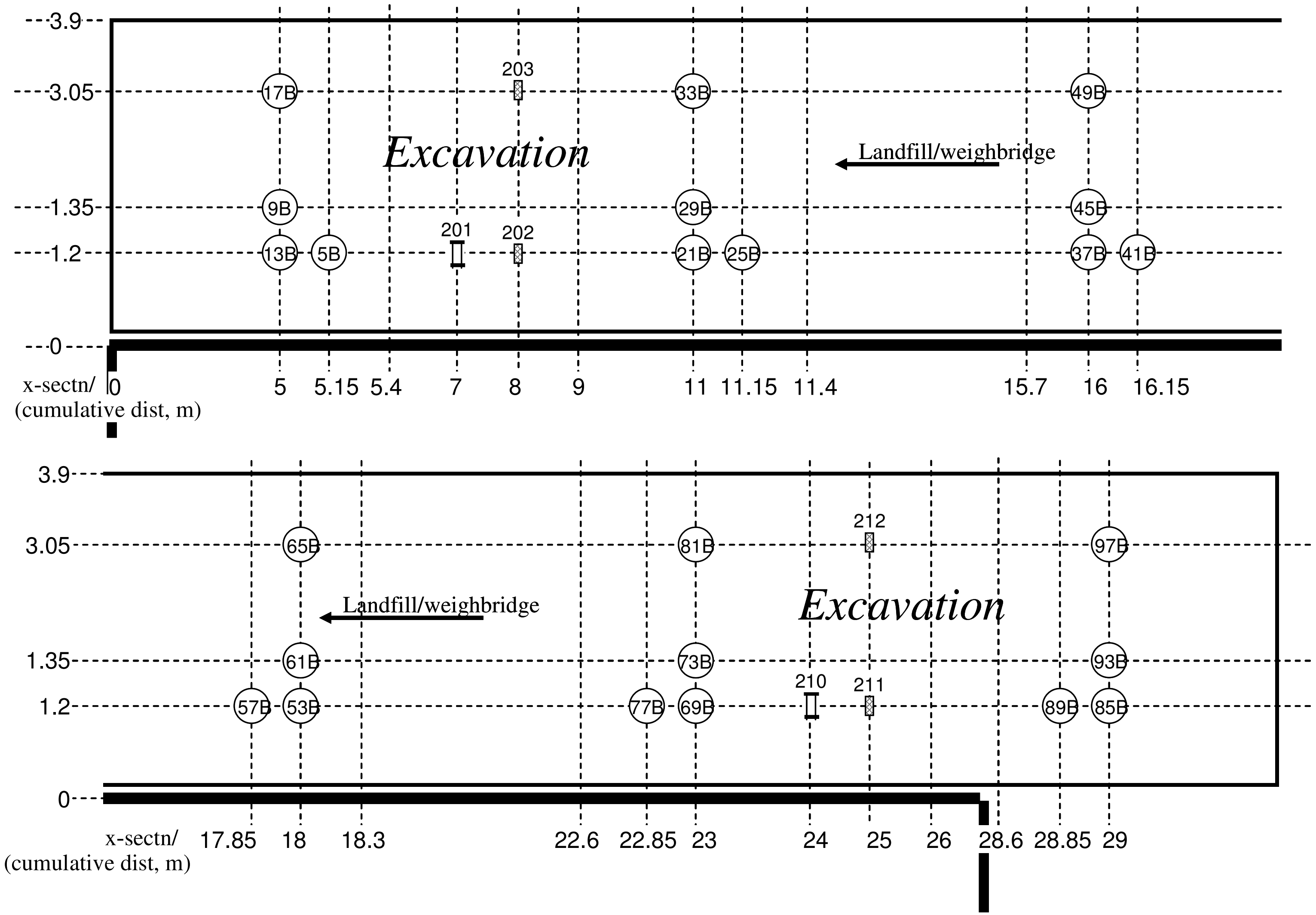

Instrumentation Layout – 1st Layer (QUB Road Trial – Ballyclare)

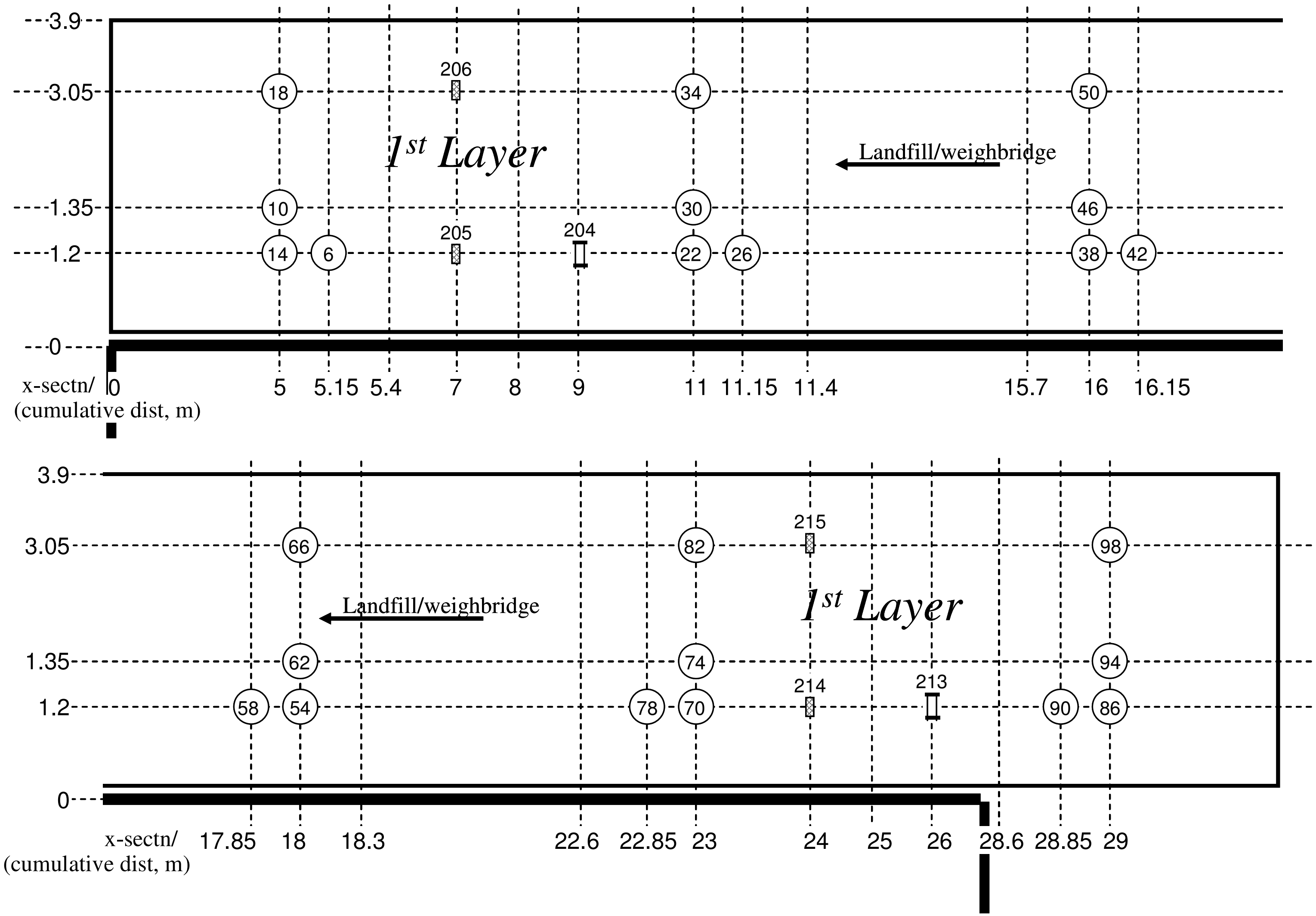

Instrumentation Layout – 2nd Layer (QUB Road Trial – Ballyclare)

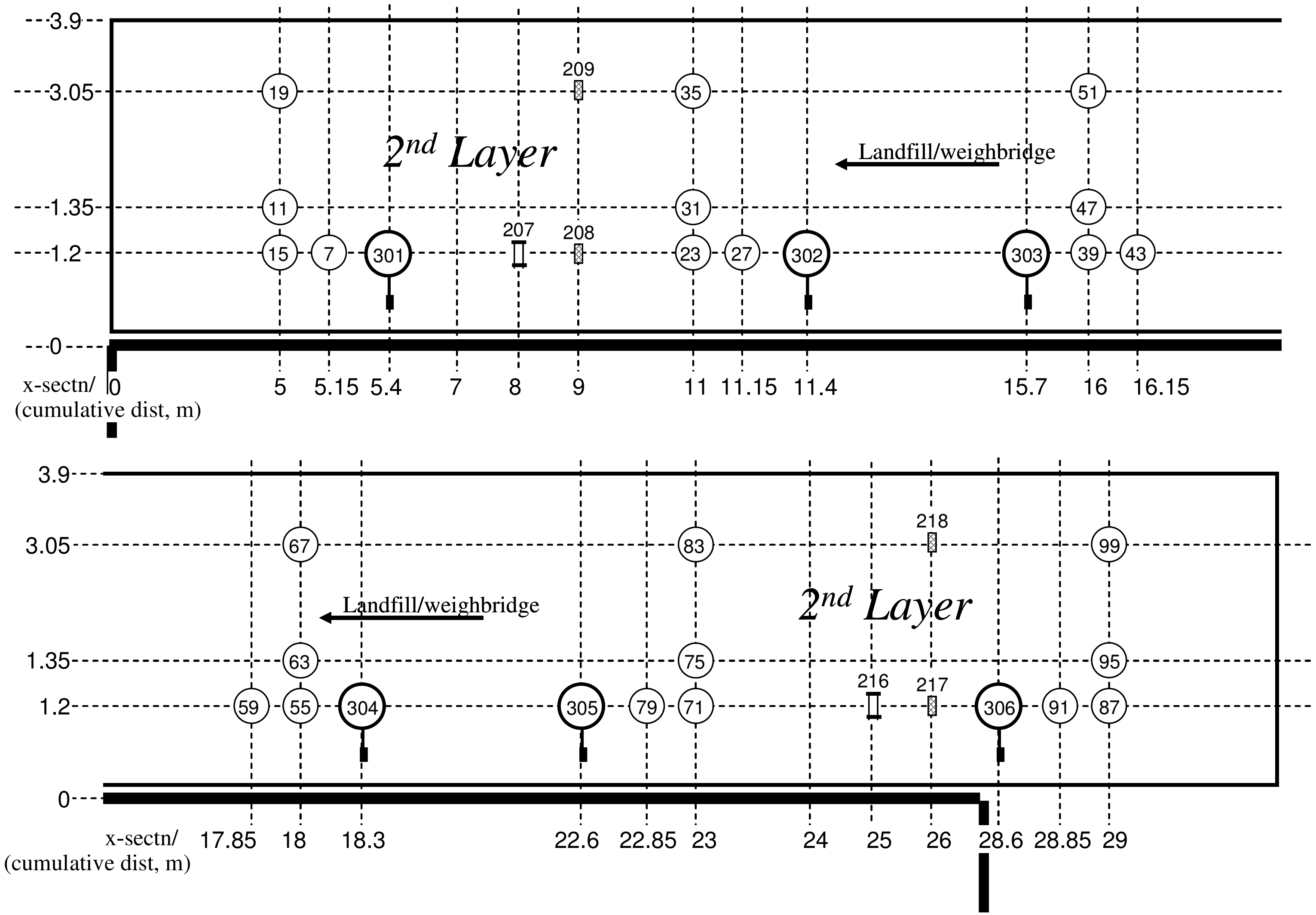

Instrumentation Layout – 3rd Layer (QUB Road Trial – Ballyclare)